Exploring the molecular underpinnings of neuropathic pain in primary afferent subtypes

Allison Marie Barry

Green Templeton College

University of Oxford

Thesis submitted for

Doctor of Philosophy

TT 2022

This thesis is dedicated to every person
who bashed down the doors I walk through.
- AMB

Abstract

Dorsal root ganglia (DRG) neurons have been well described for their role in driving both acute and chronic pain. With cell bodies clustered in the spinal column, these neurons project from the periphery into the dorsal horn. Subtypes convert a range of stimuli into electrical signals, and have been traditionally defined by size, histological markers, projection pathways, and electrophysiological phenotypes. With the advance of sequencing technologies, DRG transcriptomes have been examined through whole ganglia, single cell, and more recently, deep subpopulation sequencing in naïve lines. Here, we study the deep transcriptional profiles of multiple murine DRG populations in acute and chronic pain states while considering sex interactions.

We have exploited currently available transgenics to label and purify subtypes after injury for high throughput sequencing. Using bulk tissue samples, we are able to circumvent the issues of low transcript coverage and drop-outs seen with single cell datasets, increasing our power to detect changes in gene expression.

In one experiment, we have studied the molecular changes in five populations, classified by their functional and molecular signatures in naïve states. These include general nociceptors, peptidergic nociceptors, non-peptidergic nociceptors, C-LTMRs, and Aδ + Aβ-RA-LTMRs. We see both stereotyped and unique subtype signatures in injured states after nerve injury at both an acute and chronic timepoint. While all populations contribution to a general injury signature, subtype enrichment changes can also be seen, possibly driven by the loss of transected NP neurons by 4 weeks. Within populations, there is not a strong intersection of sex and injury, but sex differences in naïve states - particularly in Aδ + Aβ-RA-LTMRs - still contribute to differences in injured neurons.

Using an SNI model of neuropathic pain, ipsilateral DRG contain both injured and intact neurons. The contributions of these populations to pain have yet to be delineated. Mirroring the techniques above, we next used an Atf3$^{\text{creERT2}}$ line to label and sort fluorescent neurons prior to RNA-seq. We have complemented this with a pilot snATAC-seq study, showing that neurons cluster by subtype in naïve and injured states.

We have curated this data into an accessible, online platform. Together, this contributes a resource to the pain community to probe subpopulation and sex-specific differences after nerve injury at multiple timepoints.

Declaration

I declare the work within this thesis to be my own, unless otherwise stated. Key contributions include:

Transgenic characterizations Dr. Xun Jang performed the immunohistochemistry for Calca$^{\text{tm1.1(cre/ERT2)Ddg}}$/J, Mrgprd$^{\text{tm1.1(cre/ERT2)Ddg}}$/J, and Ntrk2$^{\text{tm1.1(cre/ERT2)Ddg}}$/J under my supervision. I performed all analyses.

Atf3$^{\text{creERT2}}$ sequencing Dr. Georgios Baskozos performed the alignment and initial count analysis for the Atf3$^{\text{creERT2}}$ dataset in chapter 5. He also oversaw the analysis of the subpopulation RNA-seq experiments. Dr. Greg Weir and Dr. Andrew Cooper (University of Glasgow) performed the sample collection for the snATAC-seq work from Atf3$^{\text{creERT2}}$, as well as further experiments relating to the loss of non-peptidergic neurons after spared nerve injury.

Funding This work is supported by the Wellcome Trust (215145/Z/18/Z), the MRC (MR/T020113/1), and a GTC MSDTC Scholarship.

Acknowledgements

Even the smallest moments in life are built on community, and I am privileged to have more than a few people in mine.

Prof. David Bennett, thank you. For your confidence, for sharing your passion, and for the space you provided to let me grow. Thank you for the patience at all steps along the way.

Dr. Georgios Baskozos, your unwavering enthusiasm, support, and insight for each endeavor has lightened this PhD and shaped me into a better scientist.

Prof. Stephen Tucker, thank you for being there as a pillar to turn to. Along with Prof. Dame Fran Ashcroft and the OXION programme, your love of ion channels has been inspiring, and I'm excited to have contributed even the smallest of slivers. To the rest of the Neural Injury Group, thank you for being there to celebrate the good, and, more importantly, to help navigate the bad.

To Prof. Ian Meinertzhagen - thank you for introducing me to the world of research. For showing me that I had a place here. Your acceptance, passion, and encouragement over the years cleared this path in ways I couldn't imagine when I joined your group a decade ago. I am indebted to the entire lab for having me, but within this, Dr. Lucia Caceres: thank you for taking me under your wing.

Prof. Manuela Schmidt, you inspire me. I am continuously grateful for your care and mentorship. Thank you for the continuing to support and uplift me. Dr. David Gomez-Varela, your encouragement as I entered the world of bioinformatics helped shape this work for the better. I hope you like the plots.

To every other lab I've passed through - to Prof. Vic Rafuse, to Dr. Bart Geurten, and to Dr. Livia de Hoz - there is a joy in learning that can be lost when not protected. The space you each gave me to play in your labs has kept science fun.

To my family and friends in Oxford and overseas, your love and patience has not gone unnoticed. Your undying support has given warmth to this experience. Mum and Dad - thank you for fostering my curiosity throughout life. Mel, thank you for being there to look up to, for always looking out for me, and for Wallace. Ronja, Linda, Tal, and Myrto, your love has built me up, and I am unbelievably grateful for the family you gave me. To every running partner, climbing partner, my Ashtanga community, and the Green Templeton Boat Club, for every coffee and for every hug, thank you.

Contents

List of Figures

List of Tables

1 Introduction

Contents

1.1 Somatosensation overview

Pain is a fundamental aspect of one's interaction with the physical world. It's sensory percepts are ingrained into our idea of human nature, and it's negative affect proves crucial to our survival.

In the simplest of terms, a combination of primary afferents, spinal projection

neurons, and higher order circuitry results in these percepts. Primary afferents innervate numerous organs, including the skin, the musculoskeletal system, and the viscera. These project to second-order neurons in the spinal cord where sensory signals are gated, modulated, and transmitted to the brain via projection neurons.

Disruptions to this system can turn pathological, resulting in chronic disability. The broad grouping of chronic pain conditions affects up to 25% of the global population. Neuropathic pain, as a subclass, affects about 8%. It is directly tied to nervous system damage though trauma, disease, or therapeutic use (eg. chemotherapy, antiretrovirals) [1]. Increasing lifespans, diabetic prevalence, and decreases in cancer mortality are all contributing to increases in these disorders [2].

Clinically, neuropathic pain patients experience a range of symptoms including allodynia and hyperalgesia, burning, prickling, numbness, and spontaneous pain [2]. Current treatment options are widely considered inadequate and quality of life scores remain significantly reduced [3, 4].

Primary afferent pathophysiology is thought to be a key driver: this thesis thus explores the underlying molecular mechanisms of neuropathic pain within these subpopulations. I exploit currently available transgenic models to isolate populations of interest for downstream RNA sequencing (RNA-seq). This permits subtype-specific analyses after nerve injury, as well as an interaction study of sex and injury within primary afferent populations.

1.2 Dorsal root ganglia

1.2.1 Heterogeneity and classifications

For the current study, I will focus on the sensory neurons with cell bodies residing in the dorsal root ganglia (DRG). Appropriate parallels and alternative innervation patterns will be discussed where necessary. Primarily, these neurons will be discussed for their skin innervation patterns, where they have been well described for their role in somatosensation and pain [2]. High throughput molecular profiling is discussed below.

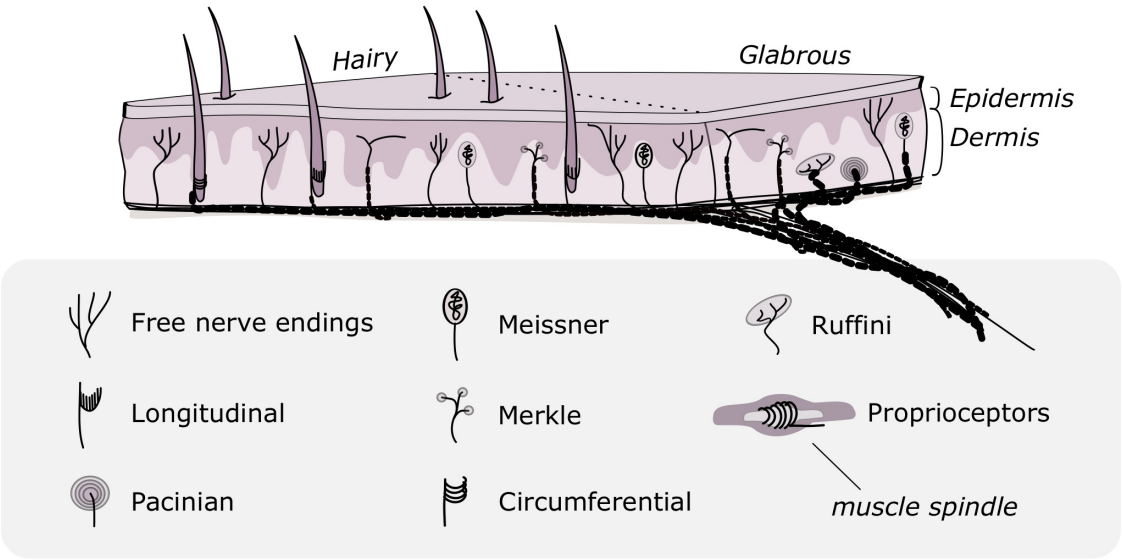

Figure 1.1: Sensory neuron terminal endings in the skin and viscera.

Sensory neuron diversity is present in various factors, each intrinsically related (Fig 1.1). Soma and axon sizes are remarkably good indicators of function due to the correlation of axon size and conduction velocity. Myelination is positively correlated to axon size, amplifying this effect. Diverse terminal endings are also seen. While free nerve endings project into the epidermis and are more indicative of high threshold stimulation, specialized touch organs in the dermis facilitate the signal transmission from a range of stimuli (1.2).

Electrophysiological response differ across subtypes due to differences in size, myelination, and end organs, as well as inherent differences in molecular composition. Within subgroups, firing patterns are well correlated to transcriptional profiles [5]. As a general rule of thumb, large diameter neurons, typically defined as a soma size $>$ 35 um in mice, have more narrow action potentials.

1.2.1.1 High threshold receptors

High threshold receptors, commonly referred to as nociceptors, are sensory neurons that traditionally activate in response to 'noxious', potentially tissue damaging stimuli (Fig 1.2). This sensory modality is associated with a negative affect, yet plays a critical role in human survival. Disruptions to this system, exemplified

in patients with congenital insensitivity to pain (CIP) result in a reduced quality of life and higher incidence of injury [6].

The majority of nociceptors are unmyelinated with small axon diameters (C-fibres). In mice, these are characterized by their small soma diameters (<25 μm) and conduction velocities less than 1.2 ms^{-1}. Afferents project "free nerve endings" into the epidermis, although the recent discovery of non-myelinating, mechanosensitive cutaneous Schwann cells suggest a more complex terminal morphology [7]. They terminate in the superficial laminae of the dorsal horn. Receptors are commonly polymodal, responding to varying combinations of temperature, chemical, and mechanical stimulation.

This population is commonly identified by the expression of *Scn10a*, encoding the voltage-gated sodium channel Nav1.8 [8, 9]. Broadly, murine nociceptors are commonly divided into two distinct, non-overlapping populations: non-peptidergic and peptidergic [10].

The non-peptidergic class corresponds to MRGPRD (MAS-related G-protein coupled receptor member D, encoded by *Mrgprd*) or P2RX3 (Purinergic ion channel type 3 receptor, *P2rx3*) expression [10]. Experimentally, this subpopulation is commonly referred to as IB4 (isolectin B4)-binding in rodents. In mice, this population is involved in mechanical and chemical pain in naïve states, with free nerve endings in the skin and projections to lamina II inner (II_i). In the dorsal horn, these neurons synapse on interneurons, which then feed into projection neurons.

The peptidergic class is identified by the expression of CGRP (Calcitonin gene-related peptide, encoded by *Calca*). This is a functionally diverse group commonly associated with noxious heat detection and with a broad grouping that can by further subdivided in various ways, including functional and transcriptional characterizations. For example, CGRP-positive nociceptors contain a subset of mechanically-insensitive (mechanoinsensitive) neurons. Referred to as "silent nociceptors", they transcriptionally unique: Silent nociceptors express both TRKA (Tropomyosin receptor kinase A, encoded by *Ntrk1*) and nAChRα3 (Neuronal

acetylcholine receptor subunit alpha-3, *Chrna3*) [11]. This population projects to lamina I and lamina II outer, with synaptic contact directly on projection neurons.

In addition to C-fibre nociceptors, a subset of Aδ fibres respond to noxious mechanical stimuli [12]. These fibres have more rapid conduction velocities than their C-fibre allies with a murine range from 1.2-10 ms^{-1}. Additionally, this class of nociceptors is thinly myelinated, expressing Nav1.8, TRKA, and the calcium binding protein B, S100β. Some of these fibres also express CGRP, and this subset can be grouped into the peptidergic class of nociceptors.

Aβ nociceptors have also been described across species [13], based on conduction velocities comparable to other Aβ fibres. These thickly myelinated nociceptors play a role in mechanical pain, and have recently been detected in humans using microneurography [14]. Electrophysiologically, the delineation between Aδ and Aβ varies with definition. As such, across species Aβ nociceptors comprise anywhere from 18-65% of high threshold A-fibres [13].

1.2.1.2 Low threshold receptors

Low threshold receptors are involved in the detection of innocuous stimuli, including pressure, stimulus velocity, and/or vibration. Typically, this category comprises the myelinated Aδ and Aβ populations. These fibres form complex terminal endings in the skin which govern the detection of innocuous mechanical stimuli, giving the name low threshold mechanoreceptors (LTMRs).

Aδ fibres can be high- or low- threshold. While Aδ nociceptors form free nerve endings, low threshold Aδ fibres, coined D-hairs, form longitudinal lanceolate endings in hairy skin. They are transcriptionally unique from their nociceptive counterparts, expressing TRKB (Tropomyosin receptor kinase B, encoded by *Ntrk2*) and the voltage-gated calcium channel 3.2 (Cav3.2, encoded by *Cav3.2*) [15–17].

Aβ-LTMRs are large, thickly myelinated sensory neurons with high conduction velocities (>10 ms^{-1} in mice). Electrophysiological recordings denote 2 subpopulations of Aβ LTMRs - rapidly adapting (RA) and slowly adapting (SA) [18]. RA-LTMRs extend into the dermis as longitudinal lanceolate endings (hair skin)

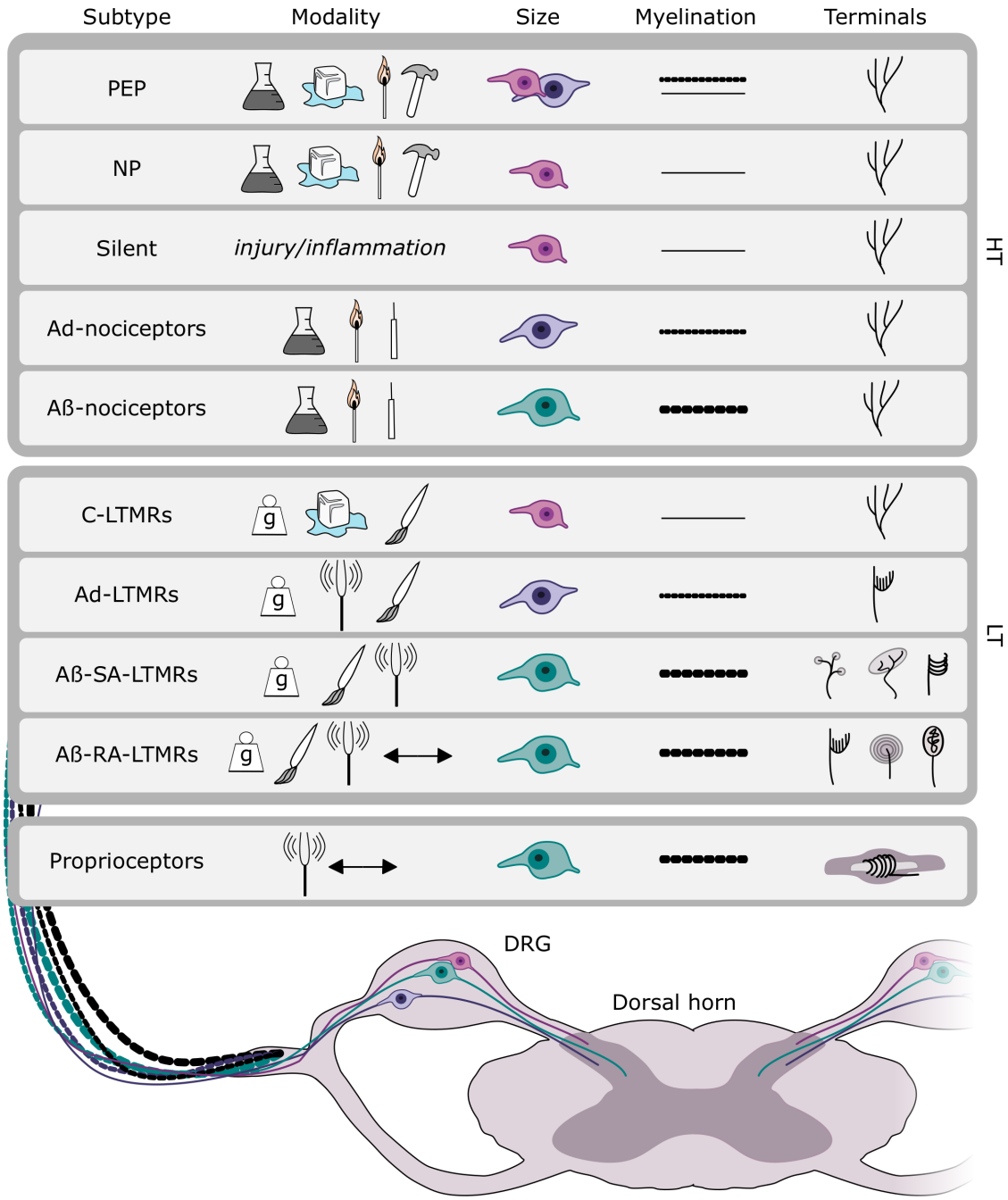

Figure 1.2: Broad sensory neuron subpopulations within the mouse dorsal root ganglia. HT: high threshold, LT: low threshold. PEP: peptidergic nociceptors, NP: non-peptidergic nociceptors. LTMR: low threshold mechanoreceptor. RA: rapidly-adapting, SA: slowly-adapting. Silent nociceptors are a functionally distinct subgroup of PEP.

and Meissner/Pacinian corpuscles in glaborous skin to give phasic responses to innocuous stimuli. SA-LTMRs are structurally unique to allow for tonic responses.

This subpopulation surrounds hair follicles with circumferential endings, as well as extend to Merkel cells (disks) and Ruffini's corpuscles [19–21].

A unique subpopulation of C-fibres termed C-low threshold mechanoreceptors (C-LTMRs) are labelled by tyrosine hydroxylase (TH) and TAFA4 in rodents. These axons form lanceolate endings in hair skin where they encode the pleasant affect of touch and innocuous cold. Similar to D-hairs, this population expresses *Cav3.2*.

1.2.2 Molecular profiling

1.2.2.1 Transcriptional profiling in naïve states

Subpopulations have been traditionally defined by size, histological markers, projection pathways, and electrophysiological phenotypes. With the advance of sequencing technologies, DRG molecular signatures have been examined through whole ganglia, single cell, and more recently, deep subpopulation sequencing in a naïve state. The single cell and subpopulation RNA-seq results have both supported and enhanced our knowledge of DRG complexity in mice [5, 22, 23], humans [24, 25], and non-human primates [26]. To our knowledge, we still lack single cell data from rat sensory neurons. A selection of these studies are highlighted in Table 1.1.

Together, this provides a detailed characterization of gene expression levels in specific states, as well as functional insights. These correlates have been highlighted in multiple cases, for example: the distribution of ion channel transcripts across subpopulations correlates to their electrophysiological properties in mice [5], and bulk human DRG transcript data correlates to neuropathic pain [27].

Bulk RNA-seq Tissue samples are commonly processed in bulk as large quantities of RNA prove easier to work with. The data complexity has been drastically increased with the advancement of sequencing techniques. Now, unbiased transcriptomic studies are becoming the norm. DRG sequencing data frequently uses whole DRG tissue samples (including neurons, glia, and immune cells). This allows in depth sequencing and detailed transcriptome details for these naïve populations.

Multiple studies have looked at DRG and related transcriptomes, including that of the naïve mouse nociceptor transcriptome [28]. Due to the variety of cell types contained in bulk tissue samples, we are limited in the types of information we can extract. Commonly, bulk sequencing is used to address more specific questions, such as transcript changes in a pathological state.

Through the use of fluorescence activated cell sorting (FACS) and transgenic labelling of subpopulations, transcript details about specific populations have also emerged [5, 29]. This has allowed for deeper sequencing of sensory neuron subtypes technically not yet available through single cell sequencing.

Single cell and single nuclear RNA-seq The development of single cell RNA sequencing (scRNA-seq) techniques has contributed significantly to our understanding of sensory neuron subpopulations. Multiple groups have published these datasets, consistently indicating that our previous population delineations fall short of grasping sensory neuron complexity [22, 23, 30].

Single nuclear sequencing (snRNA-seq) has also emerged as a useful technique. While there are known differences between single cell and single nuclear sequencing datasets [31, 32], nuclear sequencing can be technically convenient and highly informative [33]. Nuclei can be extracted from frozen tissue, reducing RNA degradation association with single cell purification methods. Additionally, this has provided a platform to sequence human sensory neurons, as the large cell size provides technical challenges.

Together, these methods have highlighted more detailed subgroupings of sensory neurons than previously available, including subgroupings of peptidergic and non-peptidergic neurons. The ability to analyse "pseudo-bulk" samples of single cells helps compensate for the lower sequencing depth and high variability associated with processing low amounts of RNA.

1.2.2.2 Molecular profiling in injured states

Initial molecular work in primary afferents has emphasized the massive changes in mRNA and protein levels across a variety of rodent pain models [34–36]. In addition to DRG profiling, datasets on immune cells [37] give insight to the vast differences between naïve and painful states, while timecourse studies have highlighted how RNA expression changes throughout an injured state [33].

Microarrays RT-PCR/qPCR and microarray assays laid decades of foundation and they remain a useful tool. At this level, massive changes in gene expression can be seen in injured state, in studies that continue to inform more high throughput, unbiased transcriptomic assays [38, 39].

Bulk transcription Using RNA-seq, large-scale transcript changes are also seen across neuropathic pain models [35]. While tissue heterogeneity complicates the interpretation of bulk datasets, emerging themes include changes in ion channel expression, immune mediators, and metabolic function [34, 40]. This also allows researchers to examine expression changes after gene manipulation, at a lower cost than single cell RNAseq, and is shaping our understanding of neuropathic pain mechanisms.

Single cell At the single cell level, recent work has emphasized the extensive transcriptome changes after nerve injury [41, 42]. Transcript markers usually associated with specific neuronal subpopulations are rapidly downregulated after injury, forming a new "injury-state" specific cell signature. The induction of this injured state is supported by a similar study of TG nuclei [33], as well as rentinal ganglion cells (RGCs) after optic crush [43]. In the TG, this effect is reversed with time, but holds true across numerous injury models including basic scratch lesions to the skin. The recovery process and related protein changes remain unclear.

Under pathological conditions, our knowledge of subpopulation-specific changes requires development, and the exact contribution of these changes to a neuropathic

pain state are needed. Furthermore, previous molecular and behavioural data support sex differences after injury. It is unclear if these differences are largely immune-related, or if individual neuronal populations behave differently. These questions are addressed in depth in chapter 4.

Transcriptomics provide just one way to examine large scale changes in pathological states. Given the complexity of neuropathic pain, researchers have employed a variety of other "-omic" technologies to tackle this problem.

1.2.2.3 Translatomics

Translatomic assays bridge the transcriptome and proteome by considering only the transcripts actively being translated into proteins. There are multiple ways to investigate a translatome, but in brief one processes ribosome-associated mRNA transcripts [44]. This provides another way of examining changes in pain states. While not as common as RNA-seq, there are published DRG translatomes investigating chemotherapy-induced neuropathic pain [45] and spared nerve injury [46].

1.2.2.4 Epigenomics

Chromatin structure is a well-known regulator of gene transcription. Whereas RNA is a transient metric of cell activity, chromatin structures and epigenetic modifications can indicate more long term changes in cell subtypes and/or pathological states. The study of these modifications, such as histone binding and base pair methylation, is referred to as epigenomics. This can be probed in a variety of ways.

DNA modification through cysteine methylation, hydroxymethylation, and other base modifications play an important role in regulating transcription. Methylation status is a common target for epigenome wide association studies (EWAS) through Methyl-seq (or bisulfite sequencing), allowing researchers to correlate cell type information to GWAS findings in an attempt to explain the molecular role of SNPs.

DNAse-seq is an extension of DNAse footprinting: here, DNA is digested with DNAse, and any DNA bound to regulatory proteins remains intact for downstream next generation sequencing (NGS) [47, 48]. This provides a general view of open

chromatin and insights to noncoding functional elements, such as transcription start sites (TSS), transcription factor binding, and nucleosome positioning.

Chromatin conformation studies have also evolved from interrogating a single loci pair via classical conformation capture (3C) to unbiased whole genome chromatin mapping, coined Hi-C [49]. This process centres around the fragmentation and ligation of fixed chromatin, such that loci in close proximity are ligated and sequenced together, revealing the multi-dimensional structure of chromatin.

The integration of classical chromatin immunoprecipitation (ChIP) with parallelized DNA sequencing (ChIP-seq) provides a high throughput way of interrogating chromatin structure through protein binding. This has been exploited for both histone modification studies of epigenetic signatures, as well as DNA-protein interactions for specific transcription and co-factor binding sites in naive and chronic pain conditions.

Recent advances in Assay for Transposase-Accessible Chromatin (ATAC) – sequencing has built on DNAse-seq and others, allowing researchers to query the accessible (ie. open chromatin) regions in DNA (Fig 1.3) [50]. This technique is high throughput and sensitive, allowing single cell sequencing of open chromatin, which reveals cell-type specific chromatin structures. These epigenetic atlases can inform disease mechanisms by guiding functional genomic variants towards possible cell type specificity. In trigeminal ganglia, this approach was recently used to investigate susceptibility to migraine in neuronal subtypes [51]. In chapter 5, we exploit this technique for a pilot study to examine changes in injured DRG neurons.

1.2.2.5 Proteomics

In addition to understanding DNA and RNA changes after injury, it is important to understand changes at the protein level. Advances in mass-spectrometry (MS) and sample preparation has facilitated the transition to high throughput proteome analyses. For disease states, human studies commonly centre around more accessible tissue, such as blood, saliva, and/or cerebral spinal fluid (CSF). Rodent proteomic studies in pain have primarily focused on SC and sciatic nerve (SN) tissue, with

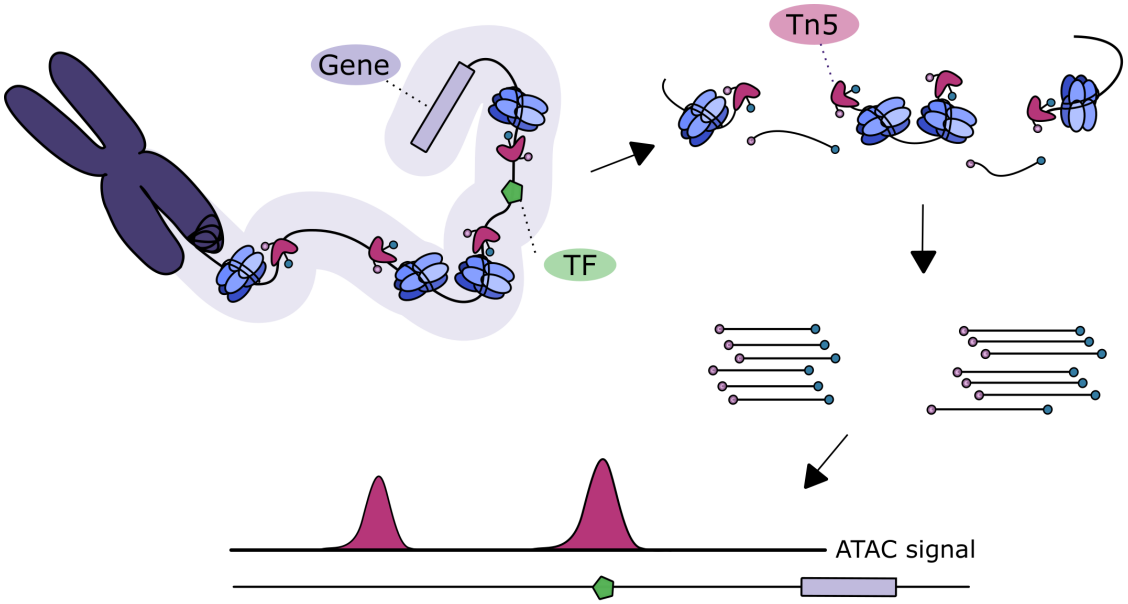

Figure 1.3: ATAC-seq schematic. Tn5 binds to accessible chromatin for transposition. Fragments are then sequenced and aligned to the appropriate genome.

some DRG data available, as well as added analyses into sex differences [52] and drug response mechanisms [53, 54]. Recent work has also highlighted protein changes in iPSCd sensory neurons in a model of chemotherapy induced peripheral neuropathy [55].

Differences in tissue processing can alter the detection of membrane proteins, and lowly expressed proteins are notoriously difficult to capture using standard data-dependant (DDS, ie. shotgun) MS techniques [56, 57]. The development of data-independent acquisition (DIA) techniques has helped with these advances [36], but our ability to probe complete proteomes is likely still lacking. Technical limitations have thus far prevented any DRG subpopulation-specific proteomes, as substantial amounts of protein are required for each experiment. Extensive immunofluorescence experiments have led to the development of a cell atlas, mapping protein locations across cell types, but does not include sensory neurons [58, 59]. It is reasonable to expect more high throughput advancements in the near future, as they are currently in development across model species [60].

Mass-spectrometry can be tailored further. It has been successfully used to interrogate protein-protein interactions of pain-implicated proteins via co- immuno-

precipitation (eg. TRPV1 [61] and TRPA1 [62]). It can be used to sequence the secretome (the collection of soluble proteins release from cells), or, using specific sample preparation methods, metabolites (metabolomics). Protein regulation can be further queried through phosphoproteomics, which provides insight to kinase and phosphotase activity within tissue.

Table 1.1: DRG and related -omics references from a selection of published works.

Group	Type	Tissue	Species	Notes	Sex	Location	Reference
	snRNA-seq	DRG	Human	naïve	Mixed	All	Nyugen *et al.* 2021 [25]
	spatial-seq	DRG	Human	naïve	M + F	Lumbar	Tavares-Ferreira *et al.* 2022 [24]
	snRNA-seq	TG	Human	naïve	M + F	All	Yang *et al.* 2022 [51]
	scRNA-seq	DRG	Macaque	naïve	Mixed	Lumbar	Kupari *et al.* 2021 [26]
	snRNA-seq	DRG	Mouse	injury	Male	Lumbar	Renthal *et al.* 2020 [42]
	scRNA-seq	DRG	Mouse	naïve	Mixed	Lumbar	Usoskin *et al.* 2014 [22]
	scRNA-seq	DRG	Mouse	naïve	Mixed	All	Zeisel *et al.* 2018 [30]
	scRNA-seq	DRG	Mouse	naïve	Male	Lumbar	Li *et al.* 2016 [23]
	scRNA-seq	DRG	Mouse	naïve	NA	All	Sharma *et al.* 2020 [63]
	scRNA-seq	DRG	Mouse	naïve	NA	Colonic	Hockley *et al.* 2019 [64]
	patch-seq	DRG	Mouse	naïve	Male	All	Parpaite *et al.* 2021 [65]
	scRNA-seq	DRG	Mouse	injury	Mixed	All	Hu *et al.* 2016 [41]
	scRNA-seq	RGC	Mouse	injury	Mixed	RGC	Tran *et al.* 2019 [43]
	snRNA-seq	TG	Mouse	naïve	Mixed	All	Nguyen *et al.* 2017 [66]
	snRNA-seq	TG	Mouse	injury	Mixed	All	Nguyen *et al.* 2019 [33]
	snRNA-seq	TG	Mouse	migraine	Mixed	All	Yang *et al.* 2022 [51]
	snRNA-seq	SN/Vagus	Mouse	naïve	Mixed	Nerve	Lim *et al.* 2022 [67]
	sc/sn RNA-seq	ON	Drosophila	naïve	NA	ORN	McLaughlin *et al.* 2021 [68]
RNA	RNA-seq	DRG/TG	Human	naïve	Male	All	Flegel *et al.* 2015 [69]
	RNA-seq	DRG	Human	naïve	Female	Lumbar	Ray *et al.* 2018 [70]
	RNA-seq	DRG	Human	injury	M + F	All	North *et al.* 2019 [27]
	RNA-seq	DRG	Mouse	naïve	Female	All	Gerhold *et al.* 2013 [71]
	RNA-seq	DRG	Mouse	naïve	Male	Lumbar	Thakur *et al.* 2014 [28]
	RNA-seq	DRG subtypes	Mouse	naïve	Mixed	All	Zheng *et al.* 2019 [5]
	RNA-seq	DRG	Mouse	injury	M+F	Lumbar	Lopes *et al.* 2017 [72]
	RNA-seq	DRG	Mouse	injury	Mixed	Lumbar	Baskozos *et al.* 2019 [73]

	RNA-seq	DRG	Mouse	injury	Male	Lumbar	Palmisano *et al.* 2019 [74]
	RNA-seq	DRG	Mouse	injury	Male	Lumbar	Pan *et al.* 2021 [75]
	RNA-seq	DRG	Mouse	injury	M + F	Lumbar	Chernov *et al.* 2021 [76]
	RNA-seq	SG (DRG)	Mouse	injury	Mixed	Lumbar	Jager *et al.* 2020 [77]
	RNA-seq	TG	Mole	naïve	Female	All	Gerhold *et al.* 2013 [71]
	RNA-seq	DRG	Mole	naïve	Female	All	Gerhold *et al.* 2013 [71]
	RNA-seq	DRG	Rat	injury	Male	Lumbar	Baskozos *et al.* 2019 [73]
	RNA-seq	DRG	Rat	injury	M + F	Lumbar	Stephens *et al.* 2019 [78]
	RNA-seq	DRG	Rat	injury	Male	Lumbar	Yin *et al.* 2019 [79]
	RNA-seq	DRG	Rat	injury	Female	Lumbar	Shin *et al.* 2020 [80]
	RNA-seq	DRG	Rat	injury	Male	Lumbar	Stephens *et al.* 2021 [81]
	*only a subset						
	TRAP-seq	DRG/TG	Mouse	naïve	Mixed	All	Megat *et al.* 2019 [82]
	TRAP-seq	DRG	Mouse	chemo	Mixed	All	Megat *et al.* 2018 [45]
	TRAP-seq	DRG	Mouse	injury	Male	Lumbar	Rozenbaum *et al.* 2018 [83]
	mRNA-seq	DRG/SC	Mouse	injury	Female	Lumbar	Uttam *et al.* 2018 [46]
DNA	snATAC-seq	TG	Human	naïve	M + F	All	Yang *et al.* 2022 [51]
	snATAC-seq	TG	Mouse	naïve	M + F	All	Yang *et al.* 2022 [51]
	ChIP-seq	DRG	Mouse	injury	Male	Lumbar	Palmisano *et al.* 2019 [74]
	ATAC-seq	DRG	Mouse	injury	Male	Lumbar	Palmisano *et al.* 2019 [74]
	ChIP-seq	DRG	Mouse	injury	Male	Lumbar	Manners *et al.* 2016 [84]
	ATAC-seq	DRG	Rat	injury	Male	Lumbar	Stephens *et al.* 2021 [81]
	ChIP-seq	DRG	Rat	chemo	Male	Lumbar	Zheng *et al.* 2019 [5]
	MeDIP-Seq	DRG	Rat	injury	Female	Lumbar	Shin *et al.* 2020 [80]
Protein	LC-MS/MS	Nerve	Human	Injury	Mixed	NA	Oki *et al.* 2012 [85]
	DIA-MS	DRG	Mouse	Injury	Male	Lumbar	Rouwette *et al.* 2015 [86]
	DIA-MS	DRG/SC/SN	Mouse	Injury	Male	Lumbar	Barry *et al.* 2018 [36]
	CoIP + MS	DRG	Mouse	Injury	Male	Lumbar	Sondermann *et al.* 2019 [61]

LC-MS/MS	SN myelin	Mouse	Naive	Male	All	Patzig *et al.* 2011 [87]
LC-MS/MS	SN myelin	Mouse	Neuropathy	NA	All	Siems *et al.* 2020 [88]
CoIP + MS	TG	Mouse	Injury	NA	Lumbar	Avenali *et al.* 2014 [62]
LC-MS/MS	SC/SN	Rat	Naive	NA	NA	Lu *et al.* 2009 [89]

DRG: dorsal root ganglia. TG: trigeminal ganglia. SN: sciatic nerve. SC: spinal cord. ORN: olfactory receptor neurons. RGC: retinal ganglion cells. Mixed: both sexes used, samples combined. M + F: male and female data available separately. LC-MS/MS: liquid chromatography mass spectrometry (MS). DIA-MS: data-independent acquisition-MS. Note: Only a subset of work is summarized in this table, as a substantial about of bulk RNA-seq studies have been performed across relevant conditions.

1.2.2.6 Additional sensory profiling

In addition to general DRG neurons, we have transcriptomic data for a subgroup of colonic sensory neurons in the DRG [64], as well as trigeminal ganglia (TG) [51, 72]. Broadly speaking, these are diverse groups of sensory neurons that share numerous overlapping features. Even so, TG comprise developmentally unique populations that benefit from tailored analyses.

Additional sensory neurons throughout the body can deepen our understanding of naïve and pathological states. Tran *et al.* 2019 have studied retinal ganglion cell response to nerve crush [43], and related subtypes of sensory neurons are seen in the autonomic nervous system (eg. the jugular and nodose ganglia) [90].

1.2.3 Human-mouse comparisons

In a naïve state, clear differences between mouse and human sensory neurons exist [91, 92]. At a subpopulation-level, there is a lack of peptidergic/non-peptidergic distinction in humans, in part due to the increased proportion of *CALCA* and *TRPV1* in human sensory neurons [24, 93]. Human DRG neurons also do not bind IB4, preventing a clear NP subtype assignment by classical definitions used in mice.

The recent addition of human DRG snRNA-seq and spatial-seq data provides more insight. Cluster analyses suggest some mouse NP-designated neurons have human analogues, with the identification of two human DRG subtypes (H10 and H11) expressing itch-related genes similar to the NP groups in mice [25]. Even so, other functionally-relevant transcripts specific to non-peptidergic neurons in mice are more broadly expressed in humans (eg. *PTGER3* and *LPAR3*) [24].

C-LTMRs also show differences between mice and humans. The human equivalent of this population remains elusive, in part due to the lack of *TH* expression in human DRG neurons [24]. Recent snRNA-seq failed to classify a distinct C-LTMR population, and suggests a possible overlap with the H10 cluster. This cluster was previously discussed in the context of non-peptidergic neurons, but *PIEZO2* expression suggests a role in low threshold mechanosensation. Spatial sequencing in human DRGs proposes *GFRA2* as a potential marker of itch and C-LTMR neurons,

due to it's shared enrichment in mouse C-LTMRs [24]. Supporting this, snRNA-seq data from trigeminal sensory neurons find a population of *GFRA2*-expressing human neurons which cluster with mouse trigeminal C-LTMRs [51].

These discrepancies highlight the importance of cross-species validation in clinically-driven work. Animal models remain an important part of translational pain research, but effective use requires species parallels.

1.3 Rodent models of neuropathic pain

A variety of rodent models are used to study the progression and maintenance of neuropathic pain. Each centres around damaging the nervous system to elicit a pain response. This can be achieved through trauma, chemicals, or inflammation, among others.

An assortment of models are summarized in Table 1.2. This list is not comprehensive, as many models can be adapted slightly for specific aims. For example, sciatic nerve (SN) ligations can involve the whole nerve or a single/combination of the three branches. The SN has also been targeted by cuffing, freezing, or transection with/without ligation [94]. A description of the models most relevant to the current thesis are thus described.

Nerve trauma Surgical models of acute nerve trauma can be used to study neuropathic pain. The condition can be reversible depending on the approach. Moreover, these models can provide an internal control with specific injury locations as ipsilateral (injured) versus contralateral (non-injured) limb comparisons are valid.

Frequently, the sciatic nerve is targeted due to its surgical accessibility and hindlimb specificity. This nerve contains a mix of ipsilateral sensory and motor neurons with cell bodies in the lumbar DRG 3-5 (L3-L5) region. With three branches, there are various transection combinations used. Full (complete) transection results in loss of limb function [95]. Partial transections are used to mitigate loss of motor function while permitting the study of injured/intact axons within the same DRG. A common model is the spared nerve injury (SNI) model [95]. SNI relies on the

transection and ligation of the tibial and common peroneal nerves, leaving the sural nerve intact. This results in a mix of injured and intact afferents within DRG. Animals develop a pronounced and long-lasting neuropathic pain phenotype, with less of an inflammatory component than chronic constriction (CCI), and less variability than partial sciatic nerve ligation (PSN).

Full and partial crush models also target the SN, relying on forceps to inflict axon damage. These models leave the epineurium intact, promoting axon regeneration and recovery [96–98]. Other options include spinal cord or spinal nerve injury, as well as trigeminal nerve lesions such as partial infraorbital trigeminal nerve transection (IOT) [99, 100].

Slight variations in pain models, such as which branches are targeted for a partial transection are important considerations. While there is a heterogenous mix of sensory and motor neurons in the peroneal nerve, the sural branch is purely sensory. Recent snRNA-seq has also found large variations in cell-type proportions, such as the domination of fibroblasts over glia in the sural nerve not seen in other sciatic nerve branches [67]. As we continue dissecting the contributions of non-neuronal cells to neuropathic pain states, these differences are likely to contribute to model-specific differences seen throughout the literature.

Diabetic neuropathies Disease states can also result in neuropathic pain, with diabetes being a key example. Many mouse models of diabetes can thus be repurposed to study the effects of diabetic-associated neuropathy and the associated pain. Recent work has centred on high fat diets and genetic models, as streptozotocin (STZ)-induced diabetes has a confounding neurotoxic effect [101].

CIPN Chemotherapy-induced peripheral neuropathy (CIPN) can also be used to study neuropathic pain. Clinically, these models are highly relevant as the administration of human chemotherapy drugs can cause nerve damage in both humans and rodents [102].

HIV-related neuropathies Human immunodeficiency viruses (HIV) can cause neuropathic pain in humans. There are multiple mouse models to study this effect, including the use of transgenics or retroviral treatment protocols [103–105].

Table 1.2: Rodent models of neuropathic pain.

Model	Technique	Location	Recovery	Reference
SNL	Spinal nerve ligation	L5 + L6	Yes	Kim *et al.* 1992 [106, 107]
SNT	Spinal nerve transection	L4 + L5	No	Sweitzer *et al.* 1999 [108]
CCI	Nerve ligation	SN	No	Bennett *et al.* 1988 [109]
PSL	Nerve ligation	SN	No	Seltzer *et al.* 1990 [110]
Sciatic NT	Nerve transection	SN	No	Wall *et al.* 1979 [111]
Full crush	Nerve crush	SN	Yes	Vogelaar *et al.* 2004 [96]
Partial crush	Nerve crush	SN	Yes	Davies *et al.* 2019 [98]
SNI	Sural + common peroneal ligation & transection	SN	No	Decosterd *et al.* 2000 [95]
IOT	Nerve transection	TGN	No	Hardt *et al.* 2019 [100]
Auto-antibody	Antibody-induced neuropathy (ie. human plasma injection)	Systemic	N/A*	Dawes *et al.* 2018 [112]
Bone cancer	Inoculation of cancerous cells	Various	No	Schwei *et al.* 1999 [113]
Chemotherapy	Drug administration causing peripheral neuropathy (ie. Cisplatin, Paclitaxel)	Systemic	Yes	Hoke *et al.* 2014 [102]
Diabetes	Strepozotocin administration	Systemic	No	Ali *et al.* 2015 [114]
Diabetes	Tg animals (ob/ob, Akita)	Systemic	No	OBrien *et al.* 2014 [115]
HIV-related	Anti-retroviral drugs	Systemic	No	Burdo *et al.* 2014 [103]
HIV-related	Tg animals (ie. gp120)	Systemic	No	Herzberg *et al.* 2001 [104, 105]

Abbreviations: CCI, chronic constriction injury; SNT, spinal nerve transection; PSL, partial sciatic nerve ligation; NT, nerve transection; SNI, spare nerve injury; SNL, spinal nerve ligation; IOT, partial infraorbital trigeminal nerve transection; Tg, transgenic; GBS, Guillaine-Barré syndrome. *Experiments not performed (personal correspondence, John Dawes).

1.4 Functional assessments of neuropathic pain

1.4.1 Behavioural assays

Various behavioural tests have been developed to quantify pain responses in rodents. Paradigms predominantly focus on allodynia (pain to an innocuous stimulus) and hyperalgesia (exaggerated pain response to a noxious stimulus). Hyposensitivity resulting from nerve damage can also be examined. Typically, assays measure withdrawal thresholds (such as von Frey or dynamic brush) or response latencies (hot/cold plates, dry ice, acetone) [95, 116, 117]. Thermal preferences can be monitored using thermal gradient assays.

Nerve damage can also affect the neuromuscular system, thus many experimenters also examine motor function (rotarod, beam walking, grip strength, etc.) to eliminate this confound.

Spontaneous pain assays Patients frequently experience debilitating spontaneous pain. In rodents, numerous assays have been used to assess this prominent disease phenotype. Overt spontaneous nocifensive behavior such as licking, biting, vocalization, facial grimace scoring, or paw-lifting can be characterized over time. Burrowing behaviour can be reduced in experimental cohorts, and researchers may infer an underlying pain experience as a root cause. These measures are likely indicative of extreme pain as many animals are known to minimize visible weaknesses.

Conditioned place preference (CPP) is an alternative way to measuring ongoing pain in rodents. As the name intuitively suggests, this assay depends on animals developing a conditioned preference within an experimental apparatus. Briefly, animals are placed in a dual-chamber setting with each chamber having distinct visual and olfactory cues. After initial baseline exploration, animals are injected with a non-addictive analgesic in one chamber and a saline control in the other. Interestingly, naïve animals do not developed a preference following analgesia, but neuropathic pain cohorts do. This suggests that analgesia has a positive effect in these animals (ie. treatment of ongoing pain) [118].

1.4.2 Primary afferent electrophysiology

Hyperexcitability is a key feature of neuropathic pain. Fortunately, this can be studied through electrical recordings at various levels. *In vivo* and *ex vivo* preparations have provided invaluable insights to sensory neuron function.

For example, skin-nerve recordings are a useful way to examine first-order sensory neurons. Typically, one dissects the hind paw hairy skin and saphenous nerve for *in vitro* recordings. With receptive fields attached, various stimulus responses can be studied, and by teasing the nerve apart, it is possible to perform single fibre recordings. Fibres can then be classified into distinct subpopulations based on a myriad of electrical properties [119]. This is commonly performed on rodents but skin nerve recordings have also been done on non-human primates [120].

DRG neurons are commonly cultured into a monolayer for single cell recordings. Changes in rheobase and altered channel conductance's have been shown to relate to painful phenotypes. Moreover, some cells exhibit low levels of spontaneous action potential generation [121]. This is considered a correlate of spontaneous pain, although direct causation remain undocumented [122–124].

While the focus of the current thesis is on primary afferents, it is important to note that higher order recordings, such as those in the dorsal horn slices, offer additional, invaluable insight to pain mechanisms.

1.4.3 Calcium imaging

Changes in cell excitability can be measured through calcium indicators. Depending on the setup, both chemical (eg. Fura-2) and biological indicators (eg. GCaMP) can be used to measure calcium influxes *in vivo* or *in vitro*. Changes in calcium levels provide an indirect overview of a cell's activity but allow for high throughput screening generally not available with electrophysiology.

1.5 Mechanisms of neuropathic pain

The sensitization of both peripheral and central components is thought to contribute to the chronicity of neuropathic pain [125, 126].

1.5.1 Spontaneous activity

Spontaneous pain is a major clinical complaint. This refers to pain without a clear stimulus, and is typically described as a shooting or burning sensation. It is hypothesized that increased firing of nociceptors results in heightened pain perception, and that ongoing activity of these fibres can result in the maintenance of a spontaneous pain percept in patients [124, 127].

Spontaneous activity (SA) refers to the presence of action potential(s) in the absence of stimuli. In the context of pain, spontaneous activity commonly refers to aberrant, non-evoked action potentials in primary afferents [124, 128]. This differs from allodynia and hyperalgesia as there is no evident trigger. Instead, the activity originates from within the nervous system, likely due to changes in ion channel functions, concentrations, and/or distributions. Changes in higher order circuitry - referred to broadly as central sensitization, can also contribute [2, 125]. SA has been correlated to pain phenotypes in various studies [27, 122, 123].

SA in high threshold C-fibres, as measured through human microneurography, has been related to spontaneous pain [122]. In patients, SA has been related to the incidence of spontaneous pain, but not to pain ratings [123]. Additionally, individuals' DRG transcriptomes have been correlated to spontaneous ectopic activity and neuropathic pain phenotypes [27]. One notable study using non-human primates looked at SA after spinal nerve ligation [120]. Using a macaque skin-nerve preparation, Ali and colleagues found aberrant, spontaneous activity in the adjacent uninjured C-fibres.

The use of local anesthetics has proven effective in minimizing spontaneous pain in humans, supporting the importance of primary afferents [127]. Unfortunately the lack of specificity to nociceptors limits therapeutic use. A thorough understanding of the molecular changes which lead to neuropathic pain will support the development of novel therapeutics.

1.5.2 Sensitization

A spectrum of sensitization processes in the peripheral and central nervous systems result in an increase responsiveness to noxious input (hyperlgesia) and/or a "pain-like" response to normally innocuous stimuli (allodynia). This helps limit further tissue damage in acute states, but is problematic in chronic conditions. To contextualize: reducing skin contact after a recent burn injury can be protective, but allodynia is maladaptive when the brush of clothing is painful for migraineurs.

Hyperalgesic priming One mechanism of sensitization is hyperalgesic priming. This refers to the plastic response of neurons through mechanisms like long-term potentiation (LTP) to increase the responsiveness pain pathways after an initial injury, pharmacological treatment, or through disease states [129–131]. It can occur either in primary afferents (eg. nociceptor priming), or more centrally, resulting in heightened responsiveness to noxious stimuli [132, 133].

Higher order circuitry For pain arising in the periphery, it is worth reiterating that primary afferents do not function in a vacuum. There is complex circuitry within the dorsal horn, as well as ascending and descending pathways which undergo changes in neuropathic states. The sensitization of these processes in pain states are broadly referred to as "central sensitization", a general term encompassing changes in neuronal plasticity, network excitability, and top-down modulation. Ultimately, this acts to amplify nociceptive processing and pain perception.

Immune response Moreover, neurons do not work in isolation. The interaction between neurons, glia, and immune cells contributes to pain states, and play a prominent role in the pathophysiology of neuropathic pain [134]. Immune cells infiltrate the injury site, DRG, and dorsal horn with varying effects. The release of immune factors sensitizes primary affects, and molecular changes within sensory neurons after injury contribute to modified interactions. Axon/myelin degeneration after injury is also inherently dependent on immune cells, and monocytes have been implicated in pain readouts after chemotherapy-induced neuropathic pain [135].

DRG macrophages affect both the initiation and maintenance of neuropathic pain [37, 136], and can alter hypersensitivity in neuropathic pain states in the spinal cord[137]. Recent work also suggests the transfer of mitochondria from macrophages into DRG neurons in inflammatory pain models [138]. Here, this transfer is shown to promote recovery from mechanical hypersensitivity, possibly by offsetting metabolic changes initiated through injury. With changes in metabolic activity seen across neuropathic pain conditions as well, it remains to be seen whether a similar mechanism for mitochondrial homeostatis exists here.

1.5.3 Subpopulation-specific mechanisms

Both high- and low- threshold receptors are involved in neuropathic pain. Evidence suggests that ectopic activity begins in Aβ fibres. As the condition progresses, SA in reduced in large diameter fibres and heightened in nociceptive C-fibres [139, 140]. Changes in receptor expression/localization, neuro-immuno interactions, and network changes are all thought to contribute to the sensitization and aberrant activity across subtypes.

In rodents, subpopulation roles have been extracted through a mix of pharmacological and genetic approaches. Ablation studies have been instrumental to our understanding of specific subpopulation contributions. The over-expression of the Diphtheria toxin receptor (DTR) combined with administration of this toxin (diphtheria toxin, DTX) allows researchers to specifically ablate subpopulations of interest. DTX-ablation of *Nav1.8* expressing cells (primarily nociceptors) suggests that this population is involved in acute and inflammatory pain, but plays a less prominent role in evoked pain during neuropathic conditions [141]. The role of this population in spontaneous, neuropathic pain remains unclear. Mrgprd$^{\text{creERT2}}$ ablation affects baseline levels of noxious mechanical sensitivity, but does not show a clear interaction with temperature or inflammatory pain [142], while subgroups of peptidergic nociceptors play a role in thermal pain [143]. Moreover, these peptidergic and non-peptidergic populations appear to play unique roles in the development of thermal and mechanical hyperalgesia in mice [142, 143], and differences in

hyperalgesic priming have been reported between subtypes [129]. It is unclear how this translates to humans as there does not exist a clear delineation between these subtypes [24, 93].

Aδ- and Aβ-LMTRs can be targeting in mice using an Ntrk2$^{\text{creERT2}}$ line. Ablation of this population reduces the expected mechanical hypersensitivity phenotype in neuropathic pain models of male mice [21] and provides strong evidence that low threshold mechanoreceptors play a prominent role in neuropathic pain.

1.5.4 Sexual dimorphism in pain

Understanding sexual dimorphism in pain states is a fundamental clinical issue. Females are much more likely to be living with chronic pain, and treatment efficacy can be sex-dependant [144, 145].

The case for studying sexual dimorphism is not new [146, 147], but systemic sexism in the research community has slowed progress. Fundamental preclinical work in neuroscience centres on male animal models. With such a strong baseline data on male subjects, the bias continues to be seen [145, 148–150]. This is due to a combination of convention, following historic protocols, and the reduced power (and added financial cost) of including sex as a factor.

More recent female-inclusive studies have revealed clear mechanistic differences between sexes at the immune and nervous system level. Sensitization, as a mechanism of neuropathic and inflammatory pain, is inherently sexually dimorphic. Within this, hyperalgesic priming has been discussed in the context of sensitization in the periphery [151, 152] as well as sex-specific responses in the basolateral amygdala [153].

Gonadal hormones play a diverse role in in acute and chronic pain. In rats, testosterone levels during development were shown to affect morphine-induced hyperalgesia later in life [154]. Prolactin has been implicated in sensitization of female, but not male sensory neurons [151, 152, 155], as well as migraine, an inherently sexually dimorphic pain condition [156, 157]. It has been shown to regulate various pain-implicated ion channels in a sex-dependent way, including

TRPV1 [158, 159], ASICS [160], and TRPM8 [159]. Furthermore, oestrogen has been implicated in a range of pain conditions through direct modulation of sensory neurons and immune interactions [161–163].

CGRP, in addition to being a classic marker of peptidergic nociceptors, plays a sexually dimorphic role in pain pathology [164], and human peptidergic nociceptors show differences in *Calca* expression across sexes [24].

Brain derived neurotrphic factor (BDNF) is also frequently discussed in the context of sexual dimorphism. In mammary glands, testosterone expression alters sensory neuron development via BDNF-TRKB [165]. Centrally, sex differences in dorsal horn hyperexcitability are driven by BDNF mediated N-methyl-D-aspartate receptor (NMDAR) potentiation in both rat and human [166].

Together, there is clear evidence for central and peripheral mechanisms in pain-relevant sexual dimorphism across species. The sensitization of primary afferents and higher order circuitry in a sex-dependant manner supports further interrogation of the underlying mechanisms.

1.6 Aims

Neuropathic pain is a widespread issue and the underlying mechanisms remain unclear. My thesis explores the underlying molecular mechanisms within the DRG subpopulations in a murine model of neuropathic pain. We set out to develop a resource for the pain community to probe subpopulation and sex-specific differences after nerve injury at multiple timepoints.

The availability of subtype-specific transgenics allows us to label and isolate numerous subpopulations of interest. We purified each cell type after injury via fluorescent activated cell sorting (FACS) for subsequent transcriptomic analysis. Using bulk tissue samples, we are able to circumvent the issues of low transcript coverage and drop-outs seen with single cell datasets, increasing our power to detect differentially expressed genes (DEGs) and explore the interaction of sex at a subtype-level.

We hypothesize this will reveal distinct patterns of differential gene expression in primary afferent subtypes after injury, and that there will be sex differences in both the control and injured samples. The intersection of sex and injury across subpopulations will also be explored openly.

2

DRG transgenics and subtype isolation

Our current understanding of neuronal subpopulation contributions to nociception and pathological pain is incomplete. To study these populations in depth, we must first appropriately target the populations of interest. Here, we set out to isolate live, bulk neuronal subpopulations for downstream sequencing. We successfully characterized 5 populations involved in acute nociception and/or chronic pain states through available transgenics using a combination of Cre-based and intersectional approaches. These include: general nociceptors (*Scn10a*), peptidergic nociceptors (*Calca*), non-peptidergic nociceptors (*Mrgprd*), C-LTMRs (*Th*), and Aβ-RA + Aδ-LTMRs (*Ntrk2*). In parallel, we characterized injured afferents after spared nerve injury, based on *Atf3*-driven tdTomato expression via Atf3$^{\text{creERT2}}$. For each population, neurons were then purified by magnetic and fluorescence sorting (MACS and FACS) for downstream analyses.

Contents

2.1 Introduction

2.1.1 Subpopulation targeting methodology

DRGs are extremely heterogeneous in nature, containing a plethora of neurons, glia, and immune cells. There are various ways to study this diverse tissue, from basic dissociation and single cell analysis to transgenic targeting of specific subpopulations. The targeting method will strongly depend on the requirements of the research question (i.e. functional modulation, live cells, labelling, etc.).

2.1.1.1 Cell sorting

To study cell subpopulation with techniques such as RNA-seq, cells are first dissociated and sorted into single cell or pure, multi-cell samples. There are

various tools for purifying cell populations available, with the most applicable to DRG sorting described here.

MACS Magnetic-activated cell sorting (MACS) exploits the use of surface antigen targeting and strong magnets to purify samples. Biotin conjugated cell-type specific antibodies are added to dissociated cells, followed by biotin-coated magnetic beads. Through secondary binding, the targeted cell type(s) will bind to these microbeads. This solution is fed through a column in a strong magnetic field. Both the non-binding flow-through and binding samples can be isolated for further analysis. Technically, MACS columns are recommended for cells <30 μm as larger cells can become trapped in the column. This size constraint is relevant when studying murine sensory neurons.

Flow cytometry and FACS Flow cytometry uses scattered light to characterize the physical parameters of single cells (or nuclei/particles). Adding a fluorescence-conjugated antibody or other fluorescent tag, you can obtain further information about cell identity. In addition to cell profiling, fluorescence-activated cell sorting (FACS) allows you to isolate and sort cells based on these modalities. This method relies on the addition of charged particles to droplets containing individual cells. These droplets are then deflected by charged plates into a collection tube/plate of interest. Numerous subpopulations can be detected concurrently, limited by sorter capabilities (primarily laser combinations) and surface antigen/labelling limitations.

2.1.1.2 Transgenic targeting

Advances in murine transgenics has drastically improved our ability to target specific cell populations. There are a variety of ways this has been achieved, including the use of congenic reporters and various recombination systems. These methods allows the insertion and expression of unique genes of interest - including fluorescent and/or functional reporters, systemically or in a cell-type specific fashion.

Congenic reporters Cell populations are commonly defined by transcript expression patterns. To express a reporter in a cell-type specific manner, sequences can be inserted under the control of an endogenous promoter unique to the cell-type of interest. Here, these are referred to as congenic reporters. For example, Thy1-GFP mice express green fluorescent protein (GFP) in a subset of peripheral and central neurons, including cells in the dorsal root ganglia, based on Thy1 expression. These mice provide a simple, effective way of targeting populations of interest.

Cre-based recombination Transgenic population targeting can also be achieved through site-specific recombination (SSR). The most common system for this is the Cre-lox system, first exploited for murine transgenics in the 1980s. This system replies on Cre recombinase - a bacteriophage-derived tyrosine recombinase - to target flanked DNA sequences in a two step process. First, Cre is expressed under the control of a promoter sequence. Second, Cre targets specific paired loxP sequence sites, excising the flanked sequence. Recombinase expression can be driven by a variety of enhancer sequences to excise a wide range of sequences. Commonly, this can be used for the expression of reporters in a cell-type specific manner.

Modified versions of Cre recombinase allow for temporal control of gene expression. A prominent example is the fusion of an estrogen receptor to the recombinase, forming a Cre-ER fusion protein. Here, Cre is fused to a modified estrogen receptor (ER) which binds tamoxifen (an estrogen analog) but not estrogen. In a naïve state, Cre-ER is sequestered to the cytoplasm through association with the heat shock protein HSP90 where it is unable to bind loxP sites. In the presence of tamoxifen, Cre-ER can dissociate from HSP90, translocate to the nucleus, and promote recombination. Tamoxifen is a widely available drug administered embryonically or post-natally to target specific windows of gene expression. Additional inducible systems include the use of tetracycline [167], the progesterone analog RU-486 [168], and antibiotic-dependent recombination with trimethoprim [169]. In each case, drug administration promotes site-specific recombination.

In addition to Cre recombinase, bacteria have inspired other recombination systems. D6 recombination system (Dre-rox) and Vika/*vox* are other tyrosine recombinases that have been used to modify the murine genome. Dre targets 'rox' sites, Vika 'vox' sites, and do not overlap with Cre-based specificity while acting in a similar manner. Like Cre, there are inducible variants available.

Serine integrases such as ϕC31 have also been implemented for murine SSR. Serine integrases depend on two DNA sites - *att*B and *att*P, which recombine into two unique sites, *att*L and *att*R. These novel sites are no longer detected by the integrase, allowing for unidirectional recombination not available with tyrosine recombinase-based systems.

Flp-based recombination Flp-FRT recombination is an alternative, analogous approach to bacteriophage-inspired SSR. This system relies on frt site recombination in the presence of flippase (Flp), originating from *Saccharomyces cerevisiae*. This yeast-derived enzyme has since been modified for use in mice (FlpO) to increase recombination efficiency towards that of Cre. A conditional FlpO variant has also been developed [170].

Intersectional transgenics The development of SSR techniques such as Flp-frt and Cre-lox has revolutionized our ability to target specific cell populations. Combining these systems can add an additional level of depth. For example, some reporters are dependant on multiple drivers (frequently Cre + Flp/Dre), allowing researchers to target the intersection of two drivers. These dual-recombinase systems are particularly useful when narrowing focus to a smaller subpopulation or when the use of a single driver results in off-target effects.

The flexibility of a recombination-based system provides a convenience not available with congenic reporters, especially when working with multiple subpopulations and multiple reporter-types. SSR-drivers can be bred to any reporter animal, reducing the overall number of stocks requiring purchasing/maintenance. Furthermore, the added benefit of inducible recombination allows us to target subpopulations otherwise unavailable through a basic promoter-reporter system.

In each case, the genetic strategy may itself produce confound, such as a toxicity of exogenous lacZ reporter enzymes in primary afferent terminals [171]. Unlike congenic reporters, recombination-based systems also have an inherent risk of 'leakiness', where recombination occurs in the absence of Cre, or Cre-induction. The rate at which this happens depends on the genetic strategy, thus characterization of each line is pertinent.

2.1.2 Populations of interest

The functionality of sensory neuron populations have been studied through a variety of loss-of-function (LOF) and gain-of-function (GOF) studies. Commonly, this involves targeted ablation/silencing or activation through genetic/chemical approaches. For the current study, our primary interest is narrowed to populations which can be targeted through SSR and play a role in painful conditions (acute or neuropathic).

2.1.2.1 Nav1.8

Nociceptors are commonly targeted through the *Scn10a* promoter [9]. *Scn10a* encodes Nav1.8, a tetrodotoxin-insensitive sodium channel widely expressed in sensory neurons. Commonly, Nav1.8 expression is discussed in the context of nociceptors. Single cell sequencing in adult mice data suggests the expression is not exclusive to C-fibres, with low levels of *Scn10a* in neurofilament-positive A-fibres. This overlap with non-nociceptive sensory neurons has also been documented in a non-inducible Cre line by immunohistochemistry, suggesting that transgenic targeting of a *Scn10a* population marks nociceptors as well as C- and Aβ-LTMRs [172].This is a broad subclass of DRG neurons that can be further subdivided including peptidergic/non-peptidergic nociceptors and C-LTMRs.

Ablation of this population in mice results in pronounced hyposenstivity to mechanical pain with no noticeable effects on light touch or motor skills [141]. Moreover, evidence suggests a more prominent role in inflammatory than neuropathic

pain in mice [141]. Given the diversity of this population, additional transgenics can be used to understand more specific subpopulation roles within the DRG.

2.1.2.2 CGRP

Peptidergic nociceptors (PEP) are defined by GCRP expression in mice, encoded by *Calca*. This population is historically considered analogous to *Ntrk1* (TRKA) nociceptors [173]. More recent single cell sequencing suggests this grouping is reasonably accurate, although *Ntrk1* and *Calca* can also be detected in low levels throughout C-fibre populations, including both non-peptidergic and C-LTMR [22].

CGRP expression denotes a broad grouping of small- to large- diameter neurons encompassing multiple functional facets. A subset of these neurons are myelinated. Genetic ablation using a CGRPα-DTR knockin enhances cold responsiveness while reducing heat sensitivity [143]. This mirrors the expression of heat-sensitive channel TRPV1, which is predominantly expressed in peptidergic neurons throughout adulthood. Additionally, CGRP+ nociceptors also include silent nociceptors and a subpopulation of myelinated Aδ fibres, predominantly involved in mechanical pain [11, 174].

Calca$^{\text{creERT2}}$ has been previously characterized, showing strong overlap with CGRP and TRKA antibody staining as expected [175]. A subset of these neurons stains weakly for isolectin B4 (IB4), a marker commonly associated with non-peptidergic (NP) neurons [175].

2.1.2.3 MRGPRD

NP C-fibres are defined by MRGPRD (encoded by *Mrgprd*), P2X3 (*P2rx3*), or the lack of CGRP expression in mice [10]. These neurons are largely described for their role in mechanical and chemical pain in naïve states. Neuronal ablation affects inflammatory but not neuropathic pain readouts in mice [142].

In rats, IB4+ ablation through Saporin toxin results in thermal and mechanical hyposensitivity [176], blurring the clear delineations between thermal/mechanical processing in peptidergic/non-peptidergic populations. With nociceptor subgroups, species conceptualization is important: peptidergic/non-peptidergic definitions don't

always hold true. In rats, there is more overlap between IB4+ and CGRP+ neurons [177]. This mirrors human DRGs, with clear overlap between P2RX3 and CGRP in over 40% human DRG neurons (compared to 15% overlap in mice) [93].

2.1.2.4 TH

In humans, C-LTMRs are involved in affective touch, playing a role in social bonding and pain relief [178]. In both humans and mice, this population responds to low threshold stimuli and cool detection. Von Frey assays suggest an additional role for mouse C-LTMRs in mechanical pain but rodent affective touch assays are lacking [179].

C-LTMRs can be targeted through various markers in mice, including TH, VGLUT3, TAFA4, and a subset of GINIP expressing (IB4-) neurons [180–182]. Comprising around 10% DRG neurons, this population projects to lamina II_i of the dorsal horn. Here, neurons synapse on both excitatory and inhibitory interneuron subpopulations [19, 183].

Due to the availability and previous classification of murine C-LTMRs through $Th^{tm1.1(cre/ERT2)Ddg}$/J in our lab, this transgenic approach was used for the current project [20, 179]. Moreover, characterizations using VGLUT3 targeting are difficult to interpret as more recent evidence suggests this marker is not unique to C-LTMRs, instead labelling additional neuronal populations in the dorsal horn [180, 184].

A subpopulation of TH+ neurons also overlap with TRKC (*Ntrk3*), in a population recently implicating in blood pressure regulation [185].

2.1.2.5 TRKB

$Ntrk2^{creERT2}$ provides an avenue to target Aδ- and Aβ-RA-LMTRs. These neurons terminate with lanceolate endings or as Meissner's corpuscles, playing a role in light touch sensation [186]. These myelinated neurons have been previously implicated in mechanical hypersensitivity following nerve injury [21]. This is an interesting example of a low threshold population contributing to pain states.

Recently published staining hints that TRKB expression isn't limited to sensory neurons, instead innervating satellite glia and Schwann cells across Cre lines [5, 21,

77]. This was further documented using a Dhh^{cre} to target TRKB specifically in Schwann cells [186]. Because of this, both a direct targeting and an intersectional transgenic approach were used, as outlined in the methodology.

2.1.3 Actively omitted populations

In addition to the transgenics described above, numerous targeting options are available but were consciously omitted from the current study.

Advillin Advillin^{cre} is a common marker of all sensory neurons in the DRG. Given the diversity already provided by the Scn10a^{cre}, as well as previously published whole DRG datasets, we omitted this generic driver to prioritize more specific populations. Moreover, we are focused on subpopulations with known roles in nociception (acute or chronic), thus the addition of low threshold fibres not covered by Scn10a^{cre} were not a priority. This marker still remains useful: I use an Advillin^{flp} driver in parallel with Ntrk2^{creERT2} to label TRKB neurons, specifically, circumventing the non-neuronal TRKB-expressing cells in the DRG.

Cav3.2 Cav3.2^{cre} labels both low threshold Aδ fibres and C-LTMRs [17]. C-LTMRs are readily targeted through Th^{creERT2}, and D-hair targeting requires a unique intersectional transgenic approach. We are primarily interested in sequencing these populations independently, thus the overlap provided by *Cav3.2* was unnecessary.

GINIP *Ginip* is expressed in a subpopulation of C-fibres. These populations can be targeted uniquely through other available transgenics (Th^{creERT2} and Mrgprd^{creERT2}) thus like *Cav3.2*, this line was not pursued.

NPY2R Neuropeptide Y receptor-2-expressing (NPY2R) labelling through Npy2r^{cre} marks a subpopulation of myelinated Aδ fibres [174]. This marker does not appear specific to the myelinated nociceptor population, as it overlaps with small populations of Calbindin and TRKB neurons (RA-LTMR and D-hairs). Positive

neurons primarily terminate as free nerve endings in hairy and glabrous skin, but few labelled lanceolate endings are also reported [19, 174]. Single cell sequencing suggests a unique group of non-peptidergic, unmyelinated C-fibres strongly express NPY2R, although this was not seen with Cre-driven expression [22, 174]. We hope to develop an S100B^{flp} in the future to allow an intersectional targeting approach for all Aδ nociceptors, negating the need for Npy2r^{cre}. Npy2r^{cre} was omitted from the current study in anticipation of that transgenic.

TRKA TRKA, encoded by *Ntrk1* is expressed in small diameter neurons. Expression is predominantly in peptidergic nociceptors but overlaps with the non-peptidergic population, as discussed above. A congenic Ntrk1-FLAG line and Ntrk1^{cre} are available, but this population is encompassed by the well characterized Calca^{creERT2} and Mrgprd^{creERT2} [187].

TRPV1 The capscaicin-sensitive channel TRPV1 is expressed developmentally throughout nociceptor populations. In adulthood, expression is largely restricted to peptidergic neurons, with further overlap to non-peptidergic nociceptors. Research suggests that approximately 25% of TRPV1+ neurons do not overlap with CGRP expression [175]. Trpv1^{cre} options are readily available, but not sufficiently unique from other lines to warrant addition to our study design.

2.1.4 Aims

Here we aim to characterize various transgenic lines in naïve conditions through immunohisotochemistry and cell sorting. This will provide a platform for downstream RNA-seq experiments examining subpopulation-specific changes after nerve injury.

2.2 Methodology

2.2.1 Animals

All work was done in accordance with the UK Home Office and the University of Oxford Policy on the Use of Animals in Scientific Research. This study conforms

to ARRIVE guidelines.

Animals were housed in standard conditions on a 12-hour light/dark cycle with food and water *ad libitum*. All animals were randomly assigned to experimental groups where applicable. Internal controls were used when not possible to randomize (ie. ipsilateral vs contralateral comparisons). Unless explicitly stated, all experiments were performed on both males and females. Adulthood refers to $\geq$8 weeks of age. Briefly, driver lines were bred with a fluorescence reporter for various experiments. When necessary, inducible lines were dosed with intraperitoneal (i.p.) injection(s) of tamoxifen. Specific details below.

2.2.1.1 Transgenic details

C57BL/6 mice were purchased from the Oxford University Breeding Unit. Cre driver lines used include: Calca$^{\text{tm1.1(cre/ERT2)Ptch}}$ (CGRP, gifted from Prof. Pao-Tien Chaung) [188], Mrgprd$^{\text{tm1.1(cre/ERT2)Wql/J}}$ (MRGPRD, JAX 031286) [189], Scn10a$^{\text{tm2(cre)Jnw}}$ (Nav1.8, gifted from Prof. John Wood) [190], Th $^{\text{tm1.1(cre/ERT2)Ddg}}$/J (TH, gifted from Prof. David Ginty) [20], Ntrk2$^{\text{tm1.1(cre/ERT2)Ddg}}$/J (TRKB, gifted from Prof. Paul Heppenstall) [21]. Cre-driver lines were bred and maintained as heterozygotes, except for Th$^{\text{creERT2}}$, which was bred as homozygous. Details are listed in Table 2A.1.

The following reporters were used to visualize DRG subpopulations: B6.129S-Gt(ROSA)26Sor$^{\text{tm32(CAG-COP4*H134R/EYFP)Hze}}$/J (JAX 012569, gifted from Prof. Simon Butt), tdTomato B6.Cg-Gt(ROSA)26Sor$^{\text{tm14(CAG-tdTomato)Hze}}$/J (JAX 007914) and ai80D B6.Cg-Gt(ROSA)26Sor$^{\text{tm80.1(CAG-COP4*L132C/EYFP)Hze}}$/J, (JAX 025109). Ai32 and ai14 use was based on initial breeding availability. Ai80 depends on both Flp- and Cre-recombinase for intersectional targeting, and was used for neuronal targeting of *Ntrk2*. Ai80 was first crossed to an Advillin$^{\text{flpO}}$ (unpublished, gifted from Prof. David Ginty). Reporters were bred as homozygotes where applicable. Advillin$^{\text{flpO}}$ was bred to a C57BL/6 background for at least 7 generations prior to experimental use.

Atf3$^{<tm1.1(cre/ERT2)Msra}$ mice were gifted from Prof. Stephen McMahon (Kings College London). This inducible Cre line was first described by Denk and colleagues [191]. This line depends on *Atf3* upregulation after injury to trigger recombination. Notably, tamoxifen dosing is not commonly used, even though the line is inducible. Instead, the high expression of *Atf3* after injury appears sufficient to override the inducible promoter and trigger recombination in injured cells [192]. This has been repeated in multiple labs (personal correspondence Dr. Greg Weir, Prof. Stephen McMahon). The mechanism of recombination has not yet been described, although unpublished data suggests small doses of tamoxifen can increase the recombination efficiency (Dr. Greg Weir, Dr. Matt Ramer).

2.2.2 Spared nerve injury

Adult mice were anesthetized with 2% inhaled isoflurane. Using sterile technique (including incision site sterilization and surgical drapes), the sciatic nerve was exposed prior to ligation and transection of the tibial and common peroneal branches. The sural nerve was left intact. Each animal was dosed with systemic (5 mg/kg Rimadyl, Pfizer) and local (2 mg/kg Marcain, AstraZeneca) postoperative analgesia. Animals were monitored daily for self-mutilation, and no animals required sacrifice due to tissue damage.

2.2.2.1 Tamoxifen regimes

Tamoxifen (Sigma-Aldrich) was dissolved 20 mg/ml in corn oil via sonification. All animals were dosed i.p. and health statuses were monitored daily for the duration of the dosing regime. Calca^{creERT2} were dosed 5x (daily) with 75 mg/kg in adulthood. Mrgprd^{creERT2} were dosed 5x i.p. (0.5 mg/animal/day), beginning between P10-P17. Body weight recovered more quickly when dosed at later stages, with no noticeable difference in reporter expression. We recommend dosing begin at P17 for this line moving forward. Th^{creERT2} were dosed 1x with 50 mg/kg above 6 weeks of age. Ntrk2^{creERT2} were dosed 5x (daily) with 75 mg/kg in adulthood. Notably,

dosing for Ntrk2^{creERT2} required optimization, and is discussed below. A subset of Atf3^{creERT2} mice were dosed at 7.5 mg/kg.

2.2.3 IHC

Adult animals were overdosed with pentobarbital and perfused transcardially with sterile saline followed by 4% paraformaldehyde. Tissue was removed and post-fixed prior to subsequent dehydration in 30% sucrose (0.1M PB) at 4°C for a minimum of 48 hours. Samples were then embedded in OCT medium (Tissue-Tek), sectioned, and stored at -80°C. Neuronal profiles were quantified across multiple sections per animal, opposed to more detailed stereology, and are presented as estimates. A detailed list of all antibodies can be found in appendix table 2A.2. In addition to subpopulation markers such as TH (C-LTMRs), CGRP (peptidergic) and parvalbumin (PV, proprioceptors), non-peptidergic neurons bind isolectin B4 (IB4) from *Griffonia simplicifolia*. Neurofilament heavy chain (NF200) labels large diameter neurons in mice, and NeuN (or FOX3) is a general neuronal marker. Glutamine synthetase is a satellite glial cell (SGC) marker.

2.2.4 DRG culturing

Adult mice were sacrificed by rising levels of CO_2. The spinal column was removed and placed in ice cold HBSS (Ca2+/Mg2+ free, Invitrogen). All DRGs were dissected into HBSS, unless otherwise noted. For paired experiments, DRGs were divided as left/right. Ganglia were digested for 90 min at 37°C (5% CO_2) using Collagenase II (4 mg/ml, Worthington)/Dispase II (4.7 mg/ml, Roche) in HBSS. Cells were subsequently mechanically dissociated with polished glass pipettes. When stated, debris was reduced using a 15% w/v BSA cushion. Once pelleted, cells were resuspended in Neurobasal medium supplemented with B27 (2% v/v, Gibco), Glutamax (1% v/v, Gibco), mouse NGF (50 ng/ml, PeproTech) and GDNF (10 ng/ml, PeproTech) for culturing. For magnetic cell sorting, samples were instead resuspended in ice cold 0.5% BSA/dPBS.

2.2.5 Magnetic-activated cell sorting (MACS)

After mechanical dissociation, cells were resuspended in 80 µl ice-cold 0.5% BSA/dPBS prior to the addition of 20 µl non-neuronal biotin antibody cocktail (Miltenyi Biotec, 130-115-390) for magnetic purification of sensory neurons. After a 5 min incubation at 4°C, suspension was topped up to 500 µl BSA/PBS and spun down. Cells were again resuspended 80 µl 0.5% BSA/dPBS prior to the addition of 20 µl biotin microbeads. After a 10 min incubation (4°C), suspension was topped up to 500 µl BSA/PBS and loaded into pre-primed MACS separation LD columns. Columns were washed 2x with to increase yield. Negative fractions were spun down (1000 RPM, 5 min) and resuspended in supplemented culture medium. Cells were plated on poly-d-lysine/laminin coated coverslips and maintained at 37°C (5% CO2).

2.2.6 Fluorescence-activated cell sorting (FACS)

After mechanical dissociation (or MACS), cells were fluorescently sorted using a Sony SH800/Sony MA900 or BD FACSAria Fusion 1/2 into culture media or applicable lysis buffer (for RNA work, see chapter 3, chapter 4 and chapter 5). Cells were first gated on forward- and side-scatter. DAPI was added to gate live/dead cells. Wildtype littermates were used as negative controls during protocol optimization for each subpopulation to confirm gating.

2.3 Results

2.3.1 Characterization

2.3.1.1 Nav1.8

Scn10a encodes Nav1.8, a voltage-gated sodium channel widely implicated in nociception and clinically-relevant sensory conditions. A non-inducible Scn10a^{cre} allows easy targeting of this population throughout development. Using this line with a tdTomato reporter, we see that *Scn10a* is widely expressed throughout the DRG, with terminal endings in the dorsal horn (Fig 2.1). Most prominently, this population encompasses both peptidergic and non-peptidergic nociceptors but

also includes C-low threshold mechanoreceptors, labelled by tyrosine hydroxylase (Fig 2.1B-D). All three populations fall under this larger denotation, with almost 100% of each population covered by this reporter line (Fig 2.1D). Recombination efficiency likely accounts for the near-total overlap.

This transgenic further labels a subset of NF200+ neuron. This is likely a population of myelinated Aδ nociceptors which co-express CGRP. Very few tdTomato expression neurons overlap with PV, but this still accounts for a notable population within this proprioceptive population. We have previously found a subset of PV neurons to overlap with Th, which would fit the current data [179].

Together, this transgenic is well placed to study nociceptive and C-fibre afferents. It encompasses a broad range of sensory neurons involved in nociception, as well as an understudied C-LTMR population.

2.3.1.2 CGRP

Calca^{creERT2} mice drive reporter expression in a smaller, but still heterogeneous neuronal population. In our hands, we see recombination in 35% of neurons, labelling 75% of CGRP-positive neurons. This recombination efficiency is slightly lower than previously reported [175], but specifically overlaps with CGRP-antibody (ab) labelled neurons (Fig 2.2A-D), as well as CGRP-positive terminals in the dorsal horn (2.2E). Differences in tamoxifen dosing regimes may account for this shift.

A small subset of these neurons bind IB4, in line with prior report [175], as well as a 20% overlap NF200, supporting previous data that *Calca* neurons includes a population of myelinated Aδ nociceptors. There is no overlap with paravalbumin-expressing neurons, as expected. Previous reports suggest less than 2% of PV neurons express CGRP in naïve and chronic pain conditions [193]. In the spinal cord, we see terminal endings in the expected laminae, overlapping with CGRP-ab but largely independent of IB4-binding.

Together, this data support the use of Calca^{creERT2}; ai14 mice to target the peptidergic nociceptor population, a subset of *Scn10a*-expressing cells.

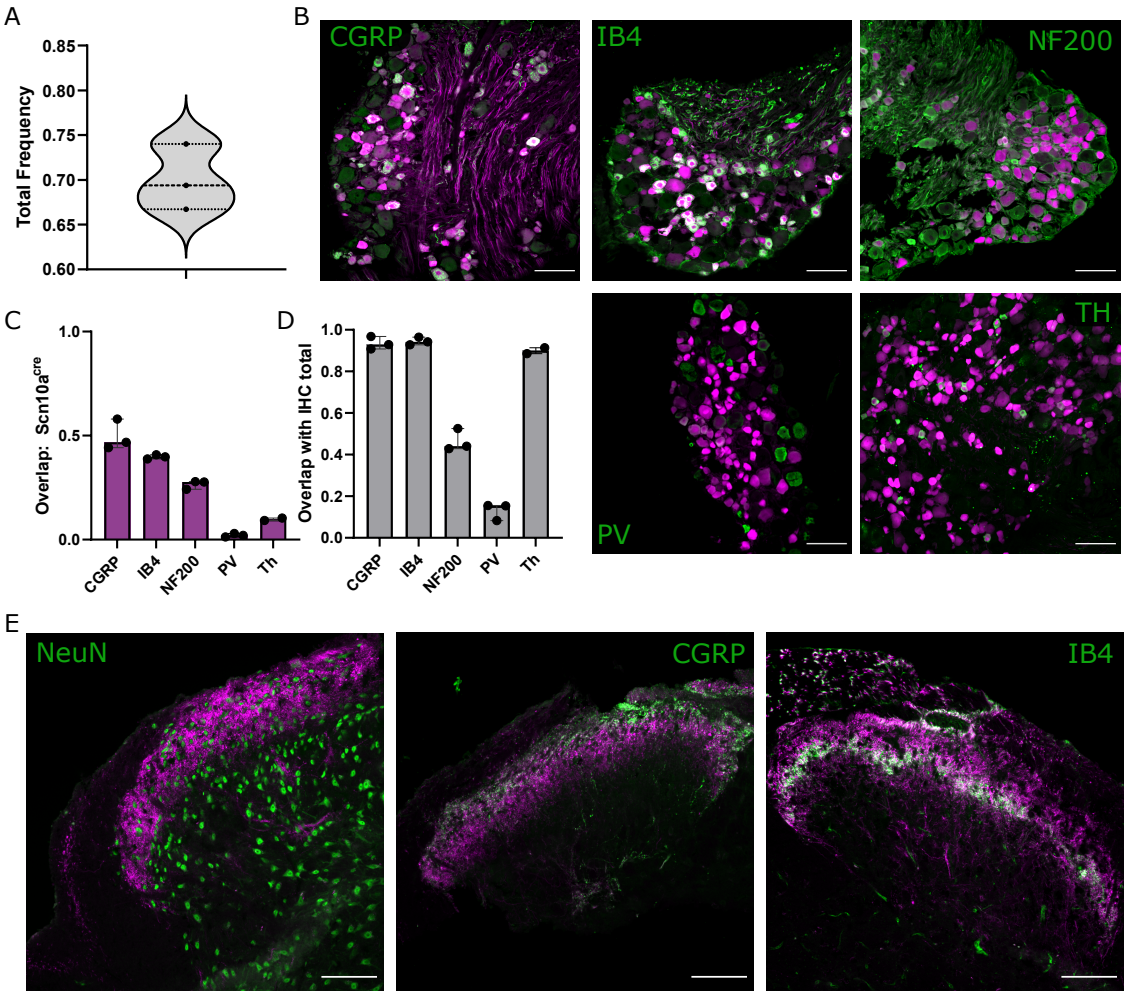

Figure 2.1: Scn10a^{cre}; ai14 validation in naïve, lumbar DRG tissue. A. Frequency of tdTomato labelled neurons by mouse. B. Immunohistochemistry of lumbar mouse DRG sections, stained for distinct subpopulations (green). All Scn10a^{cre}; ai14 is shown in magenta. C-D: tdTomato/staining overlap as a proportion of the total population: C - tdTomato population, D - IHC stained population. E. Dorsal horn spinal cord sections, with Scn10a^{cre}; ai14 in magenta and NeuN (neuronal marker), IB4 (NP) and CGRP (PEP) in green.

2.3.1.3 MRGPRD

Here, I used Mrgprd^{creERT2} to target non-peptidergic nociceptors (NP). This driver provides a specific, and near total labelling of IB4-binding non-peptidergic neurons (Figure 2.3A-D). Matching previous reports, we find approximately 30% of sensory neurons in the DRG to express *Mrgprd*. This is slightly lower than the peptidergic population, and fits historical data. Unlike the minor Calca^{creERT2}; ai14 overlap with IB4, we see no overlap with CGRP-ab staining in this line (Figures 2.2C, 2.3C). This

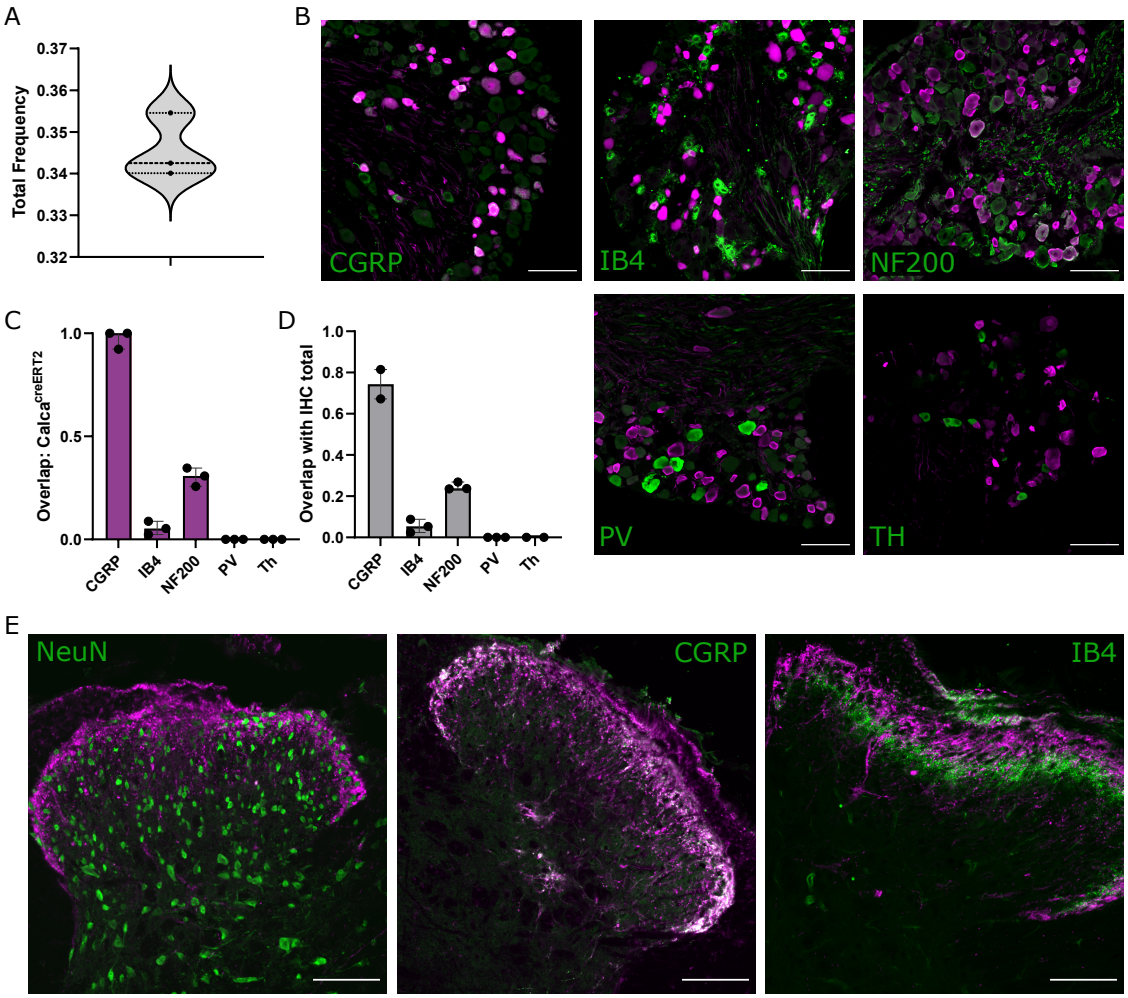

Figure 2.2: Cgrp^{creERT2}; ai14 validation in naïve, lumbar DRG tissue. A. Frequency of tdTomato labelled neurons by mouse. B. Immunohistochemistry of lumbar mouse DRG sections, stained for distinct subpopulations (green). All Calca^{creERT2}; ai14 is shown in magenta. C-D: tdTomato/Staining overlap as a proportion of the total population: C - tdTomato population, D - IHC stained population. E. Dorsal horn spinal cord sections, with Calca^{creERT2}; ai14 in magenta and NeuN (neuronal marker), IB4 (NP) and CGRP (PEP) in green. Scale bars = 100 um.

fits the dogma that in mice, specifically, these are distinct populations. Additionally, this population of small-diameter neurons remains distinct from C-LTMRs, with no documented overlap with the TH-labelled population.

As expected, afferents projecting to the dorsal horn overlap with IB4-staining, but not CGRP (Fig2.3E). This line complements Calca^{creERT2}; ai14 well by distinctly labelling the non-peptidergic nociceptor population.

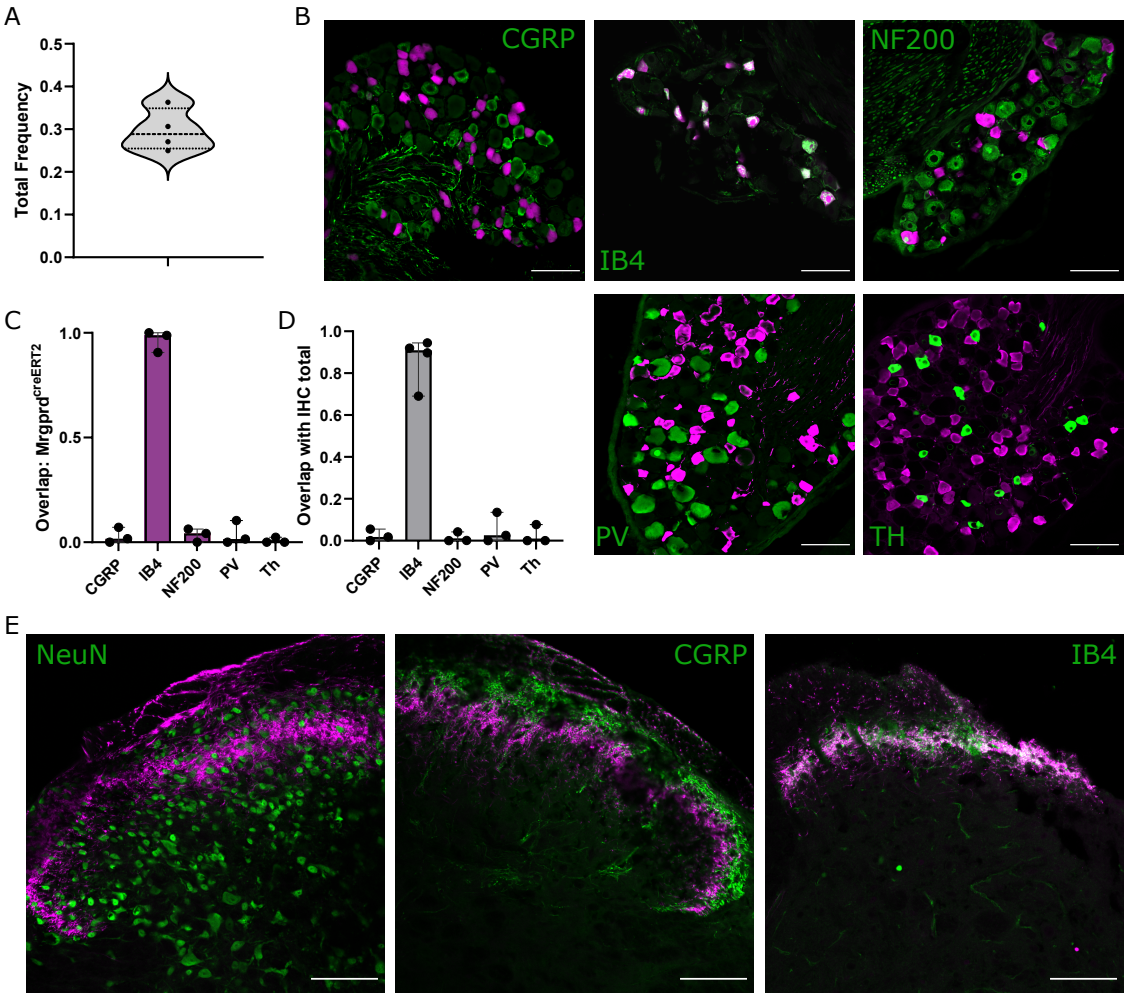

Figure 2.3: Mrgprd^{creERT2}; ai14 validation in naïve, lumbar DRG tissue. A. Frequency of tdTomato labelled neurons by mouse. B. Immunohistochemistry of mouse DRG sections, stained for distinct subpopulations (green). All Mrgprd^{creERT2}; ai14 is shown in magenta. C-D: tdTomato/Staining overlap as a proportion of the total population: C - tdTomato population, D - IHC stained population. E. Dorsal horn spinal cord sections, with Mrgprd^{creERT2}; ai14 in magenta and NeuN (neuronal marker), IB4 (NP) and CGRP (PEP) in green. Scale bars = 100 um.

2.3.1.4 Th

C-LTMRs are a unique population of small diameter unmyelinated touch receptors expressing *Scn10a*. We have successfully targeted this population in the group previously using Th^{creERT2}; ai14 [179]. To validate this driver alongside a tagged optogenetic reporter for future experiments, I validated Th^{creERT2}; ai32 for this study (Fig 2.4). Ai32 encodes a channelrhodopsin (ChR2)-reporter fusion protein (ChR2/EYFP), providing an avenue for downstream flow cytometry.

The proportion of C-LTMRs varies anterior-posterior, comprising 10% of thoracic DRG, but only 5% of lumbar neurons [179]. For this study, I focus on the lumbar region, as these neurons are directly involved in spare nerve injury model employed in subsequent experiments. In line with previous data, $Th^{creERT2}$; ai32 neurons comprise around 5% of DRG neurons in the lumbar region. As anticipated, this population does not overlap with the classically defined PEP or NP populations. A subpopulation of these neurons overlaps with PV, which fits the previous characterization of this driver line in our group with ai14 [179]. While 100% of $Th^{creERT2}$; ai32 labelled neurons are co-labelled by TH-ab, recombination efficiency is lower than in other lines used here, and lower than that previously reported when crossed to ai14. Future experimenters may benefit from increased tamoxifen amounts or a longer dosing period. Unlike the other transgenics here, this line is only dosed by i.p. once, compared to daily doses over five days for the other validated lines.

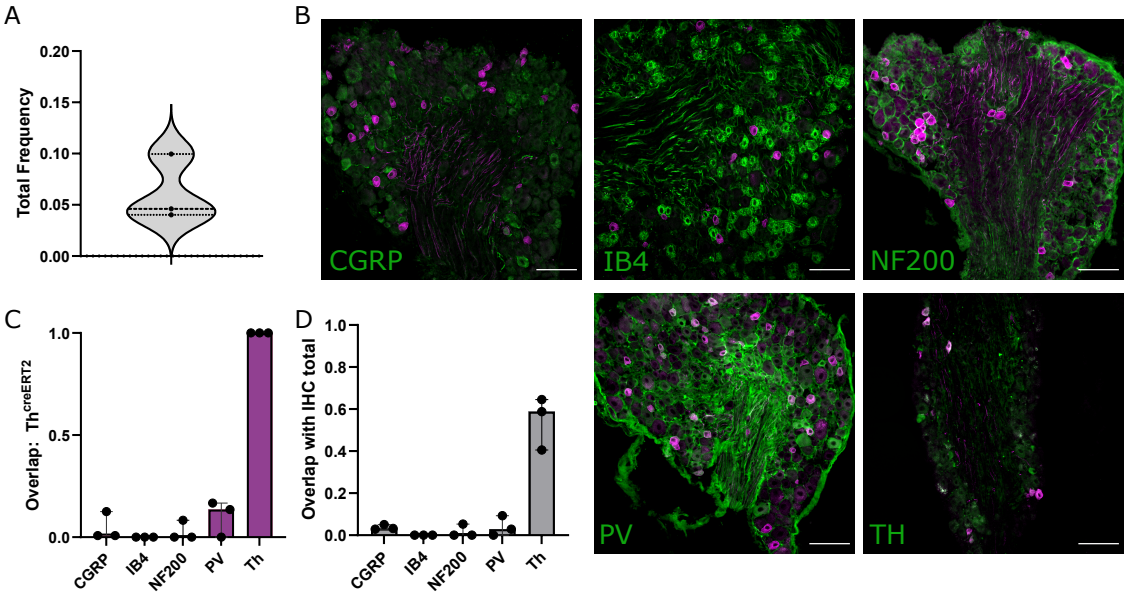

Figure 2.4: $Th^{creERT2}$;ai32 validation in naïve, lumbar DRG tissue. A. Frequency of ChR2/EYFP labelled neurons by mouse. B. Immunohistochemistry of mouse dorsal root ganglia sections, stained for distinct subpopulations (green). All $Th^{creERT2}$; ai32 is shown in magenta. Scale = 100 um. C-D: ChR2/staining overlap as a proportion of the total population: C - ai32 population, D - IHC stained population.

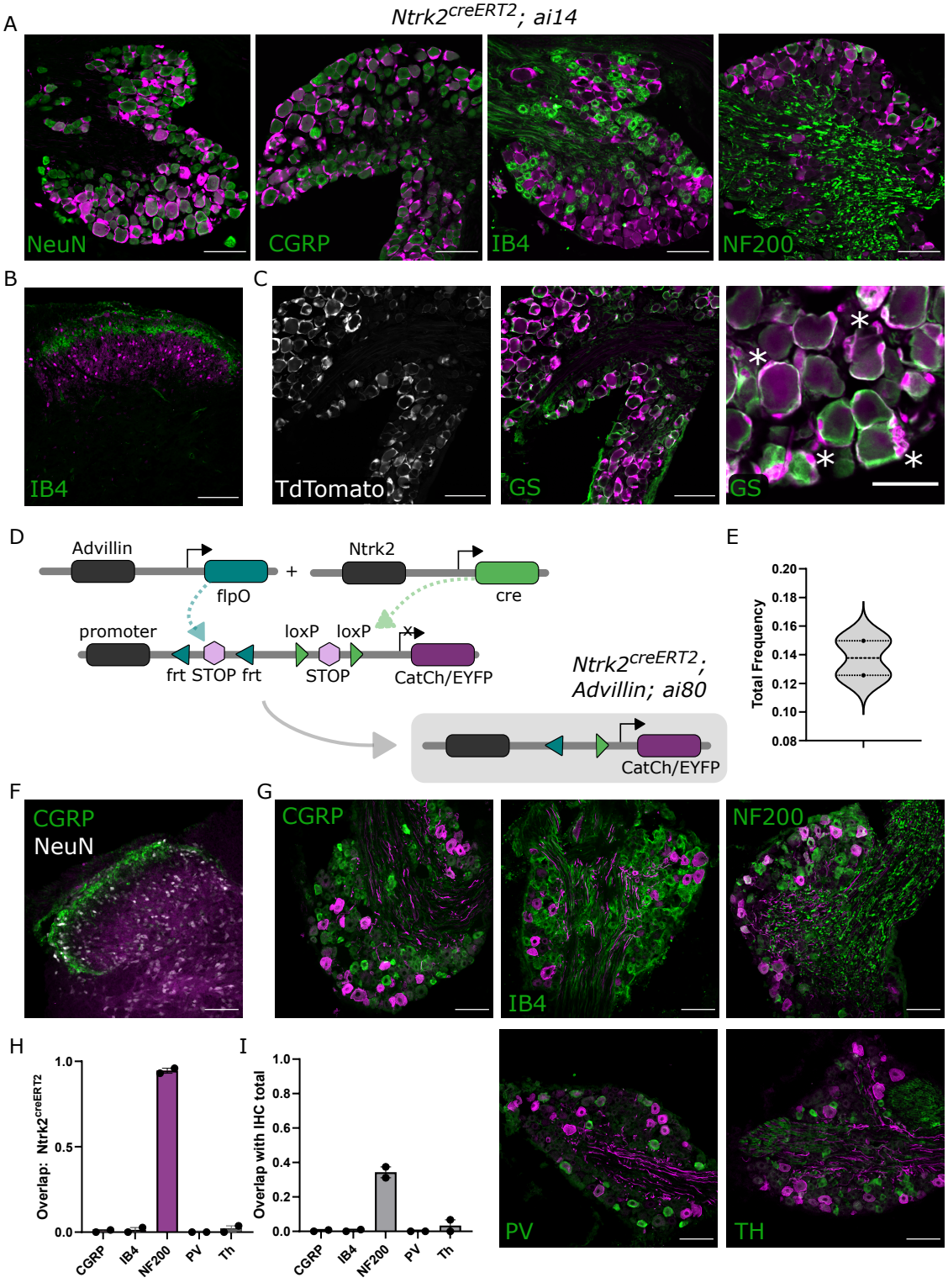

Figure 2.5: Ntrk2$^{\text{creERT2}}$ validation. Caption continued below.

Figure 2.5: A-C: Ntrk2^{creERT2}; ai14, Lumbar DRG (A) and spinal cord (B) IHC. C: Reporter expression (grey) and combined reporter (magenta) with glutamine synthatase, as marker of satellite glia (GS, green). Scale = 100 um. Far right: enlarged, scale = 50 um. * highlight overlap. D-I: Ntrk2^{creERT2}; Advillin^{flpO}; ai80 localises reporter expression to neuronal populations. D: Intersectional approach: The ai80 reporter has two stop cassettes, flanked by frt and loxP sites respectively. Only in the presence of both Flp (frt) and Cre (loxP) are both casettes excised to allow CatCH/EYFP transcription. E. Frequency of ai80 labelled neurons by mouse. F-G. IHC of mouse DRG, stained for subpopulations (green) or NeuN (general neuronal marker, white). All Ntrk2^{creERT2}; Advillin^{flpO}; ai80 is shown in magenta. Scale bars = 100 um. H-I: EYFP/staining overlap proportion: H - ai80 population, I - IHC stained population.

2.3.1.5 TRKB

Ntrk2 drives expression in large-diameter low threshold mechanoreceptors. When combined with a basic cre-driven reporter, non-neuronal labelling is evident through colocalization with the satellite glia marker glutamine synthetase (Fig 2.5A-C). This parallels published data from other groups, although it is not widely acknowledged in the field [5, 21]. Bulk sequencing of satellite glia supports this finding, with SGCs expressing a truncate form of *Ntrk2* [77].

Because satellite glial cells (SGCs) remain attached throughout the sorting process, it is important to exclusively label neurons. If not, SGC-positive, but unlabelled neurons may be sorted incorrectly. The Ntrk2^{creERT2} used here was gifted from Prof. Paul Heppenstall, and our adult dosing regime mirrors their published work [21]. The non-neuronal specificity of TRKB has been addressed in multiple ways: A photoablation study using this line initially characterized expression using a cre-driven Rosa26^{RFP} before shifting to an Advillin-tagged reporter system to limit expression to sensory neurons [21]. Another study by Zheng and colleagues suggests prenatal tamoxifen dosing increases neuronal specificity using a similar Ntrk2^{creERT2} [5]. Animal welfare and licensing limitations require pup delivery by caesarean paired to surrogacy in cases of prenatal tamoxifen dosing (due to the effects of tamoxifen on pregnant females). This, paired to their supporting immunohistochemistry which suggests non-neuronal labelling remains [5] led us to concentrate on options allowing tamoxifen dosing in adult animals.

I took an intersectional transgenic approach to do this (2.5D). B6.Cg-Gt(ROSA) 26Sor$^{tm80.1(CAG-COP4*L132C/EYFP)Hze}$/J (ai80) is a flp- and cre- dependant reporter. When combined with Advillin^{flpO} and Ntrk2^{creERT2}, it limits reporter expression to the associated sensory neurons (Fig 2.5D). Using this approach, I see LTMR-specific labelling within the DRG after tamoxifen dosing (Fig 2.5D-I). In line with previous reports, this population comprises a distinct subset of NF200-positive neurons, with no overlap to peptidergic nociceptors (CGRP) or proprioceptors (PV). Additionally, it shows no overlap with smaller diameter neurons, including C-LTMRs (TH) or non-peptidergic nociceptors (IB4).

2.3.1.6 ATF3

In many pain conditions, only a subset of neurons within a DRG are injured through direct insult. These injured neurons stand adjacent to their uninjured ("intact") counterparts. The contributions of each population to painful phenotypes remains unclear. In addition to classically defined neuronal subtypes, transgenics can also be used to define injured and intact afferents in murine injury models based on the upregulation of transcription factors in injured states (Figure 2.6) [191, 194].

We are exploiting access to an Atf3^{creERT2} line to probe the transcriptional differences within these populations after spared nerve injury, mirroring techniques used for the aforementioned populations. This sequencing is discussed separately in chapter 5.

About 35% of lumbar DRG neurons express tdTomato 4 weeks post-SNI, and in our hands tamoxifen (7.5 mg/kg) does not make a significant difference by 4 weeks ($p = 0.1780$, two-way repeated measure ANOVA) (Figure 2.6A). Correspondence with Dr. Greg Weir (Glasgow) suggests the effect of tamoxifen on recombination efficiency may relate to the specific reporter used. Tamoxifen dosing has previously been shown to induce *Atf3* upregulation in DRG neurons [191], so to reduce confound with our nerve injury model it was not used in our experiments.

Immunohistochemistry was also performed on Atf3^{creERT2} tissue after SNI to examine subpopulation overlap. While most populations showed a subset

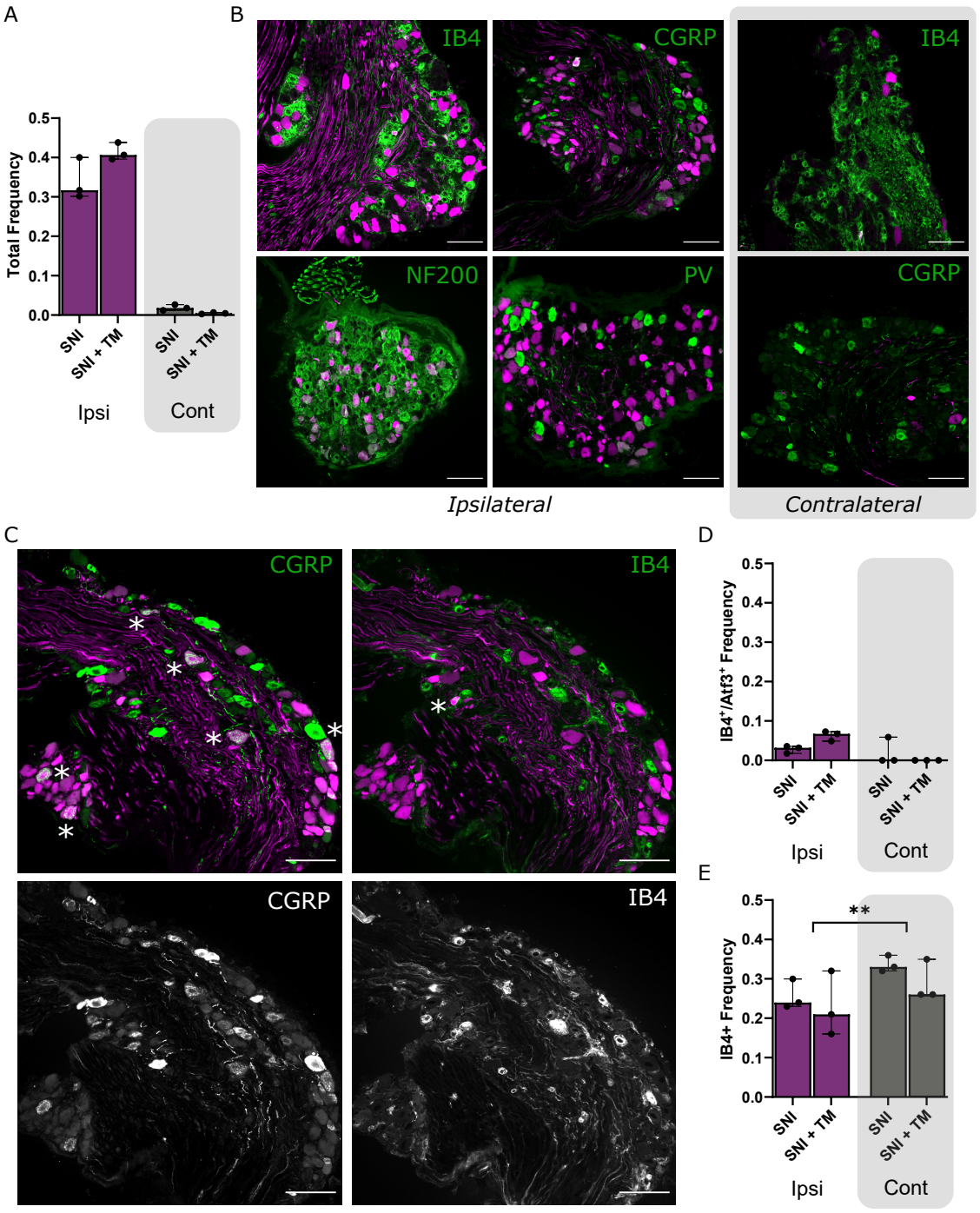

Figure 2.6: Atf3^{creERT2} validation after SNI. Caption continued below.

of cell profiles overlapping with tdTomato-labelled injured afferents, there was minimal colocalization between IB4 and tdTomato. This notable difference was quantified further (Fig 2.6D-E). There is no significant difference in overlap across ipsilateral/contralateral tissue, nor between tamoxifen dosing conditions ($p = 0.0628$

Figure 2.6: Atf3^{creERT2}; ai14, L4 DRG 4 weeks after spared nerve injury (SNI). Ipsilateral (ipsi) and contralateral (cont) lumbar DRG tissue. Surgeries were performed without tamoxifen dosing (SNI) or with a small amount of tamoxifen (SNI + TM, 7.5 mg/kg). A: Frequency of ai14 labelled neurons by mouse after SNI. Minimal recombination is seen in paired contralateral tissue after nerve injury (cont, grey box). Tamoxifen does not have a significant effect on tdTomato expression after SNI (p = 0.1780, two-way repeated measure ANOVA). Plotted as median count by mouse, with 95% confidence intervals. B: IHC of mouse DRG after SNI (no tamoxifen), stained for neuronal subpopulations (green). Far right (grey box) = contralateral lumbar tissue, stained for peptidergic (CGRP) and non-peptidergic (IB4) nociceptors. C: IB4 and CGRP expression (greyscale) and combined reporter (magenta) with subtypes (green). * = overlap. D. Colocalization of IB4 and tdTomato labelling across conditions. E. Frequency of IB4 staining across conditions. Total IB4-binding (E) is significantly different between ipsilateral and contralateral conditions (p = 0.0016, two-way repeated measure ANOVA), but there is no effect of tamoxifen on totals (p =0.4296), or overlap with tdTomato (p=0. 5525). All ai14 is shown in magenta. Scale bars = 100 um.

for condition, tamoxifen p = 0.5525, two-way repeated measure ANOVA). There is a significant reduction in the total frequency of IB4-binding profiles in injured DRG ganglia (p = 0.0016), although stereometric DRG counts are better suited to explore this phenomenon in depth (contrasting sectioned profiles, shown here). We have pursued this finding through a collaboration with partners in Glasgow, and are excited to present our data as a separate study outside of this thesis.

Given our interest in acute changes, we further examined this line on a shorter timescale. As anticipated, recombination 3 days after SNI is much lower than 4 weeks, with around 15% of neurons showing tdTomato expression, compared to double that at 4 weeks (Fig 2.7). This fits the previous validation of this line, showing 40% recombination at 4 days, compared to almost 80% by 2 weeks [194]. Co-labelling with ATF3-ab shows a large number of ATF3-expressing neurons which do not express tdTomato, likely due to the timeline for recombination and protein synthesis (Fig 2.7A).

2.3.2 MACS vs BSA

Cell suspensions have to be purified prior to FACS to eliminate debris. This is particularly important for nervous system tissue, as myelin debris prevents effective sorting. Here, I trialled multiple purification techniques. To isolate neurons, both

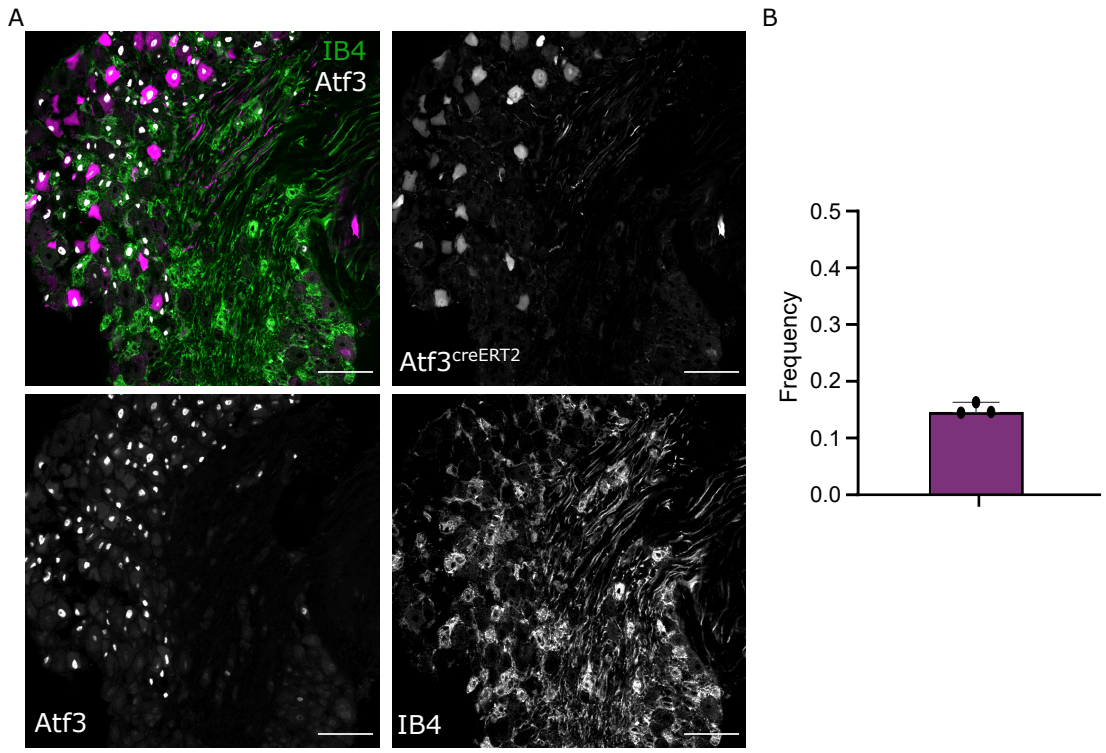

Figure 2.7: Atf3^{creERT2} ; ai14 validation three days after SNI. A. Immunohistochemistry of ATF3 and IB4 on ipsilateral lumbar tissue after injury. Atf3^{creERT2} ; ai14 in magenta (top left). B. Frequency of tdTomato-expressing neurons, by mouse. No tamoxifen was used in parallel. Scale bars = 100 um.

standard BSA gradients and magnetic sorting were trialled. Unlike BSA gradients, MACS biases the sample towards small diameter nociceptors, eliminating the classic bimodal size distribution typical of sensory neurons (Fig 2.8A-C). This is likely due to a combination a physical cell size constraint with large cells becoming stuck in the magnetic column, paired with the removal of a neuron attached to satellite glia.

Manufacturer directions recommend these columns should not be used for cells over 30 um in diameter, which fits this result. Both fire polished glass pipettes and standard filter tips are used during dissociation. Here, we see glass pipettes perform slightly better than plastic prior to MACS ($p = 0.0092$), but as expected, this fails to rescue the large diameter neurons isolate with a BSA gradient (Fig 2.8D). While MACS samples contain fewer non-neuronal cells, the bias limits our ability to study larger diameter sensory neurons. To ensure capture of each population, BSA gradients were ultimately used for subpopulation purification

(Fig 2.8E-G), although both methods are sufficient for the flow cytometry of small diameter neurons (Fig 2.8H-I).

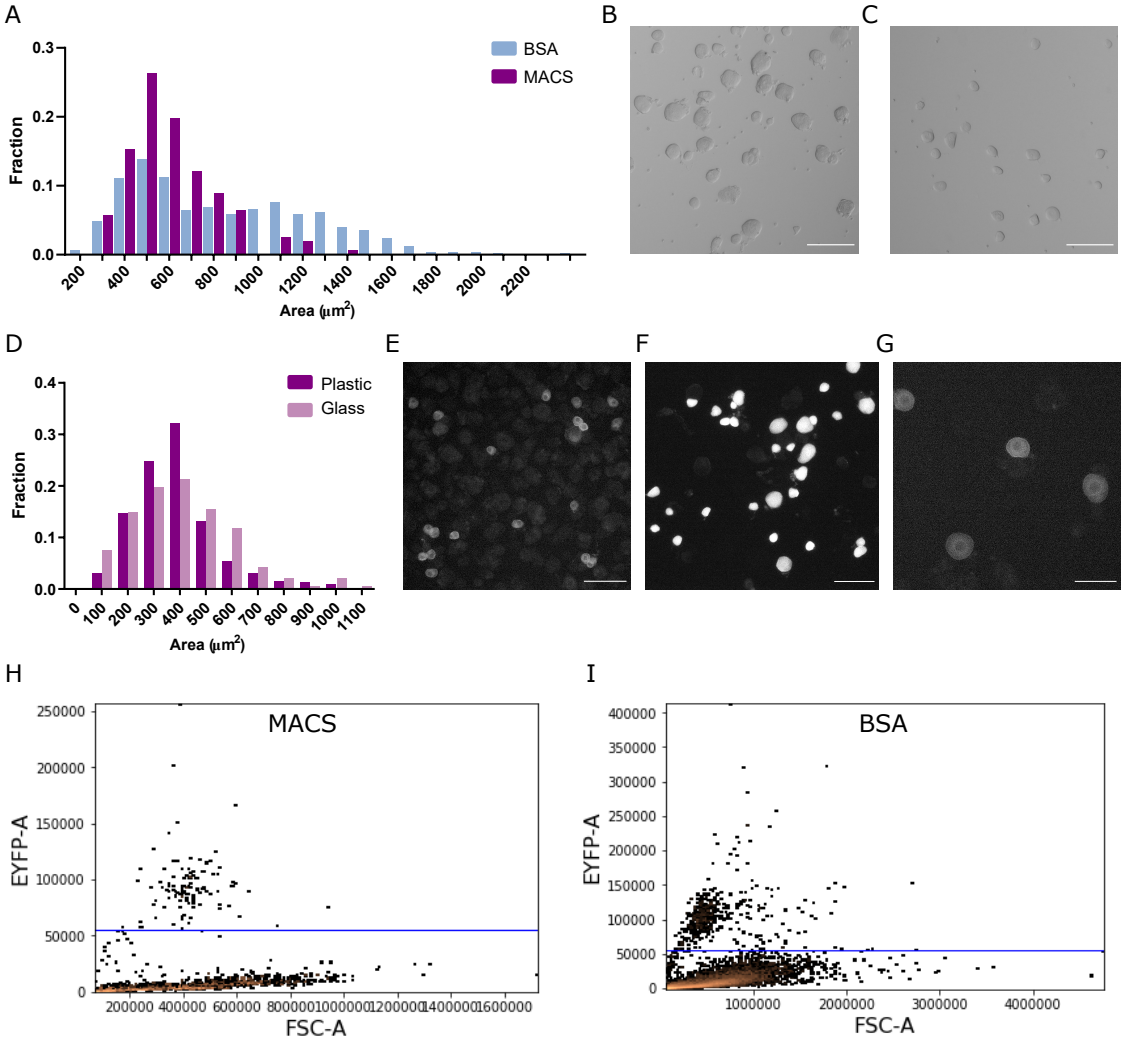

Figure 2.8: Magnetic-activated cell sorting (MACS) compared to a BSA gradient. A. Neuronal size distribution in isolated lumbar DRG cultures after BSA or MACS (n=3 mice, paired for condition. p = 0.0104*, Kolmogorov-Smirnov test). B-C: Representative culture brightfield, scale bar = 100 um. B: BSA, C: MACS. D: Fire polished glass pipettes outperform plastic pipettes during dissociation. p = 0.0092*. E-G: BSA dissociation purify neurons across supbpoulations. E: $Th^{creERT2}$, scale = 100 um. F: $Calca^{creERT2}$, scale = 100 um. G: $Ntrk2^{creERT2}$, scale = 50 um. H-I: Both MACS and BSA are sufficient for downstream flow cytometry. Example traces from $Th^{creERT2}$; ai32 DRG.

2.3.3 FACS

Cells were dissociated with a BSA gradient and sorted via fluorescence to purify each population of interest (Figure 2.9). Neurons were gated for scatter (2.9A), doublets (2.9B), live/dead (2.9C), and fluorescence (2.9D). This was then repeated, adjusting for differences in reporters (ai14, ai32, ai80). In each instance, lumber DRGs L3-L5 were used. Across populations, we were able to isolate fluorescent neurons. The proportion of positive droplets corresponds to expected population fractions, strongly supporting successful sorts. In ai14 samples, tdTomato produces a strong background signal in the 488-channel, but this does not affect these sorting conditions. Fluorescence is lower in Ntrk2$^{\text{creERT2}}$; ai80. This is due to cell size, leading to more diffuse labelling, as well as reporter differences (a CatCh/EYFP fusion). During optimization across sorting platforms, negative controls were used to ensure successful gating, as demonstrated for *Ntrk2* in figure 2.10.

2.4 Discussion

Dorsal root ganglia cells represent a diverse group of neurons and non-neuronal cells in the periphery. The development of multiple transgenic mouse lines allows specific targeting of these populations in a variety of ways. For this study I validated five distinct neuronal subpopulation transgenics with optimized tamoxifen dosing for downstream use. I also characterized Atf3$^{\text{creERT2}}$ after SNI as a way to dissecting intact and injured afferents within ganglia. Together, these populations encompass a range of neuronal subtypes implicated in acute and neuropathic pain.

Neuronal subtypes Most broadly, Scn10a$^{\text{cre}}$ labels a large majority of DRG neurons. This population can be subdivided through Calca$^{\text{creERT2}}$, Mrgprd$^{\text{creERT2}}$, and Th$^{\text{creERT2}}$, labelling peptidergic, non-peptidergic, and C-LTMRs respectively (Figures 2.1, 2.2, 2.3, 2.4).

Ntrk2$^{\text{creERT2}}$; ai14 shows a unique expression pattern in both neurons and non-neuronal cells (2.5). Colocalization with glutamine synthetase reveals prominent reporter expression in SGCs not previously documented (Fig 2.5) [5, 21]. This is

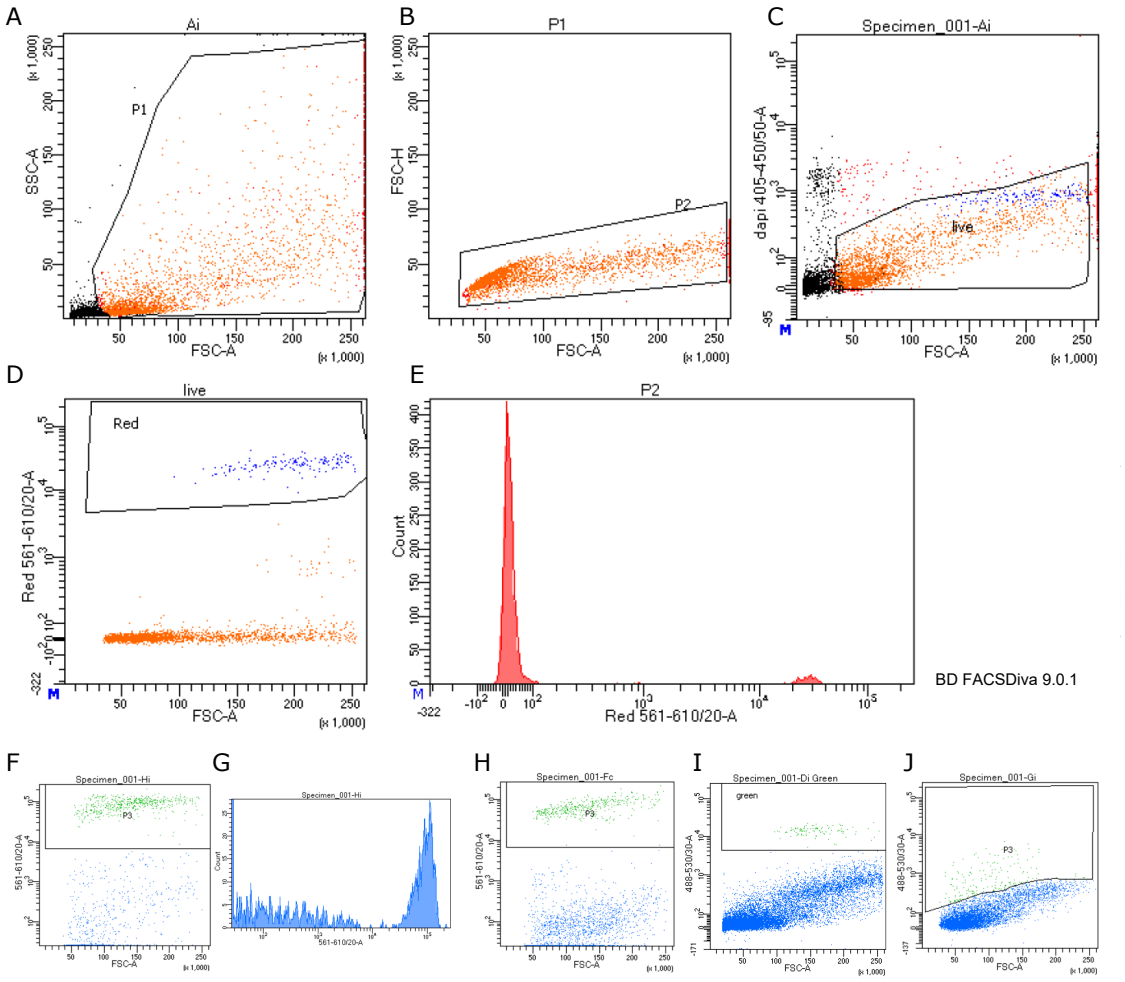

Figure 2.9: Sensory neuron populations can be sorted by fluorescence. A-E: Mrgprd$^{\text{creERT2}}$ sorted neurons, gated for scatter (A), doublets (B), live/dead (C), and ai14 fluorescence (D). F: Scn10a$^{\text{cre}}$ gating for ai14, and associated histogram (G). H: Calca$^{\text{creERT2}}$ gating for ai14. I: Th$^{\text{creERT2}}$ gating for ai32 reporter. J: Ntrk2$^{\text{creERT2}}$ gating for ai80 reporter.

problematic for downstream fluorescent sorting, as satellite glia remain attached to neurons during dissociation and FACS. Any fluorescence from positive SG could trigger a false-positive Ntrk2-lineage neuron. To circumvent this issue, Ntrk2$^{\text{creERT2}}$; Advillin$^{\text{flpO}}$; ai80 was used to limit expression to Advillin-expressing cells (ie. neurons), specifically targeting Aδ- and Aβ-LMTRs.

Injured and intact afferents Atf3$^{\text{creERT2}}$ represents a unique transgenic that targets injured afferents through their upregulation of *Atf3* after insult. Here, we are able to selectively target a subgroup of injured neurons in line with previous reports

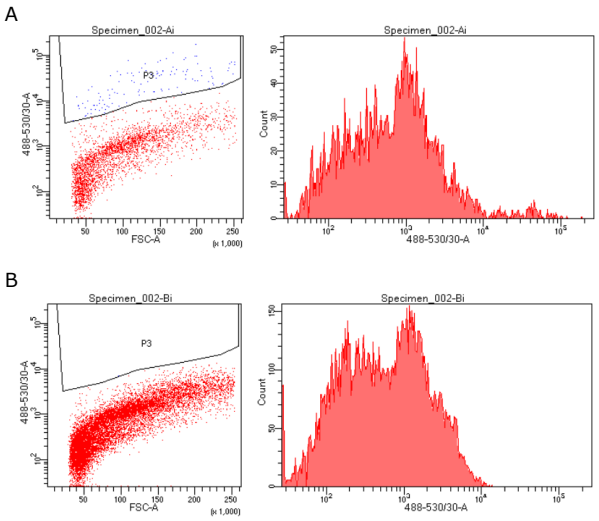

Figure 2.10: Ntrk2 positive (A) and negative control (B) gated for CatCH/EYFP fluorescence in 488.

(2.6, 2.7). Previously, recombination frequencies were quantified in more detail using retrograde labelling from the transected nerve [194]. This better represents the proportion of injured afferents expressing tdTomato, as endogenous ATF3 expression (and thus, antibody labelling) is transient. Even so, it is clear that only a subset of injured cells express tdTomato 3 days post-injury. The tdTomato-negative population thus contains a mix of injured and intact afferents. Additionally, IHC against multiple neuronal subtype markers highlighted a disjoint in IB4-labelled neurons to tdTomato-expressing cells, likely due to a loss of injured NP nociceptors.

We posit three main hypotheses for the lack of colocalization between Atf3$^{\text{creERT2}}$; ai14 and IB4-binding neurons. These hypotheses are not mutually exclusive. First, subtype differences may affect the expression of tdTomato after injury, either through differences in Atf3 regulation or another mechanism. This transgenic was developed as an inducible cre line, but it does not require tamoxifen when paired to specific reporter lines [191, 194]. Using tamoxifen as a model of cellular stress, *Atf3*-driven tdTomato expression was biased towards NF200-expressing neurons [191]. It is unclear if this subpopulation specificity arose from a biased reporter expression or a tamoxifen-sensitivity in NF200 neurons. Second, IB4-binding may be reduced in non-peptidergic neurons after injury, an interpretation which has been historically

discussed in the dorsal horn [195]. Third, NP nociceptors may be particularly susceptible to cell death after injury. Previous work in our group has shown a significant reduction in small-diameter neurons after SNI using tissue clearing and automated whole-DRG cell counting [196]. This is paired to a reduction of pre-synpatic terminals in the superficial laminae of the dorsal horn, further suggesting innervation changes in small-diameter neurons [196]. Rats also show a reduction in IB4-binding terminals after nerve injury, although the delineation between NP and PEP neurons is blurred in this species [197].

I have followed these hypotheses up in collaboration with Dr. Greg Weir and Dr. Andrew Cooper (University of Glasgow). This was done across multiple nerve injury models using stereological analyses paired to a combination of retrograde tracing of injured afferents in both Atf3^{creERT2} and Mrgprd^{creERT2} lines. Together, there appears to be a near-total loss of transected NP neurons by 4 weeks after SNI (unpublished data, Greg Weir and Andrew Cooper). This data fits with the loss of small diameter neurons reported by West [196] as well as unpublished data from dorsal horn innervation of Mrgprd^{GFP} labelled neurons after nerve injury (personal correspondence, Dr. Greg Weir and Prof. Andrew Todd). This strongly suggests that the lack of IB4 colocalization with tdTomato is biologically relevant to nerve injury, and not a confound associated with the Atf3^{creERT2} transgenic.

Data collected for this thesis relied on a simple transgenic approach, in line with previous reports. The availability of dual-recombinase reporters and FlpO drivers have since provided a refinement. Unlike our ai14 cross, tamoxifen dosing is required here, likely due to differences in the ease of recombination efficiency across reporters (personal correspondence, Greg Weir). Advillin^{flpO}; Atf3^{creERT2}; RC::FLTG allows specific labelling of injured (eGFP-expressing) and intact (tdTomato-expressing) neurons. This allows more targeted fluorescent gating during sorts, and is relevant for the sequencing data presented in chapter 5.

Cell purification and sorting Ganglia dissociation is an important processing step prior to downstream analyses. Here, we replicate MACS results from Thakur

and colleagues showing a bias towards small-diameter neurons during magnetic purification (Fig 2.8) [28]. In our hands, BSA gradients are sufficient to remove myelin debris while retaining large-diameter neurons (Fig 2.8B). In each case, cell suspensions from transgenic lines can be gated for fluorescence (2.9, 2.10).

We know from previous studies that SGCs remain attached to sensory neurons throughout the sorting process, and we expect our samples to contain both labelled neurons and unlabelled glia (personal correspondence, Prof. Fran Denk and Dr. Sara Villa). This is likely due to the wrapping structure of SGC around neurons, leading to the appearance of a single round cell. Neuronal nuclei can be isolated from SGC for nuclei-based sequencing, but this is not currently possible for bulk cell samples. As such, we expect our FACS samples to contain SGC contamination, opposed to being 100% neuronal.

Conclusions Here, we highlight effective fluorescence targeting of neuronal subtypes through murine transgenics. Combined, these lines cover a range of cell types and are well placed for downstream analyses. Using this sample preparation workflow, we subsequently used a surgical model of neuropathic pain and subpopulation purification, followed by RNA-seq or snATAC-seq to explore the molecular underpinnings of these populations. These results are presented in chapters 3, 4, and 5.

2A Appendix

Table 2A.1: Transgenic lines used in the current study

Mouse line	Source	Identifier
Atf3$^{tm1.1(cre/ERT2)Msra}$	gift: Stephen McMahon	[191]
Calca$^{tm1.1(cre/ERT2)Ptch}$	gift: Pao-Tien Chaung	[188]
Mrgprd$^{tm1.1(cre/ERT2)Wql}$/J	The Jackson Laboratory	[189], CAT#:031286
Scn10a$^{tm2(cre)Jnw}$	gift: John Wood	[190]
Tg(Ntrk2-cre/ERT2)#Phep	gift: Paul Heppenstall	[21]
Th$^{tm1.1(cre/ERT2)Ddg}$/J	gift: David Ginty	[20], CAT#:025614
Advillin^{flpO}	gift: David Ginty	[20]
B6.129S-Gt(ROSA)26Sor$^{tm32(CAG-COP4*H134R/EYFP)Hze}$/J	gift: Simon Butt	[198], CAT#:012569
B6.Cg-Gt(ROSA)26Sor$^{tm14(CAG-tdTomato)Hze}$/J	The Jackson Laboratory	[199], CAT#:007914
B6.Cg-Gt(ROSA)26Sor$^{tm80.1(CAG-COP4*L132C/EYFP)Hze}$/J	The Jackson Laboratory	[200], CAT#:025109

Table 2A.2: Antibodies used in chapter 2.

Reagent	Source	Identifier	Dilution
Donkey anti-Mouse IgG (H+L), Alexa Fluor 488	ThermoFisher Scientific	A-21202	1/200
Donkey anti-Rabbit IgG (H+L), Alexa Fluor 546	ThermoFisher Scientific	A10040	1/200
Donkey anti-Sheep IgG (H+L), Alexa Fluor 488	ThermoFisher Scientific	A-11015	1/200
Donkey anti-Sheep IgG (H+L), Alexa Fluor 546	ThermoFisher Scientific	A-21098	1/200
Goat anti-Chicken IgY (H+L), Alexa Fluor 546	ThermoFisher Scientific	A-11040	1/200
Goat anti-Rabbit IgG (H+L), Alexa Fluor 488	ThermoFisher Scientific	A-11008	1/200
Goat anti-Rabbit IgG (H+L), Alexa Fluor 546	ThermoFisher Scientific	A-11010	1/200
Goat anti-Rabbit IgG (H+L), Pacific Blue	ThermoFisher Scientific	P-10994	1/200
Streptavidin, Pacific Blue conjugate	ThermoFisher Scientific	S11222	1/100
anti-ATF3, mouse	Abcam	NA	1/500
anti-CGRP, rabbit	Peninsular Labs	T4032	1/500
anti-CGRP, sheep	Enzo	Ca1137	1/250-1/500
anti-Glutamine synthetase (GS), rabbit	Sigma-Aldrich	G2781	1/500
anti-NeuN, chicken	Merck Millipore	Abn91	1/500
anti-NeuN, rabbit	Abcam	Ab177487	1/500
anti-NF200, mouse	Sigma-Aldrich	N0142	1/250
anti-NF200, rabbit	Merck Millipore	ABN76	1/1000
anti-Parvalbumin (PV), guinea pig	Frontier Institute	Af1000	1/200-1/500
anti-Tyrosine Hydroxylase (TH) , sheep	Merck Millipore	Ab1542	1/400
IB4, streptavidin conjugated	Sigma-Aldrich	L2140	1/100

3

Deep RNA-seq of male and female sensory neuron subtypes

The diversity within DRG is well characterized, but changes by subtype after nerve injury remain unclear. Over two chapters, we study the deep transcriptional profiles of five murine DRG populations in acute and chronic pain states while considering sex interactions. First, our dataset is validated against a previously published control RNA-seq dataset, and sex differences in naïve states - particularly in Aβ-RA + Aδ-LTMRs - are presented. We have curated this dataset into an accessible, online platform as a resource for the community.

Contents

3.1 Introduction

Sensory neurons encompass a diverse collection of subtypes that are grouped by size, conduction velocity, function, and molecular profile. These subpopulations have been well documented through single cell and single nuclear RNA-seq in mice [22, 23, 30, 33] and human [24, 25].

This diversity is lost during bulk RNA-seq, due to the consolidation of all subtypes together. In single cell datasets, pseudo-bulk samples can be generated for each cluster, but this relies on a well-defined clustering that can be lost after nerve injury [33, 41].

Using transgenic targeting of neuronal subtypes paired with bulk RNA-seq, we aim to strike a unique balance of subpopulation resolution with higher sequencing depths for differential gene expression (DEG) analyses. Five sensory neuron populations were pursued. After characterizing these driver lines in chapter 2, we are here able to specifically examine the RNA expression level changes after injury across a range of neuronal subpopulations.

3.1.1 Injury models

We employ spared nerve injury (SNI) as our neuropathic pain model. It has a well established time course in mice and is a behaviourally relevant animal model, with sensory dysfunction similar to that in neuropathic pain patients (including hyperalgesia, allodynia, and spontaneous pain). As a localized model of neuropathic pain, each site of injury has an internal paired control (contralateral, uninjured tissue). This both reduces overall animal numbers and reduces the biological and technical variability introduced during the collection process to increase our power.

3.1.2 Sexual dimorphism

In addition to probing injury signatures within subtypes, we also explore sexual dimorphisms at the subpopulation-level. In naïve states, quantitative sensory testing has highlighted heightened pain sensitivity in females to a battery of acute noxious stimuli [201]. The incidence of chronic pain is also highly sex dependant, with females significantly more likely to suffer [144, 145]. Experimentally, historical biases within the research community resulted in a predominantly male focus [145, 148, 149]. The unwillingness to use female animals has stunted our knowledge.

Fortunately, numerous studies have begun probing this in depth and have found sexual dimorphisms across rodent models of neuropathic pain [151, 202, 203]. Sorge *et al.* report a prominent sex difference when studying mechanical hypersensitivity: While males depend on microglia activity, female animals depend on adaptive immune cells [203, 204]. Brain derived neurotrophic factor (BDNF) and prolactin both affect pain in a sex-dependant manner [133, 151] and there is evidence of

higher level dimorphisms affecting pain percepts in the cortex [205]. At a transcript level, sexual dimorphism is also visible [73, 206], with transcriptomic differences seen in human DRG as well [24, 27].

3.1.3 Aims

In this chapter, I focus on the deep sequencing of male and female sensory neuron subtypes in control samples. I discuss general quality control of our comprehensive RNA-seq dataset, comprising injured and control tissue from an acute (3 day) and chronic (4 week) timepoint after SNI. I validate our contralateral baseline controls against previously published data and further examine subtype-specific sexual dimorphism in sensory neuron subpopulations. Detailed results from injury phenotypes are subsequently presented in chapter 4.

3.2 Methodology

3.2.1 Animals

All work was done in accordance with the UK Home Office and the University of Oxford Policy on the Use of Animals in Scientific Research. This study conforms to ARRIVE guidelines. Transgenic details and tamoxifen dosing details are outlined in depth in chapter 2. Where necessary, animals were dosed i.p. with tamoxifen at the appropriate age, at least 14 days before surgery (see chapter 2).

3.2.2 Spared nerve injury

Adult mice were anesthetized with 2% inhaled isoflurane. Using sterile technique (including incision site sterilization and surgical drapes), the sciatic nerve was exposed prior to ligation and transection of the tibial and common peroneal branches. The sural nerve was left intact. Each animal was dosed with systemic (5 mg/kg Rimadyl, Pfizer) and local (2 mg/kg Marcain, AstraZeneca) postoperative analgesia. No animals exhibited signs of self-mutilation.

3.2.3 Immunohistochemistry and *in situ* hybridization

Adult animals were overdosed with pentobarbital and perfused transcardially with sterile saline followed by 4% paraformaldehyde. Tissue was removed and post-fixed prior to subsequent dehydration in 30% sucrose (0.1M PB) at 4°C for a minimum of 48 hours. Samples were then embedded in OCT, cryostat sectioned to 10 μm and stored at -80°C until staining. Immunohistochemistry (IHC) was performed as described in chapter 2.

In situ hybridizations (ISH) were performed using RNAscope as per manufacturer's instructions (ACDBio, Kcnk10 probe 535391) with the following modification: pretreatment step 2 was omitted. After *in situ*, tissue was co-stained using a standard protocol (above). Primary antibodies were applied overnight at RT in 3% NDS/3% NGS/0.3% Triton-X100 in PBS. Coverslips were rinsed 3x and washed 3x 5 min prior to the addition of secondary antibodies (2 hr, RT in the dark). Sections were again rinsed 3x and washed 3x 5 min prior to mounting in Vectashield Antifade (Vector Labs).

3.2.4 Sample collection

Sample size was calculated using the algorithm published by Zhao *et al.* [207]. Based on our sequencing depth, we expect to detect 10000 genes per sample. Recent data from Parisien and colleagues using whole DRG suggests that 1000 genes can be considered regulated (based on an FDR cutoff of 0.05) in DRG one week after SNI, with an average fold change of 3.3 (SNI/control) [208]. Prior data collection in our lab indicates that the minimum average read counts among the prognostic genes is 700 and the maximum expected dispersion is 0.2. Using a desired minimum fold change set to 3.3, we can achieve a power of 0.99 with 8 samples per condition. Moreover, we will be sufficiently powered to detect large fold changes between sexes (power of 0.8, n=4). All surgeries and sample collections were performed by the same experimenter to reduce variability across samples.

In total, 160 paired samples were collected (ipsilateral and contralateral) over five neuronal subtypes at an acute (3 day) and chronic (4 week) timepoint after

SNI (Fig 3.2A). Ipsilateral lumbar (L3-L5) were compared to contralateral (L3-L5) DRGs to ensure an internal control. One animal was used for each sample pair, excluding $Th^{creERT2}$, where DRGs from two animals were pooled during dissection. Male and female samples were evenly split, with the exclusion of $Mrgprd^{creERT2}$, 3 days after SNI where only 3 female mice could be used. Five males were thus processed for this group.

Sample preparation is similar to that described in chapter 2 with accelerated timing to prevent RNA degradation. Multiple animals were processed in parallel but collection times from perfusion to frozen were kept to less than 4 hours. Adult animals were first overdosed with pentobarbital and perfused transcardially with sterile, ice cold saline. Lumber DRG were quickly removed and placed into HBSS on ice. Post-dissection of all tissue, collagenase/dispase was added for a 60 min digest at 37°C followed by mechanical dissociation with polished glass pipettes. Myelin and debris was reduced using a clean 15% w/v BSA cushion. Samples were placed on ice and centrifuged at 4°C as much as possible (i.e. excluding digestion). Prior to FACS, a subset of DRG from each sample was examined under brightfield.

3.2.5 Library preparation and sequencing

Samples were transferred on ice immediately to the WIMM FACS Facility (Oxford) for sorting on a BD FACSAria Fusion 1 or Fusion 2. For each condition, 100 cells were isolated directly into low protein binding eppendorfs containing 2 µl NEBNext Single Cell Lysis Buffer (NEB, E5530S). Samples were kept on dry ice until transfer to -80°C for overnight storage.

Once all samples were collected, samples were thawed on ice, vortexed, and randomized into a 384-well 4titude Framestar skirted PCR plate (Brooks Life Science, 4ti-0384/C; Thermo Scientific, AB-0558). Non-directional libraries were prepared together using NEB Ultra low/Smarter library prep, as per manufacture instructions by the Oxford Genomics Centre at the Wellcome Trust Centre for Human Genetics. Libraries were amplified (21 cycles) on a Tetrad (Bio-Rad) using in-house unique dual indexing primers (based on [209]). Individual libraries were

normalized using Qubit, and the size profile was analysed on the 2200 or 4200 TapeStation before pooling together accordingly. The pooled library was diluted to 10 nM for storage. The 10 nM library was denatured and further diluted prior to loading on the sequencer. Sequencing was performed over three independent runs, and merged after quality control. Paired end sequencing was performed using a NovaSeq6000 platform using the S2/S4 reagent kit v1.5. Samples were sequenced with a 150 bp read length, at a depth of 30 million reads per sample.

3.2.6 Analysis

3.2.6.1 Bioinformatics overview

Reads were mapped to the GRCm38 (mm10) Mouse Genome using STAR alignment with the parameters in Figure 3.1 [210]. Samtools was used to sort, index, and merge BAM files [211]. Quality control (QC) was performed with both FastQC and Samtools prior to gene counting with HTSeq [211–213].

```
/STAR --runThreadN 16 --genomeDir /mm10_genome_index_150
    --genomeLoad LoadAndKeep --limitBAMsortRAM 20000000000
    --readFilesIn "${LANE2}/${FILE}_1.fastq.gz"
    "${LANE2}/${FILE}_2.fastq.gz" --readFilesCommand gunzip -c
    --outFileNamePrefix "$STAR_OUT/$FILE" --outTmpDir
    $STAR_OUT/STAR_TEMP --outSAMtype BAM SortedByCoordinate
    --outFilterScoreMinOverLread 0.3 --outFilterMatchNminOverLread
    0.3 --outFilterMultimapNmax 20 --alignSJoverhangMin 8
    --alignSJDBoverhangMin 1 --outFilterMismatchNmax 999
    --outFilterMismatchNoverReadLmax 0.04 --alignIntronMin 20
    --alignIntronMax 1000000 --alignMatesGapMax 1000000
```

Figure 3.1: STAR alignment

Quality control Samples were judged based on raw count numbers, as well as read assignment, alignment, and normalized gene coverage (Fig 3A.1, 3A.2). Together, six samples were removed from downstream analyses. Two samples immediately failed to sequence, as clearly highlighted by the lack of reads (3A.1A). Primary alignments to the genome (3A.1B) showed consistency across samples, and STAR mapping by sample per sequencing run shows consistency across sequencing run (3A.1C).

Normalised position against coverage was used to measure 3' prime bias, as this is often the result of RNA degradation. Here, a few samples show reduced coverage at the 5' end (Figure 3A.2). Samples which showed bias coverage towards the 3' end and had lower genome alignment to coding regions were removed from downstream analyses. High-level QC was then performed through cluster analyses and gene mapping using DESeq2 (below).

DESeq2 Counts were corrected for effective library size in R using DESeq2 [214]. Normalized gene counts were fitted to a negative binomial distribution. A batch effect was introduced during sample collection, as discussed below. A model that included this batch effect was fitted to every gene and the significance of the model's coefficients was assessed using the Wald test.

Counts were transformed via variance stabilising transformation (VST). VST transformed counts were used for all plotting, unless otherwise stated. The R package Limma was used to model the batch effect in PCA and heatmap figures. Uncorrected plots are shown in the chapter appendix. Box plots show median + interquartile range (IQR), with 1.5*IQR whiskers. Principal component analysis (PCA) was performed using the top 5000 ENSEMBL genes ranked by standard deviation. Sample distances are proportional to Mahalanobis distance, and ellipses show the 95% CI of a conditions gene expression distribution. Hierarchical clustering was done on transformed counts using Euclidean distances and complete linkage. Gene expression dot plots were created using median VST counts, and coloured by gene expression. Dot sizes are calculated as exponential VST counts to reflect differences in more highly expressed genes. Due to the range of base means in sexually dimorphic genes, dot sizes here match VST counts. Gene enrichment within neuronal subtypes was calculated using VST counts, and was defined as genes with a subpopulation mean within the top 75% of expressed genes, across contralateral samples.

Heatmaps were generated from transformed counts and visualized using "complex heatmaps" [215]. GSEA analyses were performed using ranked $\log_2$ fold changes via msigdbr [216] and clusterProfiler [217] libraries.

3.2.6.2 Custom GSEA

Deep RNA-seq of naïve DRG subpopulations has been previously performed elsewhere [5]. Eight DRG subpopulations were studied after transgenic labelling and fluorescent sorting, with 3-5 samples per population (mixed sex, multiple mice per sample). These populations include non-peptidergic (NP) and peptidergic (PEP) nociceptors, C-LTMRs, Aδ-LTMRs, Aβ-SA1-LTMRs, Aβ-Field-LTMRs, Aβ-RA-LTMRs, and proprioceptors (PROP). Full methodology can be found in their published report [5].

I curated these results into subpopulation-enriched gene sets to probe enrichment in the current data. RNA-seq count data was accessed from `https://www.ncbi.nlm.nih.gov/geo/` (GSE131230). Expression data was generated via STAR alignment and HTSeq on the same genome build, mirroring the current study [5]. Counts from Zheng and colleagues were then corrected for library size and transformed via rlog in R using DESeq2 to match their published report [214]. Principal component analysis (PCA) was performed using the top 5000 ENSEMBL genes ranked by standard deviation. Genes were then filtered across all samples for a mean rlog greater than 0, to mirror their filtering criteria. From this filtered dataset, 95% quantiles were determined for each gene. Within each subpopulation, genes with a mean rlog above the 95% quantile cut-off were curated into a 'gene set' for subpopulation enrichment. These custom gene sets were compiled for a GSEA analysis to our contralateral ("naïve"-like) samples using the clusterProfiler package in R. Here, GSEA analyses were performed using ranked fold changes from mean(subpopulation)/mean(total) VST counts per contralateral samples.

3.2.6.3 Within population sex differences

Recent spatial-seq data has highlighted within-population sex differences in humans [24]. The current study is well powered to explore this in murine DRG populations.

Hypothesis testing for each population was performed on genes with at least 10 combined reads across all contralateral samples (35609 ENSEMBL genes) and was performed using the Wald test and a weighted FDR correction (independent

hypothesis weighting, IHW). IHW first weights p-values by mean expression, before correcting for multiple hypothesis testing by Benjamini Hochberg (BH). This increases our power to detect differences in highly expressed genes. A Cook's distance cutoff was set as the .99 quantile to filter genes with excessive variation. Effect sizes were calculated using Bayesian shrinkage estimators (the *apeglm* method, via DESeq2) and are presented as moderated (shrunken) $\log_2$ fold changes (LFC) [218].

Sixteen samples were processed across time points for each population, with 8 male and 8 female samples each. The NP sample set is composed of 7F + 9M, due to breeding availability. Only 15 samples passed QC for nociceptors (7M + 8F).

Gene ontology (GO) was performed on differentially expressed genes in R using the goSeq library (FDR < 0.05, LFC > 1) [219]. P-values were calculated by the default Wallenius method. Here, filtered count data of non-DEG genes were used as a background, with a cut-off requiring 10 reads across samples. clusterProfiler (R) was used for GSEA analyses, with BH correction. Extended supplementary tables for DEGs and pathway analyses are available on github (`https://github.com/aliibarry/thesis-supp`).

3.2.7 Data accessibility

This dataset highlights molecular changes in sensory neuron subtypes across multiple timepoints in a murine neuropathic pain model. We see this as a useful resource for the field. To improve the accessibility of this data, I developed an open-source database through Shiny (R), hosted by the Interactive Data Network at the University of Oxford. This allows users to query and plot genes of interest across subtypes and conditions, as well as download corresponding results. It is currently available on a test server, at `https://trainingidn.shinyapps.io/drg-directory/`.

3.3 Results

3.3.1 RNA-seq overview

Using transgenic labelling of neuronal DRG subtypes, 160 lumbar DRG samples were sequenced 3 day and 4 weeks after SNI (Fig 3.2A). This includes five neuronal

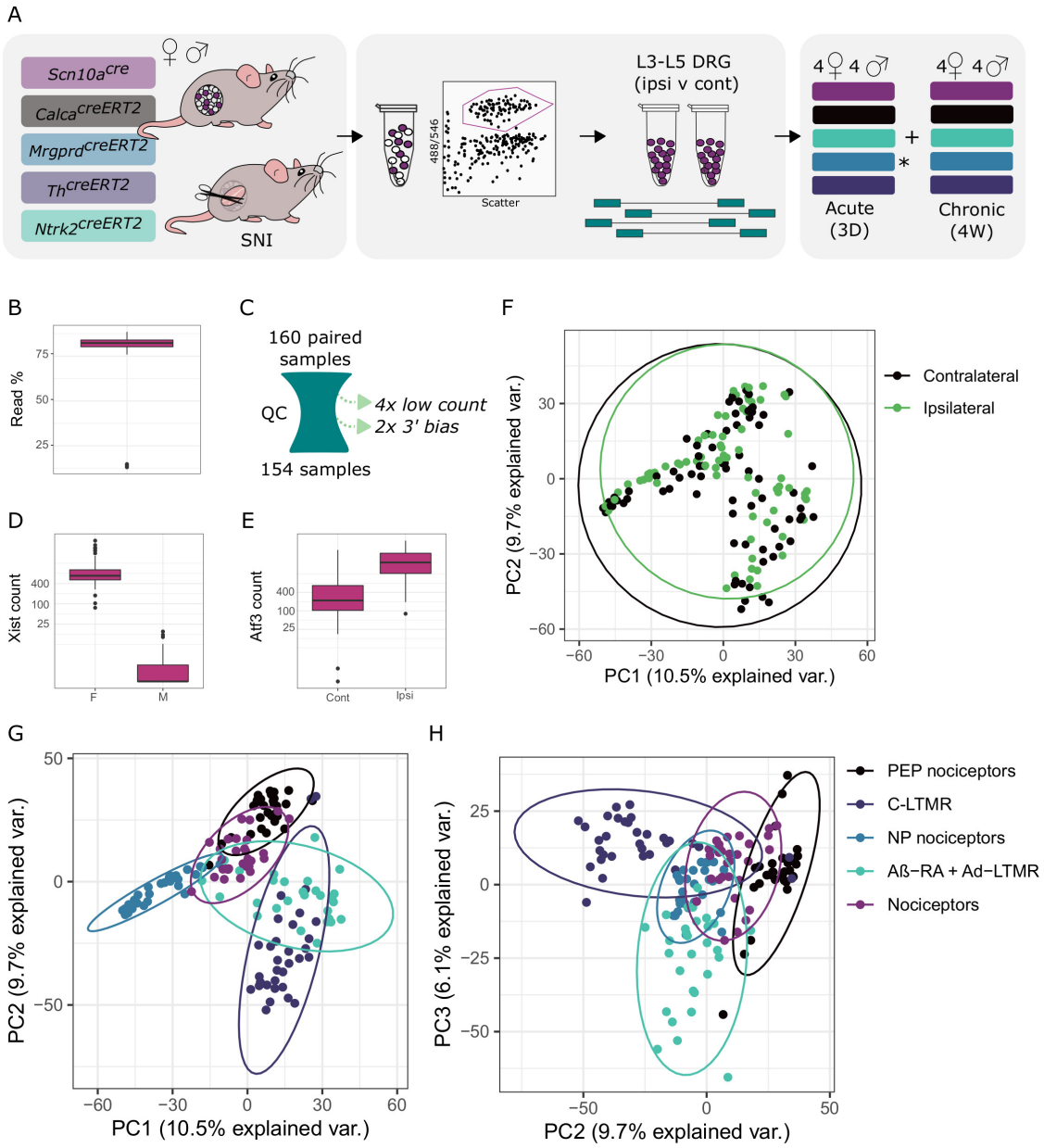

Figure 3.2: Subpopulation RNA-seq overview. A. Sample collection schematic, using transgenic mice to label five subpopulations of interest. Ipsilateral (ispi) and contralateral (cont) lumbar DRG were collected at 3 days and 4 weeks after SNI. B. Uniquely mapped reads per sample, prior to filtering. C. Six samples were removed prior to downstream analysis - 2 for low counts, and 4 for 3' bias, suggesting poor RNA quality. D. *Xist* count data for male (M) and female (F) samples. E. *Atf3* count data for contralateral (cont) and ipsilateral (ipsi) samples. F. PCA bi-plot by injury condition. G-H. PCA bi-plot by DRG subpopulation, components 1:2 (G) and 2:3 (H).

subtypes introduced in chapter 2: general nociceptors, encoded by Scn10a$^{\text{cre}}$ (nociceptors), peptidergic nociceptors from Calca$^{\text{creERT2}}$ (PEP/peptidergic), non-peptidergic nociceptors by Mrgprd$^{\text{creERT2}}$ (NP/non-peptidergic), C-low threshold

mechanoreceptors encoded by $Th^{creERT2}$ (C-LTMRs) and $Ntrk2^{creERT2}$ expressing LTMRs (Aβ-RA + Aδ-LTMRs). We recognize that our general nociceptor population expressing Scn10a is not exclusively high threshold afferents. C-LTMRs are included within this subtype, based on the coexpression of *Th* and *Scn10a*. They make up a much smaller proportion of overall cells than the peptidergic and non-peptidergic nociceptor subpopulations, resulting in a "nociceptor-like" population.

3.3.1.1 Quality control

Together, 154 samples passed QC, removing samples with low read counts or 3' bias (3.2B-C). Male and female samples are clearly distinguishable by sex-linked genes such as *Xist* (3.2D), and ipsilateral ("injured") samples can be distinguished from contralateral controls by key injury markers such as *Atf3* (3.2E).

A batch effect was introduced on the first sample collection day, affecting paired (ipsilateral and contralateral) samples for $Calca^{creERT2}$ and $Scn10a^{cre}$ females (3A.3). This effect was modelled into all downstream analyses (see methods).

Sensory neurons undergo broad, stereotyped changes after injury [33]. Even so, samples largely cluster by neuronal subtype across conditions (3.2F-H). While the bulk subpopulation methodology employed here allow deep sequencing within populations, each resulting sample contains a mix of injured and intact neurons from ipsilateral ganglia. This cell mixture likely dampens the stereotyped changes seen previously in single cell RNA-seq [33].

3.3.2 Naïve neuronal subtypes

Analyses were first performed on contralateral ("naïve") samples. As expected, samples initially cluster by batch before clustering by subpopulation. General nociceptors (nociceptors), as well as peptidergic and non-peptidergic nociceptor subpopulations largely separate from C-LTMRs and *Ntrk2*-labelled Aβ-RA + Aδ-LTMRs (Fig 3.3, 3A.3C-D).

In line with previous reports, hallmark gene expression can be seen within each population (Figure 3.4A). Voltage gated sodium (*Scn*) channels, transient receptor

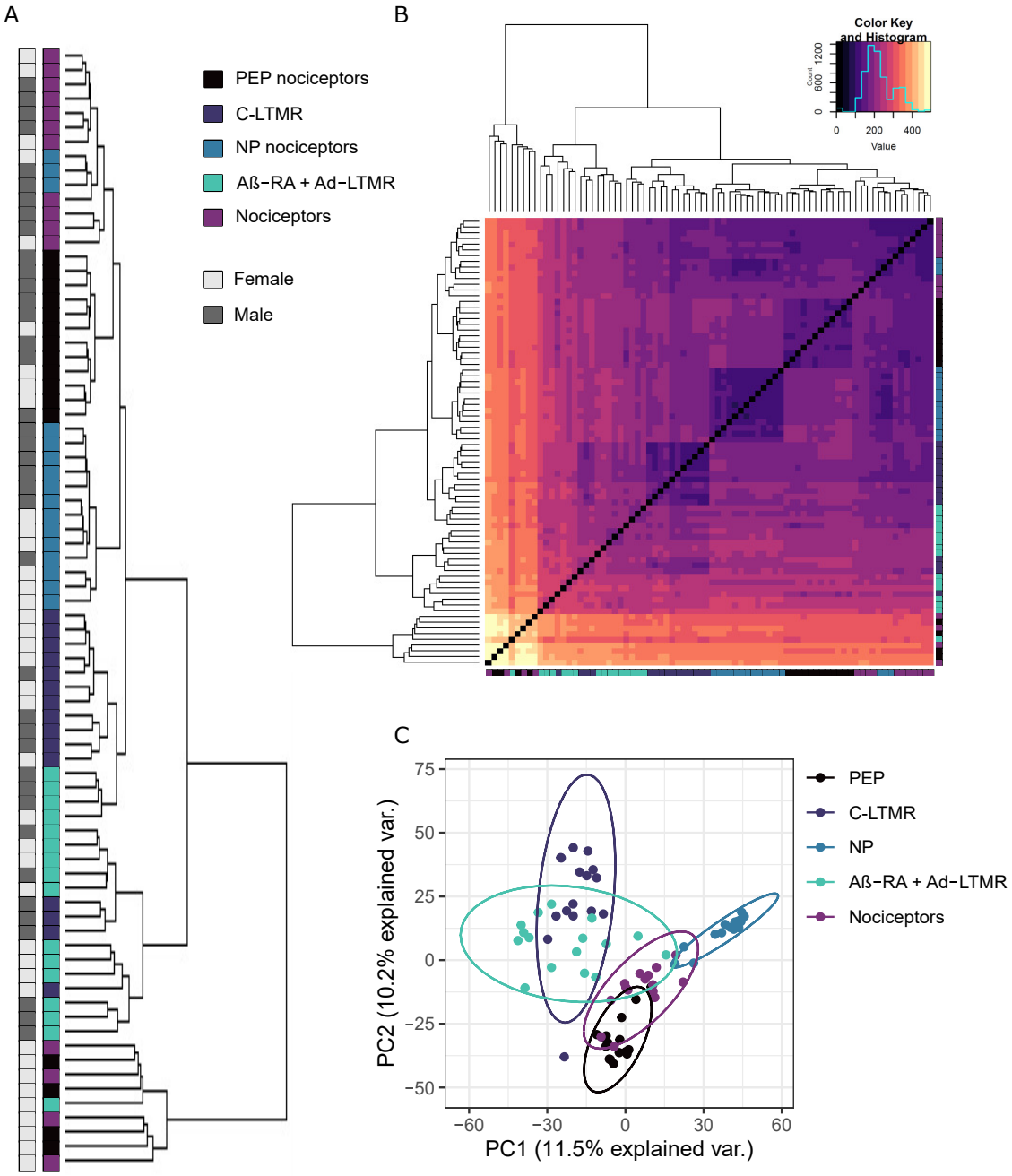

Figure 3.3: Naïve (contralateral) DRG subpopulation RNA-seq clustering from combined 3 day and 4 week samples. A. Dendrogram highlighting subpopulation and sex for each sample. B. Heatmap of contralateral sample clustering. C. PCA bi-plot for contralateral samples, coloured by population. n = 15-16 mice/subtype.

potential (*Trp*), acid-sensing (*Asic*), γ-aminobutyric acid (GABA) receptors (*Gabra*), and potassium channels (*Kcn b/c/k*) show varying subtype specificity (Figure 3.4B).

Scn10a and *Scn11a* are enriched in high threshold populations, whereas *Scn1a* is

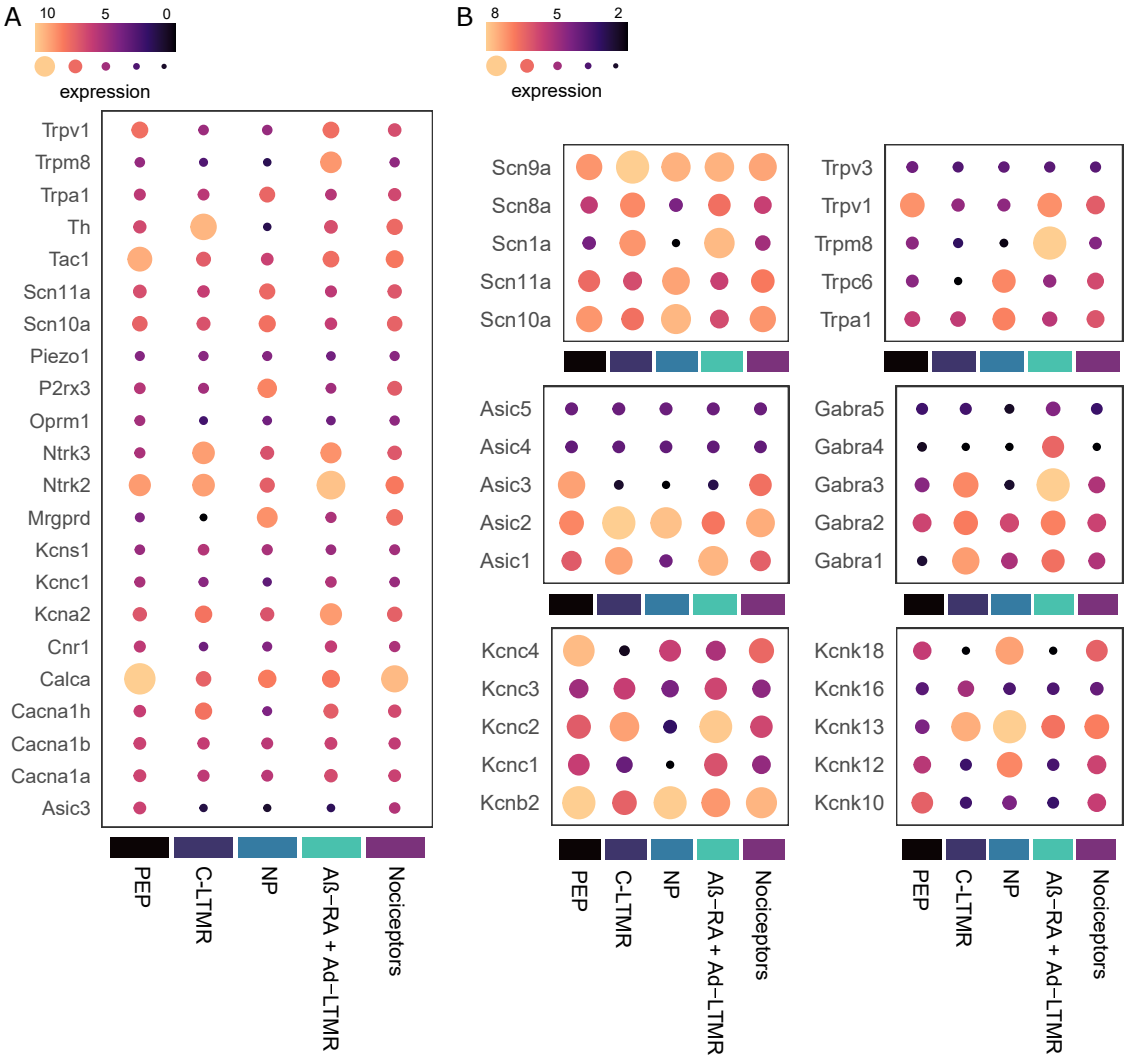

Figure 3.4: Normalized median gene expression from combined 3 day and 4 week contralateral samples. A. Selected genes across neuronal subtypes. B. Selected common ion channels across subtypes. n = 15-16 mice/subtype. Voltage gated sodium (*Scn*), transient receptor potential (*Trp*), acid-sensing (*Asic*), γ-aminobutyric acid (GABA) receptors (*Gabra*), and potassium channel (*Kcnb/c/k*) genes are highlighted

.

enriched in LTMRs. *Mrgprd* and *Mrgpr* family members, *P2rx3*, *Pirt*, and *Trpa1* are enriched in non-peptidergic nociceptors, in line with previous reports. *Ntrk2*, *Scn1a*, and *Trpc1* are enriched in Aβ-RA + Aδ-LTMRs, whereas *Th*, *Tafa4*, *Gfra2*, and *Slc17a8* (VGLUT3) are all enriched in C-LTMRs (Fig 3.4). Key peptidergic markers such as *Calca* and *Trpv1* do not hit our enrichment filtering criteria, likely due to strong expression in both peptidergic and general nociceptor populations (3.4).

Two-pore potassium channels (K2Ps) have been implicated in various pain

conditions, including the role of *Kcnk18* (TRESK) in migraine [220, 221]. We see a range of subpopulation enrichments for this gene family in our dataset. *Kcnk13* (THIK-1), *Kcnk12* (THIK-2), and *Kcnk18* (TRESK) are all enriched in non-peptidergic nociceptors. *Kcnk16* (TALK-1) is enriched in C-LTMRs. *Kcnk10*, encoding the TREK-2, has previously been implicated in spontaneous pain in rats, with expression limited to IB4-binding neurons [222]. Here, we see higher expression in peptidergic nociceptors (3.4). This peptidergic-enrichment profile is supported by the transcriptional data published by Zheng and colleagues [5], and was validated in house using *in situ* hybridization against *Kcnk10* (Fig 3A.4).

Trpm8, typically a marker of cold-sensing nociceptors, is enriched in Aβ-RA + Aδ-LTMRs, with lower expression in peptidergic nociceptors (Figure 3.4). This contrasts reports previous subpopulation RNA-seq, suggesting enrichment in C-LTMRs, peptidergic nociceptors, and Aδ-LTMRs [5]. It is unclear if this discrepancy reflects a variation across transgenic approaches, individual animal differences, or is a results of using contralateral samples as "naïve-like" controls.

3.3.3 Dataset comparisons

To validate our sequencing approach, gene enrichment analyses were performed against previously published naïve subtypes (Fig 3.5). Count data were transformed using DESeq2, mirroring our analysis to generate eight subpopulation-specific groups, as defined by Zheng and colleagues. These populations include non-peptidergic (NP) and peptidergic (PEP) nociceptors, C-LTMRs, Aδ-LTMRs, Aβ-SA1-LTMRs, Aβ-Field-LTMRs, Aβ-RA-LTMRs, and proprioceptors (PROP). Gene sets were then generated for each neuronal subtype, based on a 95% confidence interval threshold and range in size from 36 to 1583, with a median count of 546 (3.5C).

Our samples correlate strongly to this data (Fig 3.5D, Table 3A.1 + Fig 3A.5 - 3A.9). Our non-peptidergic (NP) samples are positively enriched for the NP gene set, and negatively enriched for all other gene signatures. To complement, our peptidergic (PEP) samples show strong positive enrichment for PEP, as well

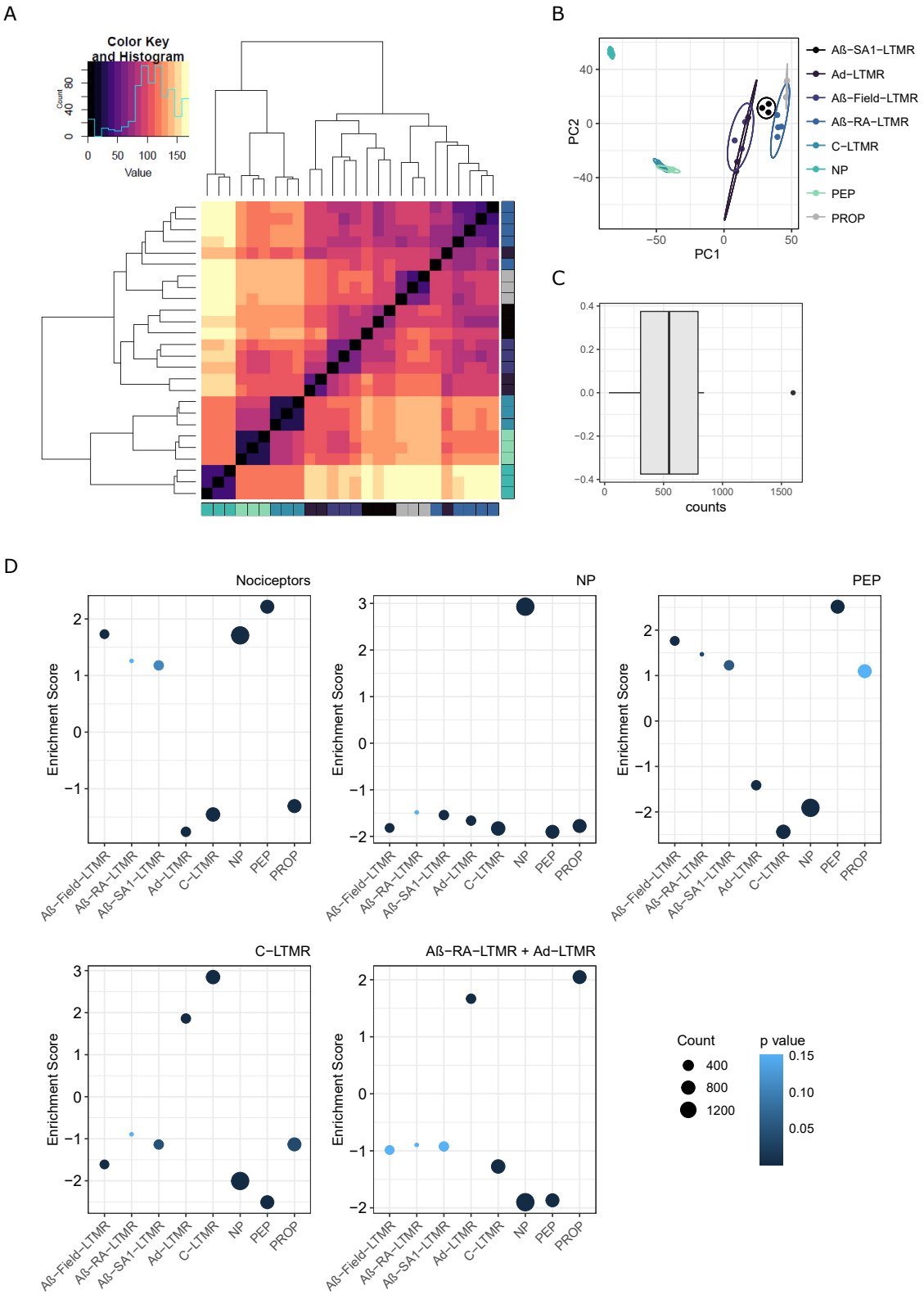

Figure 3.5: Comparison to previously published, naïve subpopulation RNA-seq. Caption continued below.

Figure 3.5: Comparison to previously published, naïve subpopulation RNA-seq. A-B. Hierarchical clustering (A) and PCA bi-plot (B) of previously published RNA-seq subpopulation transcriptomes [5]. C. Custom gene set sizes, ranging from 36 to 1599 terms. D. GSEA enrichment for each neuronal subtype, coloured by adjusted p-value. Dot sizes reflect the gene count within each set. Normalized enrichment scores and p-values are listed in Table 3A.1.

as negative enrichment for NP and C-LTMR signatures. Enrichment scores and adjusted p-values are listed in Table 3A.1.

Our *Scn10a* population appears to be largely nociceptor, with positive enrichment for both peptidergic and non-peptidergic populations. Negative enrichment is seen for C-LTMRs, likely reflecting subpopulation proportions within this broad grouping. Unlike our peptidergic population, our general nociceptor is negatively enriched for the proprioceptive signature. Both our nociceptor and peptidergic nociceptor populations show negative enrichment for the Aδ-LTMR gene set, but positive enrichment of Aβ-Field-LTMR signatures.

C-LTMRs are highly enriched for the C-LTMR gene set, along with a positive enrichment of Aδ-LTMRs. Correspondingly, this population shows negative enrichment of high threshold populations (NP and PEP), along with the proprioceptive and Aβ-Field-LTMR signatures.

Aβ-RA + Aδ-LTMRs show positive enrichment for the proprioceptive gene set, followed by enrichment for Aδ-LTMRs (3A.9). As expected, this population also shows negative enrichment of high threshold signatures.

Together, these enrichments lend confidence to our methodology and support the use of this dataset to interrogate population sex differences and as a baseline against injured neurons.

3.3.4 Subtype sex differences

With many clinically-relevant pain conditions showing sexual dimorphisms, there is a keen interest to explore sex differences within each DRG subtype transcriptome. Across subpopulations, most genes are expressed to similar levels in males and females (Fig 3.6). Differentially expressed genes (DEGs) are defined as an FDR

< 0.05 and an absolute $\log_2$ fold change (LFC) > 1. From this, only six genes were significantly regulated between males and females in all populations, each X- or Y- linked (*Kdm5d*, *Uty*, *Ddx3y*, *Eif2s3y*, *Tsix*, *Xist*) (Table 3A.2). *Gm29650*, which is also sex-linked, was differentially expressed in 4/5 populations. The only other DEG shared across any subtypes is *Sprr1a*, which is more highly expressed in male nociceptors and non-peptidergic nociceptors. *Sprr1a* has been previously described for it's upregulation in female DRGs after injury, although baseline expression differences were not studied [76].

This absence of a large sensory-neuron wide sex signature fits previous work in mice, where all but one DEG reported in adult, lumbar DRG were X- or Y-linked [223]. Nine autosomal genes were found to be regulated in sacral DRG [223], and these do not overlap with the DEGs reported within populations here, with the exception of *Clvs1* in Aβ-RA + Aδ-LTMRs.

At a subpopulation-level, a stronger sexual dimorphism emerges. The majority of DEGs are seen within unique neuronal subtypes (Fig 3.6). We see predominant changes within Aβ-RA + Aδ-LTMRs (202 genes with FDR < 0.05, LFC > 1), with few differences in the other populations. Across populations, many genes hit an FDR < 0.05, but moderated fold changes suggest negligible (near 0) fold changes in these genes (Fig 3.6C-D).

GO term analyses highlight enrichment for ion channel transport and transmembrane transport in females, although few genes are implicated in each (Fig 3.6F). GSEA analyses against all gene sets available from Molecular Signatures Database (MSigDB) show no enrichments in this population.

In the four other populations studied, most GO terms centre around sex-linked processes. Other relevant GO pathways include the detection of temperature stimulus involved in sensory perception of pain (nociceptors), immune response and cholinergic synaptic transmission (PEP), regulation of sensory perception of pain (NP), and chemosensory behavior (C-LTMR). All supplemental tables for DEGs and pathway analyses, including full DEG tables, GO, and GSEA analyses for each subpopulations are available at `https://github.com/aliibarry/thesis-supp`.

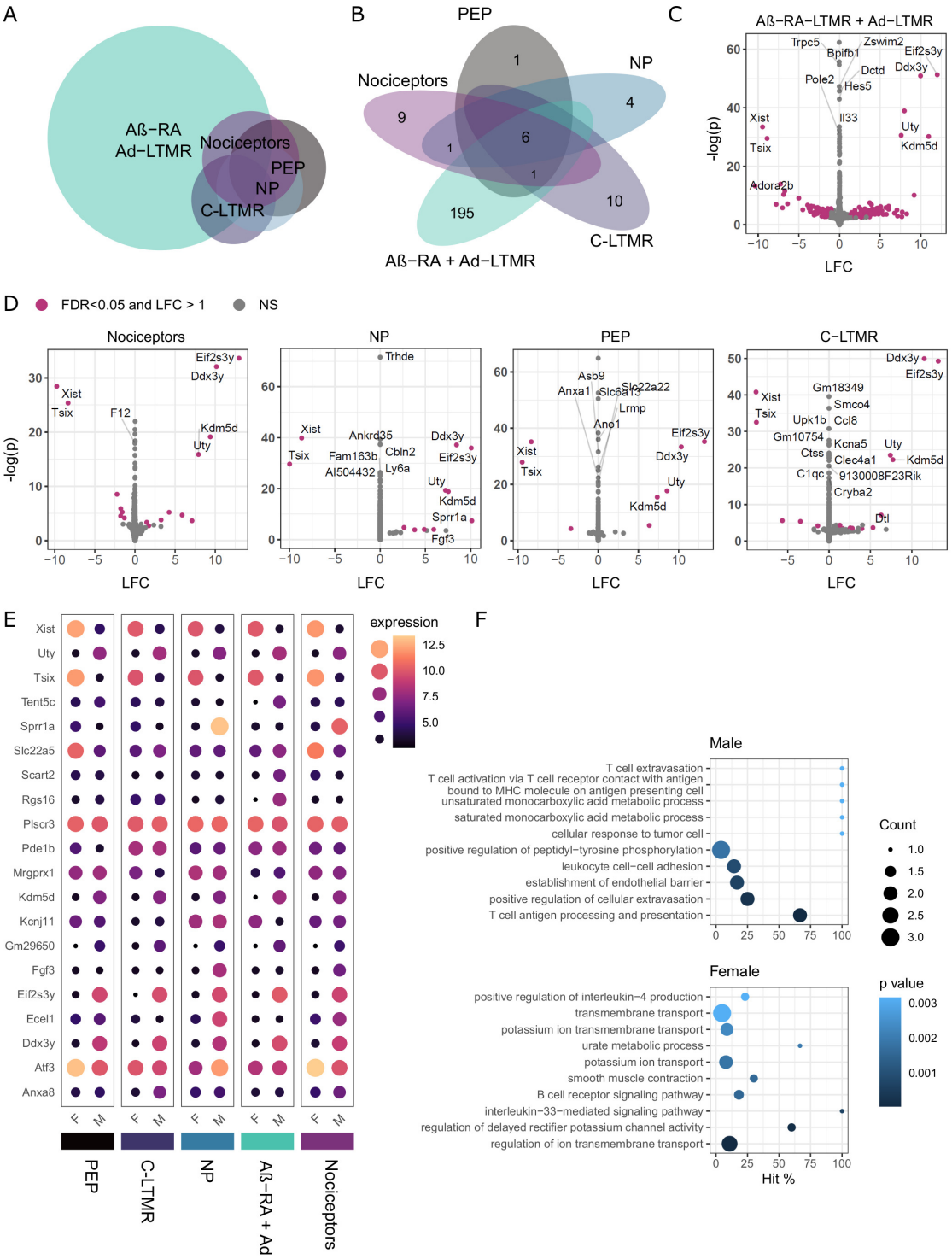

Figure 3.6: Within population sex differences for contralateral ("naïve") samples. Caption continued below.

Figure 3.6: Within population sex differences for contralateral ("naïve") samples. A. Venn diagram highlighting the number of DEGs per subtype (FDR < 0.05, log fold change (LFC) > 1). B: Euler plot highlighting proportions of DEGs by subtype. C-D. Volcano plots per subtype, showing large fold changes in sex-linked genes. LFC shrinkage was performed using the *apeglm* method in DESeq2. E. Dot plots highlighting key DEGs. F. Top 10 GO term enrichment for male (up) and female (down) regulated terms in Aβ-RA + Aδ-LTMRs.

3.4 Discussion

We performed RNA-seq on five neuronal subtypes in a neuropathic pain model. These populations were introduced in chapter 2, and include: general nociceptors, encoded by Scn10a^{cre} (nociceptors), peptidergic nociceptors from Calca^{creERT2} (PEP/ peptidergic), non-peptidergic nociceptors by Mrgprd^{creERT2} (NP/ non-peptidergic), C-low threshold mechanoreceptors encoded by Th^{creERT2} (C-LTMRs) and Ntrk2^{creERT2} expressing LTMRs (Aβ-RA + Aδ-LTMRs) (3.2). These populations are defined here by transcriptional signatures, but are known to show differences in soma and axon diameters, ligand-receptor expression profiles, and electrophysiological properties.

Initial clustering shows contralateral and ipsilateral samples clustering by population across timepoints, likely due to the heterogeneity of injured and intact neurons within the ipsilateral samples. A batch effect is visible in paired samples from one collection day, and this was included as a two-level factor in each linear model fit across genes. Across timepoints, the upregulation of injury-specific genes (eg. *Atf3*) can be seen in ipsilateral samples.

We validated our baseline dataset by combining contralateral samples from 3 day and 4 week samples (3.3). As expected, hallmark gene expression is seen within each neuronal subtype (3.4).

Recent work suggests a TRKC+/TH+ population of primary afferents involved in cardiovascular homeostasis [185]. This population appears to be enriched in lumbar DRG, and comprises a fraction of TH+ neurons. We also see higher expression of *Ntrk3* (encoding TRKC) in our C-LTMR population, suggesting a more functionally-diverse subtype targeted by Th^{creERT2}. The implications of this TRKC+/TH+ in

painful states has yet to be explored, but any genetic manipulation of $Th^{creERT2}$ should consider this added diversity.

Previous RNA-seq analyses in these naïve subtypes have correlated the underlying molecular profile to electrophysiological readout [5]. Gene signatures in our dataset parallel this data from Zheng et al. [5], with a strong correlation between related subtypes. Here, our *Scn10a* population appears largely nociceptive, with a positive enrichment for PEP and NP nociceptors paired to a negative enrichment for C-LTMRs. We also see an enrichment of the Aβ-Field-LTMR signature, possibly due to the presence of myelinated A-HTMRs in this population. Our non-peptidergic population is highly enriched for the NP signature, while our peptidergic population is enriched for the PEP signature. In our data, we also see a strong signature for proprioceptive neurons and Aδ-LTMRs in our *Ntrk2* (Aβ-RA and Aδ-LTMR) population.

Technically, these results support our use of bulk, subpopulation specific RNA-seq samples for DEG analyses. We relied on NEB Ultra low/Smarter cDNA amplification due to limited tissue access (ie. unilateral, lumbar DRGs) and were able to successfully sequence subpopulation transcriptomes to a sufficient depth for DEG analysis. These analyses lend confidence in our dataset as we shift to examining injury signatures across timepoints in chapter 4.

3.4.1 Sexual dimorphism

Building on the overlapping gene signatures between datasets, we also highlight sexual dimorphism in murine neuronal subtypes (Fig 3.6).

In control samples, shared DEGs across subtypes are limited to sex-linked transcripts, with the exception of *Sprr1a*, which is enriched in male NP nociceptor (LFC ~10) and general nociceptors (LFC ~7) populations.

Sprr1a (small proline rich protein 1A), is an autosomal gene with a role in regeneration and axon outgrowth after injury [224, 225], possibly through an interaction with SOX11 [226]. It has previously been discussed in the context of sex differences in injured states, showing up-regulation in female mice (but not

males) 24 hours after sciatic nerve transection [76], although microarray data also shows strong upregulation in male DRG one week after SN transection [225], and immunohistochemistry supports upregulation in male DRGs after one week in both SN transection and crush models of neuropathic pain [224]. Earlier work focused on the role of *Sprr1a* after injury, with low (or "null") baseline levels reported in naïve states in these studies. With the advance of deep sequencing, we are able to more accurately probe lowly expressed genes, and the expression of *Sprr1a* is also seen by Zheng and colleagues across subpopuations in naïve states [5].

NP nociceptors also show sex differences in the basal expression of *Ecel1*, *Atf3*, *Cckbr*, and *Fgf3*, whereas *Pde1b* is enriched in female naïve peptidergic nociceptors (and is the only autosomal gene regulated across sex in this subtype). C-LTMRs show sex differences in *Cenpf*, *Mrgprx1*, and *Anxa8*, among others, although previous work on C-LTMRs in our group show no differences in behavioural assays across sex in naïve states [179]. In each case, the functional implications of changes remain unclear, and warrant further study.

We see the largest number of DEGs in Aβ-RA-LTMRs and Aδ-LTMRs (D-hairs), corresponding to *Ntrk2*-expressing neurons. Few investigations have focused on sexual dimorphism in Aβ-RA-LTMRs and Aδ-LTMRs, and all behavioural readouts during the initial baseline and injury phenotype characterizations for the Ntrk2$^{\text{creERT2}}$ were performed on male mice [21]. Our data shows female GO term enrichment for transmembrane transport, potassium ion transmembrane transport, and regulation of ion transmembrane transport, as well as nervous system process, hinting at possible differences in excitability between sexes in this population. These differences is may be driven by a number of regulated channels, such as an over expression of potassium (*Kcnj11* and *Kcns1*) and calcium (*Cacng2*) channels in female samples.

BDNF and TRKB Mechanisms of sexual dimorphism in basal states suggest a developmental origin. Brain-derived neurotrophic factor (BDNF) is one of multiple well established ligands of TRKB, and is a possible candidate: It plays a role in both

early development and neuronal plasticity later in life. It shows sexual dimorphism across tissues [227]. It's general effect on Aβ-RA-LTMRs and Aδ-LTMRs through TRKB lets us speculate at a possible mechanism underlying the changes seen here.

In the skin, BDNF exerts a clear role on the development and maintenance of TRKB-expressing neurons [228, 229]. Overexpressing BDNF results in an increased hair follicle innervation, more Merkel cells, and larger Meissner corpuscles [228]. When knocked out, no Meissner corpuscles are present [229]. Female mice also show an increase in scratching behaviour in the absence of BDNF compared to males, although this behavioural assay is not exclusive to *Ntrk2*-LTMRs [230].

The BDNF-TRKB signaling pathway has been implicated in sex-specific sensory innervation, with differences in male and female mammary glands [165]. Here, TRKB-expression axons are pruned in the mammary glands of male E13 mice (but not female) in response to BDNF. This stems from the divergent expression of a truncated TRKB isoform in male neurons in response to androgen expression. This truncated form can then sequester BDNF so it no longer contributes to neuronal development [165]. Gene-level transcript abundances were quantified for the current study, but reanalysis at an isoform-level using Salmon [231] or equivalent can tease out isoform expression levels in our lumbar DRG data.

BDNF-TRKB signalling is also implicated in painful states in both mice and rats, with sexual dimorphic hyperalgesic priming reported specifically in mice [133, 232]. Taken together, this hints at a possible broader mechanism of sexual dimorphism in this population, but the functional implications in naïve, adult mice remain understudied.

Tamoxifen Studying sexual dimorphism in tamoxifen-induced Cre-lines comes with a confound, as tamoxifen is an estrogen analog. We can not exclude the possibility in the current analyses that tamoxifen administration in 4/5 transgenic lines alters gene expression in male and female mice differently. Posthoc validation in naïve tissue or pseudo-bulk analyses on annotated scRNA-seq data is required here.

Human comparisons Similar to murine sensory neurons, subtype-specific sex differences are present in humans which broad neuronal signatures fail to capture at a transcriptional level [24]. At a high level, most DEGs are not shared across studies, but transcript validation by *in situ*, as well as a detailed bioinformatic analyses of DRG sexual dimorphism between mouse and human will give better insight.

3.4.2 Conclusions

Deep sequencing of DRG subpopulations has previously been studied in a naïve state. Here, we complement these results with a lumbar-centric dataset, and build on this with subtype-specific sex differences. We validated our sequencing approach against previously published naïve data before presenting injury phenotypes in chapter 4.

3A Appendix

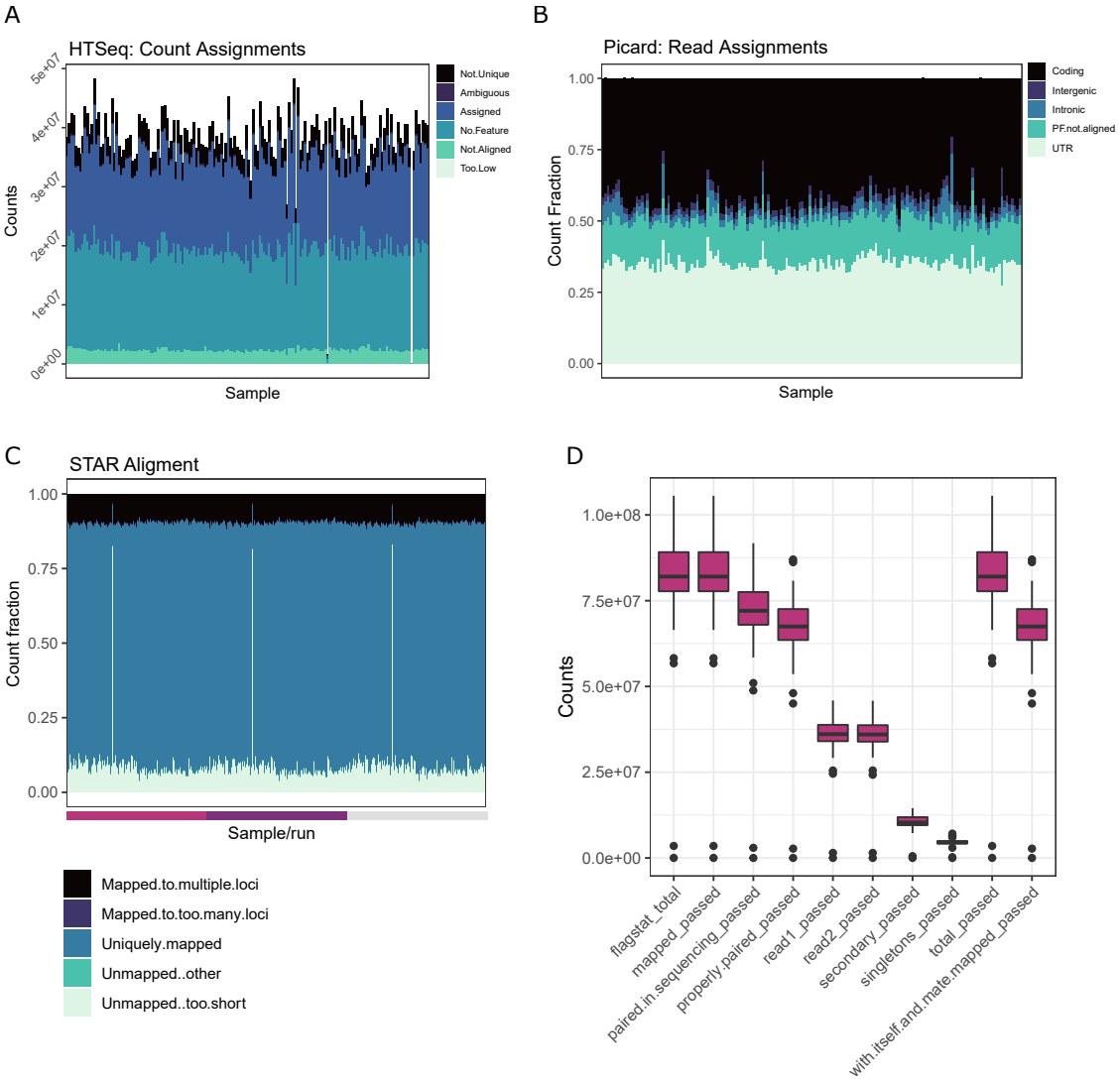

Figure 3A.1: Subpopulation RNA-seq quality control metrics (related to Figures 3.2 and 3.3). Data were compiled using MultiQC [233]. A. total count breakdown for each sample. Four samples have a noticeably lower read count and were removed from downstream analyses. B. Proportion of reads assigned to each classification. C: Proportion of reads mapped by STAR for each sample aliquot, separated by sequencing run (pink, purple, and grey sections). Mapping quality was similar across sequencing runs. D. Samtools flagstat output for key metrics

.

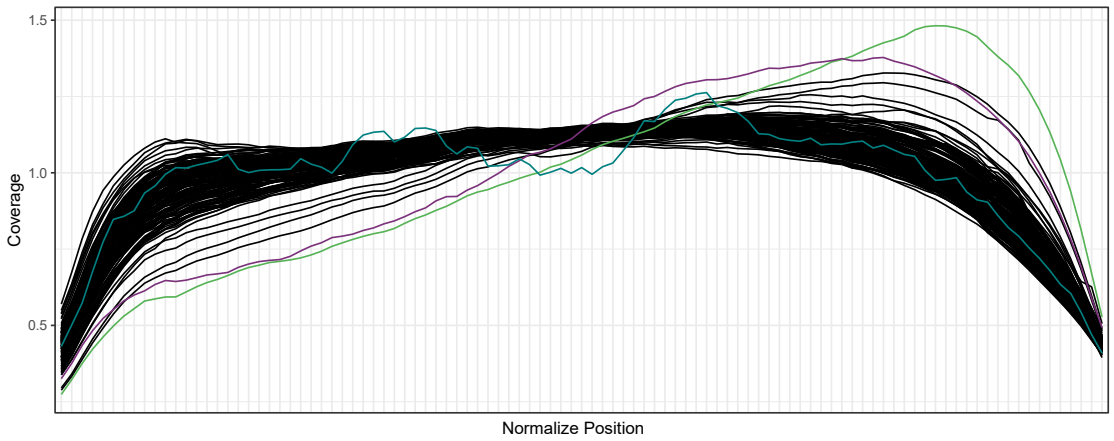

Figure 3A.2: Sequencing coverage, with biased/low-count samples coloured (purple + green). The cyan sample previously failed QC due to low read counts.

.

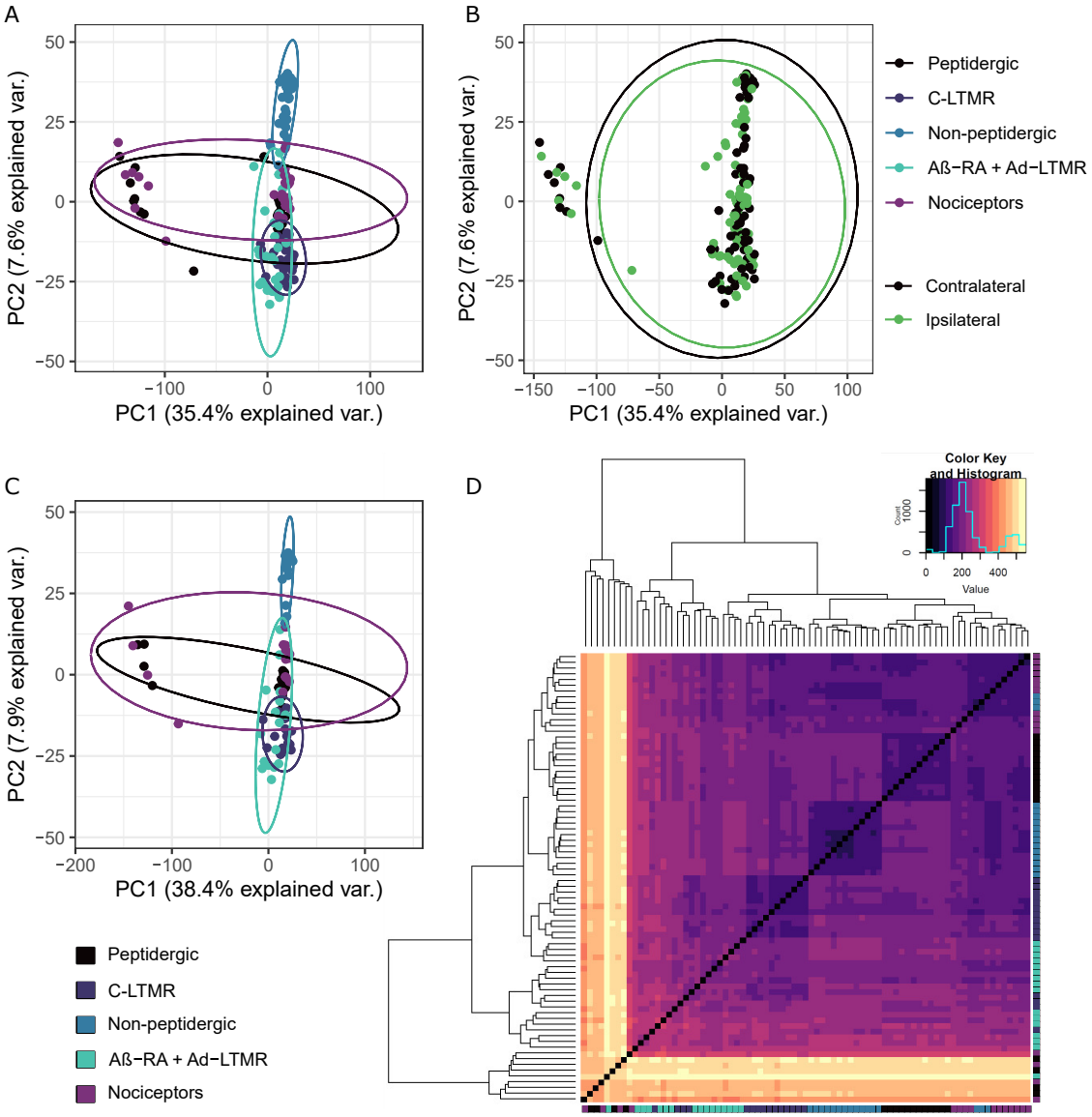

Figure 3A.3: Subpopulation RNA-seq without batch correction (related to Figures 3.2 and 3.3). A. PCA bi-plot by population, all samples. B. PCA bi-plot by condition, all samples. C: PCA bi-plot for contralateral (naïve) samples, by population. D. Hierarchical clustering of contralateral samples

.

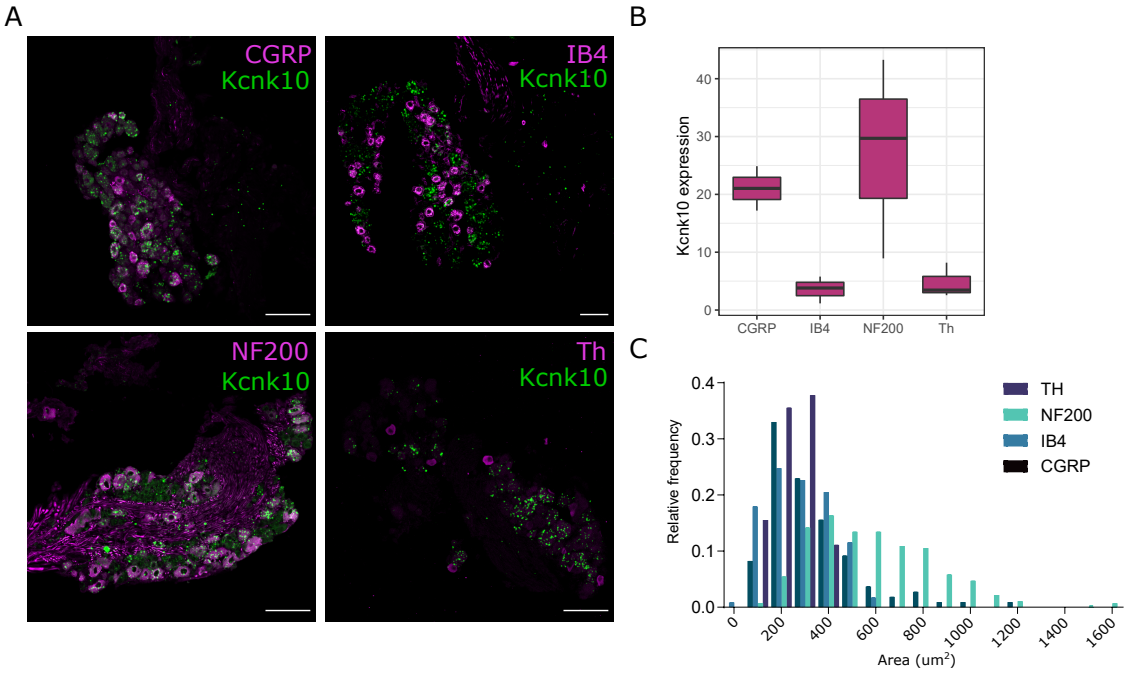

Figure 3A.4: *Kcnk10* is enriched in peptidergic nociceptors and A-LTMRs. We used *in situ* hybridization against *Kcnk10* in conjunction with antibodies to validate this finding. A. IHC and ISH for *Kcnk10* and subpopulation markers. B. Average *Kcnk10* expression by, averaged per mouse across subpopulations (n = 3 mice, excluding CGRP (n=2 mice)) C. Size profile histogram showing the range of subtypes covered by antibody stainings.

Table 3A.1: Gene set enrichment for naïve (contralateral) lumbar DRG, ranked by normalized enrichment scores within each neuronal subtype. Related to Figure 3.5

Population	Gene Set	Size	Score	p (adj)
Nociceptors	PEP	764	2.22	4.67E-69
	Aβ-field-LTMR	263	1.73	2.47E-08
	NP	1583	1.71	1.97E-34
	Aβ-RA-LTMR	35	1.26	1.51E-01
	Aβ-SA1-LTMR	317	1.18	1.06E-01
	PROP	765	-1.31	2.78E-06
	C-LTMR	836	-1.46	1.28E-09
	Aδ-LTMR	315	-1.76	4.16E-09
PEP	PEP	764	2.52	1.27E-105
	Aβ-field-LTMR	263	1.76	1.93E-07
	Aβ-RA-LTMR	35	1.47	3.79E-02
	Aβ-SA1-LTMR	317	1.23	6.47E-02
	PROP	765	1.10	1.75E-01
	Aδ-LTMR	315	-1.41	1.10E-03
	NP	1583	-1.91	4.44E-36
	C-LTMR	836	-2.44	7.43E-53
NP	NP	1583	2.93	2.40E-223
	Aβ-RA-LTMR	35	-1.48	3.14E-02
	Aβ-SA1-LTMR	317	-1.54	1.29E-04
	Aδ-LTMR	315	-1.66	1.54E-06
	PROP	765	-1.78	1.30E-18
	Aβ-field-LTMR	263	-1.82	1.17E-08
	C-LTMR	836	-1.83	1.17E-23
	PEP	764	-1.90	1.24E-26
C-LTMR	C-LTMR	836	2.85	2.49E-119
	Aδ-LTMR	315	1.86	1.70E-09
	Aβ-RA-LTMR	35	-0.89	6.16E-01
	PROP	765	-1.13	1.55E-01
	Aβ-SA1-LTMR	317	-1.14	1.90E-01
	Aβ-field-LTMR	263	-1.61	5.31E-03
	NP	1583	-2.00	6.36E-34
	PEP	764	-2.51	3.37E-66
Aβ-RA + Aδ-LTMRs	PROP	765	2.05	5.94E-30
	Aδ-LTMR	315	1.67	5.85E-08
	Aβ-RA-LTMR	35	-0.90	7.08E-01
	Aβ-SA1-LTMR	317	-0.92	7.08E-01
	Aβ-field-LTMR	263	-0.99	7.07E-01
	C-LTMR	836	-1.27	2.28E-03
	PEP	764	-1.87	6.74E-30
	NP	1583	-1.90	9.72E-72

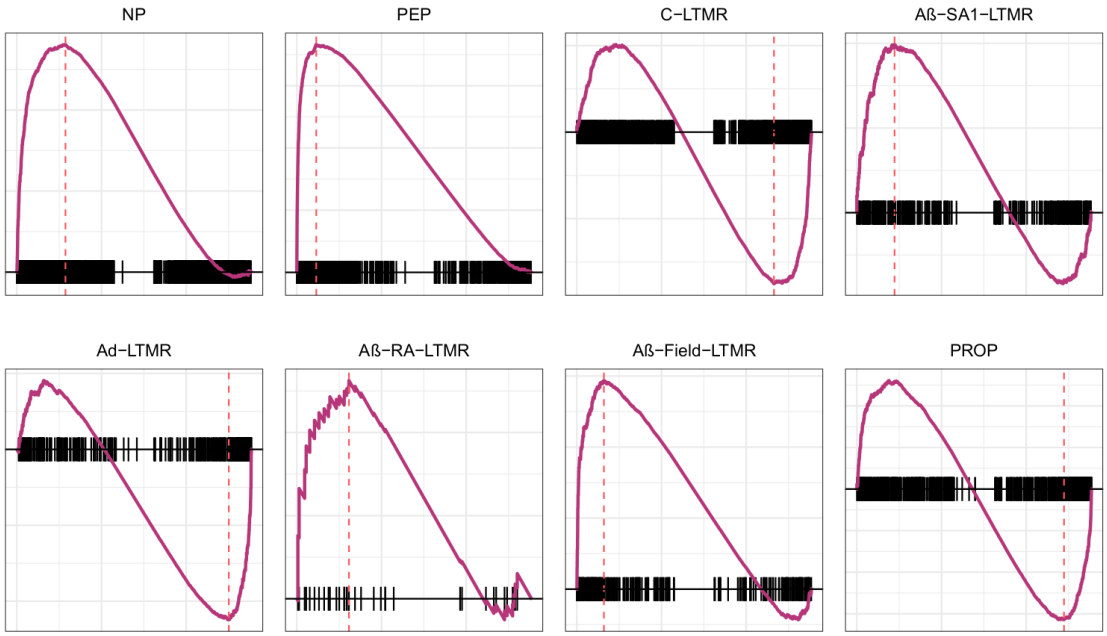

Figure 3A.5: Gene set comparison for Scn10a^{cre} to previously published, naïve subpopulation RNA-seq. Related to Figure 3.5

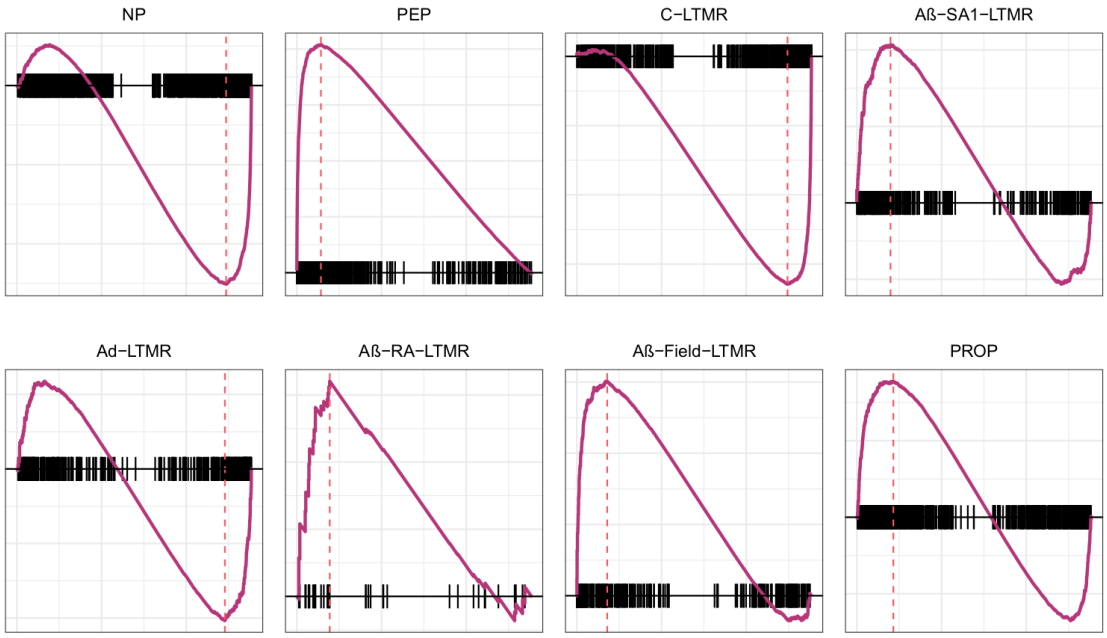

Figure 3A.6: Gene set comparison for Calca^{creERT2} to previously published, naïve subpopulation RNA-seq. Related to Figure 3.5

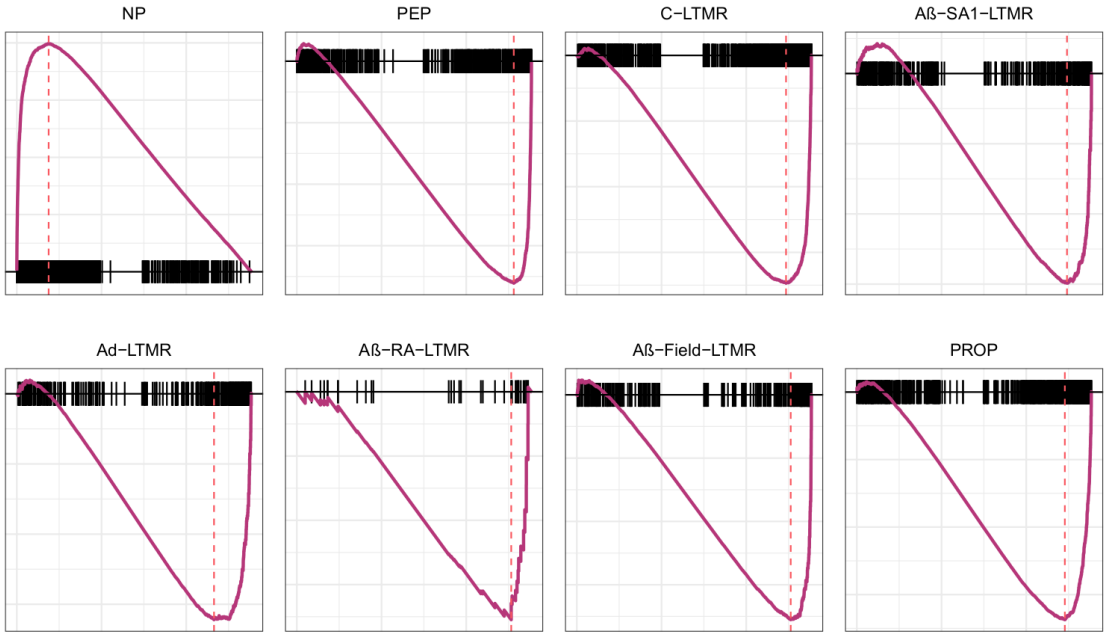

Figure 3A.7: Gene set comparison for Mrgprd^{creERT2} to previously published, naïve subpopulation RNA-seq. Related to Figure 3.5

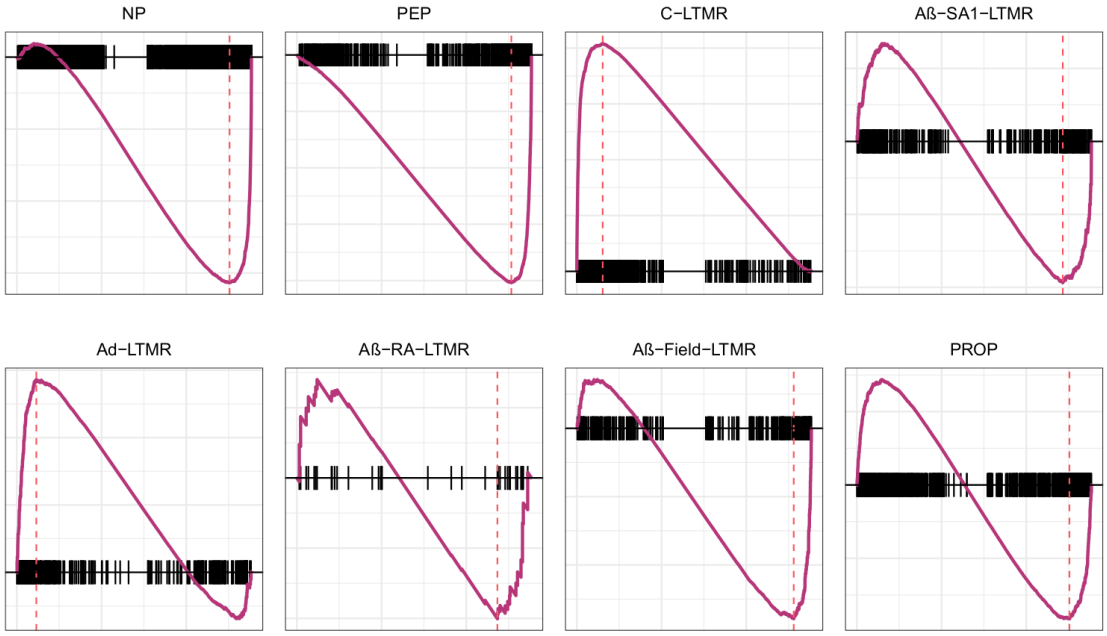

Figure 3A.8: Gene set comparison for Th^{creERT2} to previously published, naïve subpopulation RNA-seq. Related to Figure 3.5

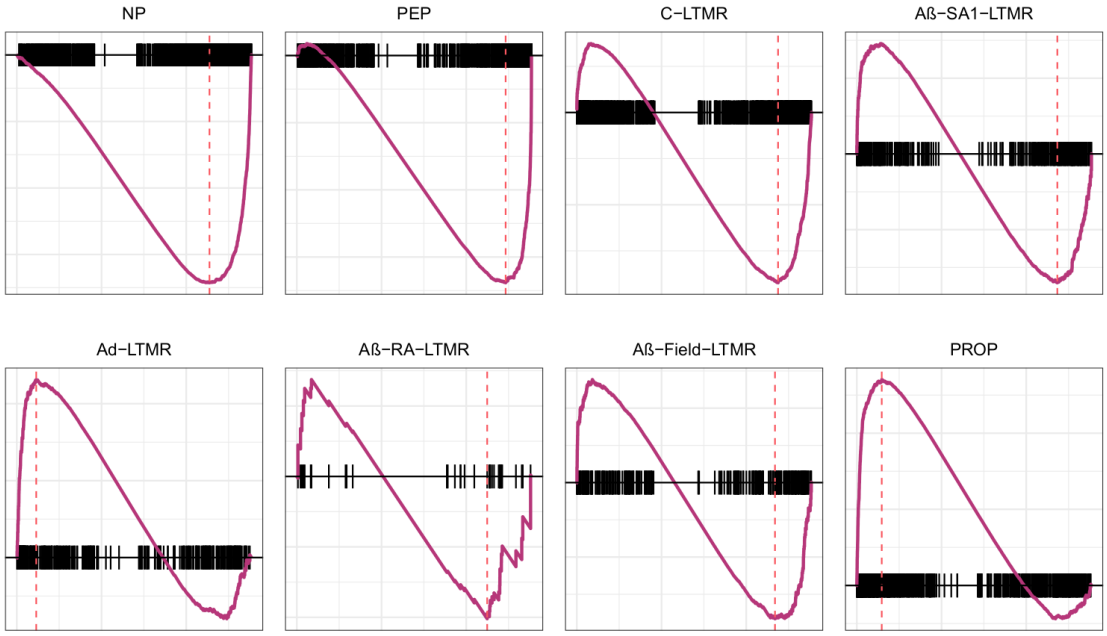

Figure 3A.9: Gene set comparison for Ntrk2^{creERT2} to previously published, naïve subpopulation RNA-seq. Related to Figure 3.5

Table 3A.2: Overlapping DEGs across multiple neuronal subtypes examined. General nociceptors (Noc.), peptidergic nociceptors (PEP), non-peptidergic nociceptors (NP), C-LTMRs (C-LT) and Aβ-RA + Aδ-LTMRs (A-LT). 1 = differentially expressed (FDR < 0.05, FC > 1), 0 = not significant. Related to Figure 3.6.

Noc.	PEP	NP	C-LT	A-LT	Gene
1	1	1	1	1	Kdm5d
1	1	1	1	1	Uty
1	1	1	1	1	Ddx3y
1	1	1	1	1	Eif2s3y
1	1	1	1	1	Tsix
1	1	1	1	1	Xist
1	1	0	1	1	Gm29650
1	0	1	0	0	Sprr1a

4

Deep RNA-seq of DRG subpopulations after injury

Sensory neuron subtypes show stereotyped and unique subpopulation signatures in injured states after nerve injury. While all populations contribution to a general injury signature at 3 days and 4 weeks post-SNI, subtype enrichment changes can also be seen, possibly driven by the loss of transected NP neurons by 4 weeks. Within populations, there is not a strong intersection of sex and injury, but sex differences in naïve states - particularly Aβ-RA + Aδ-LTMRs - still contribute to differences in injured neurons. In addition to providing injury signatures across subpopulations, we are contributing to a growing body of literature emphasizing the importance of studying sexual dimorphism in painful states.

Contents

4.1 Introduction

Here, I build on previous chapters with the deep sequencing of male and female sensory neuron subtypes in injured states. General quality control, validation against previously published work, and sex differences in naïve tissue are discussed in depth in chapter 3.

4.2 Methodology

4.2.1 Overview

Deep RNA-seq of mouse DRG subpopulations after injury was performed to query subtype-specific and shared injury signatures. Transgenic validation is described in chapter 2, and RNA-seq validation is described in chapter 3.

Briefly, spared nerve injury (SNI) was performed on transgenic animals, each labelling one of five sensory neuron subtypes of interest (general nociceptors (*Scn10a*), peptidergic nociceptors (PEP, *Calca*), non-peptidergic nociceptors (NP, *Mrgprd*), C-LTMRs (*Th*), and Aβ-RA + Aδ-LTMRs (*Ntrk2*)). Paired ipsilateral and contralateral lumbar DRG samples were then collected 3 days and 4 weeks after surgery. In each condition, both male and female samples were collected to enable sex analyses. Together, 160 samples were collected, with 154 passing QC (Figure 3.2, 3A.1). Our contralateral, naïve controls were validated against previously published data from Zheng and colleagues [5] prior to downstream analyses of injury phenotypes (3.5).

4.2.2 Bioinformatics

This work is an extension of the dataset presented in chapter 3. Detailed methodology regarding mapping (STAR), sorting/merging (Samtools) and gene counting (HTSeq) are discussed in section 3.2.6. Subsequent analyses were performed in R via DESeq2 [214].

Modelling variance Two design models were fitted and used to examine injury changes - with and without subtype information. In each case, batch was included. Design models were compared against reduced models using the likelihood ratio test (LRT), and the distribution of variance per gene by factor was calculated using the package variancePartition [234].

4.2.2.1 Differential expression analyses

Differential expression testing was performed on filtered data using the Wald test and a weighted FDR correction (independent hypothesis weighting, IHW), in line with chapter 3. Count data was first filtered to genes with an average of 5 reads in at least 10% of the samples.

GSEA analyses against "all gene sets" were performed using ranked $\log_2$ fold changes (LFC) via msigdbr [216] and clusterProfiler [217] libraries. Custom GSEA analyses were calculated against a curated list of enriched genes from previously

published subpopulation data, as described in chapter 3 [5]. Ipsilateral sample enrichment was calculated against the same combined contralateral baseline used in chapter 3. GO term analyses for DEGs were performed using the Wallenius method via goSeq (R) [219]. Mirroring chapter 3, the filtered count data of expressed, non-DEG genes were used as a background (here, 5 reads in at least 10% of the samples). Protein interaction networks were generated using STRING [235].

General injury phenotypes To compare the general effect of SNI across acute and chronic states, condition (ipsi vs cont) and time (3D vs 4W) were modelled as a grouping factor in an additive design, combining samples across neuronal subtypes ($\sim batch + Time\_Condition$).

Within population injury effects Hypothesis testing within subtypes was performed using a grouping factor for time, condition, and population ($\sim batch + Population\_Time\_Condition$).

Sexual dimorphism Sexual dimorphism in injured samples was interrogated within populations using an interaction model ($\sim Time\_Condition * Sex$), as well as by contrasting sex and injury from an additive design ($\sim Time\_Condition + Sex$). Technically, the second method requires a shift to a different Bayesian shrinkage estimator, from "approximate posterior estimation for the general linear model" (*apeglm*) using a heavy-tailed Cauchy prior distribution to a more generic adaptive shrinkage method (*ashr*) [218, 236]. While both are widely accepted shrinkage methods, the consequences of this shift are discussed throughout the results.

4.2.2.2 Injury signature enrichment

Acute and chronic injury signatures were calculated using supervised principal component analyses (SPCAs) [237] on DEGs at 3 days or 4 weeks from the general injury analysis. Eigenvectors were extracted from the first principal component (PC1) and correlated across samples as an unbiased injury signature. For the 4 week timepoint, PC2 was also analysed. Loading values were also extracted. These are a

product of the covariance between the scaled dimensions and the original variables, giving a weight to how much individual genes contribute to each principal component.

4.2.3 Data accessibility

Building on our control data, these analyses have been included on our interactive database, currently on a test server at `https://trainingidn.shinyapps.io/drg-directory/`. Data tables are available at `https://github.com/aliibarry/thesis-supp`.

4.3 Results

4.3.1 General injury phenotypes

General injury signatures were examined by combining samples across subtypes (Fig 4.1). These samples will be biased toward nociceptors, due to the inclusion of three nociceptor populations (*Scn10a*, *Calca*, and *Mrgprd*) and two LTMR populations (*Th* and *Ntrk2*) in equal numbers.

At both 3 days and 4 weeks, we see predominant upregulation of genes associated with classical injury signatures, including *Atf3*, *Jun*, *Sox11*, and *Fosl1*. The overall number of DEGs (LFC > 1, FDR < 0.05) is reduced over time, from 521 at 3 days to 162 by 4 weeks. Of these, 96 are shared across timepoints, with some highlighted in figure 4.1D-F. Subtype-enriched genes appear acutely downregulated at three days, in line with previous reports although few genes reach our significance threshold (4A.2). This is likely due to the high variability from combining samples across populations.

Timecourse progression Our experimental timecourse was selected to highlight the progression from a more acute to chronic injury state after SNI. We can probe this transition by comparing ipsilateral samples across timepoints (4.1G). At four weeks, we see the downregulation of *Atf3*, as well as an upregulation of some subtype-specific genes towards baseline, such as *Ntrk2* (TRKB). *Slc17a7* (VGLUT1), typically a marker of larger diameter DRG is positively enriched at 4 weeks compared to 3

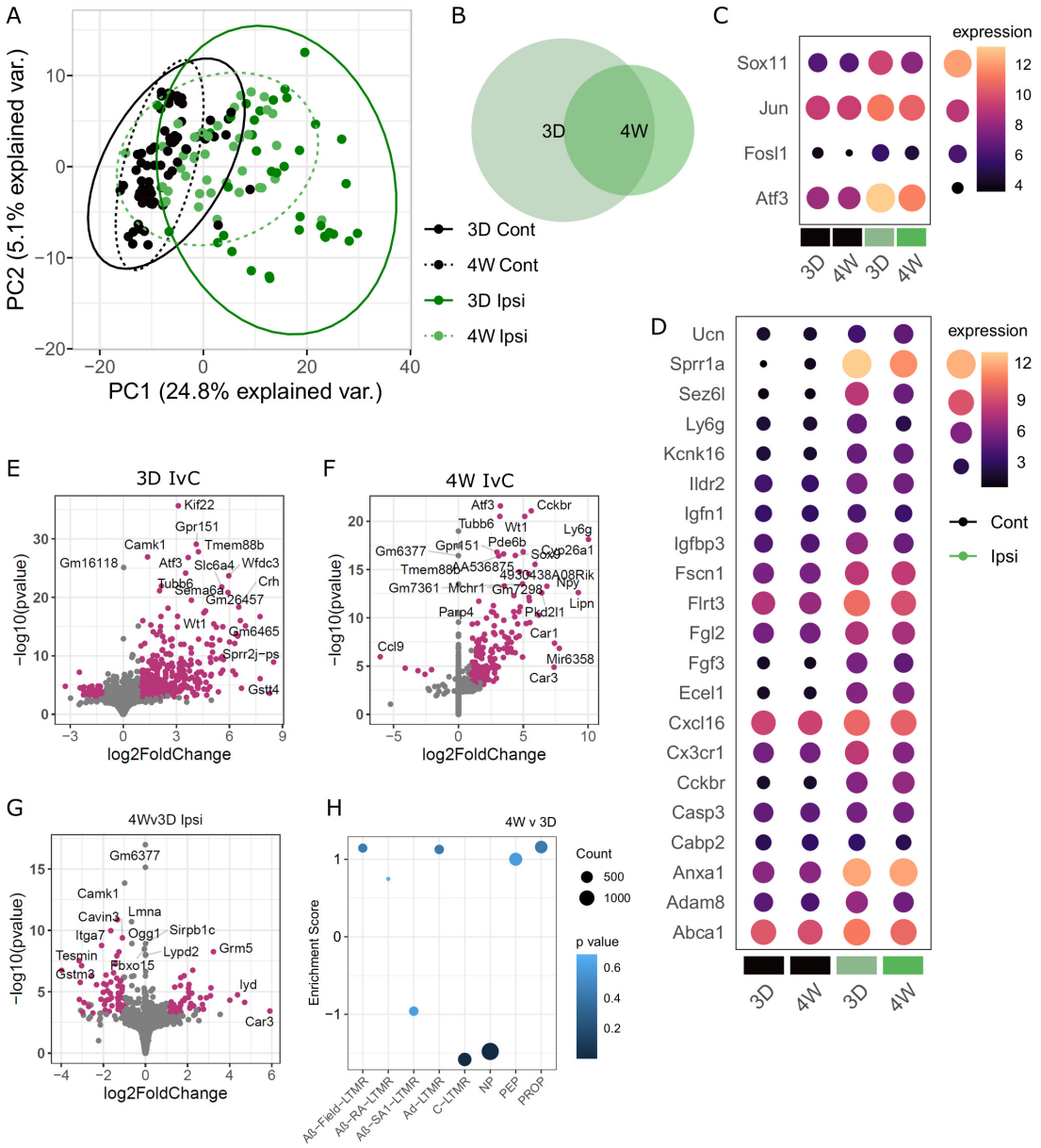

Figure 4.1: General injury signatures at acute (3 day, 3D) and chronic (4 week, 4W) timepoints after SNI. Ipsilateral (ipsi) lumbar DRG were compared to contralateral (cont) samples across neuronal subtypes. A. Supervised PCA bi-plot of 3 day DEGs (LFC > 1, FDR < 0.05). B: Overlap of 3D and 4W DEGs. C-D. Hallmark injury genes (C), and example DEGs shared across timepoints (D), plotted as median VST expression across groups. E-F. Volcano plots for ipsilateral v contralateral samples at an acute (E) and chronic (F) timepoint. G. Volcano plot for 4W v 3D ipsilateral samples. H. Subtype enrichment GSEA, based on a custom gene set for 8 neuronal subpopulations. C-LTMRs and NP nociceptors show negative enrichment in 4W ipsilateral samples compared to 3D. Normalized enrichment scores and p-values are listed in Table 4A.1

days after SNI (LFC = 2.25, p.adj = 1.7E-07), although this change is not reflected by a median expression change and is likely driven by a subgroup of samples. For

other genes, such as *Npy*, gene expression increases from 3 days to 4 weeks, where it is significantly higher than contralateral levels, suggesting a more chronic change.

In a more acute state, GO analyses show enrichment in the regulation of cell population proliferation, positive regulation of apoptotic process, and inflammatory response after injury. Many of these processes remain enriched at 4 weeks, even with the overall reduction in DEGs. GSEA enrichment at 3 days also show downregulation of electron transport and oxidative phosphorylation paired to a positive enrichment of inflammation, receptor regulator activity, and cell migration. Taken together, these results suggest we are accurately capturing injury signatures across our dataset. All supplementary tables for DEGs, GO, and GSEA analyses are provided on github.

When comparing ipsilateral samples over time, GO analyses also suggest functional changes. Three day injured samples show enrichment of apoptotic process, cytokine response and, and positive regulation of gene expression. In a more chronic state, there is an enrichment for protein import, long-term memory, and the regulation of long-term neuronal synaptic plasticity.

Cell type enrichments Injured neurons were previously shown to lose cell-type specific identifies after nerve injury in a time-dependant process [42]. At 4 weeks post-SNI, injured samples show a negative enrichment for C-LTMRs and NP nociceptors compared to their 3 day injured counterparts (4.1H).

4.3.2 Injury phenotypes by subtype

A major strength of this study is the ability to probe subtype specific patterns in a murine model of neuropathic pain. Here, we are able to explore subpopulation and common injury signatures across cell types, as well as contrast ipsilateral and contralateral samples within each population.

First, we queried cell type enrichment in our injured samples (Figures 4.2A, 4A.5-4A.9, Table 4A.2). By 4 weeks post-SNI, GSEA enrichment of subpopulation signatures varies from their naïve counterparts, previously discussed in Fig 3.5. Injured nociceptors and NP nociceptors no longer show clear subpopulation

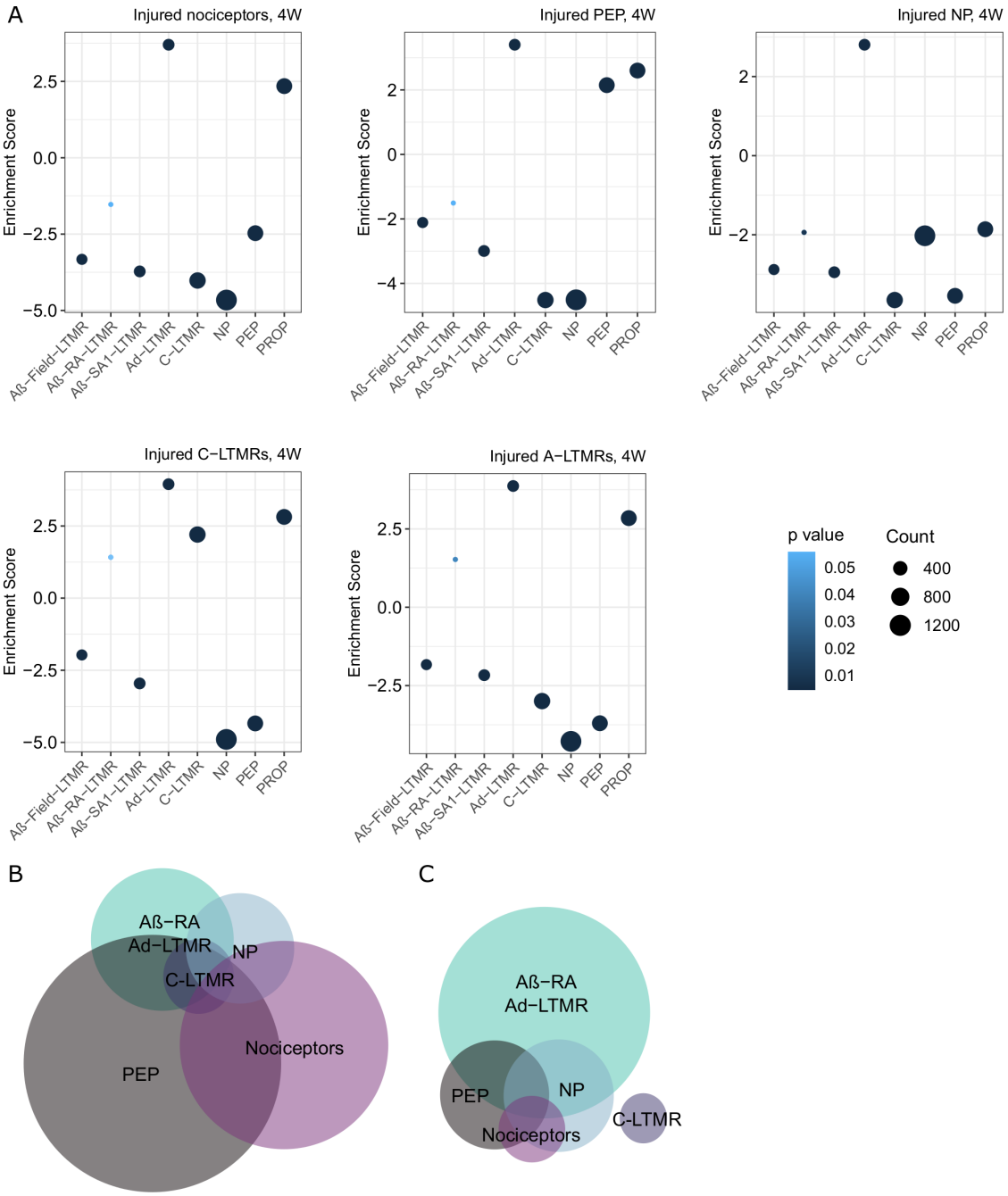

Figure 4.2: Differential gene expression across subtypes. A. GSEA analyses against previously published data [5] reveals a lack of clear subpopulation signatures in injured nociceptors and NP nociceptors by 4 weeks. All subtypes show a significant enrichment for Aδ-LTMRs, which was not seen in naïve nociceptor populations. Naïve data is shown in Fig 3.5. Normalized enrichment scores and p-values are listed in Table 4A.2. B-C: Differential expression testing at 3 days (B) and 4 weeks (C) post-SNI.

delineations, while injured PEP and C-LTMRs both show enrichment for their respective populations. Across all subtypes, there is a positive enrichment in the

Aδ-LTMR signature, previously only seen in naïve LTMR samples. Injured Aβ-RA + Aδ-LTMRs also show a new negative enrichment for Aβ-Field and Aβ-SA1-LTMRs.

4.3.2.1 Differential expression analyses

Acute gene regulation Within population testing for differentially expressed genes show a number of shared regulated genes typical of injury signatures (including *Atf3*, *Sprr1a*, and *Sox11*, Table 4A.3), as well as a subset of subtype-specific DEGs (Fig 4.2B). Over 5000 genes are regulated overall and are mostly driven by changes in the general nociceptors (2620) and peptidergic nociceptor (3270) samples. Fewer DEGs are seen in other populations, with 179 DEGs for non-peptidergic nociceptors, 640 DEGs for Aβ-RA + Aδ-LTMRs, and only 36 DEGs in C-LTMRs (with an LFC > 1, FDR < 0.05). Using an LFC cutoff of 1, we are focusing on genes with good expression changes thought to correspond to biological relevance. Even so, small changes in gene expression can be biologically relevant, and full results tables are provided online. With the populations studied, we do not see a clear LTMR-specific pattern: no genes exclusively regulated in both C-LTMRs and Aβ-RA + Aδ-LTMRs.

Most genes are either regulated in the same direction, or only regulated in a subset of populations. Even so, over 400 DEGs are regulated in opposing directions, which may provide a unique look at subtype differences after injury (Table 4A.5). For example, *Ints5* is an integrator complex involved in RNA transcription which is upregulated in PEP and general nociceptors while being downregulated in Aβ-RA + Aδ-LTMRs. The GTP binding protein *Gtpbp1* has been previously implicated in neuronal death through translational regulation [238]. Here, we see subtype differences in regulation, being upregulated in PEP and Aβ-RA + Aδ-LTMRs, but downregulated in general nociceptors (with downward trends in NP and C-LTMRs). Other genes showing bidirectional regulation include *Rnd1*, or Rho Family GTPase 1, which has been discussed previously for it's role in axon outgrowth, while *Wnk4* is related to actin cytoskeleton remodelling by Rho GTPases, as well as ion channel regulation.

Chronic gene regulation At four weeks post-SNI, there is a reduced number of DEGs across all subtypes, compared to our 3 day results (4.2C). The most changes are present in Aβ-RA + Aδ-LTMRs (217 DEGs). Non-peptidergic and peptidergic nociceptors show the next highest number of DEGs, with 25 and 36 respectively (sharing *Cckbr*, *Tubb6*, *Atf3*, *Gpr151*, *Wt1*, *Pde6b*, *Cyp26a1*, and *Cdk6*). Few changes are seen in our general nociceptor population, with only 7 DEGs with a moderated LFC > 1 (*Cckbr*, *Ttll10*, *Phox2b*, *Rpl31-ps13*, *S100a8*, *Gata5os*, and *Gm47138*). C-LTMRs also show few changes (5 DEGs), in line with the acute signature (*Hba-a1*, *Nefh*, *S100b*, *Adtrp*, *Gm35097*). No genes show regulation in opposing directions across subtypes by 4 weeks, although some, like *Rnd1* remain regulated.

Regulatory genes Many studies highlight cell-type or injury-specific gene regulation mechanisms, as they regulate important mechanisms of neuropathic pain. Additionally, they provide possible new avenues to target and modulate neurons in injured states. Our current dataset is well suited for these inquires. Across timepoints, a number of DEGs correspond to transcription factors ("GO:0003700") and/or are involved in gene regulation ("GO:0010468") (4A.10). This includes shared regulators like *Atf3*, *Hoxa2*, *Twist2*, *Cdk6*, *Prdm10*, and *Trim34b* as well as numerous subtype-specific regulators. Full results tables for these groups are available in the online supplementals.

4.3.2.2 Acute injury signatures

Differential gene expression analyses show significant differences across all samples, as well as within each subtype at both timepoints examined. To build on this, an acute injury signature was extracted from our initial list of DEGs at 3 days (from combined samples, above) through a supervised PCA (SPCA) and compared across subtypes (4.3). This provides an unbiased signature through the linear combination of individual gene expressions. All five subtypes studied show a significant difference (FDR < 0.05) between ipsilateral and contralateral samples at both timepoints (Kruskal-Wallis Rank Sum, followed by pairwise Wilcoxon with BH correction against a grouping factor (population, condition, and timepoint)). Only NP and

C-LTMR show a significant difference between 4 weeks and 3 days (FDR = 0.00185 and 0.00995 respectively), reflecting their stronger return towards baseline.

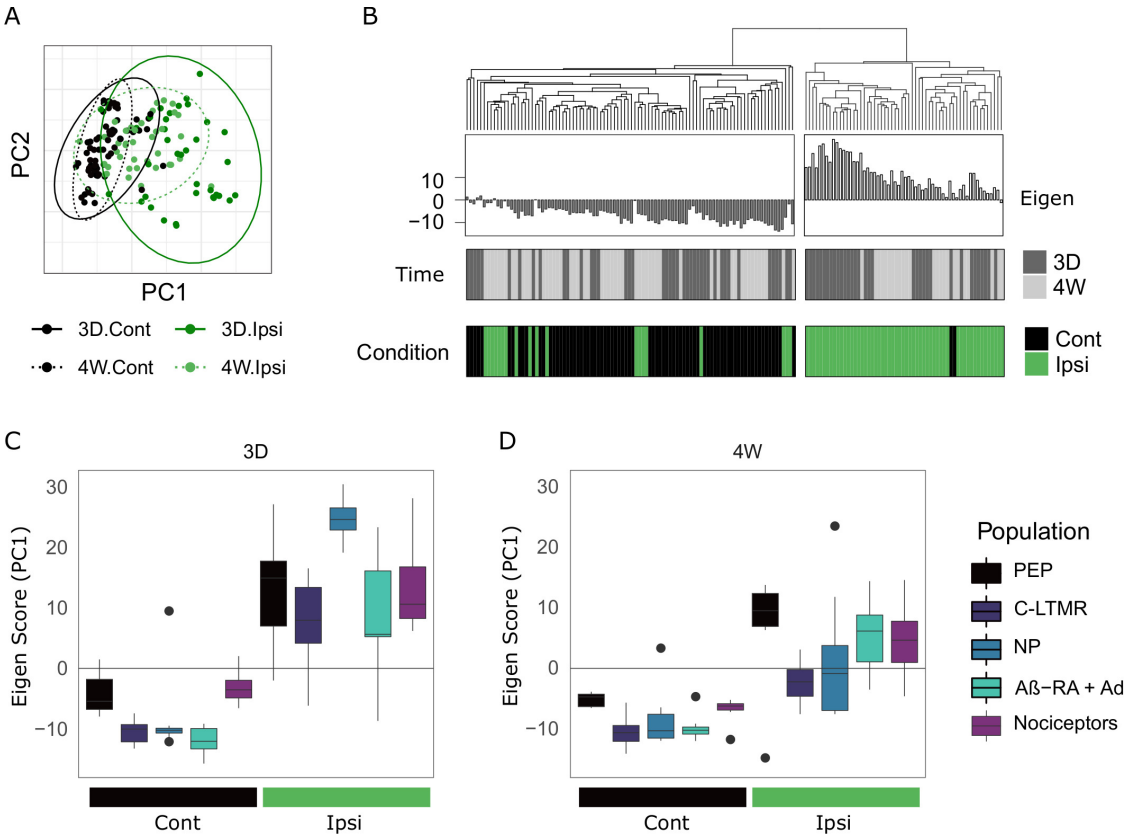

Figure 4.3: Acute injury signature analysis. A. Supervised PCA bi-plot for 3 day DEGs. B. Dendrogram split by k-means of 2, highlighting positive and negative injury scores largely correlating to sample condition. C-D. PC1 correlation across subtypes and time. Boxplot whiskers show 1.5 IQR. All five subtypes shows a significant difference between ipsilateral and contralateral samples at both timepoints (Kruskal-Wallis Rank Sum, followed by pairwise Wilcoxon with BH correction against a grouping factor (population, condition, and timepoint)). Only NP and C-LTMR ipsilateral samples are different between 4 weeks and 3 days (FDR = 0.00185 and 0.00995 respectively), reflecting their return towards baseline.

4.3.2.3 Chronic injury signatures

Eigenvectors were also extracted from an SPCA on 4W DEGs to form a chronic injury signature across populations (4.4). This signature is driven largely by general nociceptors, peptidergic nociceptors, and Aβ-RA + Aδ-LTMRs, although all subtypes show a significant difference from their contralateral counterparts at 4 weeks (Kruskal-Wallis Rank Sum, followed by pairwise Wilcoxon with BH correction

against a grouping factor (population + condition). A subset of samples share variation in PC2, so this eigenvector was also extracted for comparison (4.4C-E). Here, this variation is driven by Aβ-RA + Aδ-LTMRs ipsilateral samples, suggesting a distinct injury signature in this population not captured in the other subtypes.

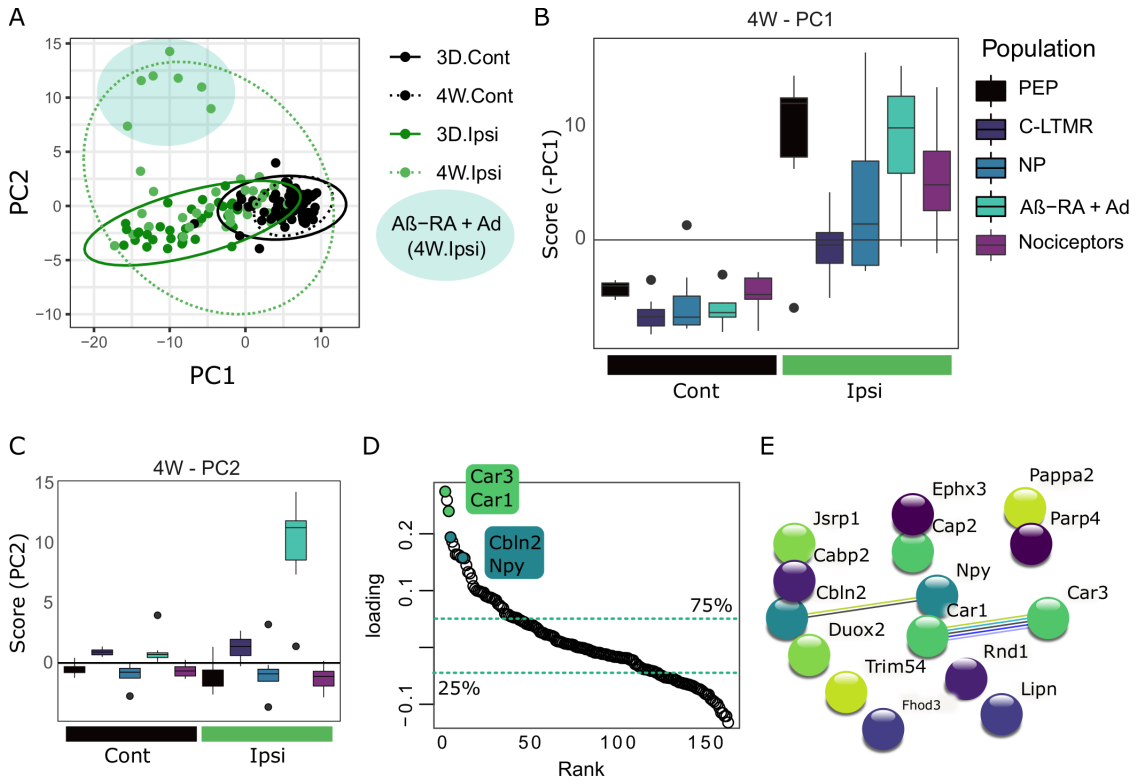

Figure 4.4: Chronic injury signature is partially driven by Aβ-RA + Aδ-LTMRs at 4 weeks. A. PCA bi-plot of differentially expressed genes, 4 weeks after SNI. Aβ-RA + Aδ-LTMRs injured samples are highlighted in cyan. B. PC1 correlations across sample, plotted as -score for consistency with the 3 day signature. C. PC2 correlations across samples. D. Ranked loadings (PC2) for all DEGs at 4 weeks after injury. Dashed lines highlight quartiles. E. STRING database interactions for top 15 DEGs (ranked by loadings).

Gene loadings for PC2 were extracted and ranked by loading for further analyses (4.4D). The top and bottom 25% quartiles were extracted for GO analyses. Both "response to stimulus" and "actin filament organization" were upregulated GO terms, while "immune response" and "synapse maturation" were downregulated. No GSEA enrichments on ranked loadings were present.

The STRING database was next queried for possible interactions between gene products. In the top quartile (41 DEGs), interactions are seen between *Car1-Car3*,

Unc-Npy-Cbln2, *Hrk-Pmaip1*, and *Uox-Mbl2*. Interactions for the genes with the highest loadings are highlighted in Fig 4.4.

Aβ-RA + Aδ-LTMRs *Ntrk2*-LTMRs represent a unique sensory neuron population because they transition functionally after injury to contribute to mechanical hypersensitivity [21]. Here, they show the largest changes 4 weeks after injury (4.2C) and contribute a unique part of the chronic injury signature (4.4C-E). There is an upregulation of *Atf3*, *Sox9*, and *Sprr1a* across timepoints in injured cells, and by 4 weeks, *Npy* is also strongly upregulated (LFC $>$ 12) in line with previous reports.

GO analysis shows an upregulation of neuropeptide signalling pathways, gene expression and actin filament organization. There is a downregulation of inflammatory response, G-protein coupled receptor signalling, and signal transduction. GSEA analysis against all gene sets also shows enrichment in neuropeptide signalling and receptor binding, driven largely by *Npy*, *Ucn* and *Nts* fold changes, as well as multiple hits for terms involving the electron transport chain and oxidative phosphorylation, which mirrors our previous analysis with a chronic injury signature.

To see if these changes were consistent across LTMRs, an SPCA on DEGs at 4 weeks was performed (Fig 4.5). There is no a clear division between high threshold and low threshold populations here, supporting the notion that *Ntrk2*-expressing neurons exhibits a unique injury signature compared to the populations studied here. In most subtypes, the injury signature correlates slightly more in male samples, with no difference at baseline (4.5D).

4.3.3 Sexual dimorphism

To see if male and female sensory neurons differ in their maintenance of chronic neuropathic pain states, we fitted an interaction model for sex and condition (4.6). Acute effects were not studied due to the colinearity of the batch and sex in a subset of the populations. Using this stringent modelling, which requires genes to be regulated in injury, as well as have a differential response to sex, we detected no differences when pooling populations at 4 weeks, or when subsetting our data to

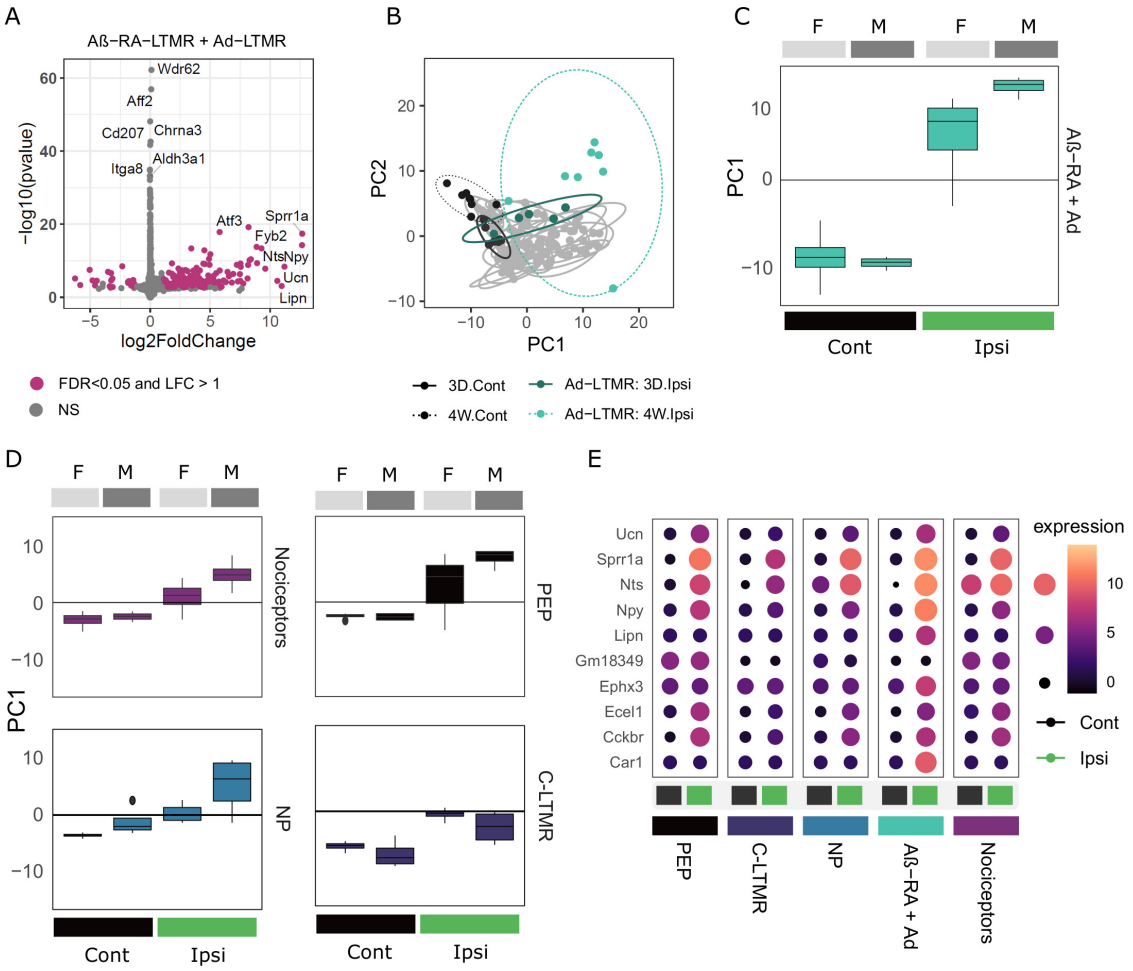

Figure 4.5: Aβ-RA + Aδ-LTMRs show a unique injury signature at four weeks. A. Volcano plot highlighting DEGs 4 weeks after SNI. B. SPCA for Aβ-RA + Aδ-LTMR DEGs at 4 weeks. Remaining populations in grey. C. Unbiased correlation analysis against the first principal component (PC1) from an SPCA on 4W DEGs for Aβ-RA + Aδ-LTMRs. D. At 4 weeks, all five subtypes shows a significant difference between ipsilateral and contralateral samples (Kruskal-Wallis Rank Sum, followed by pairwise Wilcoxon with BH correction against grouped population and condition). Effect sizes vary across populations, and do not highlight a clear difference between LTMR and HTMR populations. E. Top DEGs, ranked by LFC. Many are common in injured samples across subtypes.

interrogate within subtype (4.6A). The number of genes with FDR < 0.05 range from 9 (NP) to 212 (Aβ-RA + Aδ-LTMRs), but moderated fold changes centre towards zero, suggesting these result from the high variability in low count genes, instead of biologically meaningful differences.

By definition, interaction effects are calculated using the reference mean expression from only one sex. This can mask effects in genes which are lowly expressed

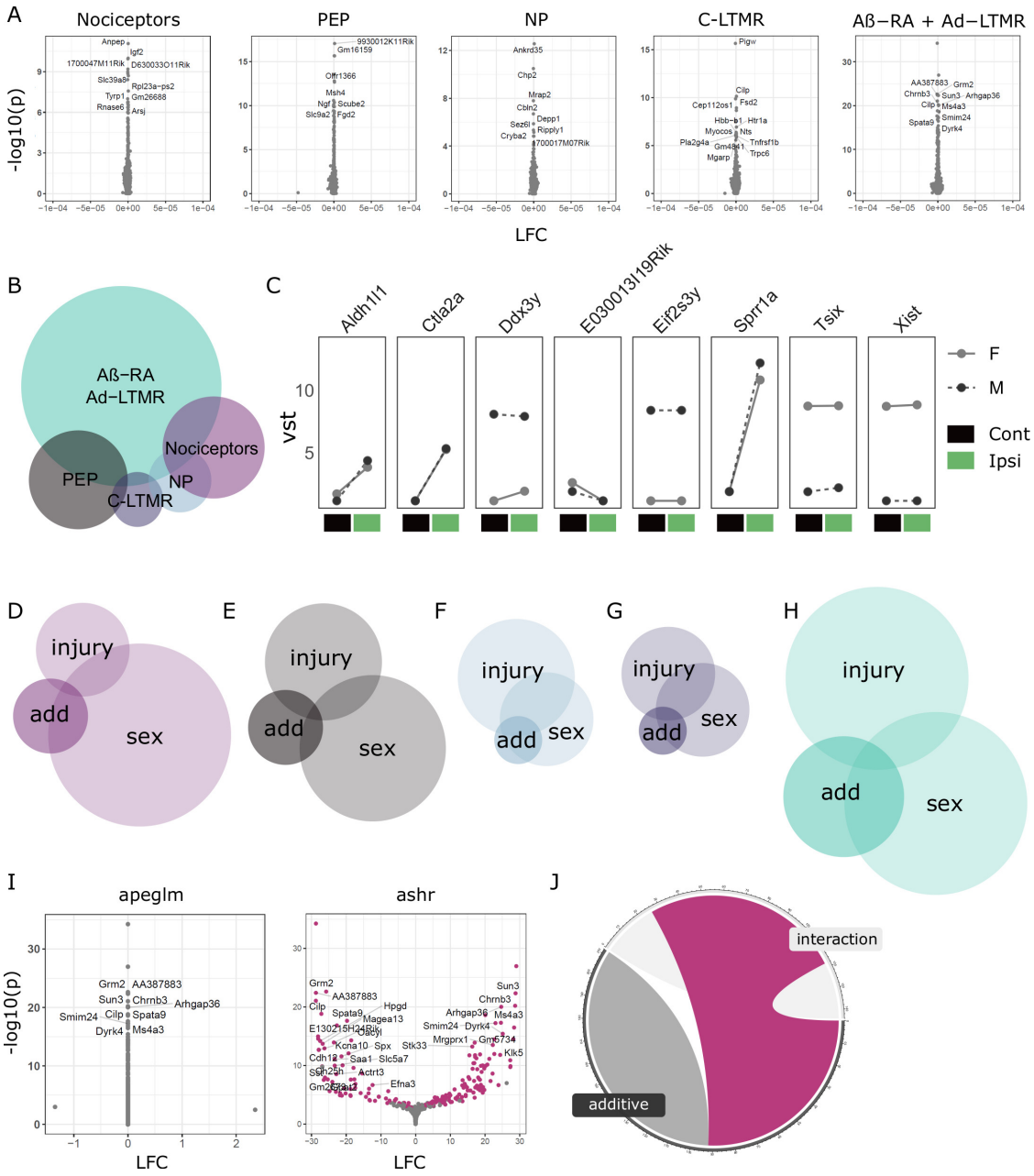

Figure 4.6: Sexual dimorphism in neuronal subtype injury responses. A. Transcriptomic analyses in primary afferents reveal no clear interaction of sex and injury 4 weeks after SNI. B. Euler plot of DEGs using an additive model contrasting sex and injury differences. C. Line plots of DEGs shared across at least two subtypes. D-H: across subtypes, DEGs from this additive modelling ("add") appear to be driven partly by sex differences in basal expression levels ("sex"), as well as some overlap with genes generally regulated in injury ("injury"). D: General nociceptors. E: PEP nociceptors. F: NP nociceptors. G: C-LTMRs. H. Aβ-RA + Aδ-LTMRs. I. Example volcano plots for the interaction of sex and injury for Aβ-RA + Aδ-LTMRs, with *apeglm* and *ashr* shrinkage. J. 42% of regulated genes are shared across our interaction and additive models (magenta) which are not regulated with *apeglm*

in one sex during control states. To overcome this, we further explored sexual dimorphism using a more relaxed additive design, subtracting sex and injury comparisons to pull out sex differences which cannot be explained by the injury effect alone (4.6B-J, 4A.11).

Using this approach a number of DEGs are seen, with the majority in Aβ-RA + Aδ-LTMRs (144 genes), followed by peptidergic nociceptors (41) and general nociceptor (34) populations (Fig 4.6B).

Eight genes show regulation in multiple subtypes. This includes a subgroup of sex-linked genes (eg. *Xist*, *Tsix*, *Kdm5d*), as well as those regulated in injured states, like *Sprr1a*. Only one, *Tsix*, shows regulation across all subtypes, but this does not appear to be a strong interaction of sex and injury (4.6C). Across subtypes, DEGs from this differential response to injury appear to be driven partly by sex differences in basal expression levels, as well as some overlap with genes generally regulated in injury (Fig 4.6D-H).

Aβ-RA + Aδ-LTMRs show the largest number of DEGs, with a selection highlighted in 4A.11. Here, there is a 32% overlap with significantly regulated genes from naïve male vs female samples and a 12% overlap with genes regulated in an injured state (4.6H). Together, 40% of DEGs overlap with significantly regulated genes for sex in control samples or injury at 4 weeks, based on an FDR < 0.05. This does not account for fold changes, due to differences in shrinkage methods (*apeglm* vs *ashr*, see methods).

To see if the difference between our interactive and additive modelling was primarily a caveat of shrinkage priors, our interaction fold changes were re-calculated using *ashr*, where 42% over DEGs detected through the additive model overlap (Fig 4.6I-J). Shrinkage priors aim to limit noise within a dataset. Plotting non-transformed counts for these genes highlights the variability present (4A.12). Some fold changes appear driven by a single sample per condition, while others show stronger trends. This highlights how the variability in lowly expressed genes can limit conclusive analyses.

Taken together, we interpret this as a lack of strong sexual dimorphism between male and female subtypes specifically in response to injury by 4 weeks. Using a less stringent analysis for sexual dimorphism, we do detect within subtype differences. These are primarily seen in Aβ-RA + Aδ-LTMRs, and is partly driven by baseline sex differences at a subpopulation-level, which were initially discussed in chapter 3. The variability in low count genes adds noise to these analyses: deeper sequencing and *in situ* validation may still reveal a clearer interaction, or lack-there-of between sex and injury.

4.4 Discussion

The availability of subtype-specific transgenics paired to advances in low input RNA-seq has allowed deep sequencing of sensory neuron subpopulations after injury. Building on our control data from chapter 3, we are able to explore changes after SNI at two timepoints, as well as probe sexual dimorphism after injury at a subpopulation-level.

4.4.1 General injury signatures

Samples cluster primarily by cell type. By collapsing these subtypes we can extract general injury signatures that mirror injury signatures seen in previous studies. There is an acute upregulation of key injury genes which decrease over time, along with the more chronic upregulation of genes like *Npy*.

This general analysis is enriched for sensory neurons, as opposed to general whole DRG sequencing. We anticipate this transcriptional signature to be similar to bulk RNA-seq of MACS-purified neurons, where researchers quantified a "nociceptor" transcriptome based on the isolation of small diameter neurons [28]. In naïve states, we see many overlapping genes, including key transcription factors they report to be enriched in their "nociceptor" sample, opposed to whole DRG. These include *Pou4f2*, *Myt1*, *Ldb2*, *Isl2*, *Bhlha9*, and *Atf3*, which show varying degrees of cell-type specificity in our data. We have built on this with added data after injury, giving insight to possible nociceptor-enriched transcription factors involved in injury. For

example, *Isl2* encodes Insulin related protein 2 and is regulated after injury in our dataset. It also shows regulation in human patients with diabetic peripheral neuropathy, suggesting cross-species, cross-model target for future experiments [239].

Timecourse developments To probe differences in acute injury and more chronic states, we examined samples at 3 days and 4 weeks. When comparing all ipsilateral samples, we see a reduction in NP and C-LTMR enrichment more chronically. Population data was pooled for GSEA analyses across timepoints, so changes in gene signatures can be difficult to interpret. For example, if we are working with the assumption that injured NP cells die after SNI, as suggested in chapter 2, the ipsilateral NP samples by 4 weeks are likely to contain primarily intact neurons (opposed to cell bodies from transected afferents). The significant reduction of an NP signature over time may thus result from changes in the intact NP neurons, or a bias in the general nociceptor population, which shows enrichment for both PEP and NP nociceptors in a naïve state. C-LTMRs show a similar pattern to NP, although we have not queried the loss of this population to the same extent as NP. Given similarities seen here, it would be interesting to follow up in a similar fashion. To address this in further detail, and amplify a major strength of the study, subtype-specific analyses were performed.

4.4.2 Subtype-specific injury changes

Previous work has explored injury signatures in whole DRG and single cells. We are adding a middle ground of "bulk", subtype-specific population analyses through deep sequencing of neuronal subtypes post-SNI. Deep sequencing allows us to interrogate genes at a larger dynamic range, including lowly expressed genes, and produces an expression matrix that is less sparse than sc/snRNA-seq.

In line with previous reports, we see a reduction in cell-type specificity within our injured samples. Primarily, we see a reduced signature in general nociceptors, as well as NP nociceptors (4.2A), while PEP nociceptors still show enrichment

for PEP, either from the contribution of intact afferents in the samples, or less change in injured cells.

There is an added enrichment for Aδ-LTMRs across all nociceptor subtypes, which remains enriched in LTMR populations. The consequence of this is unclear, with multiple, non-mutually-exclusive hypotheses available. For example, do nociceptors develop a more LTMR-like signature? Is this driven by a clear subset of genes? Is this signature simply representative of a more general, undefined or immature sensory neuron? Do Aδ-LTMRs show a more injured phenotype in naïve states? We cannot conclusively exclude this latter possibility, but key injury genes are not present in the gene set curated from Zheng and colleagues, and our contralateral *Ntrk2* samples are negatively enriched for our general injury signature at both timepoints. Together, this suggests they do not show a strong injury phenotype at baseline.

Our sequencing depth also permits differential expression testing within subpopulations. All populations show differential gene expression, but this is primarily driven by general nociceptors and PEP at 3 days, and Aβ-RA + Aδ-LTMRs at 4 weeks. Using an LFC cutoff of 1, we see significant upregulation of multiple injury genes, and a significant enrichment of a general injury signature in the ipsilateral samples across all subtypes. This suggests the low number of DEGs in other populations is not an artifact of sequencing intact neurons, but instead a biologically relevant signature. A number of these DEGs are involved in gene regulation (4A.10), and may be useful targets for genetic manipulation.

Gene signatures Using injury signatures extracted from DEG lists we can compare subtype responses over time. By four weeks, *Ntrk2* samples show a distinct injury phenotype not captured by the other populations (4.4C-E). Loading values suggest a strong involvement of *Car3* and *Car1*, which are both involved in oxidative phosphorylation. Neuropeptide Y (*Npy*) and cerebellin-2 (*Cbln2*) are also highly ranked. These have previously been implicated in mechanical hypersensitivity [240].

Npy has also been well documented for it's upregulation in large-diameter neurons after injury, which may explain the subtype-specific effect seen here [241].

4.4.3 Sexual dimorphism

In a naïve state, we see distinct sexual dimorphism across subtypes (chapter 3). This does not translate to a strong interaction of sex and injury, as the injury response seems to be consistent across sexes (4.6). With baseline differences in gene expression across sexes, a strong interaction with injury is not required for functionally relevant changes in injured states. The differences seen in control states may still contribute to painful states due to altered immune/glial interactions, baseline excitability, or differences in higher order circuitry.

Using an additive model to contrast sex and injury at 4 weeks, we are able to pull out possible gene candidates for further validation. These represent a set of genes who's different responses between sexes cannot be solely explained by the general injury response. A small subset shared across populations, which appear to be larger sex-linked, or key injury genes. Of these, *Sprr1a* was previously noted to be sexually dimorphic in naïve states, but also is strongly upregulated after injury, in line with previous reports.

Proportionally, Aβ-RA + Aδ-LTMRs show the most DEGs when contrasting sex and injury condition, in keeping with a naïve state. One third of these genes were previously reported to differ in control samples, with 12% regulated in injury at 4 weeks. As a top hit, *Slit3* is an estrogen-sensitive axonal guidance molecule previously discussed in the context of endometriosis and pelvic pain [242]. Other DEGs include a range of genes involved in inflammation and immune response (eg. *Ifi211*, *Ctla2a*, *Tlr4*), cholinergic receptors (*Chrna3*, *Chrnb3*), the transcription factor *Neurog3*, and numerous sex-linked genes.

4.4.3.1 Technical limitations

This data does not conclusively highlight an interaction of sex and injury within subtypes. The absence of a strong signature fits previous literature, but nuanced

changes in lowly expressed genes may still hold biological relevance. As discussed in chapter 3, tamoxifen dosing introduces a confound. Moreover, the variability in low count genes makes this difficult to probe with our sequencing depth. Shrinkage methods differ in their LFC estimates at this point, with a conservative shrinkage by *apeglm* showing no changes, while a more relaxed shrinkage by *ashr* captures large fold changes, some of which are driven by single samples (4A.12). To give more confidence to DEGs captured by *ashr*, more stringent filtering may be warranted to select candidates for external validation.

4.4.4 Conclusions

Using bulk RNA-seq of DRG subtypes, we build on a mountain of previous studies exploring naïve and injured molecular signatures, and have curated this data into an interactive database to improve accessibility. In addition to providing injury signatures across subpopulations, we are contributing to a growing body of literature emphasizing the importance of studying sexual dimorphism in painful states.

4A Appendix

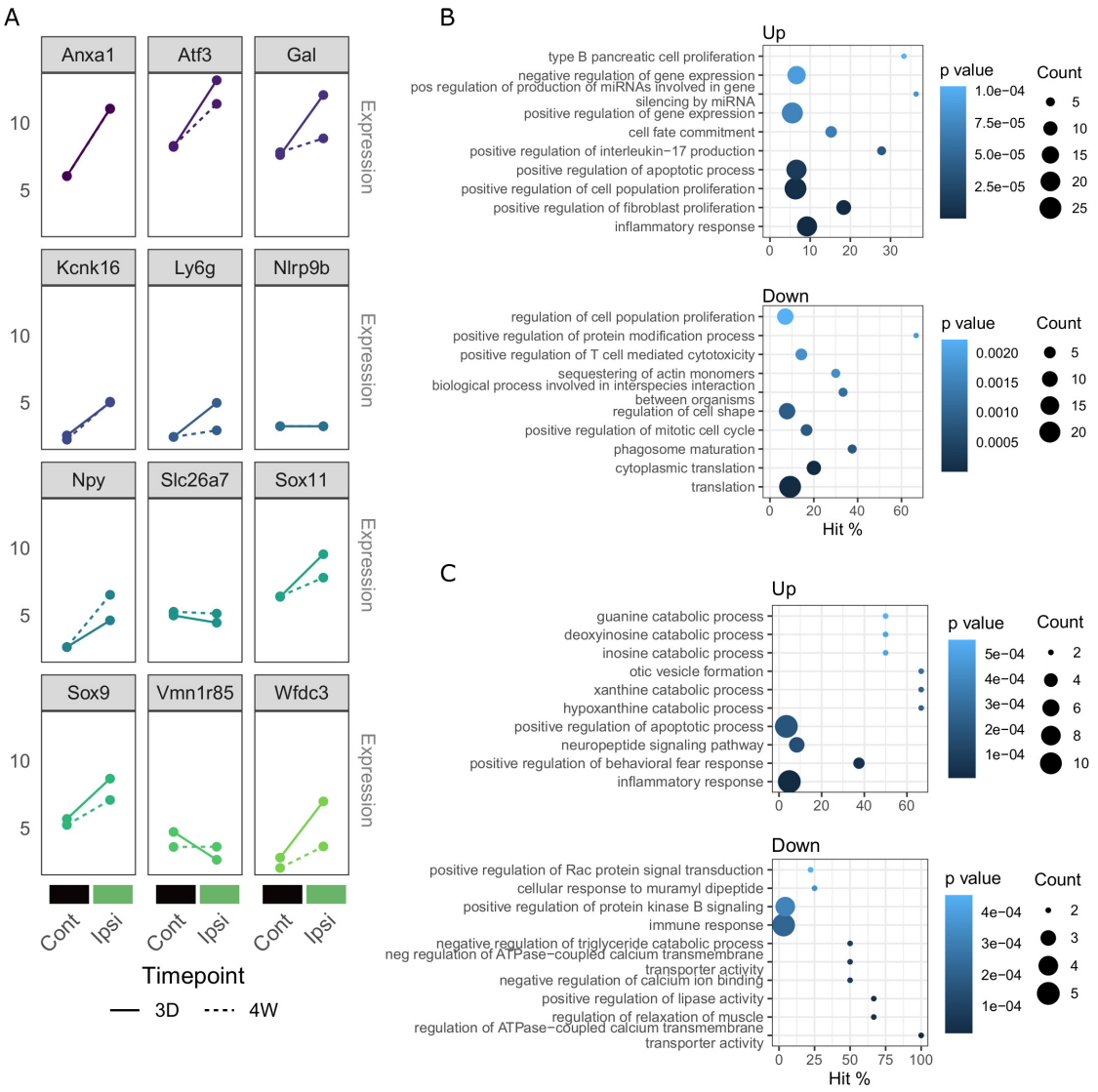

Figure 4A.1: Shared injury signatures across timepoints (3 days and 4 weeks) after SNI. A. Median expression of shared DEGs of interest between 3D and 4W, and 4W v 3D ipsilateral samples. Many genes show recovery towards baseline by 4 weeks. Solid line: 3D samples, dashed line: 4 week samples. B-C: GO term analyses for 3D (B) and 4W (C) general injury samples.

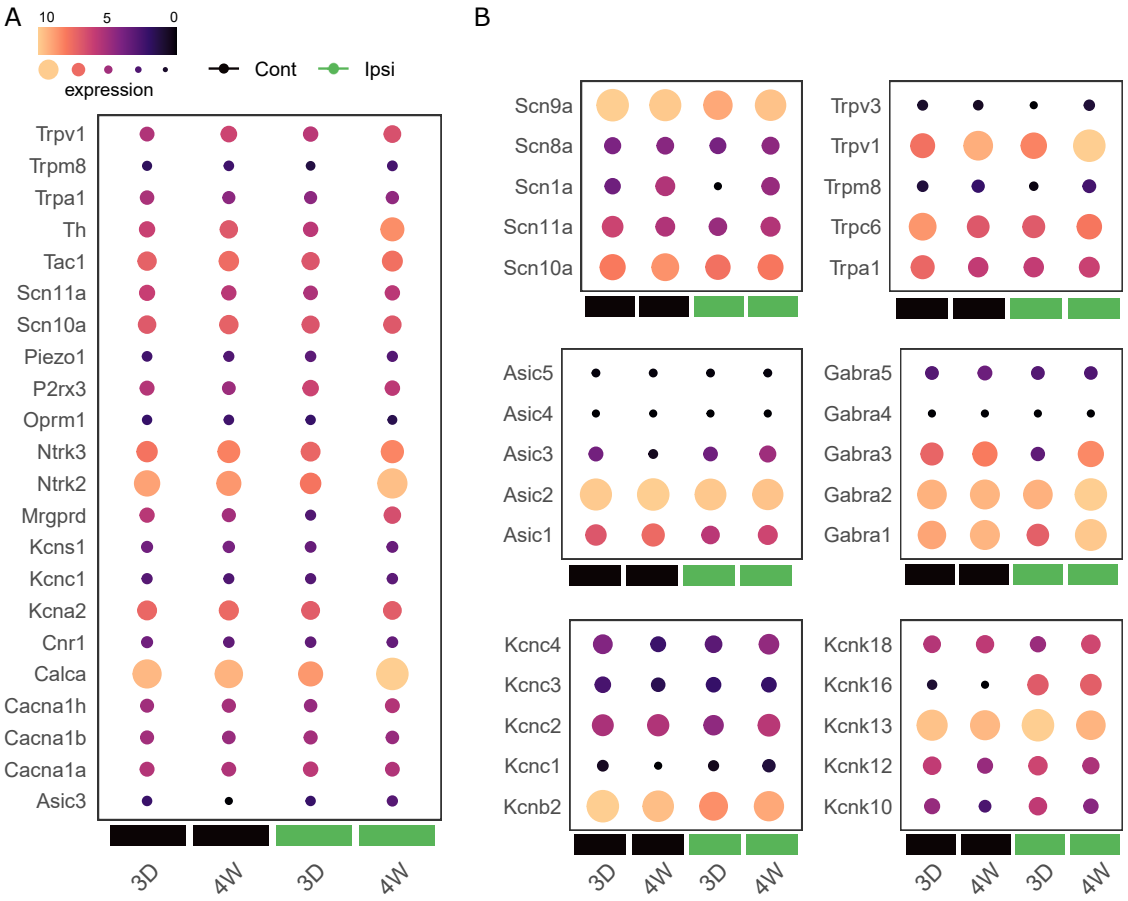

Figure 4A.2: Normalized median gene expression from 3 day and 4 week samples, combined by subpopulation. A. Selected genes across neuronal subtypes. B. Selected common ion channels across subtypes. Voltage gated sodium (*Scn*), transient receptor potential (*Trp*), acid-sensing (*Asic*), γ-aminobutyric acid (GABA) receptors (*Gabra*), and potassium channel (*Kcnb/c/k*) genes are highlighted.. Related to Figure 4.1.

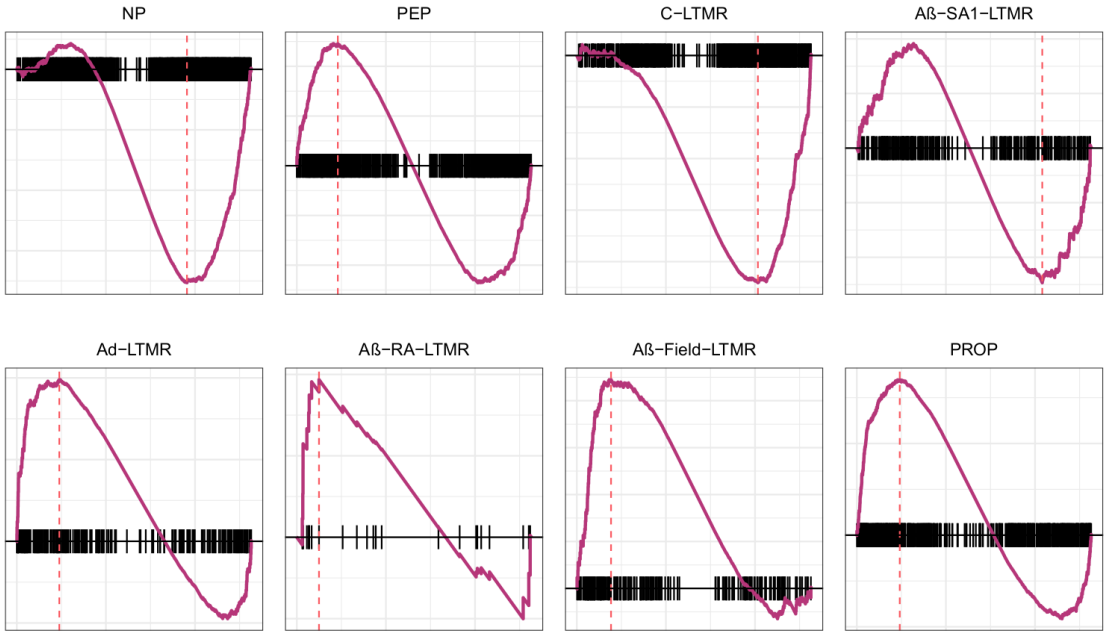

Figure 4A.3: Gene set comparison for chronic v acute injury to previously published, naïve subpopulation RNA-seq. Related to Figure 4.1.

Table 4A.1: Gene set enrichment for general injury conditions, ranked by normalized enrichment scores (score): 4W v 3D: Ipsilateral conditions across timepoints. Genes were ranked by shrunken LFC. Related to Figure 4.1

Comparison	Gene Set	Size	Score	p (adj)
4W v 3D	C-LTMR	727	-1.58	1.09E-03
	NP	1400	-1.48	1.09E-03
	PROP	594	1.16	4.25E-01
	Aβ-field-LTMR	224	1.14	4.25E-01
	Aδ-LTMR	248	1.13	4.25E-01
	PEP	666	1.00	5.86E-01
	Aβ-SA1-LTMR	250	-0.96	5.98E-01
	Aβ-RA-LTMR	24	0.75	6.88E-01

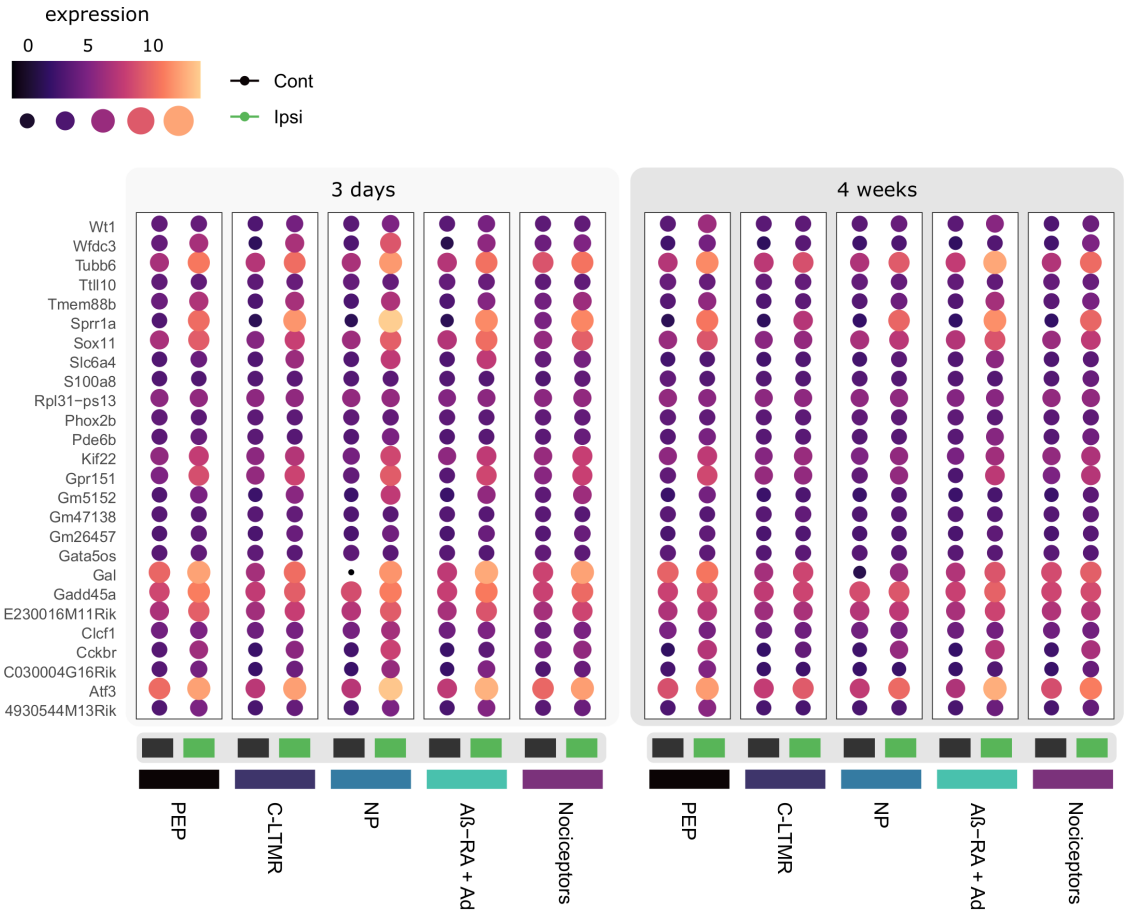

Figure 4A.4: Selection of DEGs shared across multiple populations, either at 3 days, 4 weeks, or both.

Table 4A.2: Gene set enrichment for injured lumbar DRG, 4 weeks after SNI. Ranked by normalized enrichment scores within each neuronal subtype. Related to Figure 4.2.

Population	Gene Set	Size	Score	p (adj)
Nociceptors	NP	1583	-4.66	1.27E-266
	C-LTMR	836	-4.02	8.81E-103
	Aδ-LTMR	315	3.70	9.71E-46
	Aβ-SA1-LTMR	317	-3.72	9.05E-42
	Aβ-field-LTMR	263	-3.33	1.48E-27
	PEP	764	-2.47	2.41E-24
	PROP	765	2.35	1.05E-19
	Aβ-RA-LTMR	35	-1.53	4.16E-02
PEP	NP	1583	-4.51	0.00E+00
	C-LTMR	836	-4.52	2.36E-206
	Aδ-LTMR	315	3.40	1.86E-35
	PROP	765	2.60	6.91E-30
	Aβ-SA1-LTMR	317	-2.99	2.38E-26
	PEP	764	2.15	1.52E-16
	Aβ-field-LTMR	263	-2.11	3.90E-08
	Aβ-RA-LTMR	35	-1.51	5.11E-02
NP	C-LTMR	836	-3.65	2.41E-148
	PEP	764	-3.54	4.66E-120
	Aβ-SA1-LTMR	317	-2.95	1.57E-28
	NP	1583	-2.03	1.05E-25
	Aβ-field-LTMR	263	-2.88	3.45E-22
	Aδ-LTMR	315	2.80	2.13E-21
	PROP	765	-1.86	1.82E-10
	Aβ-RA-LTMR	35	-1.94	3.68E-03
C-LTMR	NP	1583	-4.90	0.00E+00
	PEP	764	-4.34	6.78E-142
	Aδ-LTMR	315	3.95	2.80E-70
	PROP	765	2.81	8.19E-40
	Aβ-SA1-LTMR	317	-2.96	5.15E-23
	C-LTMR	836	2.20	1.49E-18
	Aβ-field-LTMR	263	-1.97	7.99E-07
	Aβ-RA-LTMR	35	1.42	8.73E-02
Aβ-RA + Aδ-LTMRs	NP	1583	-4.28	0.00E+00
	PEP	764	-3.70	6.96E-107
	Aδ-LTMR	315	3.87	1.80E-73
	C-LTMR	836	-2.99	1.61E-51
	PROP	765	2.85	4.13E-46
	Aβ-SA1-LTMR	317	-2.17	2.13E-09
	Aβ-field-LTMR	263	-1.83	1.53E-05
	Aβ-RA-LTMR	35	1.52	4.11E-02

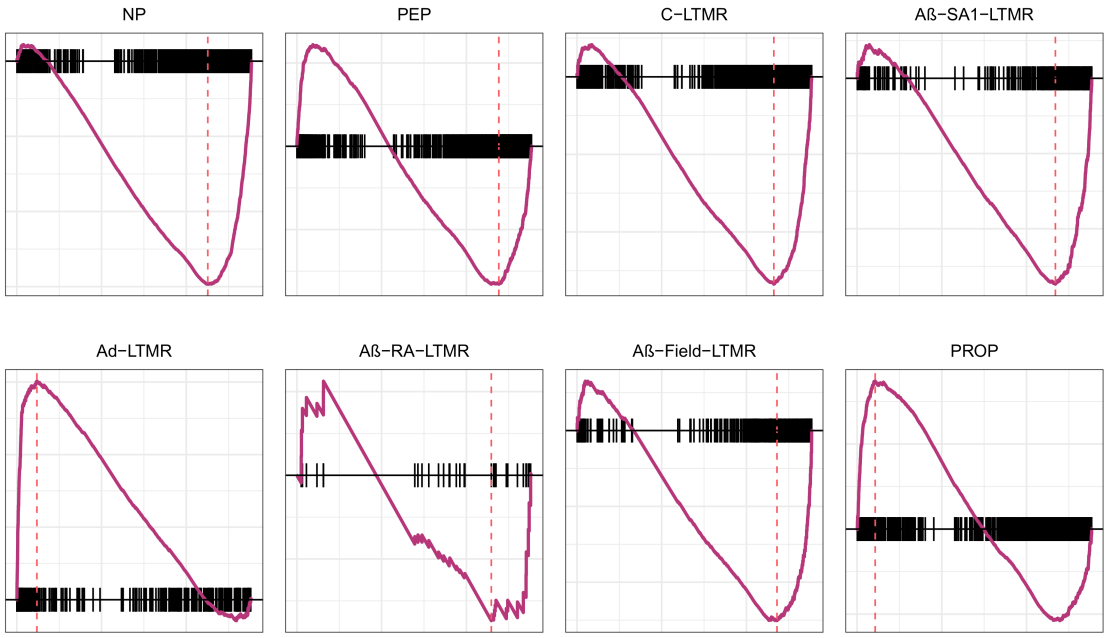

Figure 4A.5: Gene set comparison for injured nociceptors (Scn10a^{cre}), 4 weeks after SNI. Compared to previously published, naïve subpopulation RNA-seq. Related to Figures 3.5 and 4.2. Scores listed in Table 4A.2.

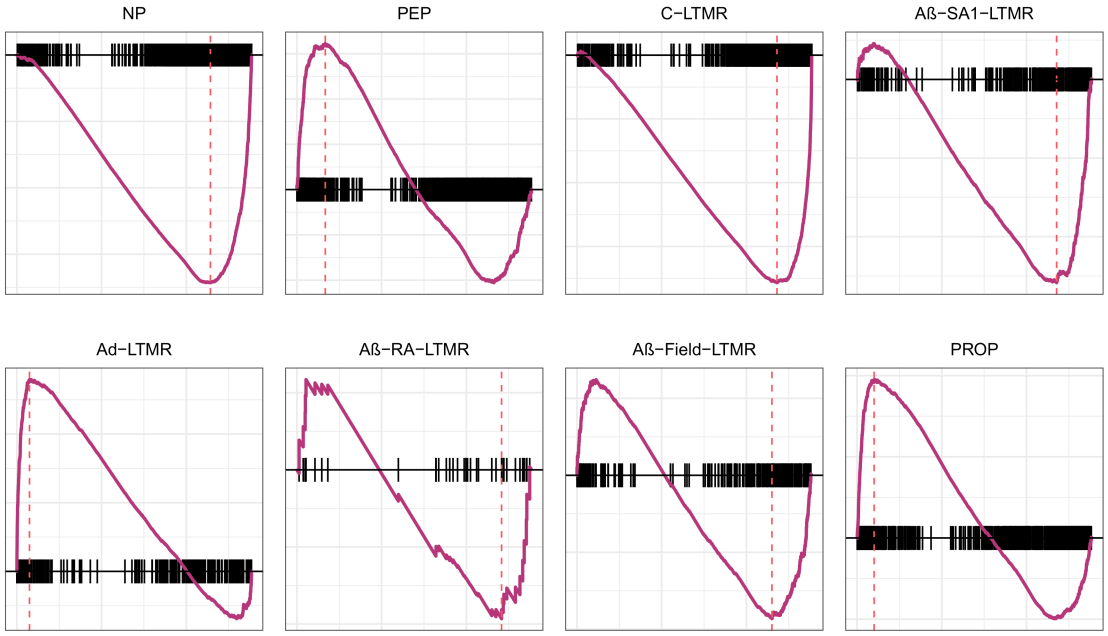

Figure 4A.6: Gene set comparison for injured PEP (Calca^{creERT2}), 4 weeks after SNI. Compared to previously published, naïve subpopulation RNA-seq. Related to Figures 3.5 and 4.2. Scores listed in Table 4A.2.

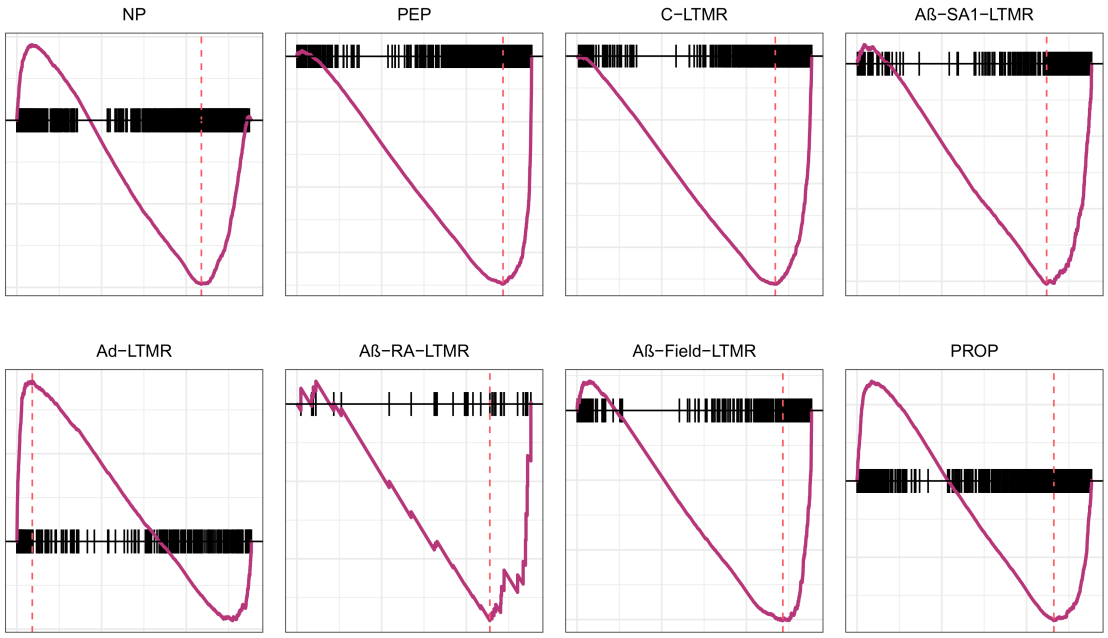

Figure 4A.7: Gene set comparison for injured NP (Mrgprd^{creERT2}), 4 weeks after SNI. Compared to previously published, naïve subpopulation RNA-seq. Related to Figures 3.5 and 4.2. Scores listed in Table 4A.2.

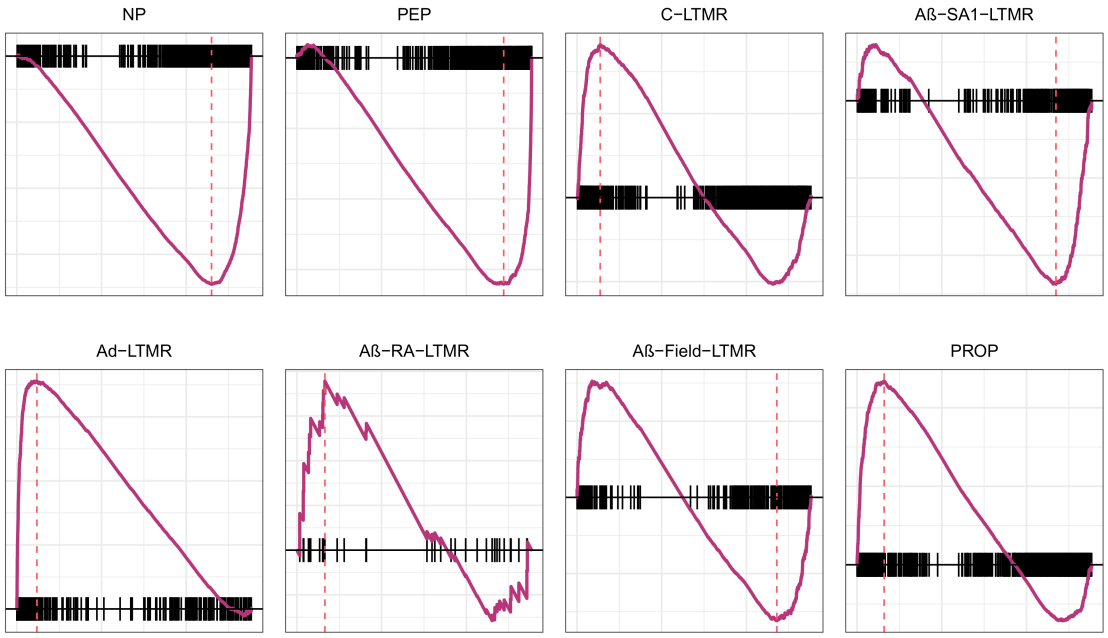

Figure 4A.8: Gene set comparison for injured C-LTMRs (Th^{creERT2}), 4 weeks after SNI. Compared to previously published, naïve subpopulation RNA-seq. Related to Figures 3.5 and 4.2. Scores listed in Table 4A.2.

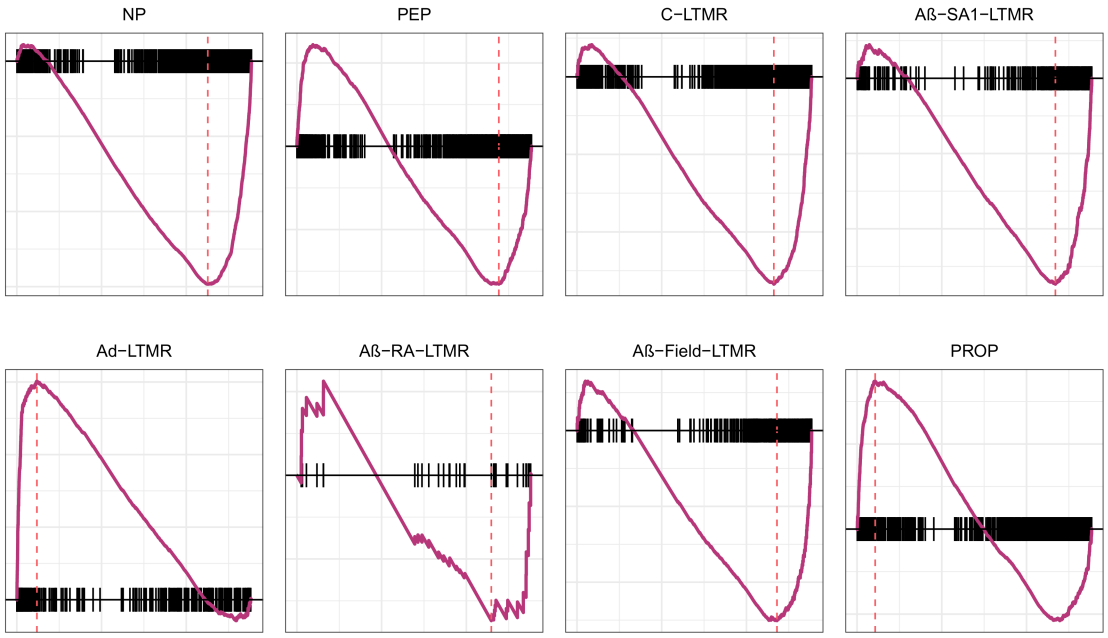

Figure 4A.9: Gene set comparison for injured Aβ-RA + Aδ-LTMRs (Ntrk2$^{\text{creERT2}}$), 4 weeks after SNI. Compared to previously published, naïve subpopulation RNA-seq. Related to Figures 3.5 and 4.2. Scores listed in Table 4A.2.

Table 4A.3: Overlapping DEGs across 4 or 5 neuronal subtypes 3 days after SNI. General nociceptors (Noc.), peptidergic nociceptors (PEP), non-peptidergic nociceptors (NP), C-LTMRs (C-LT) and Aβ-RA + Aδ-LTMRs (A-LT). 1 = differentially expressed (FDR < 0.05, LFC > 1), 0 = not significant.

Gene	Noc.	PEP	NP	C-LT	A-LT
Tubb6	1	1	1	1	1
Slc6a4	1	1	1	1	1
Atf3	1	1	1	1	1
Gadd45a	1	1	1	1	1
Gpr151	1	1	1	1	1
Sprr1a	1	1	1	1	1
Tmem88b	1	1	1	1	1
Wfdc3	1	1	1	1	0
Gal	1	1	1	0	1
Kif22	1	1	1	0	1
Clcf1	1	1	1	0	1
4930544M13Rik	1	1	1	0	1
Sox11	1	1	1	0	1
Gm26457	1	1	1	0	1
Gm5152	1	1	1	0	1
E230016M11Rik	1	1	1	0	1
C030004G16Rik	1	1	1	0	1

Table 4A.4: Overlapping DEGs across multiple neuronal subtypes 4 weeks after SNI. General nociceptors (Noc.), peptidergic nociceptors (PEP), non-peptidergic nociceptors (NP), C-LTMRs (C-LT) and Aβ-RA + Aδ-LTMRs (A-LT). 1 = differentially expressed (FDR < 0.05, LFC > 1), 0 = not significant.

Gene	Noc.	PEP	NP	C-LT	A-LT
Cckbr	1	1	1	0	1
Tubb6	0	1	1	0	1
Wt1	0	1	1	0	1
Atf3	0	1	1	0	1
Pde6b	0	1	1	0	1
Gpr151	0	1	1	0	1
Abca1	0	1	0	0	1
Krt19	0	0	1	0	1
Cyp26a1	0	1	1	0	0
Uox	0	1	0	0	1
Ttll10	1	0	1	0	0
Npy	0	1	0	0	1
Fgf3	0	1	0	0	1
Cdk6	0	1	1	0	0
Ildr2	0	0	1	0	1
Agbl2	0	1	0	0	1
Mchr1	0	1	0	0	1
Flrt3	0	1	0	0	1
Igfn1	0	1	0	0	1
Tmem88b	0	1	0	0	1
AA536875	0	1	0	0	1

Figure 4A.10: DEGs for transcription factors (A) and gene regulation (B), plotted as median VST count data.

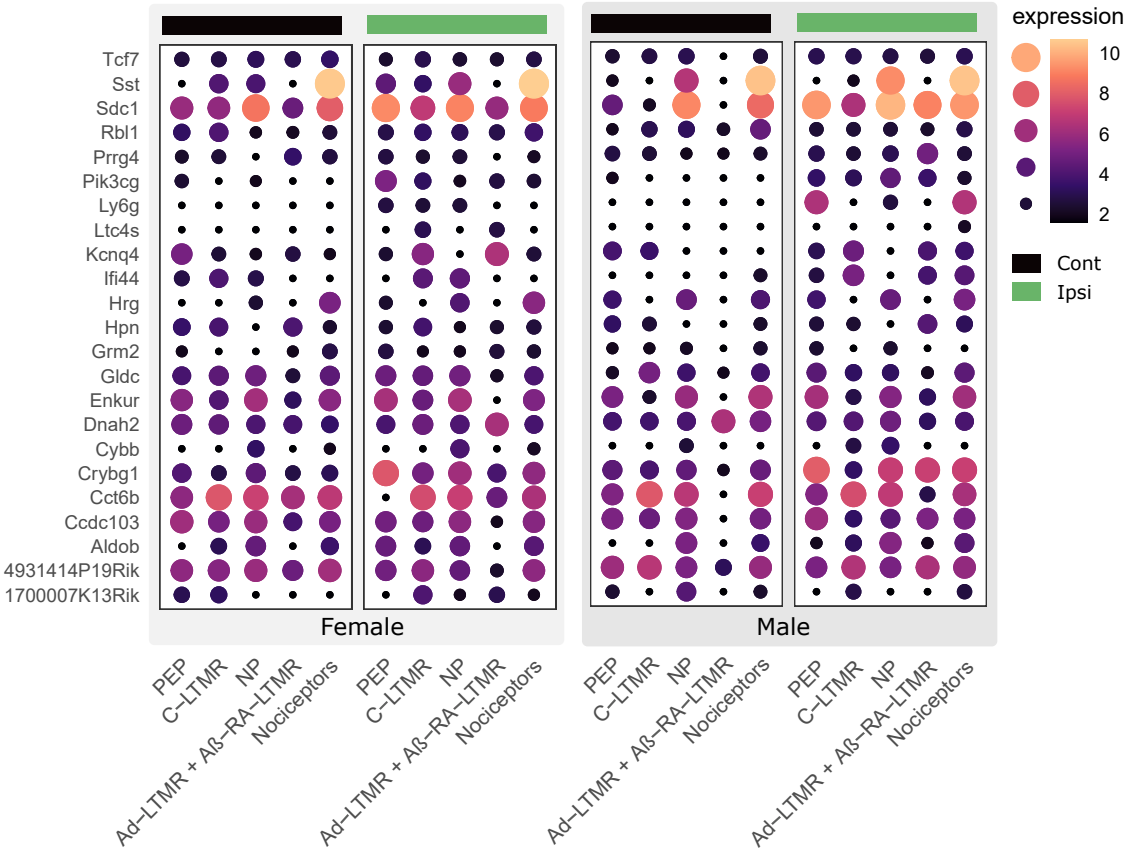

Figure 4A.11: Sexual dimorphism in *Ntrk2* afferents 4 weeks after SNI. Dot plots for median VST expression of top DEGs using an additive design to contrast sex and injury differences in Aβ-RA + Aδ-LTMRs. Related to Fig 4.6

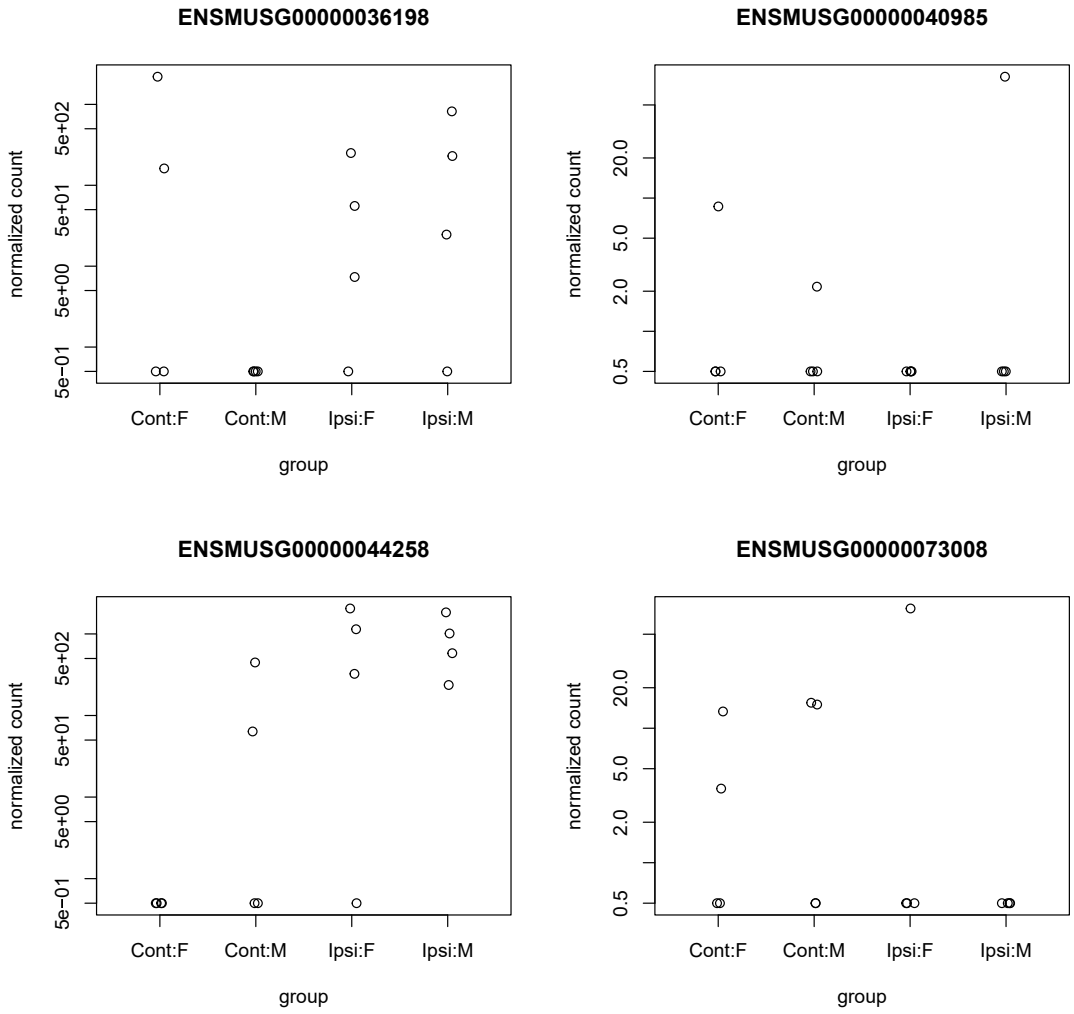

Figure 4A.12: Non-transformed count data for sexually dimorphic genes, calculated with *ashr* shrinkage (Aβ-RA + Aδ-LTMRs 4 weeks after SNI). Related to Fig 4.6.

Table 4A.5: DEGs 3 days after SNI which show regulation in opposing directions. General nociceptors (Noc.), peptidergic nociceptors (PEP), non-peptidergic nociceptors (NP), C-LTMRs (C-LT) and Aβ-RA + Aδ-LTMRs (A-LT). 1 = differentially expressed (FDR < 0.05, LFC > 1 = 1, LFC < -1 = -1, 0 = not significant.

Gene	Noc.	PEP	NP	C-LT	A-LT
Dock2	1	1	0	0	-1
Nol9	1	1	0	0	-1
Ints5	1	1	0	0	-1
Gm12061	1	1	0	0	-1
Gm17655	1	1	0	0	-1
Wnk4	1	-1	0	0	1
Mmp16	1	-1	1	0	0
Slc25a42	1	-1	0	0	0
Zfp324	1	0	0	0	-1
Mthfd2	1	-1	0	0	0
Pex1	1	-1	0	0	0
Med22	1	-1	0	0	0
Celsr1	1	-1	0	0	0
Afmid	1	-1	0	0	0
Ahr	1	-1	0	0	0
Cyb561	1	-1	0	0	0
Fgd6	1	-1	0	0	0
Sgcd	1	-1	0	0	0
Mtif2	1	-1	0	0	0
L2hgdh	1	-1	0	0	0
Galc	1	-1	0	0	0
Npas3	1	-1	0	0	0
Sptlc1	1	-1	0	0	0
Slc25a32	1	-1	0	0	0
Trmu	1	-1	0	0	0
Rabl3	1	-1	0	0	0
Grik1	1	0	0	0	-1
Odf2	1	-1	0	0	0
Arfgap1	1	-1	0	0	0
Cyp2u1	1	0	0	0	-1
Fmn2	1	-1	0	0	0
Nudt2	1	-1	0	0	0
Orc1	1	-1	0	0	0
Ipp	1	-1	0	0	0
Aldh4a1	1	-1	0	0	0
Rita1	1	-1	0	0	0
Il17rc	1	-1	0	0	0
Fbxl19	1	-1	0	0	0
Slc7a6	1	-1	0	0	0
Mns1	1	-1	0	0	0

Gab3	1	-1	0	0	0
Wdr3	1	-1	0	0	0
Daam1	1	-1	0	0	0
9530077C05Rik	1	-1	0	0	0
Tfb1m	1	-1	0	0	0
Fam222b	1	-1	0	0	0
Dhx38	1	-1	0	0	0
Arap2	1	-1	0	0	0
Abhd17c	1	-1	0	0	0
Ccdc68	1	-1	0	0	0
Znfx1	1	-1	0	0	0
Coq10a	1	-1	0	0	0
Rhou	1	-1	0	0	0
Dnph1	1	0	0	0	-1
Scamp5	1	-1	0	0	0
Hectd2	1	-1	0	0	0
Zfp236	1	-1	0	0	0
Disc1	1	0	0	0	-1
Pigv	1	-1	0	0	0
Slc36a4	1	-1	0	0	0
C130050O18Rik	1	-1	0	0	0
Slc25a26	1	-1	0	0	0
Cd109	1	-1	0	0	0
Myorg	1	0	0	0	-1
Zfp316	1	-1	0	0	0
Ccdc125	1	-1	0	0	0
Mb21d2	1	-1	0	0	0
Lrrc3	1	-1	0	0	0
Cfap300	1	0	0	0	-1
Ficd	1	-1	0	0	0
Tmem120b	1	-1	0	0	0
Mettl15	1	-1	0	0	0
Dhcr7	1	-1	0	0	0
Osm	1	-1	0	0	0
Slc27a4	1	-1	0	0	0
Ttr	1	0	0	0	-1
Clip2	1	-1	0	0	0
Spata6l	1	0	0	0	-1
Lekr1	1	-1	0	0	0
Gm14410	1	-1	0	0	0
Hsbp1l1	1	-1	0	0	0
4933413L06Rik	1	-1	0	0	0
Zfp133-ps	1	-1	0	0	0
Gm12743	1	-1	0	0	0
1700123M08Rik	1	-1	0	0	0

4930455G09Rik	1	-1	0	0	0
Gm15336	1	0	0	0	-1
Gm13066	1	-1	0	0	0
D630036H23Rik	1	-1	0	0	0
Gm4535	1	-1	0	0	0
Gm16892	1	-1	0	0	0
Gm37219	1	-1	0	0	0
Gm37274	1	-1	0	0	0
Gm38250	1	-1	0	0	0
Gm38211	1	-1	0	0	0
Gm42742	1	-1	0	0	0
Smim36	1	-1	0	0	-1
A430103D13Rik	1	-1	0	0	0
Gm34574	1	0	0	0	-1
Gm49747	1	-1	0	0	0
C030006K11Rik	1	-1	0	0	0
Gm50103	1	-1	0	0	0
Gtpbp1	-1	1	0	0	1
Gm50012	-1	1	0	0	1
Th	0	1	-1	0	0
Sema4f	-1	1	0	0	0
Hoxa4	0	1	0	0	-1
Pcbp3	-1	1	0	0	0
Itga3	-1	1	0	0	0
Fam98a	-1	1	0	0	0
Tmem25	-1	1	0	0	0
Rapsn	-1	1	0	0	0
Btbd6	-1	1	0	0	0
Cacnb3	-1	1	0	0	0
Ess2	-1	1	0	0	0
Ppfia3	-1	1	0	0	0
Clcn5	-1	1	0	0	0
Pnpla6	-1	1	0	0	0
Rfx5	-1	1	0	0	0
Aplp1	-1	1	0	0	0
Gmnn	-1	1	0	0	0
B4galnt1	-1	1	0	0	0
Mettl1	-1	1	0	0	0
Twist2	-1	1	0	0	0
Kif19a	-1	1	0	0	0
Cars	-1	1	0	0	0
Fsd1	-1	1	0	0	0
Naf1	-1	1	0	0	0
Endog	-1	1	0	0	0
Wnt11	0	1	0	0	-1

E2f3	-1	1	0	0	0
Dnttip1	-1	1	0	0	0
Zc3h18	-1	1	0	0	0
Adora2b	0	1	0	0	-1
Smyd4	-1	1	0	0	0
Plagl1	-1	1	0	0	0
Arfgef3	-1	1	0	0	0
Slc29a3	-1	1	0	0	0
Nsg2	-1	1	0	0	0
Polrmt	-1	1	0	0	0
Map2k6	-1	1	0	0	0
Sh3yl1	-1	1	0	0	0
Fbf1	-1	1	0	0	0
4930512B01Rik	-1	1	0	0	0
Pals1	-1	1	0	0	0
Galnt16	-1	1	0	0	0
Unc79	-1	1	0	0	0
Tnfaip2	-1	1	0	0	0
Trim27	-1	1	0	0	0
Rpp40	-1	1	0	0	0
Slc6a19	-1	1	0	0	0
Ercc8	-1	1	0	0	0
Rab3c	-1	1	0	0	0
Rnf180	-1	1	0	0	0
Mipep	-1	1	0	0	0
Enox1	-1	1	0	0	0
Jph4	-1	1	0	0	0
Adamts20	-1	1	0	0	0
Septin3	-1	1	0	0	0
Zfp251	-1	1	0	0	0
Gtpbp8	-1	1	0	0	0
Setd4	-1	1	0	0	0
Wiz	-1	1	0	0	0
Slc3a1	-1	1	0	0	0
Nudt12	-1	1	0	0	0
Pcdh12	-1	1	0	0	0
C330018D20Rik	0	1	0	0	-1
Pcgf6	-1	1	0	0	0
Cwf19l1	-1	1	0	0	-1
Apex2	-1	1	0	0	0
Nhej1	-1	1	0	0	0
Tmem169	0	1	0	0	-1
Bok	-1	1	0	0	0
Atg16l1	-1	1	0	0	0
Asb1	-1	1	0	0	0

Efcab2	-1	1	0	0	0
Dars2	-1	1	0	0	0
Pmpca	-1	1	0	0	0
Grin1	0	1	0	0	-1
Ly75	-1	1	0	0	0
Il1rn	-1	1	0	0	0
Nup35	-1	1	0	0	0
Tcp11l1	-1	1	0	0	0
Chgb	-1	1	0	0	0
Ttl	-1	1	0	0	0
Pcsk2	-1	1	0	0	0
Atp9a	-1	1	0	0	0
Aar2	-1	1	0	0	0
Ppa2	-1	1	0	0	0
Nudt17	-1	1	0	0	0
Dab1	-1	1	0	0	0
Dnajc6	-1	1	0	0	0
St3gal3	-1	1	0	0	0
Elavl4	-1	1	0	0	0
Fabp3	-1	1	0	0	0
Zfp362	-1	1	0	0	0
Nipal3	-1	1	0	0	0
Casp9	-1	1	0	0	0
Kcnab2	-1	1	0	0	0
Mthfr	-1	1	0	0	0
Clcn6	-1	1	0	0	0
Pex10	-1	1	0	0	0
Dvl1	-1	1	0	0	0
Zcchc4	-1	1	0	0	0
Slc30a9	-1	1	0	0	0
Sds	-1	1	0	0	0
Fbxl14	-1	1	0	0	0
Rasgef1a	-1	1	0	0	0
Klrk1	-1	1	0	0	0
Bcl2l14	0	1	0	0	-1
Slc17a6	-1	1	0	0	0
Tarsl2	-1	1	0	0	0
Synm	-1	1	0	0	0
Kctd13	-1	1	0	0	0
Cdr2	-1	1	0	0	0
Uros	-1	1	0	0	0
Cdk16	-1	1	0	0	0
Plxna3	-1	1	0	0	0
Eri1	-1	1	0	0	0
Cenpu	-1	1	0	0	-1

Phlpp2	-1	1	0	0	0
Dctn1	-1	1	0	0	0
Ddx25	-1	1	0	0	0
Rnf111	-1	1	0	0	0
Topbp1	-1	1	0	0	0
Nckipsd	-1	1	0	0	0
Abcc10	-1	1	0	0	0
Sgpp2	-1	1	0	0	0
Dis3	-1	1	0	0	0
Zdhhc15	-1	1	0	0	0
Coil	-1	1	0	0	0
Fancd2	0	1	0	0	-1
Hdac11	-1	1	0	0	0
Igsf9b	-1	1	0	0	0
Traf3ip1	-1	1	0	0	0
Cbl	-1	1	0	0	0
Ap2b1	-1	1	0	0	0
Abraxas1	-1	1	0	0	0
1810055G02Rik	-1	1	0	0	0
Ibtk	-1	1	0	0	0
Tmem59l	-1	1	0	0	0
Tmtc2	0	1	0	0	-1
Gmip	-1	1	0	0	0
Noa1	-1	1	0	0	0
Tmem177	-1	1	0	0	0
Zcwpw1	-1	1	0	0	0
Tulp1	-1	1	0	0	0
Ccdc138	-1	1	0	0	0
Dexi	-1	1	0	0	0
Primpol	-1	1	0	0	-1
Reep2	-1	1	0	0	0
Hoxb5	-1	1	0	0	0
Cfap157	-1	1	0	0	0
Mtmr7	-1	1	0	0	0
Tspyl4	-1	1	0	0	0
Ccser1	-1	1	0	0	0
Pgap4	-1	1	0	0	0
Zfp189	-1	1	0	0	0
Zer1	-1	1	0	0	0
Nploc4	-1	1	0	0	0
Ralyl	-1	1	0	0	0
Rhbdd2	-1	1	0	0	0
Phtf2	-1	1	0	0	0
Disp2	-1	1	0	0	0
Ttc12	-1	1	0	0	0

Mis12	-1	1	0	0	0
Cep126	-1	1	0	0	0
Spen	-1	1	0	0	0
C1qtnf4	-1	1	0	0	0
Atp1a3	-1	1	0	0	0
Dmxl2	-1	1	0	0	0
Katnal1	-1	1	0	0	0
Bicdl1	-1	1	0	0	0
Csdc2	-1	1	0	0	0
Dlgap3	-1	1	0	0	0
Prdm10	-1	1	0	0	0
Maneal	-1	1	0	0	0
Csrnp2	-1	1	0	0	0
Pigz	-1	1	0	0	0
Asphd1	-1	1	0	0	0
Sh2d7	-1	1	0	0	0
Zfp518b	-1	1	0	0	0
1110032F04Rik	-1	1	0	0	0
Champ1	-1	1	0	0	0
Sacs	-1	1	0	0	0
Cyb561d1	-1	1	0	0	0
Lonrf2	-1	1	0	0	0
Gpr137c	-1	1	0	0	0
Frmpd4	-1	1	0	0	0
Prmt6	-1	1	0	0	0
Proser1	-1	1	0	0	0
2310022A10Rik	-1	1	0	0	0
Morn4	-1	1	0	0	0
Zfp668	-1	1	0	0	0
Snip1	-1	1	0	0	0
Kcnb1	-1	1	0	0	0
2310061I04Rik	-1	1	0	0	0
Pgbd5	-1	1	0	0	0
Zfp52	-1	1	0	0	0
Tbc1d30	-1	1	0	0	0
St6galnac3	-1	1	0	0	0
Zfand2a	-1	1	0	0	0
Ptrh1	-1	1	0	0	0
Txlna	-1	1	0	0	0
Vapb	-1	1	0	0	0
Tmem62	-1	1	0	0	0
Arhgef33	-1	1	0	0	0
Snupn	-1	1	0	0	0
Elapor2	-1	1	0	0	0
Cars2	-1	1	0	0	0

H2bu2	-1	1	0	0	0
Usp13	-1	1	0	0	0
Camk2b	-1	1	0	0	0
Zfp809	-1	1	0	0	0
Cend1	-1	1	0	0	0
Zfp128	0	1	0	0	-1
Ccdc62	-1	1	0	0	0
Hs6st2	-1	1	0	0	0
Lhfpl5	-1	1	0	0	0
Ap3b2	-1	1	0	0	0
Hdac10	-1	1	0	0	0
Nrg1	-1	1	0	0	0
Kcnma1	-1	1	0	0	0
Zfp35	-1	1	0	0	0
Krr1	-1	1	0	0	0
Slc22a21	-1	1	0	0	0
Nr6a1	-1	1	0	0	0
Gm10176	-1	1	0	0	0
Arfgef1	-1	1	0	0	0
Gtf2f2	-1	1	0	0	0
B630019A10Rik	0	1	0	0	-1
Slc7a14	-1	1	0	0	0
Slc35g2	-1	1	0	0	0
Eid2b	-1	1	0	0	0
Ccnyl1	-1	1	0	0	0
Zfp65	-1	1	0	0	0
Bhlhb9	-1	1	0	0	0
D2hgdh	-1	1	0	0	0
Ccdc61	-1	1	0	0	0
Gm12359	-1	1	0	0	0
Cfap74	-1	1	0	0	0
Zfp566	-1	1	0	0	0
Gm17396	-1	1	0	0	0
Gm12216	-1	1	0	0	0
Gm11706	-1	1	0	0	0
Halr1	-1	1	0	0	0
Gm16976	0	1	0	0	-1
Hoxb5os	-1	1	0	0	0
Gm7805	-1	1	0	0	0
Mkln1os	0	1	0	0	-1
Gm11457	-1	1	0	0	0
4933427G23Rik	-1	1	0	0	0
Gm15860	-1	1	0	0	0
Gm16235	-1	1	0	0	0
Gm16835	-1	1	0	0	0

Gm11715	-1	1	0	0	0
5330434G04Rik	-1	1	0	0	0
Fcor	-1	1	0	0	0
A730090N16Rik	-1	1	0	0	0
A430057M04Rik	-1	1	0	0	0
Gm17484	-1	1	0	0	0
Gm17092	-1	1	0	0	0
Gm4353	-1	1	0	0	0
NA	-1	1	0	0	0
Gm21839	-1	1	0	0	0
Gm26885	-1	1	0	0	0
G630030J09Rik	-1	1	0	0	0
Gm26549	0	1	0	0	-1
Gm47512	-1	1	0	0	0
2900076A07Rik	-1	1	0	0	0
Gm26684	-1	1	0	0	0
Platr31	-1	1	0	0	0
4921504A21Rik	0	1	0	0	-1
Phf20-ps	0	1	0	0	-1
Gm28800	-1	1	0	0	0
Gm37899	-1	1	0	0	0
Gm36992	-1	1	0	0	0
Gm37446	0	1	0	0	-1
Gm43336	-1	1	0	0	0
C130013H08Rik	-1	1	0	0	0
Gm42517	-1	1	0	0	0
Gm32102	0	1	0	0	-1
Dancr	-1	1	0	0	0
Gm6261	-1	1	0	0	0
Gm44317	-1	1	0	0	0
4930588G17Rik	0	1	0	0	-1
Gm35021	-1	1	0	0	0
Gm32856	-1	1	0	0	0
Gm45892	-1	1	0	0	0
4930517E14Rik	-1	1	0	0	0
Gm48678	-1	1	0	0	0
Gm48420	-1	1	0	0	0
Gm47639	-1	1	0	0	0
Gm49743	-1	1	0	0	0
Gm41293	0	1	0	0	-1
4833415N18Rik	-1	1	0	0	0
Bcl6b	0	-1	0	0	1
Exoc3l2	0	-1	0	0	1
Aldh1a3	0	-1	0	0	1
Pigt	-1	0	0	0	1

Fbxo5	0	-1	0	0	1
Rsad2	-1	0	0	0	1
Epha1	0	-1	0	0	1
Zranb3	-1	0	0	0	1
Ppp1r13l	0	-1	0	0	1
She	0	-1	0	0	1
Rnd1	-1	0	0	0	1
Gm11532	0	-1	0	0	1
Rbm12	-1	-1	0	0	1
Sec14l5	0	-1	0	0	1
S100a2	-1	0	0	0	1
Zfp97	0	-1	0	0	1
4731419I09Rik	0	-1	0	0	1
A430110C17Rik	0	-1	0	0	1
Gm6525	0	-1	0	0	1
4732416N19Rik	-1	0	0	0	1
4930413G21Rik	-1	0	0	0	1
Eef1akmt4	-1	0	0	0	1
Galnt6	0	-1	1	0	0
Sag	-1	0	1	0	0

5

Molecular profiling of injured and intact neurons

Across models of neuropathic pain, ipsilateral DRGs can contain both injured and intact neurons. The contributions of these populations to pain remain unclear. The availability of an Atf3^{creERT2} to label and sort neurons allowed us to explore this via high throughput sequencing. Using RNA-seq, we show that intact neurons largely mirror their contralateral counterparts, with minor differences at a molecular level. In an acute state, we also see an immune-based interaction of sex and injury which is not present by 4 weeks. We have complemented this with a pilot snATAC-seq study, showing that neurons cluster by subtype in naïve and injured states.

Contents

5.1 Introduction

Our previous dataset contrasted ipsilateral and contralateral afferents after injury. In neuropathic pain conditions however, the contribution of the injured and intact neurons ipsilateral to the site of injury remains unclear. Here, we study the molecular changes within these populations after peripheral injury using a combination of bulk RNA-seq and single nuclear ATAC-seq (snATAC-seq).

Our current knowledge of injured versus intact afferents is still debated [243]. There is evidence for the role of both injured and intact afferents in painful phenotypes, which have been presented as the 'injured afferent' and 'intact afferent'

hypotheses [244]. The integration of these roles, along with higher order processes, neuro-immune interactions, and sympathetic sprouting into the dorsal root ganglia contribute to neuropathic pain states.

Injured afferents Injured afferents refer to those directly in the line of trauma, with a final common pathway of axonal degeneration. This can arise from peripheral transection/ligation, or immune mediators (if neurons are partially damaged, natural killer cells can contribute to further degeneration [98]). This frequently includes subset of neurons within a DRG, unless entire spinal nerves are affected.

The transcriptional profile of naïve neurons mirrors their function, and you can see DRG ganglia subdivided into specific functional classes based on transcript profiles. In injured states, this is not the case. Injured neurons lose this cell-type specific profile and develop a more stereotyped "injured" state, in an *Atf3*-dependent reprogramming [42]. This process is rapid, occurring over the span of a few days.

Functionally, injured afferents show changes in electrophysiological states, including the development of ectopic, spontaneous activity [245, 246], with the majority of these afferents undergoing Wallerian degeneration in response to injury [243, 247].

Intact afferents Intact afferents are DRG neurons located within the same, or adjacent DRG implicated in injury. These cells experience changes to their local environment but do not experience direct assault by the originally injury mechanism. Across species, these neurons undergo a range of electrophysiological changes in injured states, including the development of spontaneous activity [120, 248, 249].

5.1.1 Injured and intact comparisons

Seminal works exploring intact and injured afferents were published in the 1990s and early 2000s. This includes a large body of work on male rats, as well as fewer studies on mice, humans, and non-human primates [244, 250]. Together, there is a broad take home message that both injured and intact afferents are involved in a range of neuropathic pain readouts, with roles complicated by timecourse, injury type, and immune response.

Both injured and intact afferents show sensitization to TNFα after nerve injury [251], and both can develop spontaneous C-fibre activity in neuropathic states across species [120, 249, 252]. Experiments involving the removal of ganglia and/or dorsal rhizotomy implicate intact neurons in mechanical hyperexcitability [249, 253, 254], while tetrodotoxin application to ligated nerves results in a partial recovery in Von Frey withdrawal, supporting the role of injured afferents [255].

At a molecular level, differences arise. For example, Obata and colleagues have shown NPY regulation related to ERK activation in injured afferents, paired to BDNF regulation and p38 activation in intact, small diameter cells [256]. Subtype differences can also be seen. For example, *P2rx3* expression, commonly associated with NP neurons, has been shown to increase in intact neurons, paired to a reduced immunoreactivity in injured (*Atf3*+) afferents in both the DRG and TG [257]. There is also a increase in Substance P expression in injured, large diameter (but not small) afferents [258]. Here, intact afferents were not studied.

5.1.2 Pain model considerations

Differences in pain models are likely to affect the role of different afferent types. Local transections, crushes, ligations, and systemic models like chemotherapy all result in nerve damage, but differences in mechanism can translate to differences in behavioural readouts, recovery, and gene expression changes. For example, dorsal root injury - where the neurons are injured centrally - shows a distinct injury pattern from peripheral injury counterparts. In general, dorsal root injury produces a more modest transcriptional response, with less expression of regeneration associated genes: *Atf3*, for example is only upregulated in large diameter DRG neurons [259]. Additionally, "intact" neurons historically refers to afferents within DRG that are not transected, as well as those in adjacent ganglia (eg. L4 neurons are intact, after L5 spinal nerve ligation). It is thus possible that this population can be further subdivided.

5.1.3 Aims

As discussed in chapter 2, these DRG subpopulations can be isolated through a combination of transgenic labelling and fluorescent sorting. Here, we focus on changes in intact and injured afferents after spared nerve injury (SNI). It is a consistent, robust model where we spare the sural nerve in one leg, relying on the internal contralateral control to provide a unique "naive" comparison. From this, we set out to isolate intact and injured neurons for a combination of bulk RNA-seq and snATAC-seq to further explore molecular changes.

5.2 Methodology

5.2.1 Animals

All work was done in accordance with the UK Home Office and the University of Oxford Policy on the Use of Animals in Scientific Research. This study conforms to ARRIVE guidelines. Atf3^{creERT2} characterization is shown in chapter 2, section 2.3.1.6.

5.2.2 Sample collection

Sample size was calculated using the algorithm published by Zhao et al., with the same parameters in Chapter 3 [207]. Samples were collected at three days and four weeks. Techniques mirror those used in Chapter 3. To reiterate, adult animals were first overdosed and perfused transcardially with sterile, ice cold saline. Lumber DRGs L3-L5 were quickly removed and placed into HBSS on ice. Post-dissection of all tissue, collagenase/dispase was added for an hour long digest at 37°C followed by mechanical dissociation with polished glass pipettes. Myelin and debris was removed using a 15% w/v BSA cushion.

Samples were transferred on ice immediately to the WIMM FACS Facility (Oxford) for sorting on a BD FACSAria Fusion 2 using a 100 µm chip. For each condition, 100 cells were isolated directly into low protein binding eppendorfs

containing 2 µl NEBNext Single Cell Lysis Buffer (NEB, E5530S). Samples were kept on dry ice until transfer to -80°C for overnight storage.

5.2.3 RNA-seq

After collection, samples were thawed on ice and randomized into a 384-well 4titude Framestar skirted PCR plate. Samples were processed using NEB Ultra low/Smarter cDNA amplification followed by sequencing. Non-directional libraries were prepared together by the Oxford Genomics Centre, and paired-end sequencing was performed using the NovaSeq6000 platform, with a 150 bp read length, at a depth of $3.0x10^7$ reads per sample. Full library preparation details are outlined in chapter 3.

5.2.3.1 Bioinformatics

The analysis pipeline mirrored that used in chapter 3, with details in section 3.2.6. Again, reads were mapped to the GRCm38 genome using STAR aligner [210]. Samtools was used to sort, index, and merge BAM files [211]. Quality control (QC) was performed with both FastQC and Samtools prior to gene counting with HTSeq [211–213]. Count corrections for effective library sizes were performed in R using DESeq2, and normalized gene counts were fitted to a negative binomial distribution. Count transformations were performed using VST for all visualizations [214].

Injury signatures Injury signatures were previously extracted from the dataset presented in chapter 4. Differentially expressed gene lists were extracted and used in an SPCA of the current data. The first principal component (PC1) was then compared across conditions.

Differential expression analyses Count data was first filtered to genes with an average of 5 reads in at least 10% of the samples. Differential expression testing was then performed using the Wald test and a weighted FDR correction (independent hypothesis weighting, IHW), in line with chapter 3 and chapter 4, using a grouping factor for time and condition.

Gene set enrichments GSEA analyses were performed using ranked $\log_2$ fold changes (LFC) via msigdbr [216] and clusterProfiler [217] libraries. Custom GSEA analyses were calculated against a curated list of enriched genes from previously published subpopulation data, as described in chapter 3 [5]. GO term analyses for DEGs were performed using the Wallenius method via goSeq (R) [219]. As before, the filtered count data was used as a background (5 reads in at least 10% of the samples).

5.2.4 snATAC-seq

Wildtype samples were collected in Oxford, and involved MACS purification prior to FACS. MACS sorting is described in detail in Chp 2. Atf3$^{\text{creERT2}}$ samples were collected at the University of Glasgow by Dr. Gregory Weir. Samples were pooled for sex, and collected four weeks after SNI. In Glasgow, this line is crossed to ai9, instead of the ai14 tdTomato reporter used in Oxford, differing by the insertion method. Glasgow experiments were approved by the University of Glasgow.

All cells were sorted in CryoStor CS10 Freezing Media (Stem Cell Technologies, 07959). Nuclei were extracted in parallel via lysis according to the 10x Genomics protocol. Single nuclear ATAC library preparation was performed using 10x Genomics v1.1 reagents and samples were sequenced on an Illumina NextSeq 500 using the 10X Genomics pipeline at the Glasgow Polyomics Facility.

5.2.4.1 Bioinformatics

Initial analyses were performed using CellRanger-atac. Sequencing data were processed and mapped to the GRCm38 genome, and Bed files were merged via Signac. Barcodes (nuclei) with at least 500 reads were included in downstream analyses. Peaks were called through GenomicRanges [260] and filtered to a width between 20-10000. Sample normalization across cells and peaks was performed via Signac through term frequency-inverse document frequency (TF-IDF) normalization. UMAP projections were performed on dimensions 2:30, as the first dimension correlated to the total number of counts per cell. Subsequent analyses were performed in R using the Seurat and Signac libraries [261, 262].

Quality control was performed by both CellRanger-atac and Signac, and includes the total number and % of fragments per peak, as a measure of sequencing depth and quality, respectively, as well as transcription start site (TSS) enrichment scores. TSS enrichment was calculated for 2000 bp on either side of the TSS (4000 bp in total). Nuclei from the intact library were omitted due to low median fragment counts, as well as low cell counts.

Data were integrated with publicly available single cell RNA-seq data (Allen Brain Atlas) to assign population identities [263]. Annotated data was readily available in the form of a Seurat object (`https://satijalab.org/signac/articles/mouse_brain_vignette.html`). After annotation, top neuronal markers were extracted using a Wilcoxon Rank Sum test across all genes expressed in 5% of either cluster. Larger cell numbers are required for high powered differential analysis between injured and control ATAC signatures. Even so, we piloted differential expression between injured and contralateral samples using a Wilcoxon Rank Sum test.

5.3 Results

5.3.1 Overview

Using transgenic labelling of injured DRG neurons forty-eight samples were collected, processed and sequenced (Figure 5.1A). Reads were successfully mapped to the GRCm38 Mouse Genome with a median read coverage of 85.98% (Figure 5.1B-C), and one sample was removed due to poor mapping. As expected, male and female samples were identifiable by *Xist* expression (5.1D), and injured samples are distinguishable by *Atf3* expression (5.1E).

Samples readily separate by injured status (Figure 5.1F-G). A subset of tdTomato- samples (both contralateral and intact) cluster separately from the rest of their cohort. It is unclear why, and we hypothesize this to be due to an inherent variability in the sample collection. These four samples are from both male and female mice. The PCA bi-plot shows 3D and 4W injured (tdTomato+, ie. *Atf3* expressing) samples cluster separately from uninjured samples. Both contralateral and intact

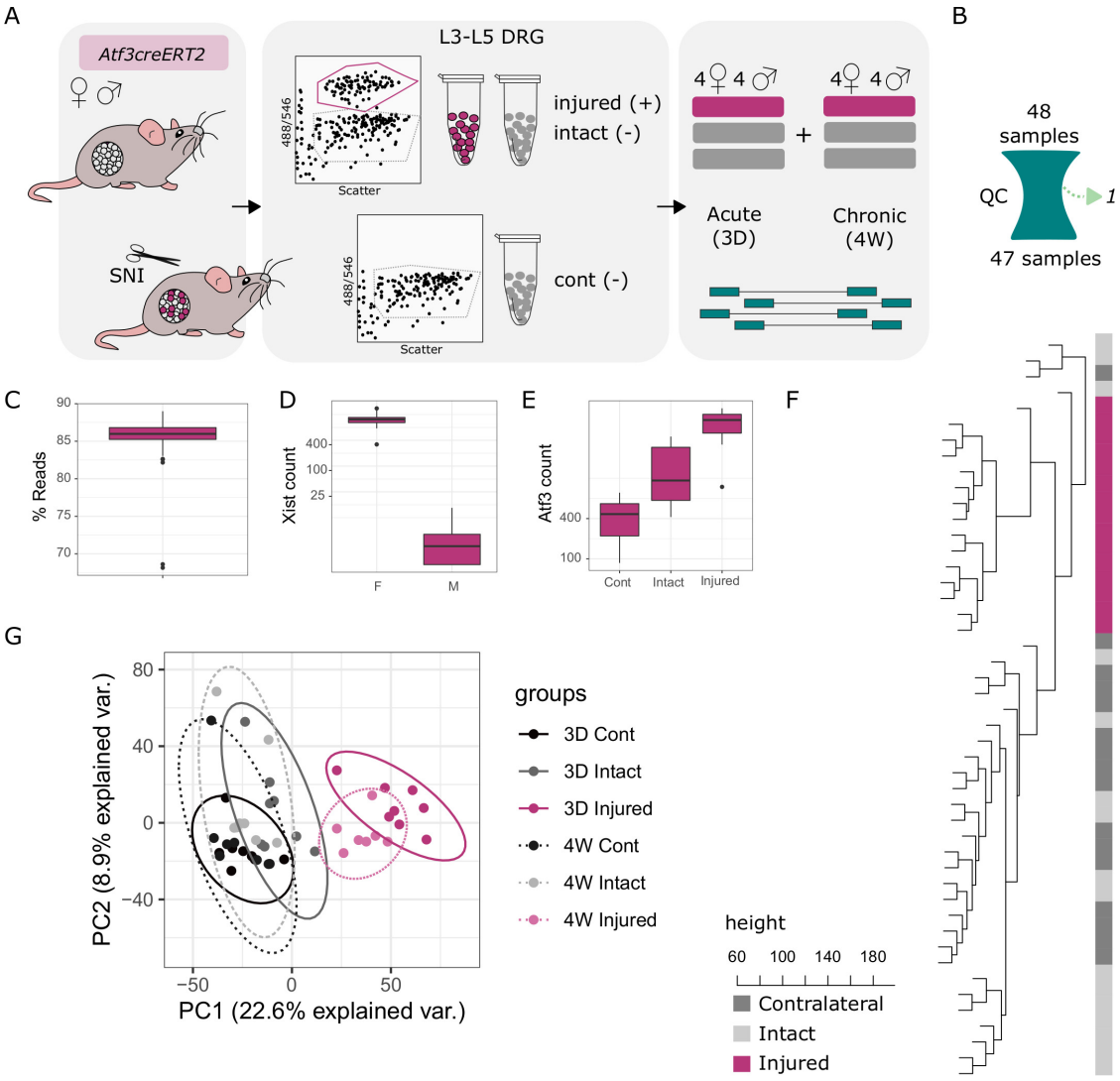

Figure 5.1: RNA-seq of Atf3^{creERT2} mice after SNI. A. Overview of the sample collection, through FACS, based on *Atf3*-driven tdTomato expression in injured neurons. B. Quality control schematic. C. Percentage of uniquely mapped reads across sample runs. D. *Xist* count data by sample. E. *Atf3* count data by sample. F. Hierarchical clustering of by euclidean distance. G. PCA bi-plot by timepoint and condition. Intact: *Atf3*-negative, ipsilateral samples. Injured: *Atf3*-positive, ipsilateral samples. Cont: *Atf3*-negative, contralateral samples.

(ipsilateral, tdTomato-) samples largely cluster together as these time points. Minor overlap between three day intact and injured samples is apparent. Due to the temporal requirements of tdTomato expression post-injury in the Atf3^{creERT2} line, this overlap would support the notion of some injured, but still unlabelled cells are present in the tdTomato- samples.

5.3.2 Injury

In our previous RNA-seq experiment, we extracted an unbiased injury signature through a supervised principal component analysis (SPCA) on DEGs. Using the same DEG list from this general injury signature (combined subpopulation samples, in 4.1), we see a clear separation of conditions at both timepoints in this distinct dataset (Kruskal-Wallis chi-squared, followed by Wilcoxon rank sum with BH adjustment) (5.2A). Across timepoints, ipsilateral samples differ from their contralateral counterparts, although no difference is seen between 3D and 4W cont ($p = 0.65$). Mirroring our previous data, injured samples are also less strongly correlated at 4 weeks than at 3 days, reflecting a return to baseline ($p = 0.00052$).

Gene enrichment analyses were next performed for injured samples across timepoints against previously published naïve subtypes (Fig 3.5). Here, we see a negative enrichment for NP at 4W, along with positive enrichments of PEP and Aβ-Field-LTMR (5.2B). No other subtypes reach significance, with values listed in Table 5A.1.

In line with previous data, we see an upregulation in injury genes in our injured afferents, as well as a moderate upregulation in intact ipsilateral samples compared to control levels (5.2C). Differential expression testing highlights a large number of regulated genes between injured and intact (3D: 1575, 4W: 1472), as well as injured and contralateral samples (3D: 2811, 4W: 1363), with a large overlap between the two lists at both timepoints (5.2D-H, 5A.1A). GO analyses for biological processes highlight a number of hits common to injury in our injured afferents. At three days, there is an upregulation in injured afferents to inflammatory response and apoptosis, paired to a reduction in the behavioural response to pain. By 4 weeks, we seen an upregulation in axon guidance, apoptosis, and cell adhesion, along with a reduction in signal transduction, oxidative stress, and endocytosis. All GO tables are available online (`https://github.com/aliibarry/thesis-supp`).

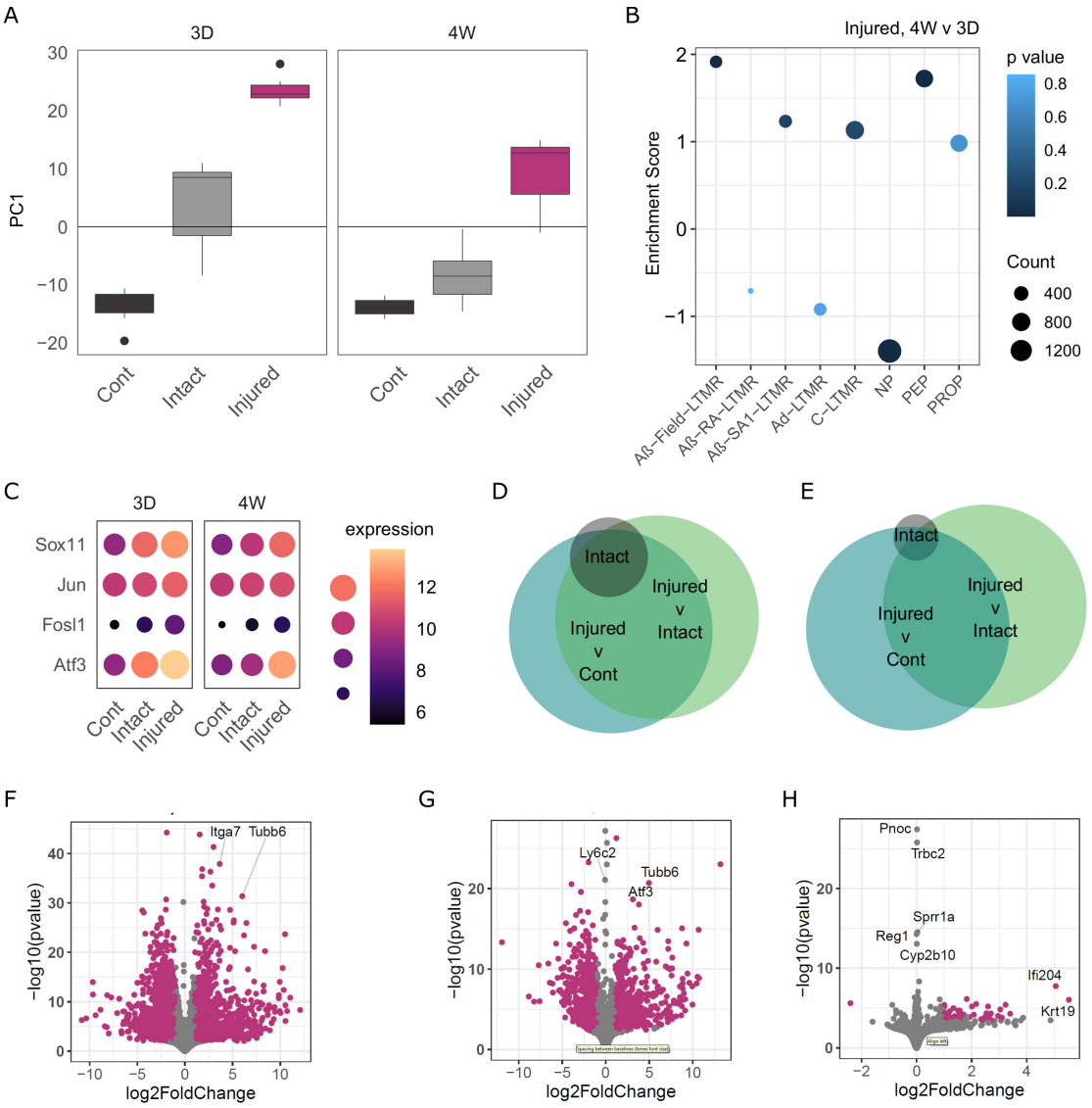

Figure 5.2: Injured and intact afferents after SNI. A. Injury signature across timepoints and conditions. Signature was derived from an SPCA of differentially expressed genes from a previous dataset (chapter 4, 4.1). B. Gene set enrichment analyses between 4W and 3D injured afferents, based on subpopulation enrichment from Zheng and colleagues [5]. C. Hallmark injury genes, plotted as median transformed counts. D-E. DEGs for 3D (D) and 4W (E) across conditions. F-H. Volcano plots highlighting DEGs (magenta, LFC > 1, FDR < 0.05), for 3D injured vs contralateral (F), 4W injured vs contralateral (G), and 4W intact vs contralateral (H).

5.3.2.1 Intact changes

Intact samples largely resemble contralateral afferents, but they exist in a different immune environment after injury. Using the ATF3$^{\text{creERT2}}$, we are able to specifically look at changes in intact afferents after SNI, instead of grouping them together in

more generalized ipsilateral samples (Fig 5.3). At three days, 153 genes are regulated against contralateral samples, with the large majority (140/153) overlapping with DEGs from injured afferents. This is likely confounded by injured neurons that have not started to express tdTomato. By four weeks, when tdTomato expression has peaked, 45 genes are regulated. This includes the upregulation of *Atf3* and *Sox11*, as well as a handful of genes involved in ligand-receptor binding or immune response, such as *Nts*, *Il13ra1*, *Cxcl16*, and *Cntfr* (5.3B-C, 5A.3). Many of these genes are also regulated in injured afferents compared to contralateral or intact samples (27/45), and eight genes show regulation across both timepoints (*Atf3*, *Sox11*, *Tubb6*, *Csf1*, *Adam8*, *Trf*, *Stx11*, *Tnfaip6*). Uniquely-regulated genes at four weeks are listed in Table 5A.2. This contains a number of transmembrane proteins, including *Tmed7*, *Tmem123*, and *Klra17*, as well as a subset of genes involved in gene regulation (*Zfp974*, *Dhx38*).

GO analyses show few hits, due to the low number of DEGs. At 3D, this includes an upregulation in inflammatory response, nervous system development, and cell population proliferation, as well as a down regulation of various catabolic processes. By four weeks, there is an upregulation of genes related in lymphocyte chemotaxis and neural tube formation, paired to a reduction in protein processing.

GSEA against all gene sets highlights additional changes across sample conditions. In an acute state, this includes a reduction in oxidative phosphorylation and DNA repair, as well as in increased signature for inflammatory response and *Tnfa* signaling via *Nfkb* (5.3D). For 4 weeks, there is still a reduction in oxidative phosphorylation, and increases in inflammatory response, *Tnfa* signaling via *Nfkb*, and *Il6-Jak-Stat3* signaling (5.3E), suggesting functional differences in intact afferents and their contralateral counterparts.

5.3.3 Sexual dimorphism

We previously noted within subpopulation sex differences in a naïve state (chapter 3), that was not strongly exacerbated by an interaction with injury (chapter 4). The inclusion of both male and female mice in this dataset allows us to query sex

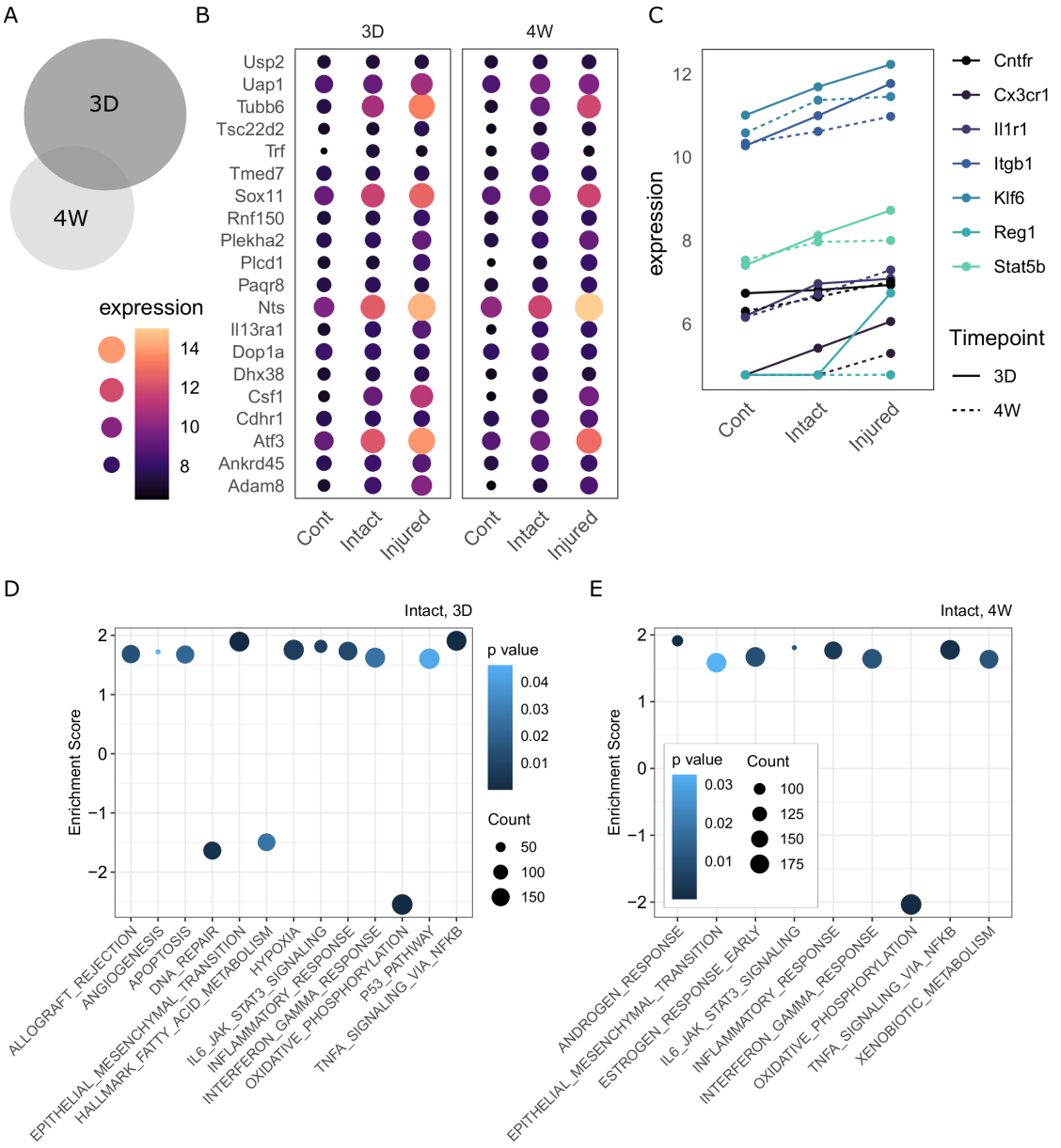

Figure 5.3: Intact afferents show changes after SNI. A. 8 genes overlap between 3D and 4W DEGs compared to contralateral tissue. B. Example DEGs from 4W. C. Immune-related DEGs from intact comparisons. D-E. GSEA plots against hallmark gene sets for 3D (D) and 4W (E).

interactions in intact and injured populations (5.4). Injured afferents do not show a strong interaction with sex (5.4A-B), with 3 DEGs (*Slc25a28*, *Gabarapl1*, *Ahnak2*) at three days, and 1 DEG (*Vars*) by four weeks. In line with our previous dataset, results are dependent on the shrinkage method, with a more relaxed shrinkage by *ashr* capturing large fold changes (5.4B).

In intact afferents, we start to see hints of sexual dimorphism emerge when

compared to contralateral tissue (5.4C-F). At 3D, 69 genes show an interaction effect (LFC > 1, FDR < 0.05). By 4 weeks, only 3 (*Gm7059*, *Rpl7-ps8*, *Gm14138*) with no overlap over time. GSEA analyses suggest sex differences in oxidative phosphorylation, as well as *Tnfa* signaling via *Nfkb*, DNA repair, and reactive oxygen species pathways. Validation of more highly expressed genes (5.4E), or those with the largest fold changes (5.4F) are required to add confidence.

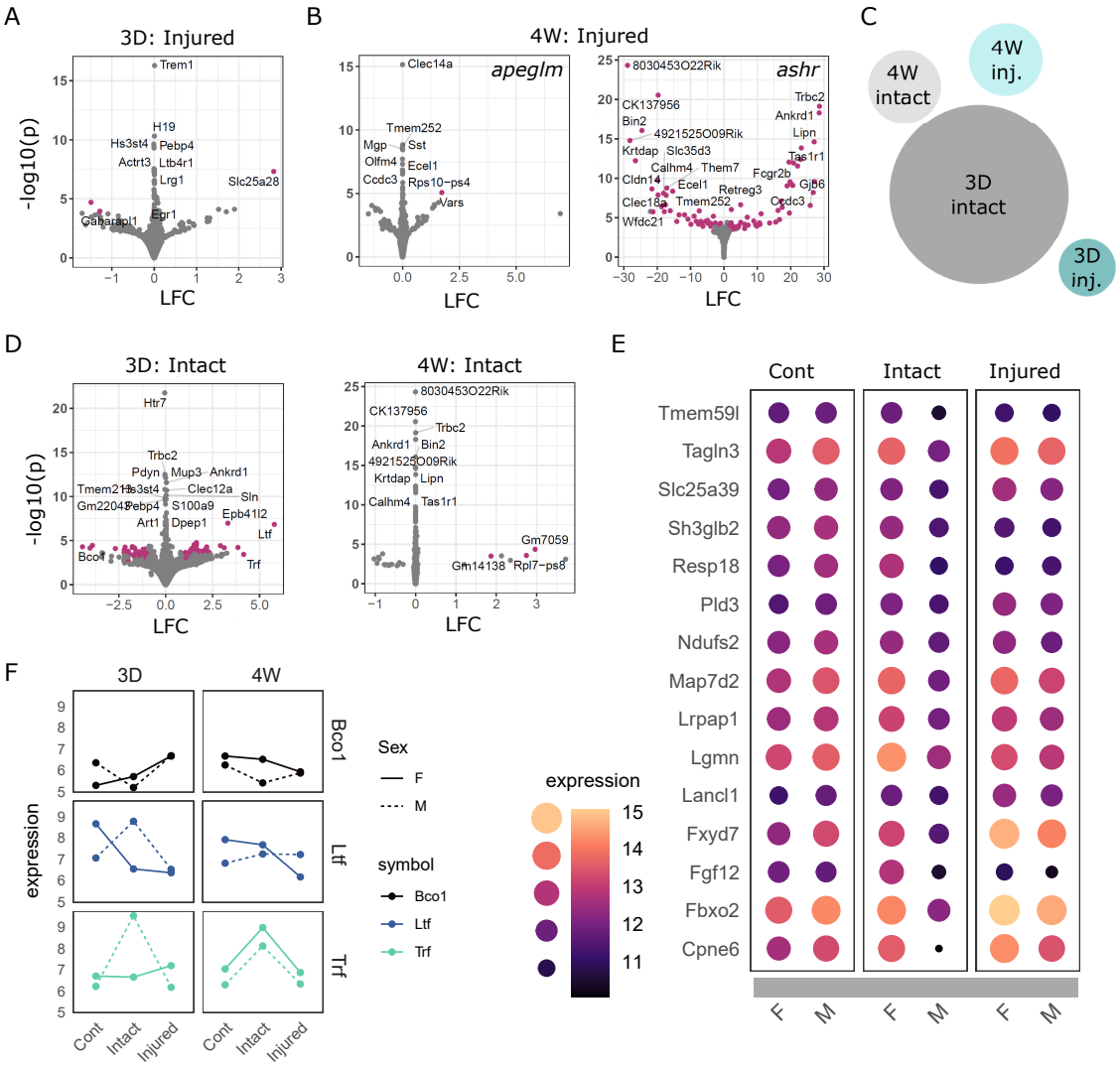

Figure 5.4: Sexual dimorphism in intact afferents. A-B. Volcano plots for DEGs between injured and contralateral DRGs, 3D (A) and 4W (B) post-SNI. Default LFC shrinkage via *apeglm*, with *ashr* shirnkage highlighted in B. C. Euler plot of DEGs across comparisons for an interaction of sex and injury. D. Intact afferent (against contralateral) volcano plots for DEGs at 3D (left) and 4W (right). E. Top expressing DEGs in 3D intact afferents, plotted as median transformed counts. F. Highest LFC DEGs for 3D intact afferents, as median transformed count.

5.3.4 snATAC-seq pilot

In parallel, we are interested in how changes in chromatic structure contribute to chronic pain states. Chromatin structure is a well-known regulator of gene transcription, and epigenetic modifications may indicate long term changes in neuronal properties. As such, we focused on four weeks post-SNI, using snATAC-seq to interrogate accessible chromatin (Fig 5.5). Here, nuclei are isolated and DNA undergoes transposition by Tn5. Fragments are then sequenced and aligned. Collection mirrored that of the RNA-seq sorting. Sexes were pooled for single nuclei ATAC-seq, with post-hoc annotation available through peak mapping of sex-linked genes.

Quality control, including TSS enrichment plots were performed on individual libraries (Fig 5.5C, 5A.4). Intact neurons were omitted for poor library quality, with very few cells passing filtering criteria. Wildtype samples show slightly skewed metrics compared to contralateral and injured libraries - a likely effect of sample preparation differences (MACS+FACS vs FACS alone). Few nuclei were sequenced in each sample: wildtype (269), contralateral (744), and injured (735). Of these, TSS enrichment scores indicate good signal to noise (wildtype (8.12), contralateral (8.45), and injured (7.69)).

DNA accessibility was calculated for specific genes, looking at peak expressing around the coding region. To annotate the cell populations, peak expression data were integrated with scRNA-seq data available from the Allen Brain Atlas [263]. Here, samples broadly cluster into five non-overlapping groups which can then be subdivided into more specific populations. Neuronal subpopulations can be distinguished, along with large populations of non-neuronal cells (5.5D-E, 5.6A).

Even with low cell counts we can see clear clustering by cell type. This annotation can be redone with PNS-specific scRNA-seq. Current labels such as oligodendrocytes likely correspond to a PNS counterpart (here, Schwann cells). Even so, we are able to define few neuronal subgroups in comparison to other cells, which correspond to top markers for neuronal groups compared to other clusters (5.6B).

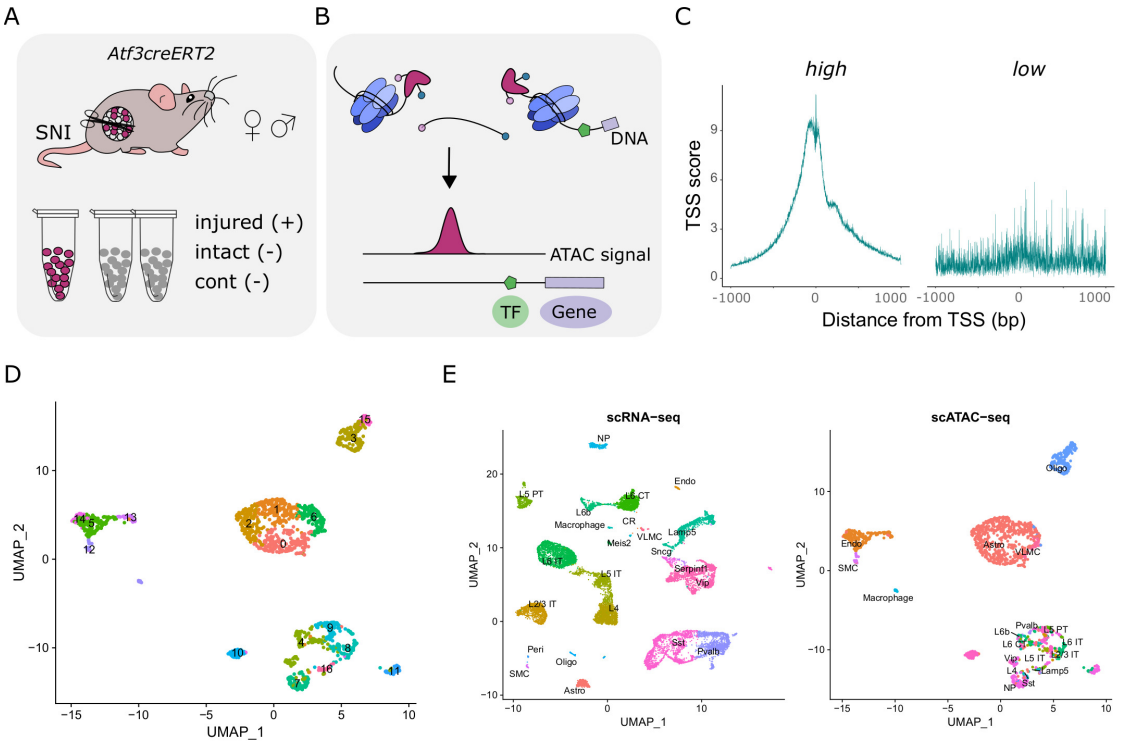

Figure 5.5: Atf3^{creERT2} snATAC-seq overview. A. Sequencing overview, looking at injured, intact, and contralateral samples after SNI. Wildtype samples were sequenced in parallel. Intact samples failed QC, and are not included in the analyses. B. ATAC-seq schematic, highlighting the accessible chromatin signal produced by ATAC. C. Transcription start site (TSS) QC plot for snATAC-seq pilot data. TSS scores per cell are sorted as 'High' = TSS > 2 or 'Low' = TSS < 2. D. UMAP projection of snATACseq data, run on dimensions 2:30. Nuclei from wildtype, contralateral, and injured libraries are included. E. snATAC-seq data were annotated against the Allen Brain Atlas (scRNA-seq, left) to assign populations. CNS-specific labels likely refer to their PNS counterparts, such as Oligo[dendrocytes] for Schwann cells.

If we interrogate specific marker differences between ipsilateral and contralateral samples within our neuronal clusters, we see hints of chromatin structure changes in pain states. The top regulated peak is *Hctr2*, a Hypocretin (Orexin) receptor previously implicated in cluster headache (5.6C) [264]. The ATAC signal is primarily found in neuronal subtypes, and minimally in satellite glia ("astrocytes"), macrophages, and endothelial cells (5.6). Chromatin accessibility is downregulated in injured neurons compared to contralateral samples, with a marginal LFC of -0.66. Higher nuclei counts are required for a more in depth, well powered analysis of chromatin accessibility in injury states. In our bulk RNA-seq dataset, *Hctr2* is not differentially expressed in injured neurons.

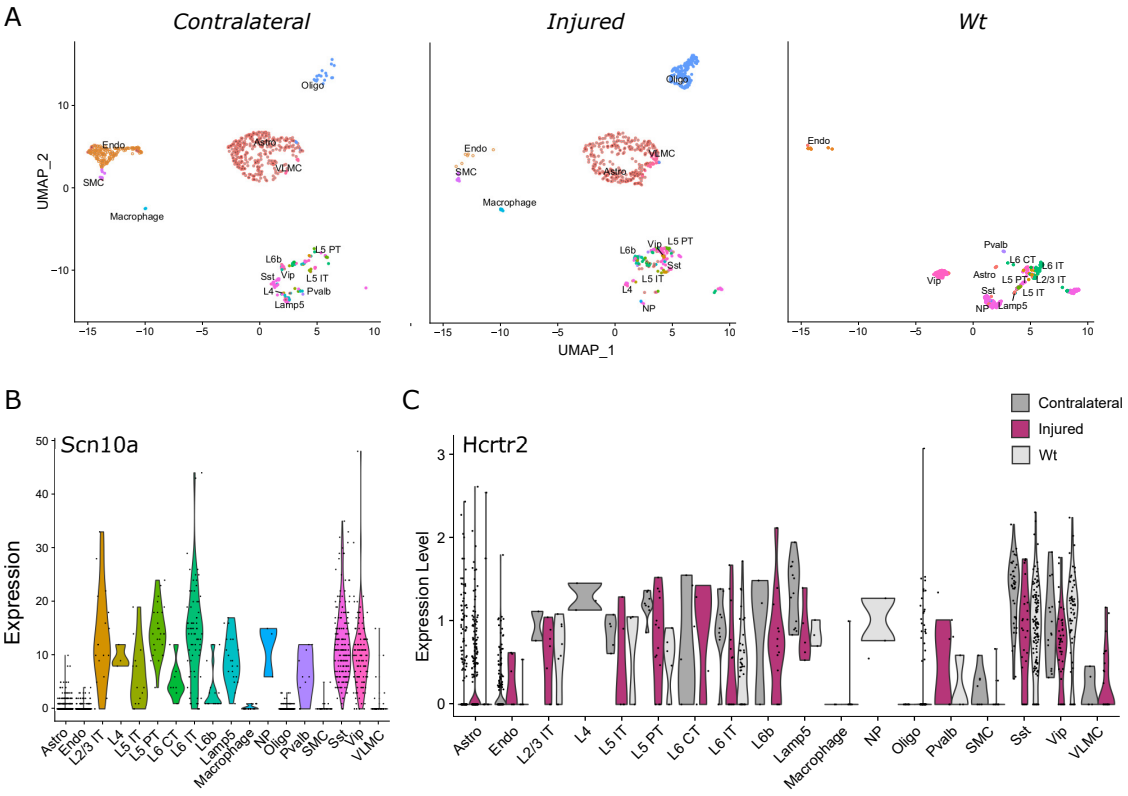

Figure 5.6: snATAC-seq pilot hints at changes after SNI. A. UMAP by sample type. Wt samples were purified by MACS, and show a larger proportion of neurons than contralateral and injured Atf3^{creERT2} samples. B. Neuronal nuclei can be distinguished by *Scn10a* peaks. C. Hcrtr2 is downregulated in injured neurons, with a LFC of -0.66 across all cells. Dots represent individual nuclei.

Because our pilot data is not exclusively neuronal, we can also study chromatin changes in other populations (5.6). In satellite glia, one gene - *Vmp1* - is significantly regulated between injured and contralateral cells (FDR = 0.000098; LFC = 0.56). *Vmp1* is an autophagy-related protein with broader expression across clusters. The regulation is not seen in the neuronal population.

5.4 Discussion

Within DRG ganglia, a mixture of injured and intact afferents can be present. Using an SNI transection model paired to a transgenic driving reporter expression in injured afferents, we probed changes in these populations through bulk RNA-seq and snATAC-seq.

5.4.1 RNA-seq

Broadly, intact neurons mirror their contralateral counterparts, while injured, tdTomato-expressing neurons show a classic injury phenotype. Intact neurons cluster with naïve cells, and show lower levels of *Atf3* than their injured neighbours (Fig 5.5). At both timepoints, injured neurons are positively correlated to an unbiased signature generated from a previous dataset, and are significantly different than the contralateral samples (5.6A). This suggests we are accurately capturing an injury phenotype which mirrors previous data. At 4 weeks, intact samples are also significantly different from contralateral samples, but with a small effect size, supporting the idea that these neurons are similar, but not the same as their contralateral afferents. At three days, intact samples more strongly correlate with the injury signature, but this may be driven by injured, non-tdTomato expressing neurons due to the timecourse of reporter expression [191].

Injured samples were next compared over time. Similar to our previous data, we see a significant downregulation of NP, paired to an upregulation of PEP signature by 4 weeks, compared to three days (5.6B, 4.2). This lends further support to the loss of NP neurons post-transection, which has been alluded to throughout this thesis. If this translates functionally, it would also align with earlier work on injured and intact afferents by Obata *et al.* that showed a lack of tactile hypersensitivity, but heightened thermal hypersensitivity in male rats with a high proportion of *Atf3*+ afferents 2 weeks after CCI [265].

Unlike our previous analyses, we do not see a significant C-LTMR enrichment. This may be biologically relevant, or an artifact of low proportions of C-LTMRs in these samples. This population typically comprises 5% of lumbar DRGs, but the previous dataset was enriched by including $Th^{creERT2}$ samples.

Differential expression testing further highlights large differences between injured afferents with both intact and contralateral samples. This includes the upregulation of multiple injury genes, as well as the downregulation of various subpopulation-specific genes (*Calca*, *Trpa1*, *Mrgprd*, *Scn10a*, *Scn11a*). In intact afferents, we see a moderate upregulation of injury genes (eg. *Atf3*, *Sox11*) at both timepoints,

with a subset of genes regulated in intact, but not injured afferents (Table 5A.2). These uniquely regulated genes in intact afferents allow mechanistic speculation. *Cdhr1* and *Dhx38* have both been studied for their roles in photoreceptor-based retinal degeneration [266, 267], suggesting functions that span sensory systems. The presence of multiple transmembrane proteins adds additional intrigue: *Tmem123* has a known role in oncosis, whereas *Tmem7* (ie. *Rtp3*) is an interferon response gene with a role in chemosensation [268, 269]. GO and GSEA analyses suggest additional functional changes in this population. The GSEA enrichment for TNFα in intact neurons fits previous data, with Schäfers *et al.* previously highlighting intact sensitization by TNFα after nerve ligation [251].

Sexual dimorphism Few genes show an interaction of sex and injury, in line with previous results (chapter 4). In an acute state, intact neurons do show sexually dimorphic changes against contralateral samples. Sixty-nine genes appear significantly regulated. This includes a number of genes directly involved in immune function, including *Ltf* and *Trf*, which show two of the highest LFC, as well as a range of other functions, like synapse regulation (*Magi2*), cell-cell interactions (*Spock1*, *Tjp2*) and protein degradation (*Fbxo2*).

GO analyses also suggests the regulation of various immune terms, including neutrophil chemotaxis, neutrophil aggregation, leukocyte chemotaxis, innate immune response, leukocyte migration involved in inflammatory response, and antibacterial humoral response. Together, we interpret this as a largely neuro-immune cross-talk, which has previously documented sexual dimorphism. For example, mechanical hypersensitivity in male mice depends on microglia activity, while adaptive immune cells are implicated in female mechanical hypersensitivity [203, 204]. At a subpopulation level, this effect was not seen in our previous data (chapter 4). Gating negative cells may capture additional non-neuronal cells and drive an immune-centric sexual dimorphism documented here. The switch to a dual-recombinase reporter, will add clarity, as will further validation and replication.

GSEA analyses also highlighted differences in TNFα signalling, with a positive enrichment for TNFα in male intact neurons, compared to females. The sensitization of injured and intact afferents by TNFα has been well documented in males [251], and our findings here suggest additional experiments are warranted to further explore the sexually dimorphic nature of this pathway.

Technical considerations Different FACS gatings between positive and negative samples add confound. Even so, the expression of neuronal genes in negative samples, paired to the significant downregulation in positive samples by comparison gives support that our negative samples are largely neuronal. Refined transgenics will still improve future experiments, as alluded to in chapter 2. RC::FLTG is a dual-recombinase reporter allowing for flp-driven expression of tdTomato, but Flp + Cre mediated eGFP expression. Paired to an Advillin$^{\text{flpO}}$ in addition to Atf3$^{\text{creERT2}}$, RC::FLTG results in the labelling of injured (eGFP-expressing) and intact (tdTomato-expressing) neurons specifically. This new approach has since been validated for downstream experiments.

5.4.2 snATAC-seq

In addition to the RNA-seq data presented, we took steps to study the underlying chromatin structure in wildtype and injured DRG, which, to our knowledge, is not currently available elsewhere. Across conditions, we see a primary clustering by subtype, in line with recently published TG snATAC-seq data for both mouse and human [51].

As a pilot, this study was informative but requires further optimization. Fewer neurons were sequenced than expected, and one library failed. Pooling samples across multiple animals does not seem to increase the number of neurons linearly, and optimal number of animals per sort still needs to be established. Additionally, cell lysis timing for nuclear extraction is very dependant on population type. Our population may have been enriched for non-neuronal cells at this stage, and lysis timing will be explored further prior to subsequent sequencing.

Building on protocol optimization, *Atf3* is also upregulated in Schwann cells after injury [270, 271]. This can label glia with tdTomato in the injured cohort, accounting for the increase in Schwann cells due to tdTomato expression (5.6A). These cells are also present in the contralateral sample, and an alternative hypothesis is that injury may increase the presence of Schwann cells in the DRG, thus increasing the contamination. The transition to Atf3^{creERT2}; Advillin^{FlpO}; RC::FLTG dual-recombinase reporter system will address this confound, although the enrichment of SG in the RNA-seq data has to be considered.

Differences in sample purity of Oxford vs Glasgow is not clear, as we have not done direct comparisons. Brightfield of samples before and after FACS suggest samples are highly enriched for neurons, but magnetic purification was also used on sequenced wildtype samples in Oxford, which is known to increase purity. Moving forward, MACS may reduce costs by focusing specifically on smaller-diameter neurons, but cell attrition through additional sorting is an issue.

We are excited to gain insights into injured versus intact ATAC signatures, and to integrate with some injury RNA-seq data – both external single cell and the bulk dataset described here. Similar to our RNA-seq results, we hypothesize that intact neurons will show a subset of unique chromatin structures compared to contralateral and injured neurons, even if the general ATAC signatures cluster by cell type. Moreover, changes in chromatin structure which overlap with transcript changes would add strength and provide an avenue for viral targeting and/or novel transgenics. This data is forthcoming.

5.4.3 Future directions

In addition to optimizing the snATAC-seq protocol, there are various ways to build on this data. While 3D intact samples come with the added caveat of a reporter expression timecourse, differences between intact and contralateral samples at 4 weeks suggest more chronic, minor changes in neurons exposed to a local immune environment. The consequence of this remains less clear, and the similarities between intact and contralateral neurons do not indicate naïvity.

As a stand-alone method, RNA-seq is not able to capture the complexity of the intact/injured afferent story. This dataset exists as a resource to query as we further interrogate differences in these populations. For example, how does the increase in apoptosis in injured afferents affect higher order circuitry? Do the innervation patterns of intact neurons change in specific ways after injury? Does afferent sensitization by immune mediators affect populations differently? What does the intersection of injured/intact look like when subtype identities are considered? Much of this work is ongoing in Glasgow, and will complement the data presented here.

Additionally, validation via previously available single cell data will strengthen our RNA-seq data. Intact neurons closely resemble contralateral samples, supporting the notion that the stereotyped changes we see after injury correspond to our tdTomato-expressing neurons, while our intact cells correspond to those considered "naïve" in previous datasets [33, 42]. Pseudo-bulk analyses of these datasets would further permit within population interrogation, and have the added advantage of multiple injury types, even though Renthal *et al.* limited their data to male mice [42].

Data accessibility remains a key priority. Our database will also be updated to host this data in parallel.

5.4.4 Conclusions

There is a long history studying the contributions of intact and injured afferents in pain states. With improving transgenics and high throughput sequencing techniques, we have been able to add deep RNA-seq of injured and intact afferents after SNI, as well as probe the chromatin structure of DRG neurons. Intact neurons largely mirror their contralateral counterparts, with small differences at a molecular level highlighting possible functional changes in oxidative phosphorylation, immune response, and *Tnfa* signaling via *Nfkb*. In an acute state, we also see an immune-based interaction of sex and injury which is not present by 4 weeks.

5A Appendix

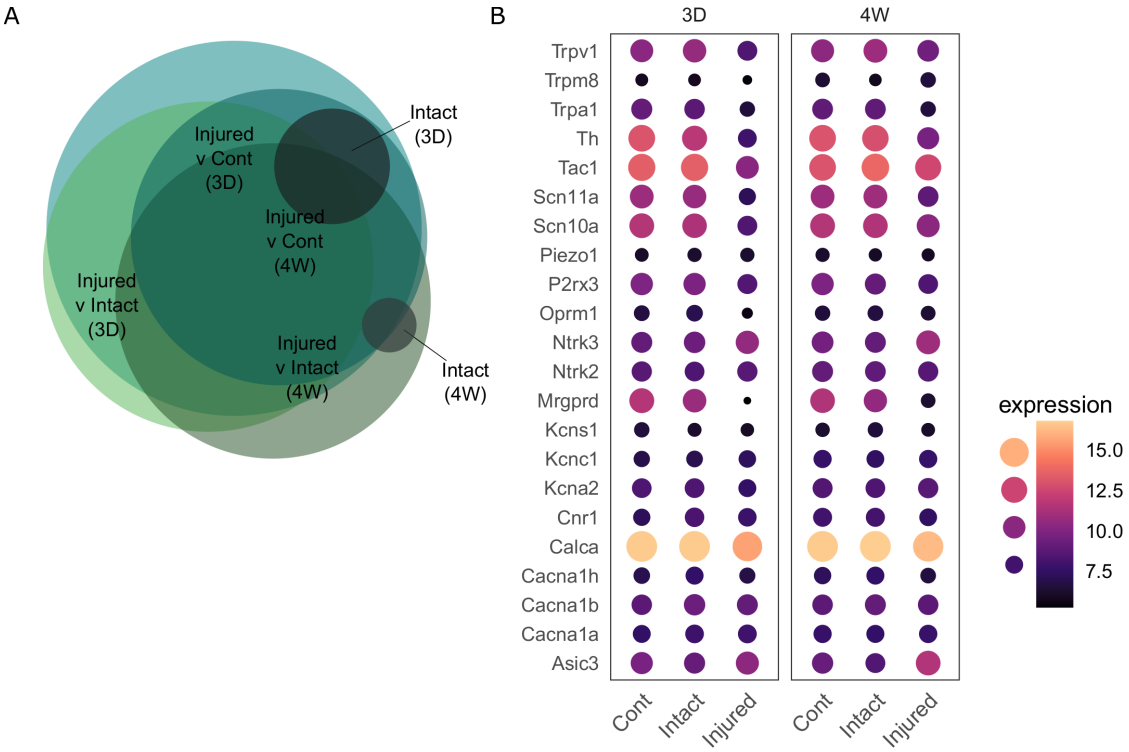

Figure 5A.1: Hallmark gene expression in Atf3$^{\text{creERT2}}$ mice after SNI. A. DEG overlap across conditions. B. Hallmark gene expression by timepoint and condition, plotted as median expression.

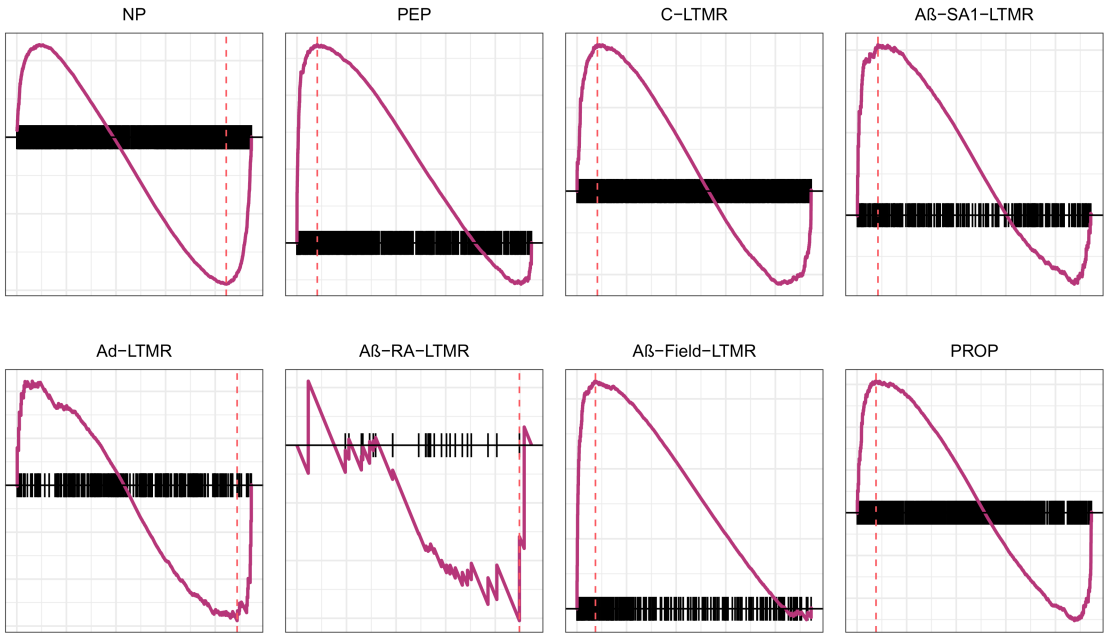

Figure 5A.2: Atf3^{creERT2} subpopulation enrichment over time. Compared to previously published, naïve subpopulation RNA-seq. Related to Figure 5.2. Scores listed in Table 5A.1.

Table 5A.1: Gene set enrichment for injured lumbar DRG over time. Ranked by normalized enrichment scores within each neuronal subtype. Related to Figure 5.2.

Population	Gene Set	Size	Score	p (adj)
Atf3^{creERT2}	PEP	725	1.72	5.52E-08
	A-field-LTMR	251	1.91	7.29E-07
	NP	1570	-1.40	5.29E-06
	AB-LTMR	292	1.23	1.71E-01
	C-LTMR	800	1.13	2.04E-01
	PROP	677	0.98	6.81E-01
	Ad-LTMR	270	-0.92	7.81E-01
	A-RA-LTMR	30	-0.71	8.55E-01

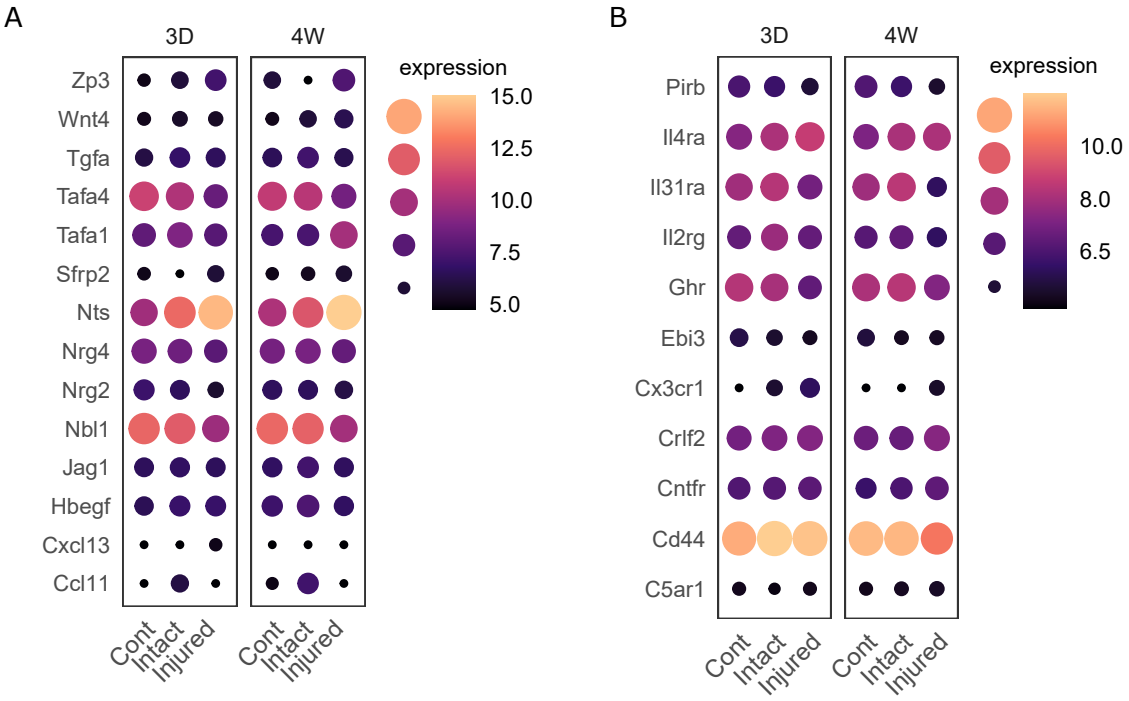

Figure 5A.3: Receptor-ligand DEGs across conditions (injured v contralateral or intact, as well as intact vs contralateral). Significantly regulated genes involved in receptor ligand activity (A) ("GO:0048018"), or immune receptor activity (B) ("GO:0140375"), plotted as median transformed count expression.

Table 5A.2: Unique DEGs between intact vs contralateral (Intact), but not in injured vs contralateral (Injured) four weeks after spared nerve injury. A subset of genes are also regulated within ipsilateral samples (Injured v Intact, "Ipsi"). Based on a LFC > 1, FDR < 0.05.

Symbol	Intact	Injured	Ipsi
Klra17	1	0	0
Cdhr1	1	0	0
Paqr8	1	0	0
Ell3	1	0	0
Tsc22d2	1	0	0
Cntfr	1	0	0
Usp2	1	0	0
Tmed7	1	0	0
Dop1a	1	0	0
Dhx38	1	0	0
Rasef	1	0	0
Ankrd45	1	0	0
Rnf150	1	0	0
Tmem123	1	0	0
Tnfaip6	1	0	0
Zfp974	1	0	0
E330034L11Rik	1	0	0
D130062J10Rik	1	0	0
Ptch1	1	0	1
Erbin	1	0	1
Trp53bp2	1	0	1
Vwa3a	1	0	1
Trf	1	0	1
Ndufa4l2	1	0	1
Gm10226	1	0	1
Hspd1-ps4	1	0	1

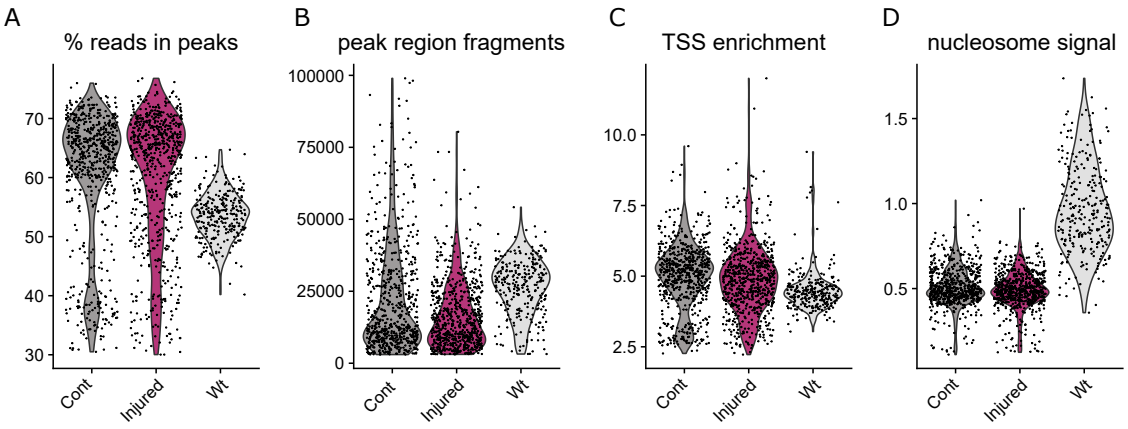

Figure 5A.4: snATAC-seq quality control. A. % reads in peaks. B. Peak region fragment counts. C. TSS enrichment score. D. Nucleosome signal. Related to Fig 5.5.

6
General discussion

Sensory neurons have a well documented role in acute and chronic pain states. In this thesis, we have added to the discussion with deep RNA-seq of murine neuronal subtypes after nerve injury. Spread over two datasets, we have curated transcriptomic data for male and female DRGs at two timepoints after SNI. In one experiment, I focus on classically defined sensory neuron subtypes (general nociceptors, peptidergic nociceptors, non-peptidergic nociceptors, C-LTMRs, and Aβ-RA + Aδ-LTMRs). In the other, I focus on differences in intact and injured neurons after injury. We have complemented these studies with a snATAC-seq pilot on DRG neurons. Taken together, these data provide unique insight to the molecular underpinnings of neuropathic pain in primary afferents.

6.1 Molecular insights

Across subtypes we can divide neurons by a general injury signature, supporting previous work highlighting stereotyped changes after injury [42]. The strength of these studies, however, comes from the ability to study subpopulations and sex differences, with DEG lists and pathway analyses providing additional foundation for future functional studies.

6.1.1 Sexual dimorphism

In naïve states, we see sexual dimorphism within sensory neuron subtypes that warrants further study. This is particularly true for *Ntrk2* afferents, which show the largest change in DEGs but have minimal data published on female animals. After injury, differences from a basal state largely remain and show negligible interaction with the injured state in our experiments, except for in intact afferents, 3 days after insult. Here, there appears to be a neuro-immune pattern emerge which may have been detected, in part, due to gating negative cells. Baseline sex differences may still contribute to painful states, regardless of interaction, due to altered immune/glial interactions, baseline excitability, or differences in higher order circuitry. All of these require further study, along with cross-species validation, as we continue to deepen our understanding of male and female pain pathways.

6.1.2 Gene signatures and enrichment

Our work was validated against previously published RNA-seq data [5], and we subsequently extracted general injury signatures from one dataset which positively correlated to injured and intact cells in a separate study. Taken together, this reproducibility adds strength to each study.

This also highlighted various injury response differences across subtypes, such as an enriched signature for Aδ-LTMRs in high threshold populations, and the reduction in NP signature across datasets by 4 weeks. Aβ-RA + Aδ-LTMRs show unique changes by 4 weeks after SNI in one dataset, but we were not well positioned to explore this further in Atf3$^{\text{creERT2}}$ samples. Additional experimentation with the Ntrk2$^{\text{creERT2}}$ in both male and female mice will be instrumental to elaborate on these current results.

6.1.3 Cell death

Throughout this thesis we have alluded to the loss of NP neurons after injury. This was initially queried in the context of the Atf3$^{\text{creERT2}}$, due to the lack of tdTomato/IB4 overlap seen by 4 weeks. Follow-up studies in collaboration with

Greg Weir and Andrew Cooper using various transgenic models paired to retrograde tracing strongly suggest this is due to a loss of almost all injured NP neurons, and is not limited to the SNI model.

Previous work in our group has highlighted the loss of small diameter neurons in cleared DRG tissue, as well as contributing to previous evidence of synapse loss in lamina II_i [196]. Hall *et al.* recently highlighted massive neuronal loss in humans with diabetic neuropathy [239]. Additional work from Prof. Andrew Todd and colleagues suggests $Mrgprd^{GFP}$-labelled afferents are lost in the dorsal horn after injury (personal correspondence). We have built on this here showing a reduction in the NP signature in injured NP neurons, as well as more broadly between ipsilateral samples at 4W compared to 3D in two separate RNA-seq datasets. Taken together, this data shifts the dialogue away from simply a loss of IB4-binding or axon degeneration after injury to a fundamental loss of neurons.

Functionally, the implications are unclear. Long-term, we have not explored whether other populations experience similar levels of cell death. Our current data also hints at a possible loss of C-LTMRs that requires further study. We hypothesize changes in higher order circuitry play a crucial role to the functional consequences. To one end, the loss of NP neurons may reduce spontaneous activity in that population. Alternatively, this may reduce inhibition and exacerbate pain, for example through aberrant sprouting/retraction of interneurons in the dorsal horn [272]. We can start teasing this out by trying to promote survival of the affected afferents. We do not know the mechanism of cell death, but the increase in "apoptosis" terms in this population suggests this is one to explore. Blocking this pathway may help, and the availability of subtype transgenics allows a targeting method.

Looking to other systems may provide further insight. Retinal ganglion cells (RGCs) are a highly diverse neuronal population that undergo a similar transcriptional reprogramming after injury to DRG neurons. The cell death after optic nerve crush is dramatic, with 80% of neurons dying by 2 weeks. The subtypes can be grouped based on susceptibility to cell death, and some subtypes die off completely [43]. By comparing differences in subtype resistance/susceptibility to

cell death through scRNA-seq, a heterogeneous group of DEGs appears. Post-hoc testing revealed a subset of these genes have neuroprotective effects, and can increase survival when modulated in susceptible cell types [43]. Some of these may be relevant in DRG neurons as well. For example, *Timp2* is an inhibitor of matrix metalloproteinasesis (MMPs), and is predominately expressed in resilient RGC subtypes. Overexpression improves survival in a subgroup of susceptible subtypes. In DRG neurons, *Timp2* is enriched in PEP nociceptors, and has the lowest expression in NP. It is mildly upregulated (LFC ~0.5) in general ipsilateral samples by 4 weeks, compared to 3 days, and has previously been discussed for in the context of MMPs and neuropathic pain [273]. Other factors explored in RGCs included *Unc*, *Crhbp*, and *Mmp12*.

6.1.4 A case for energy

Across subtypes and datasets, a downregulation of oxidative phosphorylation is seen after injury. This also shows signs of sexual dimorphism. At the level of the proteome, mitochondrial dysfunction and changes in related pathways (oxidative stress response, oxidative phosphorylation, TCA cycle) have also been shown in the DRG [36], and the transfer of mitochondria between cell types has recently been discussed in inflammatory pain models [138]. Axonal degeneration can occur by depleting energy stores, through the NADase SARM1 (sterile alpha and TIR motif—constraining 1) [247, 274], and sensory neurons in diabetic rats have shown lower respiratory chain activity than healthy controls [275]. Partial sciatic nerve ligation in mice results in metabolic changes [276], and in basal states, mitochondrial trafficking occurs in response to sensory neuron activation [277].

Clinically, mitochondrial disease often affects sensory neurons, and more than 50% of patients experience chronic pain, many with distal limb "neuropathic-like" pain [278]. Mitochondrial dysfunction has also been related to sensory neuropathy in HIV patients and non-human primates, with differences in organelle density across neuronal subtypes [279]. This pathway, as it relates to electron transport and ATP synthesis, is thus an intriguing candidate for further study.

6.2 Data access and integration

Accessible, effective data use reduces the need for new dataset generation and accelerates research [280]. The integration with human data further increases translatability, thus refining the impact of current data. Additionally, the use of meta-analyses to interrogate transcriptional data has been shown to improve candidate selection and reproducibility [281]. Long-term, there is a case for a centrally-hosted, integrated database for -omics work that moves beyond raw data repositories. Effective data sharing should have a low barrier of entry, and user-friendly data access is important.

Until that is possible, we have curated our data in house for others to dissect. The addition of a database greatly strengthens the work, and is expected to increase it's impact. Currently this database is in development, with a functional, base version presented in this thesis. More effective data integrate with other studies, as well as more efficient search functions will help refine outputs.

6.3 Limitations and refinements

Transgenics These lines were studied with the goal of bulk sorting subpopulations after injury. Currently, we are able to probe either injured versus intact neurons, or subtype-specific populations using simple transgenic approaches. We employ a Flp-based Advillin to limit *Ntrk2* targeting to neuronal populations, but the addition of dual-recombinase reporters against a FlpO driver for neuronal subpopulations or injured afferents would allow further refinement. For example, a Mrgprd$^{\text{flpO}}$; Atf3$^{\text{creERT2}}$ against an intersectional reporter such as RC::FLTG would allow distinct tdTomato/eGFP labelling of Mrgprd-lineage intact vs injured neurons ipsilateral to the site of injury, with contralateral labelled intact neurons in parallel. Pairing an *Atf3* driver with our subtype drivers would allowed injured and intact ipsilateral samples for each subtype, opposed to the current mixed samples produced here.

To our knowledge, many of these transgenics are not readily available for intersectional labelling. Alternatively, a pain model which targets all neurons within

a specific ganglia would circumvent this mixed intact and injured populations see in subtype-specific samples. Here, animal welfare must be considered, as many nerves contain a mix of sensory and motor neurons from both the periphery and viscera. Pain models should also be relevant in the context of human translation. Few traumatic nerve injuries seen in humans would transect all afferents in a specific ganglia. Even systemic conditions such as chemotherapy-induced peripheral neuropathy and diabetic neuropathy affect a subset of neurons.

Spared nerve injury was chosen as a well documented model used in both mouse and rat, with large amounts of associated behavioural data at both acute and chronic time points. Other models would also have been appropriate choices too, and future work can compare and contrast profiling in these cases. Technically, systemic models would also provide more cells per animal, although you lose the internal, paired control available with contralateral tissue.

Validation Cross-comparisons to previously published RNA-seq data adds confidence to our results. Further validation of new candidates, particularly for lowly-expressed, sexually-dimorphic genes, will be required in the future.

Timecourse Our studies selected 4 weeks as a "chronic" timepoint, but what happens after 4 weeks? Recent work suggests long-term sexually dimorphic changes in the spinal cord, including a reduction in telomere length in males, but not female mice by 4 months [282]. How DRG subtypes develop long-term remains unclear and would be an interesting avenue for a follow-up study.

System-level analyses We exclusively looked at molecular changes in DRG soma. Gene regulation can also occur along axons [283], suggesting that even within primary afferents, we are likely missing information. Crucially still, DRG neurons are not isolated. They exist as a part of the larger system. Detailed interrogations of ligand-receptor binding, neurites, and spinal cord innervation patterns are required to add context in the larger system.

6.4 Conclusions

Through bulk RNA-seq of primary afferent subtypes, we reveal molecular underpinnings in naïve, intact, and injured neurons after injury. This data was compiled into a user-friendly online platform to increase accessibility. In naïve states, we find within subtype sex difference, including a large number of regulated genes in Aβ-RA + Aδ-LTMRs. After injury, we are able to detect stereotyped injury changes, as well as differences at a subpopulation level, with changes in NP enrichment patterns and a unique response of Aβ-RA + Aδ-LTMRs 4 weeks after injury. At this timepoint, there is not a strong interaction of injury with sex, but differences in naïve states continue to contribute. Within ipsilateral tissue, differences in intact and injured afferents are also seen, with intact neurons largely resembling their contralateral counterparts. Interestingly, changes are still visible between intact and contralateral neurons, with differences in oxidative phosphorylation, immune response, and *Tnfa* signaling via *Nfkb*.

Collectively, this thesis explored the molecular underpinnings of neuropathic pain in murine sensory neurons. We see this work as an important resource for the field as we continue to probe new ways of understanding and treating neuropathic pain.

References

[1] Michael Costigan et al. "T-Cell Infiltration and Signaling in the Adult Dorsal Spinal Cord Is a Major Contributor to Neuropathic Pain-Like Hypersensitivity". In: *Journal of Neuroscience* 29.46 (Nov. 2009), pp. 14415–22. DOI: 10.1523/JNEUROSCI.4569-09.2009.

[2] Luana Colloca et al. "Neuropathic pain". In: *Nature Reviews Disease Primers* 3 (Feb. 2017), p. 17002. ISSN: 2056676X. DOI: 10.1038/nrdp.2017.2.

[3] Nadine Attal et al. "The neuropathic components of chronic low back pain: A prospective multicenter study using the DN4 questionnaire". In: *Journal of Pain* 12.10 (Oct. 2011), pp. 1080–1087. ISSN: 15265900. DOI: 10.1016/j.jpain.2011.05.006.

[4] Alec B. O'Connor. *Neuropathic pain: Quality-of-life impact, costs and cost effectiveness of therapy*. Sept. 2009. DOI: 10.2165/00019053-200927020-00002.

[5] Yang Zheng et al. "Deep Sequencing of Somatosensory Neurons Reveals Molecular Determinants of Intrinsic Physiological Properties". In: *Neuron* 103.4 (2019), 598–616.e7. ISSN: 08966273. DOI: 10.1016/j.neuron.2019.05.039.

[6] David L.H. Bennett and C. Geoffrey Woods. *Painful and painless channelopathies*. 2014. DOI: 10.1016/S1474-4422(14)70024-9.

[7] Hind Abdo et al. "Specialized cutaneous schwann cells initiate pain sensation". In: *Science* 365.6454 (Aug. 2019), pp. 695–699. ISSN: 10959203. DOI: 10.1126/science.aax6452.

[8] Armen N. Akopian, Lucia Sivilotti, and John N. Wood. "A tetrodotoxin-resistant voltage-gated sodium channel expressed by sensory neurons". In: *Nature* 379.6562 (Jan. 1996), pp. 257–262. ISSN: 00280836. DOI: 10.1038/379257a0.

[9] Armen N. Akopian et al. "The tetrodotoxin-resistant sodium channel SNS has a specialized function in pain pathways". In: *Nature Neuroscience* 2.6 (June 1999), pp. 541–548. ISSN: 10976256. DOI: 10.1038/9195.

[10] Claire E. Le Pichon and Alexander T. Chesler. *The functional and anatomical dissection of somatosensory subpopulations using mouse genetics*. Apr. 2014. DOI: 10.3389/fnana.2014.00021.

[11] Vincenzo Prato et al. "Functional and Molecular Characterization of Mechanoinsensitive "Silent" Nociceptors". In: *Cell Reports* 21.11 (2017). ISSN: 22111247. DOI: 10.1016/j.celrep.2017.11.066.

[12] Nima Ghitani et al. "Specialized Mechanosensory Nociceptors Mediating Rapid Responses to Hair Pull". In: *Neuron* 95.4 (2017). ISSN: 10974199. DOI: 10.1016/j.neuron.2017.07.024.

[13] Laiche Djouhri and Sally N. Lawson. "Aβ-fiber nociceptive primary afferent neurons: a review of incidence and properties in relation to other afferent A-fiber neurons in mammals". In: *Brain Research Reviews* 46.2 (Oct. 2004), pp. 131–145. ISSN: 01650173. DOI: 10.1016/j.brainresrev.2004.07.015.

[14] Saad S. Nagi et al. "An ultrafast system for signaling mechanical pain in human skin". In: *Science Advances* 5.7 (July 2019), eaaw1297. ISSN: 23752548. DOI: 10.1126/sciadv.aaw1297.

[15] Jung Bum Shin et al. "A T-type calcium channel required for normal function of a mammalian mechanoreceptor". In: *Nature Neuroscience* 6.7 (July 2003), pp. 724–730. ISSN: 10976256. DOI: 10.1038/nn1076.

[16] Amaury François et al. "The Low-Threshold Calcium Channel Cav3.2 Determines Low-Threshold Mechanoreceptor Function". In: *Cell Reports* 10.3 (Jan. 2015), pp. 370–382. ISSN: 22111247. DOI: 10.1016/j.celrep.2014.12.042.

[17] Yinth A. Bernal Sierra et al. "Genetic tracing of Cav 3.2 t-type calcium channel expression in the peripheral nervous system". In: *Frontiers in Molecular Neuroscience* 10 (Mar. 2017), p. 70. ISSN: 16625099. DOI: 10.3389/fnmol.2017.00070.

[18] Victoria E. Abraira and David D. Ginty. "The sensory neurons of touch". In: *Neuron* 79.4 (Aug. 2013), pp. 618–639. ISSN: 08966273. DOI: 10.1016/j.neuron.2013.07.051.

[19] Lishi Li et al. "The functional organization of cutaneous low-threshold mechanosensory neurons". In: *Cell* 147.7 (Dec. 2011), pp. 1615–1627. ISSN: 00928674. DOI: 10.1016/j.cell.2011.11.027.

[20] Masahiko Watanabe et al. "The Cellular and Synaptic Architecture of the Mechanosensory Dorsal Horn". In: *Cell* 168.1-2 (2017), 295–310.e19. ISSN: 10974172. DOI: 10.1016/j.cell.2016.12.010.

[21] Rahul Dhandapani et al. "Control of mechanical pain hypersensitivity in mice through ligand-targeted photoablation of TrkB-positive sensory neurons". In: *Nature Communications* 9.1 (2018). ISSN: 20411723. DOI: 10.1038/s41467-018-04049-3.

[22] Dmitry Usoskin et al. "Unbiased classification of sensory neuron types by large-scale single-cell RNA sequencing". In: *Nature Neuroscience* 18.1 (2015), pp. 145–153. ISSN: 15461726. DOI: 10.1038/nn.3881.

[23] Chang Lin Li et al. "Somatosensory neuron types identified by high-coverage single-cell RNA-sequencing and functional heterogeneity". In: *Cell Research* 26.1 (2016), pp. 83–102. ISSN: 17487838. DOI: 10.1038/cr.2015.149.

[24] Diana Tavares-Ferreira et al. "Spatial transcriptomics of dorsal root ganglia identifies molecular signatures of human nociceptors." In: *Science translational medicine* 14.632 (Feb. 2022), eabj8186. ISSN: 1946-6242. DOI: 10.1126/SCITRANSLMED.ABJ8186/SUPPL_FILE/SCITRANSLMED.ABJ8186_FILES_S1_TO_S31.ZIP.

[25] Minh Q. Nguyen et al. "Single-nucleus transcriptomic analysis of human dorsal root ganglion neurons". In: *eLife* (2021). ISSN: 2050084X. DOI: 10.7554/eLife.71752.

[26] Jussi Kupari et al. “Single cell transcriptomics of primate sensory neurons identifies cell types associated with chronic pain”. In: *Nature Communications* (2021). ISSN: 20411723. DOI: 10.1038/s41467-021-21725-z.

[27] Robert Y. North et al. “Electrophysiological and transcriptomic correlates of neuropathic pain in human dorsal root ganglion neurons”. In: *Brain : a journal of neurology* 142.5 (2019), pp. 1215–1226. ISSN: 14602156. DOI: 10.1093/brain/awz063.

[28] Matthew Thakur et al. “Defining the nociceptor transcriptome”. In: *Frontiers in Molecular Neuroscience* 7.November (2014), pp. 1–11. DOI: 10.3389/fnmol.2014.00087.

[29] Ana Reynders et al. “Transcriptional Profiling of Cutaneous MRGPRD Free Nerve Endings and C-LTMRs”. In: *Cell Reports* 10.6 (Feb. 2015), pp. 1007–1019. ISSN: 22111247. DOI: 10.1016/j.celrep.2015.01.022.

[30] Amit Zeisel et al. “Molecular Architecture of the Mouse Nervous System”. In: *Cell* 174.4 (2018). ISSN: 1097-4172. DOI: 10.1016/j.cell.2018.06.021.

[31] R. V. Grindberg et al. “RNA-sequencing from single nuclei”. In: *Proceedings of the National Academy of Sciences* 110.49 (2013), pp. 19802–19807. ISSN: 0027-8424. DOI: 10.1073/pnas.1319700110.

[32] Lars J. von Buchholtz et al. “Assigning transcriptomic class in the trigeminal ganglion using multiplex in situ hybridization and machine learning”. In: *PAIN* (May 2020), p. 1. ISSN: 0304-3959. DOI: 10.1097/j.pain.0000000000001911.

[33] Minh Q. Nguyen, Claire E. Le Pichon, and Nicholas Ryba. “Stereotyped transcriptomic transformation of somatosensory neurons in response to injury”. In: *eLife* 8 (2019). ISSN: 2050084X. DOI: 10.7554/eLife.49679.

[34] A. K. Reinhold et al. “Differential transcriptional profiling of damaged and intact adjacent dorsal root ganglia neurons in neuropathic pain differential transcriptional profiling of damaged and intact adjacent dorsal root ganglia neurons in neuropathic pain”. In: *PLoS ONE* 10.4 (2015), pp. 1–17. ISSN: 19326203. DOI: 10.1371/journal.pone.0123342.

[35] M.A. A. Bangash et al. “Distinct transcriptional responses of mouse sensory neurons in models of human chronic pain conditions [version 1; referees: 2 approved]”. In: *Wellcome Open Research* 3.0 (2018), p. 78. ISSN: 2398502X. DOI: 10.12688/wellcomeopenres.14641.1.

[36] Allison M Barry et al. “Region-resolved quantitative proteome profiling reveals molecular dynamics associated with chronic pain in the PNS and spinal cord”. In: *Frontiers in Molecular Neuroscience* 11.August (2018), p. 259. ISSN: 1662-5099. DOI: 10.3389/fnmol.2018.00259.

[37] Elke Ydens et al. “Profiling peripheral nerve macrophages reveals two macrophage subsets with distinct localization, transcriptome and response to injury”. In: *Nature Neuroscience* 23.May (2020), pp. 676–689. ISSN: 15461726. DOI: 10.1038/s41593-020-0618-6.

[38] Michael Costigan et al. “Replicate high-density rat genome oligonucleotide microarrays reveal hundreds of regulated genes in the dorsal root ganglion after peripheral nerve injury”. In: *BMC neuroscience* 3 (Oct. 2002). ISSN: 1471-2202. DOI: 10.1186/1471-2202-3-16.

[39] Hua Sheng Xiao et al. "Identification of gene expression profile of dorsal root ganglion in the rat peripheral axotomy model of neuropathic pain". In: *Proceedings of the National Academy of Sciences of the United States of America* 99.12 (June 2002), pp. 8360–8365. ISSN: 00278424. DOI: 10.1073/PNAS.122231899/SUPPL_FILE/2318TABLE5.XLS.

[40] Enrique J. Cobos et al. "Mechanistic Differences in Neuropathic Pain Modalities Revealed by Correlating Behavior with Global Expression Profiling". In: *Cell Reports* 22.5 (Jan. 2018), pp. 1301–1312. ISSN: 22111247. DOI: 10.1016/j.celrep.2018.01.006.

[41] Ping Hu et al. "Single Cell Isolation and Analysis". In: *Frontiers in Cell and Developmental Biology* 4.October (2016), pp. 1–12. ISSN: 2296-634X. DOI: 10.3389/fcell.2016.00116.

[42] William Renthal et al. "Transcriptional Reprogramming of Distinct Peripheral Sensory Neuron Subtypes after Axonal Injury". In: *Neuron* 108.1 (Oct. 2020), 128–144.e9. ISSN: 1097-4199. DOI: 10.1016/J.NEURON.2020.07.026.

[43] Nicholas M. Tran et al. "Single-Cell Profiles of Retinal Ganglion Cells Differing in Resilience to Injury Reveal Neuroprotective Genes". In: *Neuron* 104.6 (Dec. 2019), 1039–1055.e12. ISSN: 10974199. DOI: 10.1016/J.NEURON.2019.11.006/ATTACHMENT/E091CDB1-E8A4-45BC-9F1B-517EEC865444/MMC1.PDF.

[44] Helen A King and André P Gerber. "Translatome profiling: methods for genome-scale analysis of mRNA translation". In: *Briefings in Functional Genomics* 15.1 (2016), pp. 22–31. DOI: 10.1093/bfgp/elu045.

[45] Salim Megat et al. "Nociceptor translational profiling reveals the Ragulator-Rag GTPase complex as a critical generator of neuropathic pain". In: *The Journal of Neuroscience* (2018), pp. 2661–18. ISSN: 0270-6474. DOI: 10.1523/JNEUROSCI.2661-18.2018.

[46] Sonali Uttam et al. "Translational profiling of dorsal root ganglia and spinal cord in a mouse model of neuropathic pain". In: *Neurobiology of Pain* 4 (Aug. 2018), pp. 35–44. ISSN: 2452-073X. DOI: 10.1016/j.ynpai.2018.04.001.

[47] Alan P. Boyle et al. "High-Resolution Mapping and Characterization of Open Chromatin across the Genome". In: *Cell* 132.2 (Jan. 2008), pp. 311–322. ISSN: 00928674. DOI: 10.1016/J.CELL.2007.12.014/ATTACHMENT/A6266970-4D15-43AC-9B59-2F337B97AE66/MMC1.PDF.

[48] Lingyun Song and Gregory E. Crawford. "DNase-seq: a high-resolution technique for mapping active gene regulatory elements across the genome from mammalian cells". In: *Cold Spring Harbor protocols* 2010.2 (Feb. 2010). ISSN: 1559-6095. DOI: 10.1101/PDB.PROT5384.

[49] Erez Lieberman-Aiden et al. "Comprehensive mapping of long range interactions reveals folding principles of the human genome". In: *Science (New York, N.Y.)* 326.5950 (Oct. 2009), p. 289. ISSN: 00368075. DOI: 10.1126/SCIENCE.1181369.

[50] Jason D. Buenrostro et al. "Transposition of native chromatin for fast and sensitive epigenomic profiling of open chromatin, DNA-binding proteins and nucleosome position". In: *Nat. Methods* 10.12 (Dec. 2013), pp. 1213–1218. ISSN: 15487091. DOI: 10.1038/nmeth.2688.

[51] Lite Yang et al. “Human and mouse trigeminal ganglia cell atlas implicates multiple cell types in migraine”. In: *Neuron* 0.0 (Mar. 2022). ISSN: 0896-6273. DOI: 10.1016/J.NEURON.2022.03.003.

[52] Valentina Vacca et al. “Higher pain perception and lack of recovery from neuropathic pain in females: A behavioural, immunohistochemical, and proteomic investigation on sex-related differences in mice”. In: *Pain* (2014). ISSN: 18726623. DOI: 10.1016/j.pain.2013.10.027.

[53] Anna Bodzon-Kułakowska et al. “Morphinome - A meta-analysis applied to proteomics studies in morphine dependence”. In: *PROTEOMICS* 11.1 (Jan. 2011), pp. 5–21. ISSN: 16159853. DOI: 10.1002/pmic.200900848.

[54] Ohannes K. Melemedjian et al. “Proteomic and functional annotation analysis of injured peripheral nerves reveals ApoE as a protein upregulated by injury that is modulated by metformin treatment”. In: *Molecular Pain* 9.1 (Mar. 2013). ISSN: 17448069. DOI: 10.1186/1744-8069-9-14.

[55] Sybil C.L. Hrstka et al. “Proteomic analysis of human iPSC-derived sensory neurons implicates cell stress and microtubule dynamics dysfunction in bortezomib-induced peripheral neurotoxicity”. In: *Experimental Neurology* 335 (Jan. 2021), p. 113520. ISSN: 0014-4886. DOI: 10.1016/J.EXPNEUROL.2020.113520.

[56] David Gomez-Varela and Manuela Schmidt. “Exploring novel paths towards protein signatures of chronic pain”. In: *Molecular Pain* (2016). ISSN: 17448069. DOI: 10.1177/1744806916679658.

[57] Roland Bruderer et al. “Optimization of Experimental Parameters in Data-Independent Mass Spectrometry Significantly Increases Depth and Reproducibility of Results”. In: *Molecular & Cellular Proteomics* 34 (2017), mcp.RA117.000314. ISSN: 1535-9476. DOI: 10.1074/mcp.RA117.000314.

[58] Mathias Uhlén et al. “Tissue-based map of the human proteome”. In: *Science* 347.6220 (Jan. 2015). ISSN: 10959203. DOI: 10.1126/SCIENCE.1260419/SUPPL_FILE/1260419_UHLEN.SM.PDF.

[59] Peter J. Thul et al. “A subcellular map of the human proteome”. In: *Science* 356.6340 (May 2017). ISSN: 10959203. DOI: 10.1126/SCIENCE.AAL3321/SUPPL_FILE/AAL3321_THUL_SM_TABLE_S9.XLSX.

[60] Shunsuke Aburaya et al. “Neuronal subclass-selective proteomic analysis in Caenorhabditis elegans”. In: *Scientific Reports 2020 10:1* 10.1 (Aug. 2020), pp. 1–9. ISSN: 2045-2322. DOI: 10.1038/s41598-020-70692-w.

[61] Julia R. Sondermann et al. “Vti1b promotes TRPV1 sensitization during inflammatory pain”. In: *Pain* 160.2 (Feb. 2019), pp. 508–527. ISSN: 18726623. DOI: 10.1097/j.pain.0000000000001418.

[62] L. Avenali et al. “Annexin A2 Regulates TRPA1-Dependent Nociception”. In: *Journal of Neuroscience* (2014). ISSN: 0270-6474. DOI: 10.1523/JNEUROSCI.1801-14.2014.

[63] Nikhil Sharma et al. “The emergence of transcriptional identity in somatosensory neurons”. In: *Nature* 577.7790 (Jan. 2020), pp. 392–398. ISSN: 1476-4687. DOI: 10.1038/S41586-019-1900-1.

[64] James R.F. Hockley et al. "Single-cell RNAseq reveals seven classes of colonic sensory neuron". In: *Gut* 68.4 (2019), pp. 633–644. ISSN: 14683288. DOI: 10.1136/gutjnl-2017-315631.

[65] Thibaud Parpaite et al. "Patch-seq of mouse DRG neurons reveals candidate genes for specific mechanosensory functions". In: *Cell Reports* 37.5 (Nov. 2021), p. 109914. ISSN: 22111247. DOI: 10.1016/J.CELREP.2021.109914.

[66] Minh Q. Nguyen et al. "Diversity amongst trigeminal neurons revealed by high throughput single cell sequencing". In: *PLOS ONE* 12.9 (Sept. 2017), e0185543. ISSN: 1932-6203. DOI: 10.1371/JOURNAL.PONE.0185543.

[67] Aldrin K.Y. Yim et al. "Disentangling glial diversity in peripheral nerves at single-nuclei resolution". In: *Nature Neuroscience 2022 25:2* 25.2 (Feb. 2022), pp. 238–251. ISSN: 1546-1726. DOI: 10.1038/s41593-021-01005-1.

[68] Colleen N. McLaughlin et al. "Single-cell transcriptomes of developing and adult olfactory receptor neurons in drosophila". In: *eLife* 10 (Feb. 2021), pp. 1–37. ISSN: 2050084X. DOI: 10.7554/ELIFE.63856.

[69] Caroline Flegel et al. "RNA-Seq analysis of human trigeminal and dorsal root ganglia with a focus on chemoreceptors". In: *PLoS ONE* 10.6 (June 2015), pp. 1–30. ISSN: 19326203. DOI: 10.1371/journal.pone.0128951.

[70] Pradipta Ray et al. "Comparative transcriptome profiling of the human and mouse dorsal root ganglia". In: *Pain* 159.7 (Mar. 2018), p. 1. ISSN: 0304-3959. DOI: 10.1097/j.pain.0000000000001217.

[71] Kristin A. Gerhold et al. "The Star-Nosed Mole Reveals Clues to the Molecular Basis of Mammalian Touch". In: *PLoS ONE* 8.1 (Jan. 2013), p. 55001. ISSN: 19326203. DOI: 10.1371/JOURNAL.PONE.0055001.

[72] Douglas M. Lopes, Franziska Denk, and Stephen B. McMahon. "The Molecular Fingerprint of Dorsal Root and Trigeminal Ganglion Neurons". In: *Frontiers in Molecular Neuroscience* (2017). DOI: 10.3389/fnmol.2017.00304.

[73] Georgios Baskozos et al. "Comprehensive analysis of long noncoding RNA expression in dorsal root ganglion reveals cell-type specificity and dysregulation after nerve injury". In: *Pain* 160.2 (Feb. 2019), pp. 463–485. ISSN: 18726623. DOI: 10.1097/j.pain.0000000000001416.

[74] Ilaria Palmisano et al. "Epigenomic signatures underpin the axonal regenerative ability of dorsal root ganglia sensory neurons". In: *Nat. Neurosci.* 22.11 (Nov. 2019), pp. 1913–1924. ISSN: 15461726. DOI: 10.1038/s41593-019-0490-4.

[75] Zhiqiang Pan et al. "Downregulation of a Dorsal Root Ganglion-Specifically Enriched Long Noncoding RNA is Required for Neuropathic Pain by Negatively Regulating RALY-Triggered Ehmt2 Expression". In: *Advanced Science* 8.13 (July 2021), p. 2004515. ISSN: 2198-3844. DOI: 10.1002/ADVS.202004515.

[76] Andrei V. Chernov and Veronica I. Shubayev. "Sexual Dimorphism of Early Transcriptional Reprogramming in Dorsal Root Ganglia After Peripheral Nerve Injury". In: *Frontiers in Molecular Neuroscience* 14 (Dec. 2021). ISSN: 16625099. DOI: 10.3389/FNMOL.2021.779024/FULL.

[77] Sara E. Jager et al. "Changes in the transcriptional fingerprint of satellite glial cells following peripheral nerve injury". In: *Glia* 68.7 (July 2020), pp. 1375–1395. ISSN: 1098-1136. DOI: 10.1002/GLIA.23785.

[78] Kimberly E. Stephens et al. "Sex differences in gene regulation in the dorsal root ganglion after nerve injury". In: *BMC Genomics* 20.1 (Feb. 2019), pp. 1–18. ISSN: 14712164. DOI: 10.1186/S12864-019-5512-9/FIGURES/7.

[79] Chengyu Yin et al. "Transcriptome profiling of dorsal root ganglia in a rat model of complex regional pain syndrome type-I reveals potential mechanisms involved in pain". In: *Journal of Pain Research* 12 (2019), p. 1201. ISSN: 11787090. DOI: 10.2147/JPR.S188758.

[80] Hae Young Shin et al. "Alteration in global DNA methylation status following preconditioning injury influences axon growth competence of the sensory neurons". In: *Experimental Neurology* 326 (Apr. 2020), p. 113177. ISSN: 0014-4886. DOI: 10.1016/J.EXPNEUROL.2020.113177.

[81] Kimberly E. Stephens et al. "Global gene expression and chromatin accessibility of the peripheral nervous system in animal models of persistent pain". In: *Journal of Neuroinflammation* 18.1 (Dec. 2021), pp. 1–16. ISSN: 17422094. DOI: 10.1186/S12974-021-02228-6/FIGURES/5.

[82] Salim Megat et al. "Differences between Dorsal Root and Trigeminal Ganglion Nociceptors in Mice Revealed by Translational Profiling". In: *The Journal of neuroscience : the official journal of the Society for Neuroscience* 39.35 (Aug. 2019), pp. 6829–6847. ISSN: 15292401. DOI: 10.1523/JNEUROSCI.2663-18.2019.

[83] Meir Rozenbaum et al. "Translatome Regulation in Neuronal Injury and Axon Regrowth". In: *eNeuro* 5.2 (Mar. 2018). ISSN: 2373-2822. DOI: 10.1523/ENEURO.0276-17.2018.

[84] Melissa T. Manners et al. "Genome-wide redistribution of MeCP2 in dorsal root ganglia after peripheral nerve injury". In: *Epigenetics & chromatin* 9.1 (June 2016). ISSN: 1756-8935. DOI: 10.1186/S13072-016-0073-5.

[85] Gosuke Oki et al. "Metallothionein deficiency in the injured peripheral nerves of complex regional pain syndrome as revealed by proteomics". In: *Pain* 153.3 (Mar. 2012), pp. 532–539. ISSN: 1872-6623. DOI: 10.1016/J.PAIN.2011.11.008.

[86] Tom Rouwette et al. *Modulation of nociceptive ion channels and receptors via protein-protein interactions: Implications for pain relief*. 2015. DOI: 10.1080/19336950.2015.1051270.

[87] Julia Patzig et al. "Quantitative and integrative proteome analysis of peripheral nerve myelin identifies novel myelin proteins and candidate neuropathy loci". In: *The Journal of neuroscience : the official journal of the Society for Neuroscience* 31.45 (Nov. 2011), pp. 16369–16386. ISSN: 1529-2401. DOI: 10.1523/JNEUROSCI.4016-11.2011.

[88] Sophie B. Siems et al. "Proteome profile of peripheral myelin in healthy mice and in a neuropathy model". In: *eLife* 9 (Mar. 2020). ISSN: 2050084X. DOI: 10.7554/eLife.51406.

[89] Aiping Lu, Jacek R. Wiśniewski, and Matthias Mann. "Comparative proteomic profiling of membrane proteins in rat cerebellum, spinal cord, and sciatic nerve". In: *Journal of Proteome Research* 8.5 (May 2009), pp. 2418–2425. ISSN: 15353893. DOI: 10.1021/PR8010364/SUPPL_FILE/PR8010364_SI_004.PDF.

[90] Jussi Kupari et al. "An Atlas of Vagal Sensory Neurons and Their Molecular Specialization". In: *Cell Reports* 27.8 (May 2019), 2508–2523.e4. ISSN: 22111247. DOI: 10.1016/j.celrep.2019.04.096.

[91] Pradipta R. Ray et al. "Transcriptome Analysis of the Human Tibial Nerve Identifies Sexually Dimorphic Expression of Genes Involved in Pain, Inflammation, and Neuro-Immunity". In: *Frontiers in Molecular Neuroscience* 12.March (2019). DOI: 10.3389/fnmol.2019.00037.

[92] Steven J. Middleton et al. "Studying human nociceptors: From fundamentals to clinic". In: *Brain* (2021). ISSN: 14602156. DOI: 10.1093/brain/awab048.

[93] Stephanie Shiers, Rebecca M. Klein, and Theodore J. Price. "Quantitative differences in neuronal subpopulations between mouse and human dorsal root ganglia demonstrated with RNAscope in situ hybridization". In: *Pain* 161.10 (Oct. 2020), pp. 2410–2424. ISSN: 1872-6623. DOI: 10.1097/J.PAIN.0000000000001973.

[94] Nicholas S. Gregory et al. "An overview of animal models of pain: Disease models and outcome measures". In: *Journal of Pain* 14.11 (2013), pp. 1255–1269. ISSN: 15288447. DOI: 10.1016/j.jpain.2013.06.008.

[95] Isabelle Decosterd and Clifford J. Woolf. "Spared nerve injury: An animal model of persistent peripheral neuropathic pain". In: *Pain* 87.2 (Aug. 2000), pp. 149–158. ISSN: 03043959. DOI: 10.1016/S0304-3959(00)00276-1.

[96] Christina F. Vogelaar et al. "Sciatic nerve regeneration in mice and rats: Recovery of sensory innervation is followed by a slowly retreating neuropathic pain-like syndrome". In: *Brain Research* 1027.1-2 (Nov. 2004), pp. 67–72. ISSN: 00068993. DOI: 10.1016/j.brainres.2004.08.036.

[97] Andrew R. Bauder and Toby A. Ferguson. "Reproducible mouse sciatic nerve crush and subsequent assessment of regeneration by whole mount muscle analysis". In: *Journal of Visualized Experiments* 60 (Feb. 2012). ISSN: 1940087X. DOI: 10.3791/3606.

[98] Alexander J Davies et al. "Natural Killer Cells Degenerate Intact Sensory Afferents following Nerve Injury Article Natural Killer Cells Degenerate Intact Sensory Afferents following Nerve Injury". In: *Cell* 176 (2019), pp. 716–728. DOI: 10.1016/j.cell.2018.12.022.

[99] Allan I. Basbaum et al. "Cellular and Molecular Mechanisms of Pain". In: *Cell* 139.2 (2009), pp. 267–284. ISSN: 00928674. DOI: 10.1016/j.cell.2009.09.028.

[100] Stefanie Hardt et al. "Distal infraorbital nerve injury: A model for persistent facial pain in mice". In: *Pain* 160.6 (June 2019), pp. 1431–1447. ISSN: 18726623. DOI: 10.1097/j.pain.0000000000001518.

[101] Joyshree Biswas et al. "Streptozotocin alters glucose transport, connexin expression and endoplasmic reticulum functions in neurons and astrocytes". In: *Neuroscience* 356 (July 2017), pp. 151–166. ISSN: 18737544. DOI: 10.1016/j.neuroscience.2017.05.018.

[102] Ahmet Höke and Mitali Ray. "Rodent models of chemotherapy-induced peripheral neuropathy". In: *ILAR Journal* 54.3 (Apr. 2014), pp. 273–281. ISSN: 10842020. DOI: 10.1093/ilar/ilt053.

[103] Tricia H. Burdo and Andrew D. Miller. *Animal models of HIV peripheral neuropathy*. 2014. DOI: 10.2217/fvl.14.28.

[104] Uri Herzberg and Jacqueline Sagen. "Peripheral nerve exposure to HIV viral envelope protein gp120 induces neuropathic pain and spinal gliosis". In: *Journal of Neuroimmunology* 116.1 (May 2001), pp. 29–39. ISSN: 01655728. DOI: 10.1016/S0165-5728(01)00288-0.

[105] Victoria C.J. Wallace et al. "Pharmacological, behavioural and mechanistic analysis of HIV-1 gp120 induced painful neuropathy". In: *Pain* 133.1-3 (Dec. 2007), pp. 47–63. ISSN: 03043959. DOI: 10.1016/j.pain.2007.02.015.

[106] Sun Ho Kim and Jin Mo Chung. "An experimental model for peripheral neuropathy produced by segmental spinal nerve ligation in the rat". In: *Pain* 50.3 (1992), pp. 355–363. ISSN: 03043959. DOI: 10.1016/0304-3959(92)90041-9.

[107] Jin Mo Chung, Hee Kee Kim, and Kyungsoon Chung. "Segmental spinal nerve ligation model of neuropathic pain." In: *Methods in molecular medicine* 99 (2004), pp. 35–45. ISSN: 15431894. DOI: 10.1385/1-59259-770-X:035.

[108] S. M. Sweitzer et al. "Acute peripheral inflammation induces moderate glial activation and spinal IL-1β expression that correlates with pain behavior in the rat". In: *Brain Research* 829.1-2 (May 1999), pp. 209–221. ISSN: 00068993. DOI: 10.1016/S0006-8993(99)01326-8.

[109] Gary J. Bennett and Y. K. Xie. "A peripheral mononeuropathy in rat that produces disorders of pain sensation like those seen in man". In: *Pain* 33.1 (1988), pp. 87–107. ISSN: 03043959. DOI: 10.1016/0304-3959(88)90209-6.

[110] Ze'ev Seltzer, Ronald Dubner, and Yoram Shir. "A novel behavioral model of neuropathic pain disorders produced in rats by partial sciatic nerve injury". In: *Pain* 43.2 (1990), pp. 205–218. ISSN: 0304-3959. DOI: 10.1016/0304-3959(90)91074-S.

[111] P. D. Wall et al. "Autotomy following peripheral nerve lesions: experimental anesthesia dolorosa". In: *Pain* 7.2 (Oct. 1979), pp. 103–113. ISSN: 0304-3959. DOI: 10.1016/0304-3959(79)90002-2.

[112] John M. Dawes et al. "Immune or Genetic-Mediated Disruption of CASPR2 Causes Pain Hypersensitivity Due to Enhanced Primary Afferent Excitability". In: *Neuron* 97.4 (2018). ISSN: 10974199. DOI: 10.1016/j.neuron.2018.01.033.

[113] Matthew J. Schwei et al. "Neurochemical and cellular reorganization of the spinal cord in a murine model of bone cancer pain". In: *Journal of Neuroscience* 19.24 (Dec. 1999), pp. 10886–10897. ISSN: 02706474. DOI: 10.1523/jneurosci.19-24-10886.1999.

[114] Gowhar Ali et al. "A streptozotocin-induced diabetic neuropathic pain model for static or dynamic mechanical allodynia and vulvodynia: Validation using topical and systemic gabapentin". In: *Naunyn-Schmiedeberg's Archives of Pharmacology* 388.11 (Nov. 2015), pp. 1129–1140. ISSN: 14321912. DOI: 10.1007/s00210-015-1145-y.

[115] Phillipe D. O'Brien, Stacey A. Sakowski, and Eva L. Feldman. "Mouse Models of Diabetic Neuropathy". In: *ILAR Journal* 54.3 (2014), p. 259. DOI: 10.1093/ILAR/ILT052.

[116] K. Hargreaves et al. "A new and sensitive method for measuring thermal nociception in cutaneous hyperalgesia". In: *Pain* 32.1 (1988), pp. 77–88. ISSN: 03043959. DOI: 10.1016/0304-3959(88)90026-7.

[117] Jennifer R. Deuis, Lucie S. Dvorakova, and Irina Vetter. "Methods used to evaluate pain behaviors in rodents". In: *Frontiers in Molecular Neuroscience* 10 (Sept. 2017), p. 284. ISSN: 16625099. DOI: 10.3389/fnmol.2017.00284.

[118] Tamara King et al. "Unmasking the tonic-aversive state in neuropathic pain". In: *Nature Neuroscience* 12.11 (2009), pp. 1364–1366. ISSN: 10976256. DOI: 10.1038/nn.2407.

[119] Martin Koltzenburg, Cheryl L. Stucky, and Gary R. Lewin. "Receptive Properties of Mouse Sensory Neurons Innervating Hairy Skin". In: *Journal of Neurophysiology* 78.4 (Oct. 1997), pp. 1841–1850. ISSN: 0022-3077. DOI: 10.1152/jn.1997.78.4.1841.

[120] Z. Ali et al. "Uninjured C-Fiber Nociceptors Develop Spontaneous Activity and α-Adrenergic Sensitivity Following L ₆ Spinal Nerve Ligation in Monkey". In: *Journal of Neurophysiology* 81.2 (Feb. 1999), pp. 455–466. ISSN: 0022-3077. DOI: 10.1152/jn.1999.81.2.455.

[121] Greg A. Weir et al. "Using an engineered glutamate-gated chloride channel to silence sensory neurons and treat neuropathic pain at the source". In: *Brain* 140.10 (2017), pp. 2570–2585. ISSN: 14602156. DOI: 10.1093/brain/awx201.

[122] Inge Petter Kleggetveit et al. "High spontaneous activity of C-nociceptors in painful polyneuropathy". In: *Pain* 153.10 (Oct. 2012), pp. 2040–2047. ISSN: 03043959. DOI: 10.1016/j.pain.2012.05.017.

[123] Jordi Serra et al. "Microneurographic identification of spontaneous activity in C-nociceptors in neuropathic pain states in humans and rats". In: *Pain* 153.1 (Jan. 2012), pp. 42–55. ISSN: 03043959. DOI: 10.1016/j.pain.2011.08.015.

[124] Martin Schmelz. *Does spontaneous activity in C-nociceptors provide a readout to quantify neuropathic pain?* 2012. DOI: 10.1016/j.pain.2011.09.027.

[125] Alban Latremoliere and Clifford J. Woolf. "Central Sensitization: A Generator of Pain Hypersensitivity by Central Neural Plasticity". In: *Journal of Pain* 10.9 (Sept. 2009), pp. 895–926. ISSN: 15265900. DOI: 10.1016/j.jpain.2009.06.012.

[126] Clifford J Woolf. "Review series introduction What is this thing called pain ?" In: *The Journal of Clinical Investigation* 120.11 (2010), pp. 10–12. ISSN: 15588238. DOI: 10.1172/JCI45178.3742.

[127] Simon Haroutounian et al. "Primary afferent input critical for maintaining spontaneous pain in peripheral neuropathy". In: *Pain* 155.7 (2014), pp. 1272–1279. ISSN: 18726623. DOI: 10.1016/j.pain.2014.03.022.

[128] Laiche Djouhri et al. "Spontaneous pain, both neuropathic and inflammatory, is related to frequency of spontaneous firing in intact C-fiber nociceptors". In: *Journal of Neuroscience* 26.4 (Jan. 2006), pp. 1281–1292. ISSN: 02706474. DOI: 10.1523/JNEUROSCI.3388-05.2006.

[129] David B. Reichling and Jon D. Levine. "Critical role of nociceptor plasticity in chronic pain". In: *Trends in neurosciences* 32.12 (Dec. 2009), pp. 611–618. ISSN: 1878-108X. DOI: 10.1016/J.TINS.2009.07.007.

[130] Dioneia Araldi et al. "Fentanyl Induces Rapid Onset Hyperalgesic Priming: Type I at Peripheral and Type II at Central Nociceptor Terminals". In: *J. Neurosci* 10 (2018), pp. 3476–17. DOI: 10.1523/JNEUROSCI.3476-17.2018.

[131] Kufreobong E. Inyang et al. "Alleviation of paclitaxel-induced mechanical hypersensitivity and hyperalgesic priming with AMPK activators in male and female mice". In: *Neurobiology of Pain* 6 (Aug. 2019), p. 100037. ISSN: 2452-073X. DOI: 10.1016/J.YNPAI.2019.100037.

[132] Luiz F. Ferrari, Dionéia Araldi, and Jon D. Levine. "Regulation of Expression of Hyperalgesic Priming by Estrogen Receptor α in the Rat". In: *The journal of pain* 18.5 (May 2017), pp. 574–582. ISSN: 1528-8447. DOI: 10.1016/J.JPAIN.2016.12.017.

[133] Jamie K. Moy et al. "Temporal and sex differences in the role of BDNF/TrkB signaling in hyperalgesic priming in mice and rats". In: *Neurobiology of Pain* 5.October 2018 (Jan. 2019), p. 100024. ISSN: 2452-073X. DOI: 10.1016/j.ynpai.2018.10.001.

[134] Ru Rong Ji, Alexander Chamessian, and Yu Qiu Zhang. *Pain regulation by non-neuronal cells and inflammation*. Nov. 2016. DOI: 10.1126/science.aaf8924.

[135] Elizabeth A. Old et al. "Monocytes expressing CX3CR1 orchestrate the development of vincristine-induced pain". In: *Journal of Clinical Investigation* 124.5 (2014), pp. 2023–2036. ISSN: 15588238. DOI: 10.1172/JCI71389.

[136] Xiaobing Yu et al. "Dorsal root ganglion macrophages contribute to both the initiation and persistence of neuropathic pain". In: *Nature Communications* 11.1 (Dec. 2020), pp. 1–12. ISSN: 20411723. DOI: 10.1038/s41467-019-13839-2.

[137] Jesse K. Niehaus et al. "Spinal macrophages resolve nociceptive hypersensitivity after peripheral injury". In: *Neuron* 109.8 (Apr. 2021), 1274–1282.e6. ISSN: 10974199. DOI: 10.1016/J.NEURON.2021.02.018.

[138] Michiel van der Vlist et al. "Macrophages transfer mitochondria to sensory neurons to resolve inflammatory pain". In: *Neuron* 110.4 (Feb. 2022), 613–626.e9. ISSN: 10974199. DOI: 10.1016/J.NEURON.2021.11.020/ATTACHMENT/97A4F6F1-8A18-4CC7-A7F2-7E148DE13764/MMC3.ZIP.

[139] Patrick D. Wall and Michael Gutnick. "Properties of afferent nerve impulses originating from a neuroma". In: *Nature* 248.5451 (1974), pp. 740–743. ISSN: 00280836. DOI: 10.1038/248740a0.

[140] Marshall Devor. *Ectopic discharge in Aβ afferents as a source of neuropathic pain*. June 2009. DOI: 10.1007/s00221-009-1724-6.

[141] Bjarke Abrahamsen et al. "The cell and molecular basis of mechanical, cold, and inflammatory pain". In: *Science* 321.5889 (Aug. 2008), pp. 702–705. ISSN: 00368075. DOI: 10.1126/science.1156916.

[142] Daniel J. Cavanaugh et al. "Distinct subsets of unmyelinated primary sensory fibers mediate behavioral responses to noxious thermal and mechanical stimuli". In: *Proceedings of the National Academy of Sciences of the United States of America* 106.22 (June 2009), pp. 9075–9080. ISSN: 10916490. DOI: 10.1073/PNAS.0901507106.

[143] Eric S. McCoy et al. "Peptidergic CGRPα Primary Sensory Neurons Encode Heat and Itch and Tonically Suppress Sensitivity to Cold". In: *Neuron* 78.1 (Apr. 2013), pp. 138–151. ISSN: 08966273. DOI: 10.1016/j.neuron.2013.01.030.

[144] Joel D. Greenspan et al. *Studying sex and gender differences in pain and analgesia: A consensus report*. Nov. 2007. DOI: 10.1016/j.pain.2007.10.014.

[145] Jeffrey S Mogil. *Sex differences in pain and pain inhibition: multiple explanations of a controversial phenomenon*. Tech. rep. 2012. DOI: 10.1038/nrn3360.

[146] Karen J. Berkley. "Vive la différence!" In: *Trends in Neurosciences* 15.9 (Sept. 1992), pp. 331–332. ISSN: 0166-2236. DOI: 10.1016/0166-2236(92)90048-D.

[147] Anita M. Unruh. "Gender variations in clinical pain experience". In: *Pain* 65.2-3 (1996), pp. 123–167. ISSN: 03043959. DOI: 10.1016/0304-3959(95)00214-6.

[148] Rebecca M. Shansky. "Are hormones a "female problem" for animal research? Outdated gender stereotypes are influencing experimental design in laboratory animals". In: *Science* 364.6443 (May 2019), pp. 825–826. ISSN: 10959203. DOI: 10.1126/science.aaw7570.

[149] Chelsea Wald and Corinna Wu. "Of Mice and Women: The Bias in Animal Models". In: *Science* 327.5973 (Mar. 2010), 1571 LP –1572. DOI: 10.1126/science.327.5973.1571.

[150] Jeffrey S. Mogil. "Qualitative sex differences in pain processing: emerging evidence of a biased literature". In: *Nature Reviews Neuroscience 2020* (2020), pp. 1–13. ISSN: 1471-003X. DOI: 10.1038/s41583-020-0310-6.

[151] Mayur Patil et al. "Prolactin Regulates Pain Responses via a Female-Selective Nociceptor-Specific Mechanism". In: *iScience* 20 (Oct. 2019), pp. 449–465. ISSN: 25890042. DOI: 10.1016/j.isci.2019.09.039.

[152] Candler Paige et al. "Neuroendocrine Mechanisms Governing Sex Differences in Hyperalgesic Priming Involve Prolactin Receptor Sensory Neuron Signaling". In: *Journal of Neuroscience* 40.37 (Sept. 2020), pp. 7080–7090. ISSN: 0270-6474. DOI: 10.1523/JNEUROSCI.1499-20.2020.

[153] Daniela Baptista-de-Souza et al. "Sex differences in the role of atypical PKC within the basolateral nucleus of the amygdala in a mouse hyperalgesic priming model". In: *Neurobiology of Pain* 8 (Aug. 2020). ISSN: 2452073X. DOI: 10.1016/J.YNPAI.2020.100049.

[154] Theodore J Cicero et al. "Role of steroids in sex differences in morphine-induced analgesia: activational and organizational effects". In: *J Pharmacol Exp Ther* 300.2 (2002), pp. 695–701. DOI: 10.1124/jpet.300.2.695.

[155] Yanxia Chen et al. "An Emerging Role for Prolactin in Female-Selective Pain". In: *Trends in Neurosciences* 43.8 (Aug. 2020), pp. 635–648. ISSN: 0166-2236. DOI: 10.1016/J.TINS.2020.06.003.

[156] Authors Amanda Avona et al. "Dural calcitonin gene-related peptide produces female-specific responses in rodent migraine models Title : Dural calcitonin gene-related peptide produces female-specific responses in rodent migraine models Abbreviated Title : Female-specific responses to ". In: (2019).

[157] Daigo Ikegami et al. "A prolactin-dependent sexually dimorphic mechanism of migraine chronification". In: *Cephalalgia* 42.3 (Mar. 2022), pp. 197–208. ISSN: 14682982. DOI: 10.1177/03331024211039813.

[158] Anibal Diogenes et al. "Prolactin modulates TRPV1 in female rat trigeminal sensory neurons". In: *The Journal of neuroscience* 26.31 (Aug. 2006), pp. 8126–8136. ISSN: 1529-2401. DOI: 10.1523/JNEUROSCI.0793-06.2006.

[159] Mayur J. Patil et al. "Prolactin regulates TRPV1, TRPA1, and TRPM8 in sensory neurons in a sex-dependent manner: Contribution of prolactin receptor to inflammatory pain". In: *American journal of physiology. Endocrinology and metabolism* 305.9 (Nov. 2013). ISSN: 1522-1555. DOI: 10.1152/AJPENDO.00187.2013.

[160] Ting Ting Liu et al. "Prolactin potentiates the activity of acid-sensing ion channels in female rat primary sensory neurons". In: *Neuropharmacology* 103 (Apr. 2016), pp. 174–182. ISSN: 0028-3908. DOI: 10.1016/J.NEUROPHARM.2015.07.016.

[161] Rebecca M. Craft. "Modulation of pain by estrogens". In: *Pain* (2007). ISSN: 1872-6623. DOI: 10.1016/J.PAIN.2007.09.028.

[162] Tim Hucho and Jon D Levine. "Signaling pathways in sensitization: toward a nociceptor cell biology." In: *Neuron* 55.3 (Aug. 2007), pp. 365–76. ISSN: 0896-6273. DOI: 10.1016/j.neuron.2007.07.008.

[163] Rebecca S. Hornung et al. "Progesterone and Allopregnanolone Rapidly Attenuate Estrogen-Associated Mechanical Allodynia in Rats with Persistent Temporomandibular Joint Inflammation". In: *Frontiers in Integrative Neuroscience* 14 (May 2020), p. 26. ISSN: 16625145. DOI: 10.3389/FNINT.2020.00026/BIBTEX.

[164] Candler Paige et al. "A Female-Specific Role for Calcitonin Gene-Related Peptide (CGRP) in Rodent Pain Models". In: *Journal of Neuroscience* 42.10 (Mar. 2022), pp. 1930–1944. ISSN: 0270-6474. DOI: 10.1523/JNEUROSCI.1137-21.2022.

[165] Yin Liu et al. "Sexually dimorphic BDNF signaling directs sensory innervation of the mammary gland". In: *Science* 338.6112 (Dec. 2012), pp. 1357–1360. ISSN: 10959203. DOI: 10.1126/SCIENCE.1228258/SUPPL_FILE/1228258.LIU.SM.PDF.

[166] Annemarie Dedek et al. "Sexual dimorphism in a neuronal mechanism of spinal hyperexcitability across rodent and human models of pathological pain". In: *Brain : a journal of neurology* 145.3 (Mar. 2022), pp. 1124–1138. ISSN: 1460-2156. DOI: 10.1093/BRAIN/AWAB408.

[167] Gusztav Belteki et al. "Conditional and inducible transgene expression in mice through the combinatorial use of Cre-mediated recombination and tetracycline induction". In: *Nucleic acids research* 33.5 (2005), pp. 1–10. ISSN: 1362-4962. DOI: 10.1093/NAR/GNI051.

[168] Christoph Kellendonk et al. "Regulation of Cre Recombinase Activity by the Synthetic Steroid RU 486". In: *Nucleic Acids Research* 24.8 (Apr. 1996), pp. 1404–1411. ISSN: 0305-1048. DOI: 10.1093/NAR/24.8.1404.

[169] Richard Sando et al. “Inducible control of gene expression with destabilized Cre”. In: *Nature methods* 10.11 (Nov. 2013), p. 1085. ISSN: 15487091. DOI: 10.1038/NMETH.2640.

[170] Nina L. Hunter et al. “Ligand-activated Flpe for temporally regulated gene modifications”. In: *genesis* 41.3 (Mar. 2005), pp. 99–109. ISSN: 1526-968X. DOI: 10.1002/GENE.20101.

[171] Liam J. Peck et al. “Studying Independent Kcna6 Knock-out Mice Reveals Toxicity of Exogenous LacZ to Central Nociceptor Terminals and Differential Effects of Kv1.6 on Acute and Neuropathic Pain Sensation”. In: *Journal of Neuroscience* 41.44 (Nov. 2021), pp. 9141–9162. ISSN: 0270-6474. DOI: 10.1523/JNEUROSCI.0187-21.2021.

[172] Shannon D. Shields et al. “Nav1.8 expression is not restricted to nociceptors in mouse peripheral nervous system”. In: *Pain* 153.10 (Oct. 2012), pp. 2017–2030. ISSN: 0304-3959. DOI: 10.1016/j.pain.2012.04.022.

[173] S. Averill et al. “Immunocytochemical Localization of trkA Receptors in Chemically Identified Subgroups of Adult Rat Sensory Neurons”. In: *European Journal of Neuroscience* 7.7 (July 1995), pp. 1484–1494. ISSN: 1460-9568. DOI: 10.1111/J.1460-9568.1995.TB01143.X.

[174] Alice Arcourt et al. “Touch Receptor-Derived Sensory Information Alleviates Acute Pain Signaling and Fine-Tunes Nociceptive Reflex Coordination”. In: *Neuron* 93.1 (Jan. 2017), pp. 179–193. ISSN: 10974199. DOI: 10.1016/j.neuron.2016.11.027.

[175] Mayur J. Patil, Anahit H. Hovhannisyan, and Armen N. Akopian. “Characteristics of sensory neuronal groups in CGRP-cre-ER reporter mice: Comparison to Nav1.8-cre, TRPV1-cre and TRPV1-GFP mouse lines”. In: *PLOS ONE* 13.6 (June 2018). Ed. by David D. McKemy, e0198601. ISSN: 1932-6203. DOI: 10.1371/journal.pone.0198601.

[176] Jason W. Tarpley, Martin G. Kohler, and William J. Martin. “The behavioral and neuroanatomical effects of IB 4-saporin treatment in rat models of nociceptive and neuropathic pain”. In: *Brain Research* 1029.1 (Dec. 2004), pp. 65–76. ISSN: 00068993. DOI: 10.1016/j.brainres.2004.09.027.

[177] Theodore J. Price and Christopher M. Flores. “Critical Evaluation of the Colocalization Between Calcitonin Gene-Related Peptide, Substance P, Transient Receptor Potential Vanilloid Subfamily Type 1 Immunoreactivities, and Isolectin B4 Binding in Primary Afferent Neurons of the Rat and Mouse”. In: *Journal of Pain* 8.3 (Mar. 2007), pp. 263–272. ISSN: 15265900. DOI: 10.1016/j.jpain.2006.09.005.

[178] Jaquette Liljencrantz and Håkan Olausson. “Tactile C fibers and their contributions to pleasant sensations and to tactile allodynia”. In: *Frontiers in behavioral neuroscience* 8.MAR (Mar. 2014). ISSN: 1662-5153. DOI: 10.3389/FNBEH.2014.00037.

[179] Steven J. Middleton et al. “Nav1.7 is required for normal C-low threshold mechanoreceptor function in humans and mice”. In: *Brain : a journal of neurology* (Dec. 2021). ISSN: 1460-2156. DOI: 10.1093/BRAIN/AWAB482.

[180] Rebecca P. Seal et al. "Injury-induced mechanical hypersensitivity requires C-low threshold mechanoreceptors". In: *Nature* 462.7273 (Dec. 2009), pp. 651–655. ISSN: 00280836. DOI: 10.1038/nature08505.

[181] Marie Claire Delfini et al. "TAFA4, a Chemokine-like Protein, Modulates Injury-Induced Mechanical and Chemical Pain Hypersensitivity in Mice". In: *Cell Reports* 5.2 (Oct. 2013), pp. 378–388. ISSN: 22111247. DOI: 10.1016/j.celrep.2013.09.013.

[182] Louise Urien et al. "Genetic ablation of GINIP-expressing primary sensory neurons strongly impairs Formalinevoked pain". In: *Scientific Reports* 7.1 (Feb. 2017), pp. 1–12. ISSN: 20452322. DOI: 10.1038/srep43493.

[183] Max Larsson and Jonas Broman. "Synaptic organization of VGLUT3 expressing low-threshold mechanosensitive C fiber terminals in the rodent spinal cord". In: *eNeuro* 6.1 (Jan. 2019). ISSN: 23732822. DOI: 10.1523/ENEURO.0007-19.2019.

[184] Cedric Peirs et al. "Dorsal Horn Circuits for Persistent Mechanical Pain". In: *Neuron* 87.4 (Aug. 2015), pp. 797–812. ISSN: 10974199. DOI: 10.1016/j.neuron.2015.07.029.

[185] Chiara Morelli et al. "Identification of a population of peripheral sensory neurons that regulates blood pressure". In: *Cell Reports* 35.9 (June 2021). ISSN: 22111247. DOI: 10.1016/J.CELREP.2021.109191.

[186] Nicole L Neubarth et al. "Meissner corpuscles and their spatially intermingled afferents underlie gentle touch perception". In: *Science* 368.6497 (June 2020), p. 2751. DOI: 10.1126/science.abb2751.

[187] Kenji Mandai et al. "LIG Family Receptor Tyrosine Kinase-Associated Proteins Modulate Growth Factor Signals during Neural Development". In: *Neuron* 63.5 (Sept. 2009), pp. 614–627. ISSN: 08966273. DOI: 10.1016/j.neuron.2009.07.031.

[188] Hai Song et al. "Functional characterization of pulmonary neuroendocrine cells in lung development, injury, and tumorigenesis." In: *Proceedings of the National Academy of Sciences of the United States of America* 109.43 (Oct. 2012), pp. 17531–6. ISSN: 00278424. DOI: 10.1073/pnas.1207238109.

[189] William Olson et al. "Sparse genetic tracing reveals regionally specific functional organization of mammalian nociceptors". In: *eLife* 6 (Oct. 2017). ISSN: 2050-084X. DOI: 10.7554/eLife.29507.

[190] Mohammed A. Nassar et al. "Nociceptor-specific gene deletion reveals a major role for Nav1.7 (PN1) in acute and inflammatory pain". In: *Proceedings of the National Academy of Sciences of the United States of America* 101.34 (Aug. 2004), pp. 12706–12711. ISSN: 0027-8424. DOI: 10.1073/PNAS.0404915101.

[191] Franziska Denk et al. "Tamoxifen induces cellular stress in the nervous system by inhibiting cholesterol synthesis". In: *Acta neuropathologica communications* 3 (Nov. 2015), p. 74. ISSN: 20515960. DOI: 10.1186/s40478-015-0255-6.

[192] Seth D Holland et al. "An ATF3-CreERT2 Knock-In Mouse for Axotomy-Induced Genetic Editing: Proof of Principle." In: *eNeuro* 6.2 (). ISSN: 2373-2822. DOI: 10.1523/ENEURO.0025-19.2019.

[193] Tom Medici and Peter J. Shortland. "Effects of peripheral nerve injury on parvalbumin expression in adult rat dorsal root ganglion neurons". In: *BMC neuroscience* 16.1 (Dec. 2015). ISSN: 1471-2202. DOI: 10.1186/S12868-015-0232-9.

[194] Seth D. Holland et al. "An ATF3-CreERT2 Knock-in mouse for axotomy- induced genetic editing: Proof of principle". In: *eNeuro* 6.2 (2019), pp. 1–17. ISSN: 23732822. DOI: 10.1523/ENEURO.0025-19.2019.

[195] C. Molander et al. "Early decline and late restoration of spinal cord binding and transganglionic transport of isolectin B4 from Griffonia simplicifolia I after peripheral nerve transection or crush". In: *Restorative Neurology and Neuroscience* 10.3 (1996), pp. 123–133. ISSN: 09226028. DOI: 10.3233/RNN-1996-10301.

[196] Steven J. West, Damien Bonboire, and David L Bennett. "StereoMate: 3D Stereological Automated Analysis of Biological Structures". In: *bioRxiv* (Jan. 2020), p. 648337. DOI: 10.1101/648337.

[197] A. L. Bailey and A. Ribeiro-Da-Silva. "Transient loss of terminals from non-peptidergic nociceptive fibers in the substantia gelatinosa of spinal cord following chronic constriction injury of the sciatic nerve". In: *Neuroscience* 138.2 (Jan. 2006), pp. 675–690. ISSN: 0306-4522. DOI: 10.1016/J.NEUROSCIENCE.2005.11.051.

[198] Linda Madisen et al. "A toolbox of Cre-dependent optogenetic transgenic mice for light-induced activation and silencing." In: *Nature neuroscience* 15.5 (Mar. 2012), pp. 793–802. ISSN: 1546-1726. DOI: 10.1038/nn.3078.

[199] Linda Madisen et al. "A robust and high-throughput Cre reporting and characterization system for the whole mouse brain". In: *Nature neuroscience* 13.1 (Jan. 2010), pp. 133–140. ISSN: 1546-1726. DOI: 10.1038/NN.2467.

[200] Tanya L. Daigle et al. "A Suite of Transgenic Driver and Reporter Mouse Lines with Enhanced Brain-Cell-Type Targeting and Functionality". In: *Cell* 174.2 (July 2018), 465–480.e22. ISSN: 0092-8674. DOI: 10.1016/J.CELL.2018.06.035.

[201] E.J. Bartley and R.B. Fillingim. "Sex differences in pain: a brief review of clinical and experimental findings". In: *Br. J. Anaesth.* 111 (2013), pp. 52–58.

[202] Jeffrey S. Mogil et al. "Pain sensitivity and vasopressin analgesia are mediated by a gene-sex-environment interaction". In: *Nature Neuroscience* 14.12 (Dec. 2011), pp. 1569–1573. ISSN: 10976256. DOI: 10.1038/nn.2941.

[203] Robert E. Sorge et al. "Different immune cells mediate mechanical pain hypersensitivity in male and female mice". In: *Nature Neuroscience* 18.8 (2015). ISSN: 15461726. DOI: 10.1038/nn.4053.

[204] Robert E. Sorge et al. "Spinal cord toll-like receptor 4 mediates inflammatory and neuropathic hypersensitivity in male but not female mice". In: *Journal of Neuroscience* 31.43 (Oct. 2011), pp. 15450–15454. ISSN: 02706474. DOI: 10.1523/JNEUROSCI.3859-11.2011.

[205] Loren J. Martin et al. "Male-Specific Conditioned Pain Hypersensitivity in Mice and Humans". In: *Current Biology* 29.2 (Jan. 2019), 192–201.e4. ISSN: 18790445. DOI: 10.1016/J.CUB.2018.11.030.

[206] Jennifer Mecklenburg et al. "Transcriptomic sex differences in sensory neuronal populations of mice". In: *Scientific Reports 2020 10:1* 10.1 (Sept. 2020), pp. 1–18. ISSN: 2045-2322. DOI: 10.1038/s41598-020-72285-z.

[207] Shilin Zhao et al. "RnaSeqSampleSize: Real data based sample size estimation for RNA sequencing". In: *BMC Bioinformatics* 19.1 (2018), pp. 1–8. ISSN: 14712105. DOI: 10.1186/s12859-018-2191-5.

[208] Marc Parisien et al. "Genetic pathway analysis reveals a major role for extracellular matrix organization in inflammatory and neuropathic pain". In: *Pain* 00.00 (2019), p. 1. ISSN: 0304-3959. DOI: 10.1097/j.pain.0000000000001471.

[209] Sarah Lamble et al. "Improved workflows for high throughput library preparation using the transposome-based nextera system". In: *BMC Biotechnology* 13.1 (Nov. 2013), pp. 1–10. ISSN: 14726750. DOI: 10.1186/1472-6750-13-104/FIGURES/4.

[210] Alexander Dobin and Thomas R Gingeras. "Comment on " TopHat2 : accurate alignment of transcriptomes in the presence of insertions , deletions and gene fusions " by Kim et al . Comment on " TopHat2 : accurate alignment of transcriptomes in the presence of insertions , deletions and gene fusions ". In: *Genome Biology* 14.4 (2013), pp. 0–9. ISSN: 1465-6906. DOI: 10.1101/000851.

[211] Heng Li et al. "The Sequence Alignment/Map format and SAMtools". In: *Bioinformatics* 25.16 (Aug. 2009), pp. 2078–2079. ISSN: 1367-4803. DOI: 10.1093/BIOINFORMATICS/BTP352.

[212] S Andrews. *FastQC: A Quality Control Tool for High Throughput Sequence Data*. 2010.

[213] Simon Anders, Paul Theodor Pyl, and Wolfgang Huber. "HTSeq–a Python framework to work with high-throughput sequencing data". In: *Bioinformatics* 31.2 (Jan. 2015), pp. 166–169. ISSN: 14602059. DOI: 10.1093/BIOINFORMATICS/BTU638.

[214] Michael I. Love, Wolfgang Huber, and Simon Anders. "Moderated estimation of fold change and dispersion for RNA-seq data with DESeq2". In: *Genome Biology 2014 15:12* 15.12 (Dec. 2014), pp. 1–21. ISSN: 1474-760X. DOI: 10.1186/S13059-014-0550-8.

[215] Zuguang Gu, Roland Eils, and Matthias Schlesner. "Complex heatmaps reveal patterns and correlations in multidimensional genomic data". In: *Bioinformatics (Oxford, England)* 32.18 (Sept. 2016), pp. 2847–2849. ISSN: 1367-4811. DOI: 10.1093/BIOINFORMATICS/BTW313.

[216] Igor Dolgalev. *msigdbr: MSigDB Gene Sets for Multiple Organisms in a Tidy Data Format version 7.4.1 from CRAN*. Tech. rep. 2021.

[217] Tianzhi Wu et al. "clusterProfiler 4.0: A universal enrichment tool for interpreting omics data". In: *The Innovation* 2.3 (Aug. 2021), p. 100141. ISSN: 2666-6758. DOI: 10.1016/J.XINN.2021.100141.

[218] Anqi Zhu, Joseph G. Ibrahim, and Michael I. Love. "Heavy-tailed prior distributions for sequence count data: removing the noise and preserving large differences". In: *Bioinformatics* 35.12 (June 2019), pp. 2084–2092. ISSN: 1367-4803. DOI: 10.1093/BIOINFORMATICS/BTY895.

[219] Matthew D. Young et al. "Gene ontology analysis for RNA-seq: accounting for selection bias". In: *Genome Biology* 11.2 (Feb. 2010), pp. 1–12. ISSN: 14747596. DOI: 10.1186/GB-2010-11-2-R14/TABLES/4.

[220] Perrine Royal et al. "Migraine-Associated TRESK Mutations Increase Neuronal Excitability through Alternative Translation Initiation and Inhibition of TREK". In: *Neuron* 101.2 (2019), 232–245.e6. ISSN: 10974199. DOI: 10.1016/j.neuron.2018.11.039.

[221] Xiang Yao Li and Hiroki Toyoda. *Role of leak potassium channels in pain signaling*. 2015. DOI: 10.1016/j.brainresbull.2015.08.007.

[222] C. Acosta et al. "TREK2 Expressed Selectively in IB4-Binding C-Fiber Nociceptors Hyperpolarizes Their Membrane Potentials and Limits Spontaneous Pain". In: *Journal of Neuroscience* 34.4 (2014), pp. 1494–1509. ISSN: 0270-6474. DOI: 10.1523/JNEUROSCI.4528-13.2014.

[223] C. J.A. Smith-Anttila et al. "Identification of a Sacral, Visceral Sensory Transcriptome in Embryonic and Adult Mice". In: *eNeuro* 7.1 (Jan. 2020). ISSN: 2373-2822. DOI: 10.1523/ENEURO.0397-19.2019.

[224] Michelle L. Starkey et al. "Expression of the regeneration-associated protein SPRR1A in primary sensory neurons and spinal cord of the adult mouse following peripheral and central injury". In: *The Journal of comparative neurology* 513.1 (Mar. 2009), pp. 51–68. ISSN: 00219967. DOI: 10.1002/CNE.21944.

[225] Iris E. Bonilla, Katsuhisa Tanabe, and Stephen M. Strittmatter. "Small proline-rich repeat protein 1A is expressed by axotomized neurons and promotes axonal outgrowth". In: *The Journal of neuroscience : the official journal of the Society for Neuroscience* 22.4 (Feb. 2002), pp. 1303–1315. ISSN: 1529-2401. DOI: 10.1523/JNEUROSCI.22-04-01303.2002.

[226] Xiaotang Jing et al. "The transcription factor Sox11 promotes nerve regeneration through activation of the regeneration-associated gene Sprr1a". In: *Experimental Neurology* 233.1 (Jan. 2012), pp. 221–232. ISSN: 0014-4886. DOI: 10.1016/J.EXPNEUROL.2011.10.005.

[227] Chi Bun Chan and Keqiang Ye. "Sex differences in brain-derived neurotrophic factor signaling and functions". In: *Journal of Neuroscience Research* 95.1-2 (Jan. 2017), pp. 328–335. ISSN: 1097-4547. DOI: 10.1002/JNR.23863.

[228] Ann M. LeMaster et al. "Overexpression of Brain-Derived Neurotrophic Factor Enhances Sensory Innervation and Selectively Increases Neuron Number". In: *Journal of Neuroscience* 19.14 (July 1999), pp. 5919–5931. ISSN: 0270-6474. DOI: 10.1523/JNEUROSCI.19-14-05919.1999.

[229] Tatiana González-Martínez et al. "BDNF, but not NT-4, is necessary for normal development of Meissner corpuscles". In: *Neuroscience Letters* 377.1 (Mar. 2005), pp. 12–15. ISSN: 03043940. DOI: 10.1016/J.NEULET.2004.11.078.

[230] Todd Dembo et al. "Primary Afferent-Derived BDNF Contributes Minimally to the Processing of Pain and Itch". In: *eNeuro* 5.December (Nov. 2018). ISSN: 23732822. DOI: 10.1523/ENEURO.0402-18.2018.

[231] Rob Patro et al. "Salmon provides fast and bias-aware quantification of transcript expression". In: *Nature Methods 2017 14:4* 14.4 (Mar. 2017), pp. 417–419. ISSN: 1548-7105. DOI: 10.1038/nmeth.4197.

[232] Jeffrey A.M. Coull et al. "BDNF from microglia causes the shift in neuronal anion gradient underlying neuropathic pain". In: *Nature 2005 438:7070* 438.7070 (Dec. 2005), pp. 1017–1021. ISSN: 1476-4687. DOI: 10.1038/nature04223.

[233] Philip Ewels et al. "MultiQC: summarize analysis results for multiple tools and samples in a single report". In: *Bioinformatics* 32.19 (Oct. 2016), pp. 3047–3048. ISSN: 1367-4803. DOI: 10.1093/BIOINFORMATICS/BTW354.

[234] Gabriel E. Hoffman and Eric E. Schadt. "variancePartition: Interpreting drivers of variation in complex gene expression studies". In: *BMC Bioinformatics* 17.1 (Nov. 2016), pp. 1–13. ISSN: 14712105. DOI: 10.1186/S12859-016-1323-Z/FIGURES/5.

[235] Damian Szklarczyk et al. "The STRING database in 2021: customizable protein–protein networks, and functional characterization of user-uploaded gene/measurement sets". In: *Nucleic Acids Research* 49.D1 (Jan. 2021), p. D605. ISSN: 13624962. DOI: 10.1093/NAR/GKAA1074.

[236] Matthew Stephens. "False discovery rates: a new deal". In: *Biostatistics* 18.2 (Apr. 2017), pp. 275–294. ISSN: 1465-4644. DOI: 10.1093/BIOSTATISTICS/KXW041.

[237] Eric Bair et al. "Prediction by Supervised Principal Components". In: *https://doi.org/10.1198/016214505000000628* 101.473 (Mar. 2012), pp. 119–137. ISSN: 01621459. DOI: 10.1198/016214505000000628.

[238] Markus Terrey et al. "GTPBP1 resolves paused ribosomes to maintain neuronal homeostasis". In: *eLife* 9 (Oct. 2020), pp. 1–22. ISSN: 2050084X. DOI: 10.7554/ELIFE.62731.

[239] Bradford E. Hall et al. "Transcriptomic analysis of human sensory neurons in painful diabetic neuropathy reveals inflammation and neuronal loss". In: *Scientific reports* 12.1 (Dec. 2022). ISSN: 2045-2322. DOI: 10.1038/S41598-022-08100-8.

[240] Katalin Sandor et al. "Spinal injection of newly identified cerebellin-1 and cerebellin-2 peptides induce mechanical hypersensitivity in mice". In: *Neuropeptides* 69 (June 2018), pp. 53–59. ISSN: 1532-2785. DOI: 10.1016/J.NPEP.2018.04.004.

[241] Satoshi Wakisaka, Keith C. Kajander, and Gary J. Bennett. "Increased neuropeptide Y (NPY)-like immunoreactivity in rat sensory neurons following peripheral axotomy". In: *Neuroscience letters* 124.2 (Apr. 1991), pp. 200–203. ISSN: 0304-3940. DOI: 10.1016/0304-3940(91)90093-9.

[242] Erin Greaves et al. "Estrogen receptor (ER) agonists differentially regulate neuroangiogenesis in peritoneal endometriosis via the repellent factor SLIT3". In: *Endocrinology* 155.10 (Oct. 2014), pp. 4015–4026. ISSN: 1945-7170. DOI: 10.1210/EN.2014-1086.

[243] Richard A. Meyer and Matthias Ringkamp. "A role for uninjured afferents in neuropathic pain." In: *Acta Physiologica Sinica* 60.5 (Oct. 2008), pp. 605–609. ISSN: 0371-0874.

[244] James N. Campbell and Richard A. Meyer. "Mechanisms of Neuropathic Pain". In: *Neuron* 52.1 (Oct. 2006), p. 77. ISSN: 08966273. DOI: 10.1016/J.NEURON.2006.09.021.

[245] H. Blumberg and W. Jänig. "Discharge pattern of afferent fibers from a neuroma". In: *Pain* 20.4 (1984), pp. 335–353. ISSN: 03043959. DOI: 10.1016/0304-3959(84)90111-8.

[246] Marshall Devor, Patrick D. Wall, and Naor Catalan. "Systemic lidocaine silences ectopic neuroma and DRG discharge without blocking nerve conduction". In: *Pain* 48.2 (Feb. 1992), pp. 261–268. ISSN: 0304-3959. DOI: 10.1016/0304-3959(92)90067-L.

[247] Robert O. Hughes et al. "Small Molecule SARM1 Inhibitors Recapitulate the SARM1 -/- Phenotype and Allow Recovery of a Metastable Pool of Axons Fated to Degenerate". In: *Cell reports* 34.1 (Jan. 2021). ISSN: 2211-1247. DOI: 10.1016/J.CELREP.2020.108588.

[248] Beom Shim et al. "Activity-dependent slowing of conduction velocity in uninjured L4 C fibers increases after an L5 spinal nerve injury in the rat". In: *Pain* 128.1-2 (Mar. 2007), pp. 40–51. ISSN: 03043959. DOI: 10.1016/J.PAIN.2006.08.023.

[249] Gang Wu et al. "Degeneration of myelinated efferent fibers induces spontaneous activity in uninjured C-fiber afferents". In: *Journal of Neuroscience* 22.17 (Sept. 2002), pp. 7746–7753. ISSN: 02706474. DOI: 10.1523/jneurosci.22-17-07746.2002.

[250] Matthias Ringkamp and Richard A. Meyer. "Injured versus uninjured afferents: Who is to blame for neuropathic pain?" In: *Anesthesiology* 103.2 (2005), pp. 221–223. ISSN: 0003-3022. DOI: 10.1097/00000542-200508000-00002.

[251] Maria Schäfers et al. "Increased sensitivity of injured and adjacent uninjured rat primary sensory neurons to exogenous tumor necrosis factor-alpha after spinal nerve ligation". In: *The Journal of neuroscience : the official journal of the Society for Neuroscience* 23.7 (Apr. 2003), pp. 3028–3038. ISSN: 1529-2401. DOI: 10.1523/JNEUROSCI.23-07-03028.2003.

[252] M. Devor and P. D. Wall. "Cross-excitation in dorsal root ganglia of nerve-injured and intact rats". In: *https://doi.org/10.1152/jn.1990.64.6.1733* 64.6 (1990), pp. 1733–1746. ISSN: 00223077. DOI: 10.1152/JN.1990.64.6.1733.

[253] Yongbo Li et al. "Mechanical hyperalgesia after an L5 spinal nerve lesion in the rat is not dependent on input from injured nerve fibers". In: *Pain* 85.3 (Apr. 2000), pp. 493–502. ISSN: 03043959. DOI: 10.1016/S0304-3959(00)00250-5.

[254] Rishi N. Sheth et al. "Mechanical hyperalgesia after an L5 ventral rhizotomy or an L5 ganglionectomy in the rat". In: *Pain* 96.1-2 (2002), pp. 63–72. ISSN: 0304-3959. DOI: 10.1016/S0304-3959(01)00429-8.

[255] Yeoung Su Lyu et al. "Low dose of tetrodotoxin reduces neuropathic pain behaviors in an animal model". In: *Brain research* 871.1 (July 2000), pp. 98–103. ISSN: 0006-8993. DOI: 10.1016/S0006-8993(00)02451-3.

[256] Koichi Obata et al. "Differential activation of MAPK in injured and uninjured DRG neurons following chronic constriction injury of the sciatic nerve in rats". In: *European Journal of Neuroscience* 20.11 (Dec. 2004), pp. 2881–2895. ISSN: 1460-9568. DOI: 10.1111/J.1460-9568.2004.03754.X.

[257] Kenzo Tsuzuki et al. "Differential regulation of P2X3 mRNA expression by peripheral nerve injury in intact and injured neurons in the rat sensory ganglia". In: *Pain* 91.3 (2001), pp. 351–360. ISSN: 03043959. DOI: 10.1016/S0304-3959(00)00456-5.

[258] Koichi Noguchi et al. "Substance P induced by peripheral nerve injury in primary afferent sensory neurons and its effect on dorsal column nucleus neurons". In: *The Journal of neuroscience : the official journal of the Society for Neuroscience* 15.11 (Nov. 1995), pp. 7633–7643. ISSN: 0270-6474. DOI: 10.1523/JNEUROSCI.15-11-07633.1995.

[259] W. L. Huang et al. "Spinal cord compression and dorsal root injury cause up-regulation of activating transcription factor-3 in large-diameter dorsal root ganglion neurons". In: *The European journal of neuroscience* 23.1 (Jan. 2006), pp. 273–278. ISSN: 0953-816X. DOI: 10.1111/J.1460-9568.2005.04530.X.

[260] Michael Lawrence et al. "Software for Computing and Annotating Genomic Ranges". In: *PLOS Computational Biology* 9.8 (Aug. 2013), e1003118. ISSN: 1553-7358. DOI: 10.1371/JOURNAL.PCBI.1003118.

[261] Tim Stuart et al. "Single-cell chromatin state analysis with Signac". In: *Nature Methods* 18.11 (Nov. 2021), pp. 1333–1341. ISSN: 1548-7091. DOI: 10.1038/S41592-021-01282-5.

[262] Yuhan Hao et al. "Integrated analysis of multimodal single-cell data". In: *Cell* 184.13 (June 2021), 3573–3587.e29. ISSN: 0092-8674. DOI: 10.1016/J.CELL.2021.04.048.

[263] Ed S. Lein et al. "Genome-wide atlas of gene expression in the adult mouse brain". In: *Nature 2006 445:7124* 445.7124 (Dec. 2006), pp. 168–176. ISSN: 1476-4687. DOI: 10.1038/nature05453.

[264] Philip R. Holland and Peter J. Goadsby. "Cluster headache, hypothalamus, and orexin". In: *Current pain and headache reports* 13.2 (2009), pp. 147–154. ISSN: 1534-3081. DOI: 10.1007/S11916-009-0025-X.

[265] Koichi Obata et al. "Contribution of injured and uninjured dorsal root ganglion neurons to pain behavior and the changes in gene expression following chronic constriction injury of the sciatic nerve in rats". In: *Pain* 101.1-2 (2003), pp. 65–77. ISSN: 0304-3959. DOI: 10.1016/S0304-3959(02)00296-8.

[266] Zahid Latif et al. "Confirmation of the Role of DHX38 in the Etiology of Early-Onset Retinitis Pigmentosa". In: *Investigative Ophthalmology & Visual Science* 59.11 (Sept. 2018), pp. 4552–4557. ISSN: 1552-5783. DOI: 10.1167/IOVS.18-23849.

[267] Katarina Stingl et al. "CDHR1 mutations in retinal dystrophies". In: *Scientific Reports 2017 7:1* 7.1 (Aug. 2017), pp. 1–11. ISSN: 2045-2322. DOI: 10.1038/s41598-017-07117-8.

[268] Maik Behrens et al. "Members of RTP and REEP gene families influence functional bitter taste receptor expression". In: *The Journal of biological chemistry* 281.29 (July 2006), pp. 20650–20659. ISSN: 0021-9258. DOI: 10.1074/JBC.M513637200.

[269] Xiaoling Zhou et al. "The interferon-alpha responsive gene TMEM7 suppresses cell proliferation and is downregulated in human hepatocellular carcinoma". In: *Cancer genetics and cytogenetics* 177.1 (Aug. 2007), pp. 6–15. ISSN: 0165-4608. DOI: 10.1016/J.CANCERGENCYTO.2007.04.007.

[270] Harukazu Saito and Lars B. Dahlin. "Expression of ATF3 and axonal outgrowth are impaired after delayed nerve repair". In: *BMC Neuroscience* 9.1 (Sept. 2008), pp. 1–10. ISSN: 14712202. DOI: 10.1186/1471-2202-9-88/FIGURES/3.

[271] Lena Stenberg et al. "Expression of activating transcription factor 3 (ATF 3) and caspase 3 in Schwann cells and axonal outgrowth after sciatic nerve repair in diabetic BB rats". In: *Neuroscience letters* 515.1 (Apr. 2012), pp. 34–38. ISSN: 1872-7972. DOI: 10.1016/J.NEULET.2012.03.011.

[272] David I. Hughes and Andrew J. Todd. "Central Nervous System Targets: Inhibitory Interneurons in the Spinal Cord". In: *Neurotherapeutics* 17.3 (July 2020), pp. 874–885. ISSN: 18787479. DOI: 10.1007/S13311-020-00936-0/FIGURES/4.

[273] Ru Rong Ji et al. "MMP regulation of neuropathic pain". In: *Trends in pharmacological sciences* 30.7 (July 2009), p. 336. ISSN: 01656147. DOI: 10.1016/J.TIPS.2009.04.002.

[274] Josiah Gerdts et al. "SARM1 activation triggers axon degeneration locally via NAD+ destruction". In: *Science* 348.6233 (Apr. 2015), pp. 453–457. ISSN: 10959203. DOI: 10.1126/SCIENCE.1258366/SUPPL_FILE/1258366-GERDTS.SM.PDF.

[275] Eli Akude et al. "Diminished Superoxide Generation Is Associated With Respiratory Chain Dysfunction and Changes in the Mitochondrial Proteome of Sensory Neurons From Diabetic Rats". In: *Diabetes* 60.1 (Jan. 2011), pp. 288–297. ISSN: 0012-1797. DOI: 10.2337/DB10-0818.

[276] Tony K.Y. Lim et al. "Mitochondrial and bioenergetic dysfunction in trauma-induced painful peripheral neuropathy". In: *Molecular Pain* 11.1 (Sept. 2015), p. 58. ISSN: 17448069. DOI: 10.1186/S12990-015-0057-7.

[277] Marija Sajic et al. "Impulse Conduction Increases Mitochondrial Transport in Adult Mammalian Peripheral Nerves In Vivo". In: *PLOS Biology* 11.12 (Dec. 2013), e1001754. ISSN: 1545-7885. DOI: 10.1371/JOURNAL.PBIO.1001754.

[278] Jelle van den Ameele et al. "Chronic pain is common in mitochondrial disease". In: *Neuromuscular Disorders* 30.5 (May 2020), pp. 413–419. ISSN: 18732364. DOI: 10.1016/J.NMD.2020.02.017/ATTACHMENT/FD32D64A-E465-4FB4-8B5A-5410BF471675/MMC2.PDF.

[279] Helmar C. Lehmann et al. "Mitochondrial dysfunction in distal axons contributes to human immunodeficiency virus sensory neuropathy". In: *Annals of Neurology* 69.1 (Jan. 2011), pp. 100–110. ISSN: 1531-8249. DOI: 10.1002/ANA.22150.

[280] James Brian Byrd et al. "Responsible, practical genomic data sharing that accelerates research". In: *Nature Reviews Genetics 2020 21:10* 21.10 (Oct. 2020), pp. 615–629. ISSN: 1471-0064. DOI: 10.1038/S41576-020-0257-5.

[281] Laurence A. Brown and Stuart N. Peirson. "Improving Reproducibility and Candidate Selection in Transcriptomics Using Meta-analysis". In: *Journal of Experimental Neuroscience* (2018). ISSN: 11790695. DOI: 10.1177/1179069518756296.

[282] Arjun Muralidharan et al. "Long-term male-specific chronic pain via telomere- and p53-mediated spinal cord cellular senescence". In: *The Journal of Clinical Investigation* 132.8 (Apr. 2022). ISSN: 1558-8238. DOI: 10.1172/JCI151817.

[283] Lulu I T. Korsak et al. "Regulation of neuronal gene expression by local axonal translation". In: *Current genetic medicine reports* 4.1 (Mar. 2016), p. 16. DOI: 10.1007/S40142-016-0085-2.